Étude de la variabilité des conditions océanographiques et climatiques en Antarctique de l'Est (Terre Adélie-Georges V) au cours de l'Holocène tardif et de la période instrumentale

Philippine Campagne

université de BORDEAUX

THÈSE

Présentée à

L'UNIVERSITÉ DE BORDEAUX

ÉCOLE DOCTORALE DES SCIENCES ET ENVIRONNEMENTS

Par **Philippine CAMPAGNE**

Pour obtenir le grade de docteur

SPÉCIALITÉ/ SÉDIMENTOLOGIE MARINE ET PALÉOCLIMATS

Étude de la variabilité des conditions océanographiques et climatiques en Antarctique de l'Est (Terre Adélie-Georges V) au cours de l'Holocène tardif et de la période instrumentale

---

Directeurs de recherche: Xavier Crosta, Guillaume Massé

Soutenue le 18 Décembre 2015

Devant la commission d'examen formée de :

Mme BÁRCENA PERNÍA María Ángeles, Professeur, Université de Salamanque	Rapporteur
M. GOOSSE Hugues, Professeur, TECLIM, Université Catholique de Louvain	Rapporteur
Mme VIMEUX Françoise, Directrice de recherche IRD, LSCE, Université de Versailles	Examinateur
M. GIRAUDEAU Jacques, Directeur de recherche CNRS, EPOC, Université de Bordeaux	Examinateur
M. CROSTA Xavier, Directeur de Recherche CNRS, EPOC, Université de Bordeaux	Directeur de thèse
M. MASSÉ Guillaume, Chargé de Recherche CNRS, TAKUVIK, Université Laval	Directeur de thèse

Remerciements

La thèse est loin d'être un travail solitaire. Je n'aurais jamais pu réaliser mon doctorat sans la participation et le soutien d'un grand nombre de personnes qui grâce à leur humour, intérêt et patience dont ils ont fait preuve m'ont permis de progresser dans mon projet de recherche. Je remercie donc grandement toutes ces personnes. Et comme le disait Confucius, dont je ne connais pas grand chose, "une image vaut mille mots", surtout lorsqu'il sagit des miens.

Abstract

Antarctic sea ice has large impacts on the heat and gas transfers between the ocean and the atmosphere, on the global oceanic circulation, on the Earth albedo and on the primary productivity of the Southern Ocean. However, because of its remote and ice-covered location, the climate of the Antarctic continent and of the Southern Ocean is still poorly studied and constitutes a challenge for climate model predictions. Recent observations highlighted opposite patterns of climate variability between Western and Eastern Antarctica, but poorly resolved the mechanisms and forcing involved. Reconstructions of temperature signals indicate that regional disparities have persisted over the Holocene period. The Late Holocene period includes the recent climate change (so-called modern global warming) as well as preceding rapid climate variabilities though of lower amplitude. Achieving paleoenvironmental reconstructions in the Antarctic region at high temporal resolution over this period therefore offers the opportunity to improve the understanding of climate changes in response to both natural and anthropogenic forcing. While paleoenvironmental records obtained from ice cores provide robust information on the past atmospheric conditions over Antarctica, the paleoceanography of the nearby ocean is constrained by a limited set of rather low resolution, discontinuous records from sediment cores. Our study focuses on the marginal zone of the Adélie-Georges V Land, East Antarctica, a region which has been poorly studied so far, despite the presence of thick and laminated sedimentary deposits that allow accurate and high resolution paleoclimate reconstructions. Our work is based on several marine sedimentary records, made of diatom oozes and covering the instrumental period to the last 2,000 years. Our results show that diatom assemblages, diatom specific biomarkers (HBI) and elemental geochemistry in the sediment effectively testify of local but also regional oceanographic and climatic variations at decadal to centennial scales. Coupled atmospheric and oceanic dynamics linked to major climate modes of the Southern Hemisphere, along with glacial dynamics constitute major forcing mechanisms of ice covered changes during the late Holocene.

Key words: Late Holocene, Adélie Land, Sea ice, Diatoms, HBIs, forcings

Résumé

La banquise Antarctique joue un rôle important sur les flux de chaleur et les échanges de gaz à l'interface océan-atmosphère, sur la circulation océanique globale, sur l'albédo et la productivité primaire de l'Océan Austral. Cependant, du fait de son éloignement et d'un climat extrême, cette région reste à ce jour encore peu étudiés, et représente un verrou pour les modèles prédictifs du climat. De plus, de récentes observations ont montré que le continent Antarctique présente des tendances régionales, dont les causes et les mécanismes sont encore mal compris. Les reconstructions paléoclimatiques de températures tendent à montrer que ces disparités régionales ont également caractérisé la période Holocène. L'Holocène tardif représente la période sur laquelle le réchauffement récent se produit et est également caractérisée par des variations climatiques rapides généralement de plus faibles amplitudes. Afin de mieux évaluer ces changements, l'étude fine des conditions environnementales passées en Antarctique au cours de l'Holocène tardif est essentielle afin d'isoler la part de variabilité climatique naturelle de la part anthropique. Bien qu'un vaste réseau de carottes de glace en Antarctique constitue une base d'informations robuste sur la variabilité atmosphérique passée dans l'Hémisphère Sud, l'étude des conditions paléocéanographiques est contrainte dans la région par le nombre limité d'enregistrements sédimentaires marins, et qui de plus, tendent à être de faible résolution, trop courts ou discontinus. Notre étude porte sur la zone marginale du plateau de la Terre Adélie-Georges V en Antarctique de l'Est, qui a reçu peu d'attention jusqu'à présent, malgré la présence de séquences sédimentaires très épaisses et laminées, permettant la reconstruction fine des variations climatiques passées. Nos travaux ont été réalisés à partir de plusieurs enregistrements sédimentaires marins, couvrant la période instrumentale et jusqu'aux deux derniers millénaires. Nos résultats montrent que les assemblages de diatomées, les biomarqueurs spécifiques des diatomées, ainsi que de la géochimie élémentaire du sédiment traduisent efficacement des variations océanographiques et climatiques locales et aussi régionales à l'échelle interannuelle à centennale. La dynamique couplée océan-atmosphère en lien avec les modes climatiques principaux de l'Hémisphère Sud, ainsi que la dynamique glaciaire constituent les mécanismes de forçage majeurs des changements du couvert de banquise au court de l'Holocène tardif.

Mots clés: Holocène tardif, Terre Adélie, Banquise, Diatomées, HBIs, forçages.

Table des matières

Liste des figures

Liste des acronymes

AA: Antarctic ou Antarctique

AABW: Antarctic Bottom Water

AACC: Antarctic Circumpolar Current

AAIW: Antarctic Intermediate Water

AAO: Antarctic Oscillation

AASW: Antarctic Surface Water

ACC: Antarctic Coastal Current

AD: Antarctic Divergence

AGVL: Adélie Georges V Land

ALBW: Adelie Land Bottom Water

ASSW: Antarctic Summer Surface Water

AWS: Automatic Weather Station

CB: Commonwealth Bay

CCSZ: Coastal and Continental Shelf Zone

CDW: Circumpolar Deep Water

CE: Common Era

CPT: Circumpolar Trough

CRS: *Chaetoceros* resting spores

CWT: Continuous Wavelet Transform

DDU: Dumont D'Urville

DDUP: Dumont D'Urville Polynya

DDUT: Dumont D'Urville Trough

ENSO: El Niño Southern Oscillation

EWD: East Wind Drift

FCC: *Fragilariopsis curta + F. cylindrus*

FFT: Fast Fourier Transform

HBI: Highly Branched isoprenoids

HSSW: High Salinity Shelf Water

LSSW: Low Salinity Shelf Water

MG: Mertz Glacier

MGP: Mertz Glacier Polynya

MGT: Mertz Glacier Tongue

MIZ: Marginal Ice Zone

NH: Northern Hemisphere

PA ou AP: Péninsule Antarctique

PDO: Pacific Decadal Oscillation

PF: Polar Front

PP: Primary Production

SAF: Sub Antarctic Front

SAM: Southern Annual Mode

SH: Southern Hemisphere

SO: Southern Ocean

SOI: Southern Oscillation Index

SSIZ: Seasonal Sea Ice Zone

STF: Sub Tropical Front

SWW: Southern Westerly Winds

TA: Terre Adélie

TA-GV: Terre Adélie Georges V

Ti: titane ou titanium

XRF: X Ray Fluorescence

XWT: Cross Wavelet Transform

Liste des tables

Liste des annexes

Introduction générale

Problématique et objectifs de cette thèse

Le réchauffement climatique, en grande partie attribué aux activités humaines, a des conséquences amplifiées dans les zones polaires où certaines régions montrent un réchauffement jusqu'à deux fois plus important que dans les régions tempérées, entraînant la diminution progressive de certaines zones englacées. Cependant, la réponse de la cryosphère face à ce changement climatique rapide n'est pas linéaire et uniforme et pointe une hétérogénéité spatiale importante, traduisant une complexité du système atmosphère/océan/banquise. Particulièrement, en Antarctique, alors que la Péninsule Antarctique montre un réchauffement important, la partie orientale du continent indique au contraire un léger refroidissement au cours des dernières décennies. Cette asymétrie est encore très mal appréhendée dans cette région du globe, notamment en raison du manque de données instrumentales et de leur trop courte étendue temporelle (débutant dans les années 1950 pour les mesures automatisées et 1980 pour les données satellites).

L'Antarctique est pourtant un acteur primordial de la machine climatique, où chacun des sous-systèmes climatiques (cryosphère, atmosphère, océan et biosphère) entretient des connections étroites avec les autres régions du globe *via* la circulation océanique mondiale et les téléconnexions atmosphériques avec les basses et moyennes latitudes sud. La banquise antarctique joue également un rôle important sur les flux de chaleur et les échanges de gaz à l'interface océan-atmosphère, sur la circulation océanique globale, sur l'albédo et la productivité primaire de l'Océan Austral et de l'Océan global. Ainsi la communauté internationale a développé ces dernières années de nombreux programmes de larges envergures (ex: SCAR -Scientific committee on AntarcticResearch ; PAGES 2k Network; WCRP-CLIC-PCPI - World ClimateResearch Program, Climate and cryosphere, Polar Climate Predictability Initiative) visant à développer la recherche en Antarctique ainsi que dans l'Océan Austral, et à appréhender le rôle de cette région dans la machine climatique globale. La communauté scientifique tente également d'améliorer les modèles prédictifs, afin de mieux comprendre la machine climatique au travers de ses différents compartiments mais aussi leurs interactions, et de mieux appréhender les changements environnementaux, sociétaux et économiques futurs. Cependant, le peu de données acquises en Antarctique représente un verrou pour des modèles prédictifs. Il apparait alors nécessaire d'étudier la

climatologie actuelle mais aussi passée à travers une approche couplée modèles-données pour bâtir des prédictions réalistes et comprendre les processus climatiques en jeu.

Des études récentes suggèrent l'existence de variations climatiques rapides pendant l'Holocène. Cette période sur laquelle le réchauffement récent se produit est essentielle pour isoler la part de variabilité climatique naturelle de la part anthropique. Bien qu'un vaste réseau de carottes de glace en Antarctique constitue un base d'informations importante sur la nature de cette variabilité climatique Holocène, seulement quelques enregistrements marins sont disponibles dans cette région, et de plus, tendent à être de faible résolution, trop courts ou encore discontinus. La communauté scientifique de la recherche sur le climat passé tente de comprendre les liens entre les différents composants du système climatique, les processus ainsi que les forçages climatiques au cours de l'Holocène, et notamment vise à documenter à très haute résolution l'évolution du cycle saisonnier de la banquise au cours de l'Holocène. Cette thèse s'inscrit dans la continuité des ces recherches au sein de thématiques de recherche des projets ESF Polar Climate HOLOCLIP (Holocene climate variability at high-southern latitudes: an integrated perspective), FP7 PAST4FUTURE (Climate change - Learning from the pastclimate) et ANR CLIMICE (Banquise et variabilité climatique passée), à travers la collecte d'enregistrements sédimentaires haute-résolution afin de documenter la variabilité climatique d'ordre inter-annuelle à pluri-centennale en Antarctique ainsi que les forçages associés.

Notre étude porte sur la zone marginale du plateau continental de la Terre Adélie-Georges V en Antarctique de l'Est, qui a reçu peu d'attention jusqu'à présent, malgré la présence de séquences sédimentaires très épaisses et laminées, permettant de reconstruire finement les variations climatiques. Les diatomées constituent une part importante de la production primaire dans les eaux côtières des marges continental en Antarctique. Longtemps utilisées d'un point de vue micropaléontologique, les diatomées ont été plus récemment associées à des biomarqueurs spécifiques (HBI) afin de reconstruire les conditions de glace passées dans l'Océan Austral. Notre étude s'inscrit parmi les quelques études sédimentaires qui existent dans la zone marginale de glace en Antarctique.

Nos travaux ont été réalisés à partir de plusieurs enregistrements sédimentaires marins continus composés de boues à diatomées, et ayant été récoltés sur le plateau de la Terre Adélie-Georges V. Ces séquence sédimentaires sont pour la plupart laminés saisonnièrement (2 lamines saisonnières par an), et couvrent des périodes allant des quatre dernières décennies

aux deux derniers millénaires. L'analyse haute résolution des assemblages de diatomées, de biomarqueurs spécifiques de diatomées (HBI), ainsi que l'étude de l'abondance d'éléments majeurs et mineurs dans ces sédiments permet la reconstruction des conditions passées du couvert de banquise à une résolution sans précédent à L'Holocène tardif. L'analyse de sédiments marins récents, et leur comparaison avec des données instrumentales, a permis, dans un premier temps de valider nos outils, et donc de mieux appréhender les modalités d'utilisation des diatomées ainsi que des biomarqueurs pour les reconstructions paléoenvironnementales. Puis, l'analyse de séries sédimentaires plus longues a permis de reconstruire les conditions de surface de la région de la Terre Adélie-Georges V, et de documenter les connections entre l'océan, l'atmosphère et de la cryosphère, et la biosphère marine au cours de l'Holocène tardif jusque sur la période instrumentale. Nous nous sommes également attachés à replacer nos reconstructions environnementales dans un contexte plus régional, en les confrontant avec des enregistrements glaciaires, afin de dessiner un schéma général des forçages et de la variabilité climatique en Antarctique de l'Est au cours des derniers 2,000 ans. Nos résultats attestent de variations océanographiques et climatiques locales et aussi régionales à l'échelle interannuelle à centennale. De plus, à travers l'analyse statistique et spectrale de nos enregistrements, nous avons mis en évidence des forçages climatiques et leur mécanismes associés, qui agissent à différentes échelle spatio-temporelles. Il resort de nos résultats que la dynamique couplée océan-atmosphère en lien avec les modes climatiques principaux de l'Hémisphère Sud, ainsi que la dynamique glaciaire constituent les mécanismes de forçage majeurs des changements du couvert de banquise au court de l'Holocène tardif.

Organisation du manuscrit

Dans le premier chapitre, nous introduisons les motivations scientifiques de ce travail par la présentation des particularités géographiques et climatiques du continent Antarctique et de l'Océan Austral. Nous présentons également une synthèse des connaissances actuelles sur le climat à l'Holocène tardif ainsi que sur la période récente dans la région de l'Océan Austral. Ce Chapitre I constitue ainsi un prélude au travail de recherche effectué qui permettra au lecteur de mieux situer les différentes périodes de temps étudiées.

Dans le Chapitre II, nous nous sommes particulièrement intéressé aux compartiments atmosphère/banquise/océan au large de la Terre Adélie-Georges V, et à leurs interconnections

au cours des dernières décennies, afin de présenter les connaissances sur le système actuel en Terre Adélie-Georges V. Nous présentons également les caractéristiques des différents outils utilisés ainsi que des sites étudiés dans cette thèse.

Dans le Chapitre III, nous étudions les relations entre les divers outils utilisés dans cette thèse, ainsi que leurs liens avec les conditions environnementales sur la période instrumentale. Grace à l'analyse statistique de nos données sédimentaires, que nous confrontons à un panel de données météorologiques, nous tentons de valider nos outils et de documenter la réponse sédimentaire dans notre zone d'étude. Nous affinons ainsi à l'échelle annuelle à interannuelle les connaissances sur l'écologie des diatomées et les conditions environnementales auxquelles les biomarqueurs HBI sont associés, afin de proposer un outil robuste pour la reconstruction paléoclimatique des conditions de surface au large de Terre Adélie-Georges V. Ce troisième chapitre se compose d'un article scientifique:

Sedimentary response to sea ice and atmospheric variability over the instrumental period off Adélie Land, East Antarctica

Campagne, P., Crosta, X., Schmidt, S., Houssais, M. N.,Ther, O., and Massé, G.

Soumis à *Biogeosciences*

Dans le Chapitre IV de cette thèse, nous reconstruisons les changements de la dynamique saisonnière du couvert de banquise et de l'activité des polynies régionales au cours des derniers siècles. Nous tentons également de mettre en évidence les mécanismes sous-jacents de forçages climatiques agissant à l'échelle pluri décennale et pluri centennale en Terre Adélie-Georges V. Grace à l'analyse spectrale des enregistrements (diatomées, HBI et XRF core-scanner) par la méthode des ondelettes, nous comparons ainsi deux séquences sédimentaires issus de deux zones distinctes, afin d'appréhender les forçages locaux, régionaux et synoptiques au cours des derniers siècles. Ce travail a fait l'objet d'un article scientifique publié qui constitue la première partie du Chapitre IV, sous l'intitulé :

Glacial ice and atmospheric forcing on the Mertz Glacier Polynya over the past 250 years

Campagne, P., Crosta, X., Houssais, M. N., Swingedouw D., Schmidt, S., Martin, A., Devred, E., Capo, S., Marieu, V., Closset, I. and Massé, G. (2015).

Nature communications, 6: 6642, doi: 10.1038/ncomms7642.

Ce travail sera aussi valorisé sous la forme d'un deuxième article, en préparation, qui constitue la deuxième partir du Chapitre IV sous l'intitulé :

Sea ice variability and potential related forcing in the Adélie-Georges V Land over the last 500 years

Campagne, P., Massé, G., Schmidt, S. and Crosta, X.

En préparation

Enfin, dans le Chapitre V, nous reconstruisons les conditions de surface, l'activité des polynies et la saisonnalité de la banquise à haute résolution au cours des 2,000 ans à partir d'une séquence sédimentaire à lamines saisonnières. Nous étudions également ,grâce à l'analyse de nos données par ondelettes, la cyclicité décennale à pluri-centennale au cours de l'Holocène tardif, dans le but d'étudier les forçages synoptiques de l'Hémisphère Sud. De plus, nous tentons de mettre en évidence des forçages plus régionaux à l'échelle de l'Antarctique de l'Est à travers la comparaison de nos enregistrements avec des enregistrements glaciaires couvrant la même période temporelle. Ce travail fait l'objet d'un article en préparation sous l'intitulé :

High resolution reconstruction of climate and sea ice seasonality in Adélie Land, East Antarctica, over the Late Holocene

Campagne, P., Etourneau, J., Massé, G., Crosta, X. and IODP Expedition 318 Scientists

En préparation

Les données produites au cours de ce travail de thèse sont injectées dans les compilations des grands programmes internationaux tels que PAGES 2k Network et WCRP-CLIC-PCPI. Le travail effectué pendant cette thèse a contribué à une autre publication, portant sur l'étude des évènements de fonte de la marge glaciaire en Antarctique de l'Est à partir de l'analyse isotopique du ^{18}O des sédiments marins dans la région. Cet article (Annexe 4) fournit des informations complémentaires à nos données notamment du point de vue de la réponse des glaciers locaux aux forçages globaux.

Holocene glacial discharge fluctuations and recent instability in East Antarctica

Crespin, J., Yam, R., Crosta, X., Massé, G., Schmidt, S., Campagne, P., & Shemesh, A. (2014).

Earth and Planetary Science Letters, 394, 38-47.

Chapitre I: Généralités

Les deux premières parties de ce chapitre présentent l'état actuel des connaissances concernant l'Antarctique et l'Océan Austral, à savoir les caractéristiques géographiques et environnementales qui jouent un rôle dans le climat aux hautes latitudes de l'Hémisphère Sud. Nous présentons également dans un troisième volet une synthèse des connaissances actuelles sur la variabilité climatique ainsi que sur les forçages impliqués à l'Holocène tardif et au cours de la période récente dans la région de l'Océan Austral et en Antarctique. Ce Chapitre I constitue ainsi un prélude au travail de recherche effectué qui permettra au lecteur de mieux situer les différentes périodes de temps étudiées.

1 L'Océan Austral et le continent Antarctique

L'Océan Austral forme une ceinture océanique d'une superficie de $20.10^6 km^2$ sur toute la circonférence autour du continent Antarctique (Fig. 1a) et s'étend jusqu'à 35°S. L'Océan Austral est parcouru par le Courant Circumpolaire Antarctique qui circule d'Ouest en Est. L'Océan Austral est lié à une intense activité de transformation des masses d'eau et joue un rôle prépondérant dans la circulation thermohaline, en permettant la redistribution globale de nombreux éléments clefs du système climatique tels que la chaleur, la salinité, les nutriments etc. L'océan Austral est divisé en trois grands bassins séparés par des dorsales, la plaine abyssale de Weddell-Enderby (secteur Atlantique), le bassin Australo-Antarctique (secteur Indien) et la plaine abyssale d'Amundsen-Bellingshausen (secteur Pacifique).

Le continent Antarctique à une surface de $12{,}5.10^6$ km^2 recouverte à 98 % de glace sur environ 1,6 km d'épaisseur, représentant à lui seul 10% des terres émergées de la surface du globe et 90% des réserves de glace continentale. Le continent Antarctique se divise en deux régions (Fig. 1b), orientale et occidentale, délimitées naturellement par la chaine des Montagnes Transantarctiques d'environ 3.000 km de long (Fig. 1a). Ainsi la partie Est de l'Antarctique inclus la Coats Land, Queen Maud Land, Enderby Land, Kemp Land, Mac. Robertson Land, Princess Elizabeth Land, Wilhelm II Land, Queen Mary Land, Wilkes Land, Adélie Land, George V Land, Oates Land and Victoria Land (Fig. 1a). La partie Ouest du continent comprend les zones suivantes: Antarctic Peninsula, Ellsworth Land, Marie Byrd Land and King Edward VII Land, diverses îles (ex: Adelaide Island), divers ice shelves tels que le Filchner-Ronne Ice Shelf (Weddell Sea) et le Ross Ice Shelf (Ross Sea) (Fig. 2a). Outre l'effet isostasique, le socle rocheux de la partie Ouest du continent se situe en dessous du niveau marin (Fig. 1b), conférant une plus grande sensibilité de la calotte glaciaire aux variations eustatiques dans cette région. De par sa position méridionale et donc son faible ensoleillement, l'Antarctique est le continent le plus froid (record à -90°C dans les terres), le plus sec (- de 200 mm/an de pluie) et le plus venteux (record autour de 360km/h sur les côtes) au monde.

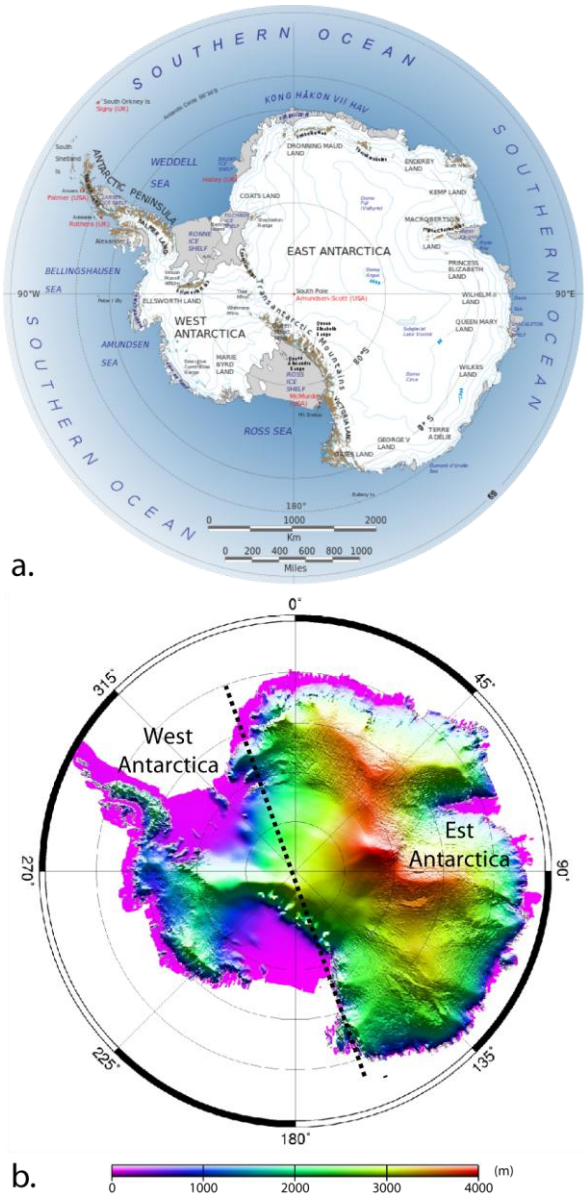

Figure 1. a) Carte montrant la géographie principale du continent Antarctique, d'après Wikipedia. b) Topographie du continent Antarctique (http://remy.omp.free.fr/FTP/image-satellite-poles/).

2 Système océan/banquise/atmosphère

2.1 Circulation atmosphérique grande échelle dans l'Hémisphère Sud

Le système climatique global est gouverné par le gradient d'insolation équateur-pôle à la surface du globe. L'énergie solaire reçue à l'équateur est environ cinq fois supérieure par rapport aux pôles ce qui engendre un fort gradient de température entre les basses et les hautes

latitudes, ainsi qu'un transport de chaleur vers les pôles, par le biais notamment de la circulation atmosphérique (Fig. 2).

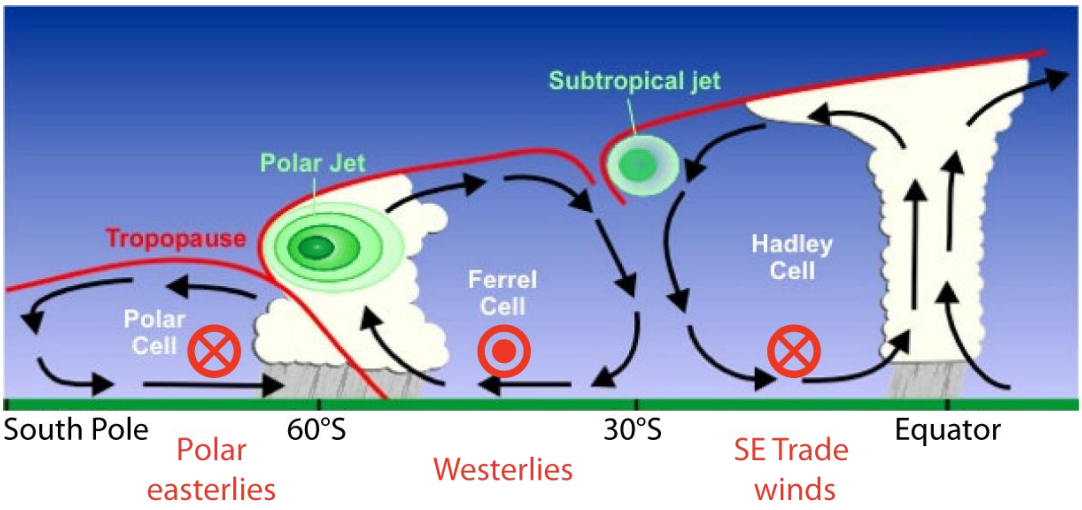

Figure 2. Circulation atmosphérique méridionale et zonale dans l'Hémisphère Sud (https://skepticalscience.com/jetstream-guide.html).

2.1.1 Circulation aux basses latitudes

L'atmosphère est composée de plusieurs cellules sous l'action de la force de Coriolis, due à la rotation de la Terre. Dans la région équatoriale, la convergence des vents d'Est, chauds et chargés en humidité, forcent l'air à s'élever, créant des zones de basses pressions autour de l'Equateur (Fig. 2). A la tropopause, vers 15 km d'altitude, ces masses d'air ayant perdu une grande partie de leur humidité sous forme de précipitations, divergent et redescendent vers 30°S. Lors de cette subsidence, l'air se réchauffe et perd son humidité conférant ainsi un régime anticyclonique générateur d'un climat sec aux régions subtropicales. Cette boucle de circulation est appelée cellule de Hadley (Fig. 2).

2.1.2 Circulation aux moyennes latitudes

La cellule de Ferrel (Fig. 2) assure la circulation de l'air entre les cellules de hautes pressions subtropicales et les dépressions subpolaires. Vers 50°S, les masses d'air tropicales s'écoulant vers le sud s'élèvent en pente douce au-dessus des masses d'air polaires, plus froides et denses

s’écoulant vers le nord, créant ainsi un mouvement d’air dirigé vers l’Est sous l’influence de la rotation de la Terre, à l'origine des vents appelés Westerlies (Fig. 2). Ces vents rencontrent peu de résistances à la surface de l'océan et peuvent alors être très violents (ex: 40° rugissants). Les Westerlies contribuent à la dynamique de l'AACC et jouent un rôle important en transportant chaleur et humidité à l’Océan Austral.

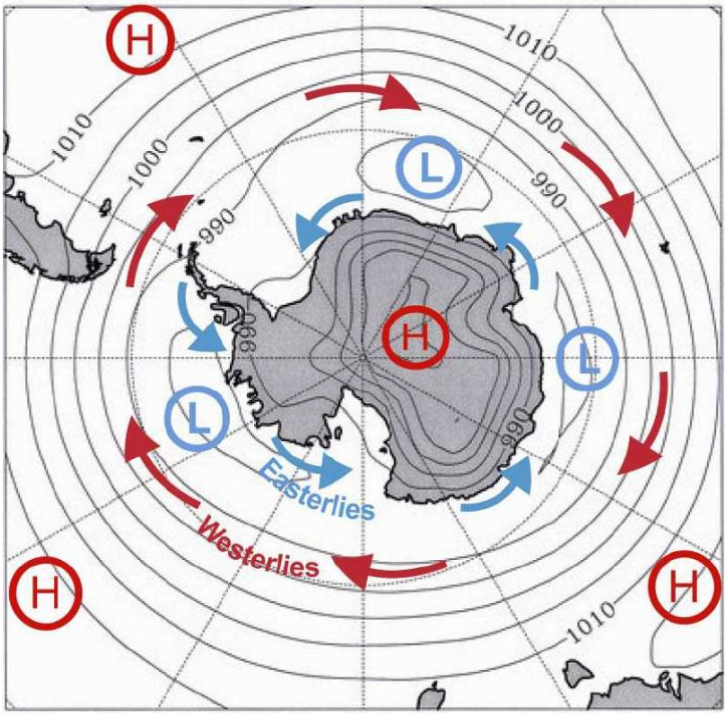

Figure 3. Position des hautes (H) et basses pressions (L) au sud de 30° S dans l’Hémisphère Sud, ainsi que la position des Westerlies et des Easterlies (d’après Tchernia, 1978 ; Fond de carte : modifié d’après Simmonds, 2003).

2.1.3 Circulation aux hautes latitudes

Des dépressions subpolaires sont localisées autour du continent Antarctique vers 60-65°S (Fig. 3), et forment la zone dépressionnaire circumpolaire Antarctique (Antarctic Circumpolar Trough, CPT). Ainsi, au niveau de la cellule polaire, les mouvements atmosphériques ascendants s’écoulent vers le pole (Fig. 2) et résultent ultimement en un mouvement d'air en surface orienté vers l'Ouest longeant les côtes antarctiques (Polar easterlies). Ces vents sont froids et très secs, mais généralement de faible intensité. L’air ascendant à 60-65°S se refroidit en se déplaçant vers le sud, entrainant sa descente jusqu’au pôle (Fig. 2) et formant

ainsi une zone de haute pression centrée sur le continent Antarctique (Fig. 3). Cette zone, appelée 'vortex polaire', est caractérisée par un cyclone permanent et particulièrement puissant dans l'Hémisphère Sud, dû à la forme circulaire du continent.

En surface, le continent Antarctique est exposé à des vents gravitaires parmi les plus violents et persistants jamais enregistrés à la surface du globe, appelés vents catabatiques (Adolphs and Wendler, 1995; Parish and Bromwich, 2007). La position géographique de l'Antarctique (faible insolation), de même que les caractéristiques physiques de la couche de glace qui la recouvre (ex: albédo), sont à l'origine d'un bilan radiatif de surface négatif. Les vents catabatiques trouvent leur origine dans le refroidissement intense de la couche atmosphérique de surface sur le continent, provoquant l'écoulement de l'air froid le long des pentes topographiques de l'Antarctique et, ainsi, des vents remarquables perpendiculaires à la côte antarctique (Fig. 4). Ces vents catabatiques s'écoulent de manière quasi perpendiculaire à la côte (Fig. 4), et sont d'autant plus forts que la pente (ex: présence de vallée glaciaires proche de la côte) et le refroidissement sont importants. Persistants plusieurs mois par an, les vents catabatiques sont cependant plus intenses en hiver en raison du resserrement des ceintures barométriques dû à une augmentation des écarts de température entre les pôles et l'équateur. Leur vitesse moyenne annuelle augmente des régions centrales (10 à 20 km/h) jusqu'aux côtes (30 à 90 km/h), où des rafales peuvent atteindre des vitesses record (360 km/h). Les vents catabatiques peuvent impacter l'océan en surface jusqu'à 120 km au large (Adolphs and Wendler, 1995). Ces vents sont impliqués dans la circulation océanique de surface et sub-surface, ainsi que dans la répartition spatiale et la formation du couvert de banquise, qui en retour impacte la circulation atmosphérique à petite et à grande échelle. Ainsi au niveau des marges continentales, l'océan, l'atmosphère et la cryosphère forment des compartiments climatiques étroitement interconnectés.

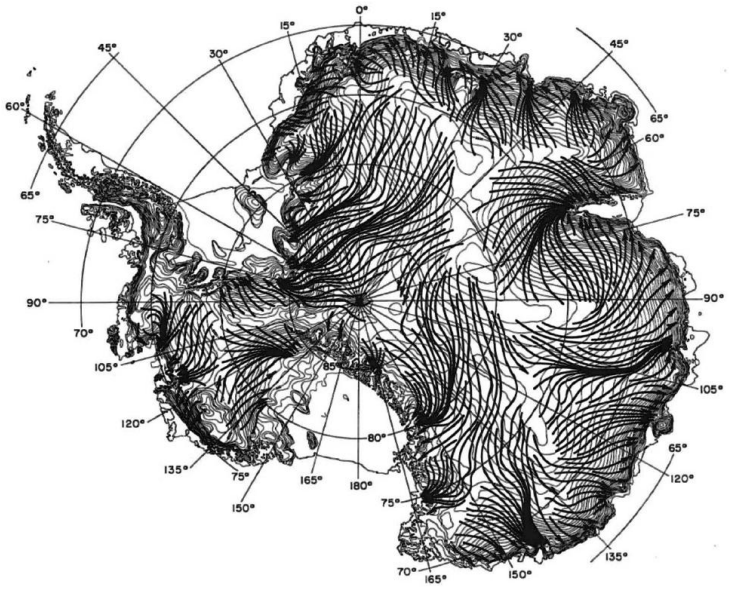

Figure 4. Position hivernale moyenne des lignes de vent au-dessus du continent antarctique (d'après Parish and Bromwhich, 2007).

2.2 Circulation océanique grande échelle

2.2.1 Circulation zonale

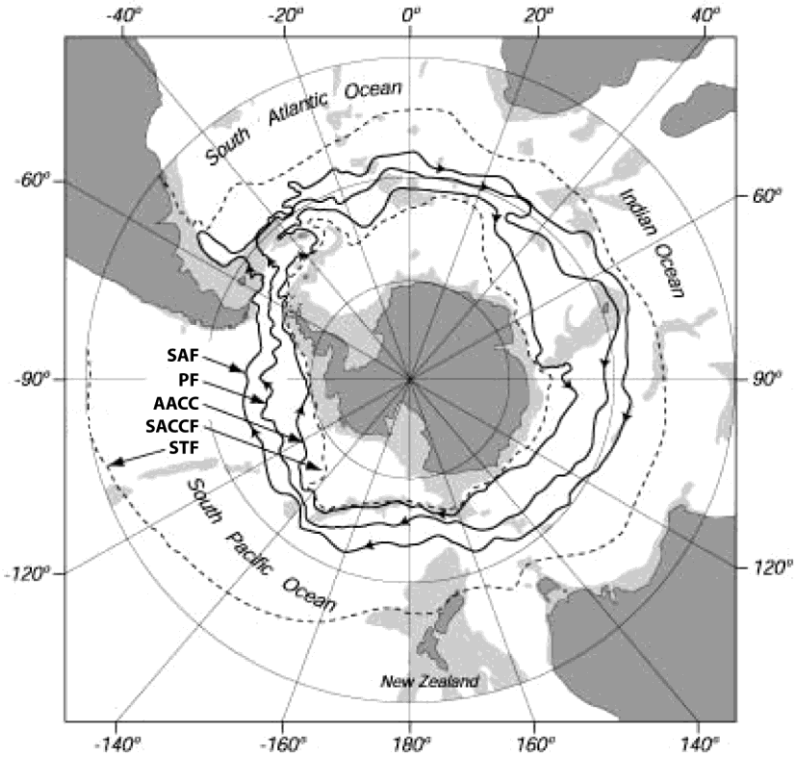

Figure 5. Position des principaux fronts atmosphériques et océaniques dans l'Océan Austral, au Sud de 30° (d'après Orsi et al., 1995). Fond de carte : Subtropical Front (STF),Subantarctic Front (SAF), Polar Front (PF), Antarctic Circumpolar Current (AACC) et le Southern Antarctic Circumpolar Front (SACCF).

L'Océan Austral est composé de plusieurs fronts circumpolaires, correspondant à des changements hydrologiques, relatifs à la présence de différentes masses d'eau (Orsi et al., 1995). Le Subtropical Front (STF; Fig. 5) marque la limite de l'Océan Austral et le sépare des eaux chaudes et salées subtropicales. Plus au Sud, le Subantarctic Front (SAF; Fig. 5) correspond à un minimum de salinité des eaux intermédiaires antarctiques au Nord du front, et marque la limite Nord de la Polar Front Zone (PFZ). La PFZ est bornée au Sud par le Polar Front (PF; Fig. 6),lieu de plongée des eaux de surface antarctiques se déplaçant vers le nord sous les eaux subantarctiques. Dans l'océan Austral, la circulation est dominée par un transport circumpolaire (zonal), l'Antarctic Circumpolar Current (ici AACC) (Fig. 5), qui est délimité au Nord par le SAF, et au Sud par la présence d'un front profond et persistant appelé le Southern Antarctic Circumpolar Front (SACCF; Fig. 5) (Orsi et al., 1995). L'AACC est un courant océanique froid (2 à 14 °C) le plus puissant au monde, et a été reporté pour la première fois par James Cook en 1775. L'AACC, qui s'écoule vers l'Est sous le régime quasi-permanent des Westerlies, connecte les grands bassins océaniques de l'Atlantique Sud, du Pacifique Sud et de l'Océan Indien (Fig. 6).

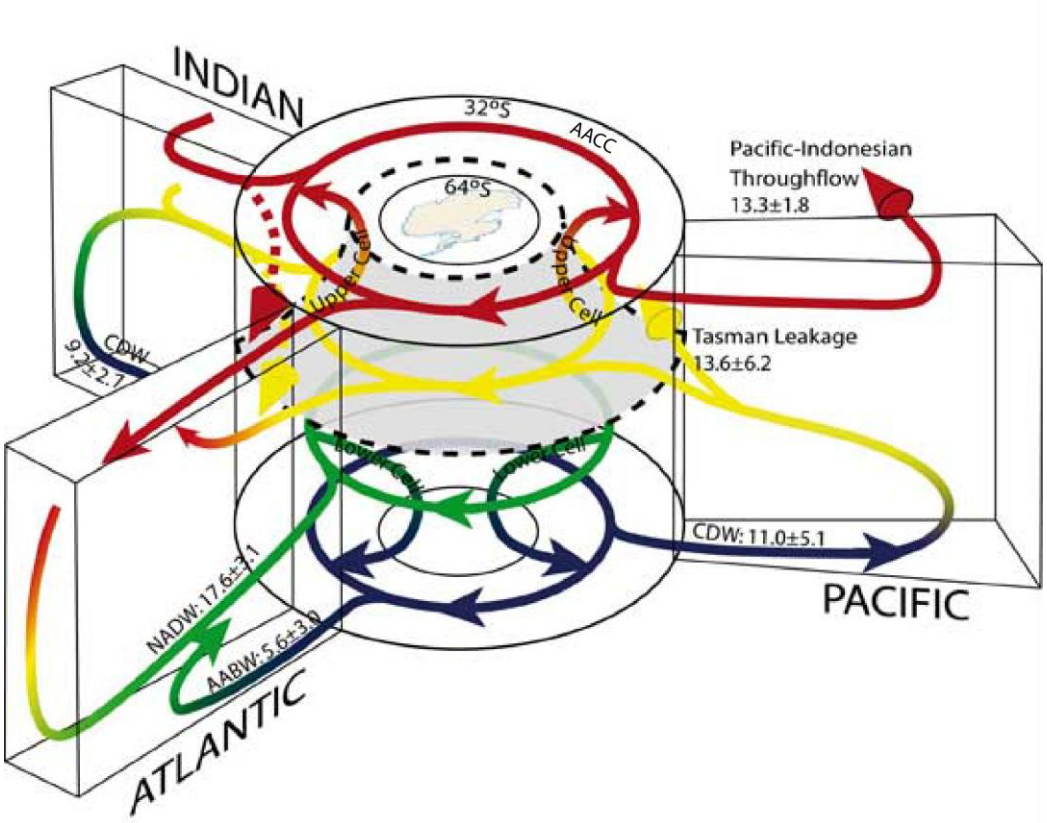

Figure 6. La circulation océanique schématique zonale et méridionale de l'Hémisphère Sud, et ses connexions avec les grands bassins Atlantique, Pacifique et Indien. Antarctic Bottom Water (AABW), Circumpolar Deep Water (CDW), Antarctic Circumpolar Current (AACC) (d'après Lumpkin et Speer, 2007).

La Circumpolar Deep Water (CDW) est la masse d'eau la plus volumineuse transportée par l'AACC (Dinniman et al., 2012). Elle est caractérisée par une température et une salinité relativement élevées. La CDW est issue du mélange des eaux de fond de l'Océan Mondial (Antarctic Bottom Water, North Atlantic Deep Water, eaux denses des bassins Indien et Pacifique), et des eaux intermédiaires Antarctique (AAIW; *cf.* circulation méridionale) (Orsi et al., 1995). La CDW remonte au Sud du PF au niveau de la Antarctic Divergence, zone de cisaillement entre l'AACC et l'Antarctic Coastal Current (ici ACC; Fig. 7) qui circule à l'opposé, d'Est en Ouest le long des cotes antarctiques, entraîné par les Easterlies près du continent Antarctique. Le trajet de l'ACC suit la ligne de côte, dépendant ainsi des structures telles que les baies, langues de glace, etc. Le transport de l'ACC est plus faible (~30 Sv; Bindoff et al., 2000) que celui de l'AACC.

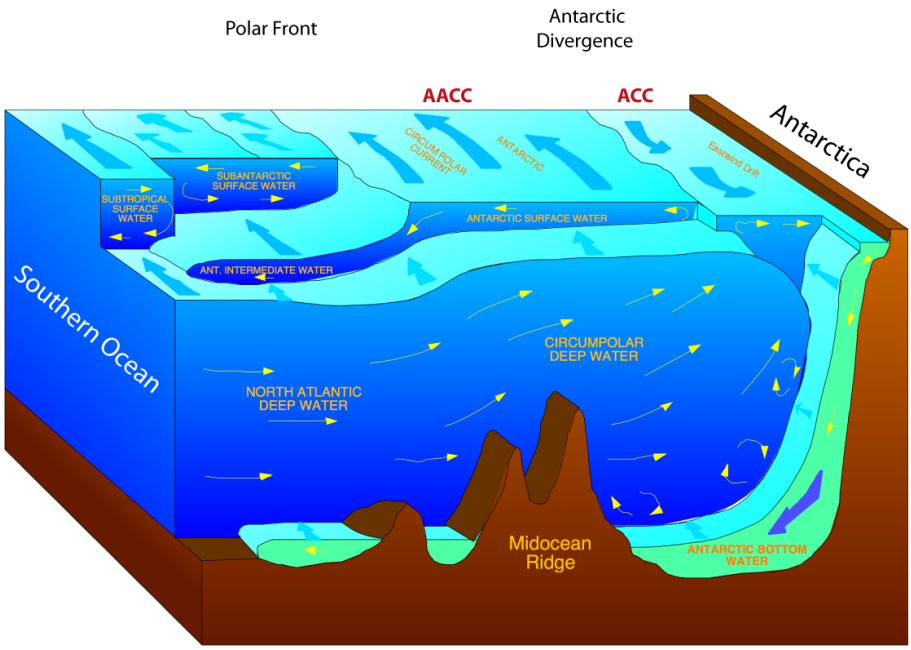

Figure 7. Schéma de la circulation océanique et des différentes masses d'eau de l'Océan Austral, Antarctic Circumpolar Current (AACC) et Antarctic Coastal Current (ACC), modifié d'après Wikipedia (http://en.wikipedia.org/wiki/North_Atlantic_Deep_Water).

2.2.2 Circulation méridionale

La circulation méridionale dans l'Océan Austral est largement contrôlée par les interactions atmosphère/océan et notamment par les vents de surface. En effet, les transports d'Ekman associés à ces vents créent des zones de divergence (Fig. 7) et de convergence, forçant la remontée (upwelling) et plongée (downwelling) des masses d'eaux (Speer et al., 2000), respectivement. Ainsi, au niveau de l'Antarctic Divergence, entre les Easterlies au Sud (et la présence de l'ACC) et les Westerlies plus au Nord (et la présence de l'AACC), l'effet de la pompe d'Ekman provoque la remontée en sub-surface de la CDW (Orsi et al., 1995) (Fig. 7). Une partie de cette masse d'eau s'écoule vers le Nord sous la forme d'Antarctic Surface Water (AASW), couche de surface des eaux estivales du plateau, jusqu'au Front Polaire où elle participe à la formation de l'AAIW, par subduction sous les Eaux de Surface Subantarctiques plus chaudes et moins denses (Fig. 7). L'AAIW qui s'écoule jusqu'à 1000-1500 m de profondeur, est caractérisée par un minimum en salinité associé à un maximum en oxygène. L'autre partie de la CDW transite le long du talus continental et fait saisonnièrement

résurgences sur le plateau, apportant des eaux « chaudes » et riches en nutriment, participant ainsi à la fonte saisonnière de la banquise et à la croissance du phytoplancton. En hiver, la prise en glace et le refroidissement augmentent drastiquement la densité des eaux de surface, qui plongent et s'écoulent vers le Nord le long du plateau et du talus continental jusqu'aux plaines abyssales sous la forme d'Antarctic Bottom Water (AABW). L'AABW est une composante majeure de la circulation thermohaline globale (THC), permettant la ventilation de fond des trois bassins océaniques du globe (Atlantique, Pacifique, Indien) et la redistribution globale de chaleur, de nutriments et de salinité (Orsi et al., 1995 ; Gordon et al., 2001). L'étude de la dynamique de l'AABW constitue donc un enjeu climatique, puisque la variabilité de la production d'eau dense peut avoir des répercussions importantes à l'échelle globale (Jacobs et al., 2004; Jonhson et al., 2008).

2.3 Banquise

2.3.1 Caractéristiques

Il existe plusieurs types de glace de mer, suivant l'âge de la glace, son épaisseur etc. Pour notre problématique, nous nous focaliserons sur deux types principaux de banquise. Premièrement, la « Fast Ice », qui se forme en milieu côtier, est attachée au continent (rivage, glacier, etc.) ou plateau continental dans des zones de faibles profondeurs. Ce type de glace, dont l'épaisseur varie de plusieurs dizaines de centimètres à plusieurs mètres, est généralement pluriannuel et localisé en un anneau autour du continent Antarctique quand présente. A l'inverse, le « Pack Ice », généralement saisonnier, représente tous les types de glace de mer autres que le « Fast Ice » et s'étend largement au nord dans l'Océan Austral. Sa compaction et son épaisseur dépendent de l'influence des températures atmosphériques et océaniques ainsi que de l'intensité et de la direction des vents et des courants océaniques. La zone couverte par le Pack Ice s'appelle la Seasonal Sea Ice Zone (SSIZ). La limite Nord de la couverture de banquise est dictée par l'interaction entre advection/prise en glace au Sud et fonte au Nord. La frange de banquise non-consolidée, constituant sur 100-200 km la limite entre la glace de mer et l'océan ouvert, se nomme la Marginal Ice Zone (MIZ). De la côte jusqu'à la MIZ, les caractéristiques de la banquise ne sont donc pas homogènes, et présentent parfois de manière persistante et/ou récurrente des polynies, zones d'eau libre de glace de taille variable (*cf.* paragraphe polynies).

2.3.2 Dynamique/cycle saisonnier

Contrairement à la banquise arctique, la glace de mer en Antarctique est en grande partie saisonnière et fond à l'été, à l'exception de quelques régions comme la mer de Weddell ou la mer d'Amundsen. Le continent Antarctique est entouré d'un couvert de banquise dont l'étendue varie saisonnièrement de ~3.10^6 km^3 en Février-Mars à ~20.10^6 km^3 en Septembre-Octobre, où sa limite atteint ~55°S dans les secteurs Atlantique et Ouest Indien et ~60°S dans les secteurs Est Indien et Pacifique(Fig. 8) (ACCE report, 2009).

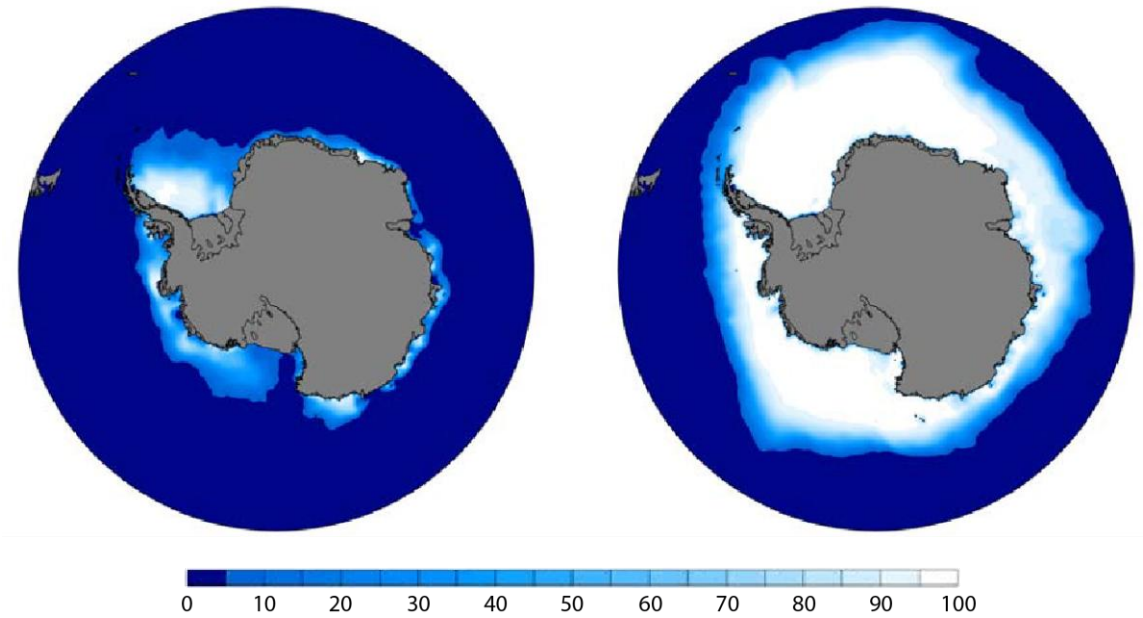

Figure 8. Etendue de la glace de mer en Antarctique, moyennée sur la période 1979-2007 durant l'été austral (gauche) et l'hiver austral (droite); NSIDC (http://nsidc.org/cgibin/bist/bist.pl?config=seaice_index).

La dynamique du couvert de banquise est contrôlée par plusieurs facteurs environnementaux tels que le cycle saisonnier d'insolation, les températures de surface atmosphérique et océanique, le régime des vents et les courants océaniques. En fin d'été, l'eau de surface se refroidit au contact de l'air jusqu'à atteindre le point de congélation de l'eau de mer, soit environ -1.8°C en surface. Les premiers cristaux de glace formés, appelés "frazil", flottent en surface et finissent par constituer une couche visqueuse appelée "pancake". Durant la congélation de l'eau de mer, le sel est massivement rejeté à travers le drainage de saumures, et contribue à augmenter la densité de la couche en surface, qui engendre alors la formation d'eau dense sur le plateau. Plus le taux de formation de glace est élevé, plus le flux de sel est

important et donc plus la quantité d'eau dense formée est importante. C'est particulièrement le cas de certaines structures au sein de la banquise, appelées polynies (*cf.* paragraphe polynie), où la production de glace et l'advection au large sont constantes. Au printemps, l'augmentation de l'insolation et des températures atmosphériques a un effet thermique direct sur la concentration de glace et initie la fonte printanière de la banquise. Les vents, et la houle résultante, ont un impact mécanique sur le couvert de glace, et peuvent contribuer à l'ouverture de celui ci par fracturation, facilitant la fonte de la glace de mer.

2.3.3 Rôle de la banquise dans le système climatique

La banquise antarctique a une influence majeure sur le climat régional et global. Outre l'impact sur la circulation thermohaline à travers la formation d'eau dense qui alimente l'AABW contribuant ainsi à l'oxygénation de l'océan profond, la formation et la fonte de la banquise affectent également la "Pompe Biologique", définie par l'ensemble de processus impliquant le piégeage et le stockage du gaz carbonique et des nutriments inorganiques dissous, par les organismes marins durant la photosynthèse (Fig. 9), ainsi que leur transport jusqu'au fonds marins, par sédimentation. Ainsi, la production primaire (PP) est étroitement liée à la dynamique de la banquise. En effet, le couvert de glace agit sur l'interface océan/atmosphère, et donc impacte la durée de la saison de croissance, la stabilité de la colonne d'eau, la disponibilité en nutriments et métaux (Arrigo et al., 2008). Malgré une saison de croissance courte, la stabilité de la colonne d'eau induite par la fonte de la banquise et les fortes teneurs en nutriments soutiennent une forte PP sur les marges continentales antarctiques (Arrigo et al., 1998). De plus, la présence de la banquise antarctique affectent significativement les échanges de chaleur entre l'océan et l'atmosphère (jusqu'à dix fois moins d'échange en présence de glace; Rutgers van der Loeff et al., 2014) , et modifie l'albédo à la surface de l'océan (Fig. 9). De nombreuses études s'accordent sur le fait que la banquise contrôle les changements de CO_2, notamment entre les cycles Glaciaire/Interglaciaire (Ferrari et al., 2014).

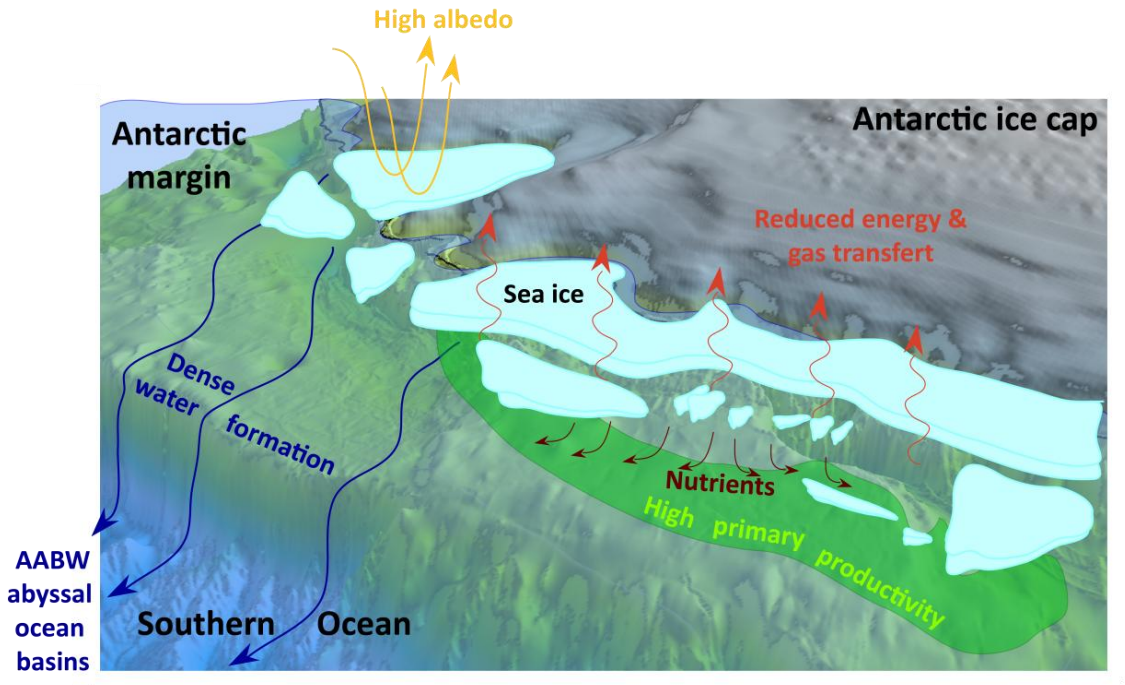

Figure 9. Schéma du rôle de la banquise dans le système climatique. Fond de carte d'après www.deepreef.org.

2.4 Climatologie

2.4.1 Variabilité interannuelle et saisonnière: principaux modes climatiques

La distribution Nord-Sud des cellules atmosphériques, qui forment une succession de ceintures barométriques, dépend de l'intensité des gradients de pression et de température entre les moyennes et les hautes latitudes. La circulation atmosphérique de l'Hémisphère Sud connaît d'importantes variations zonales et méridionales dans l'intensité de ces gradients, dues au couplage océan/atmosphère/banquise qui existe dans l'Océan Austral. Par exemple, le resserrement de ces ceintures barométriques engendre des vents plus intenses et inversement si elles se dilatent. Cette variabilité est représentée par les modes climatiques, dont le principal aux hautes latitudes est le Southern Annular Mode (SAM) aussi appelé Antarctic Oscillation (Thompson and Wallace, 2000). Toutefois, El Niño-Southern Oscillation (ENSO) ou le Southern Oscillation Index (SOI) exercent également un impact important dans l'HS, notamment en Péninsule Antarctique (Turner et al., 2004; Stammerjohn et al., 2008).

a SAM

Le SAM est caractérisé par la différence de pression, calculées sous forme d'indice, entre les moyennes (40°S) et hautes latitudes (65°S). La structure atmosphérique associée à un SAM positif est marquée par une intensification des Westerlies aux moyennes latitudes (Marshall, 2003; Liu et al., 2004), et une diminution des Polar Easterlies autour du continent. Cette compression des ceintures barométriques vers les pôles provoque le renforcement du vortex polaire au-dessus de la région polaire (Fig. 10). Ce processus qui isole l'Antarctique en réduisant les transferts d'air chaud avec les moyennes latitudes, se traduit par un refroidissement du continent (Thompson and Solomon, 2002), à l'exception de la Péninsule Antarctique (PA) qui au contraire se réchauffe, dû au renforcement des Westerlies et ainsi de l'apport d'air océanique relativement doux (Fig. 11b). De plus, alors que les précipitations augmentent en PA, elles diminuent sur le continent Antarctique qui est plus sec. On observe les phénomènes inverses en phase négative du SAM.

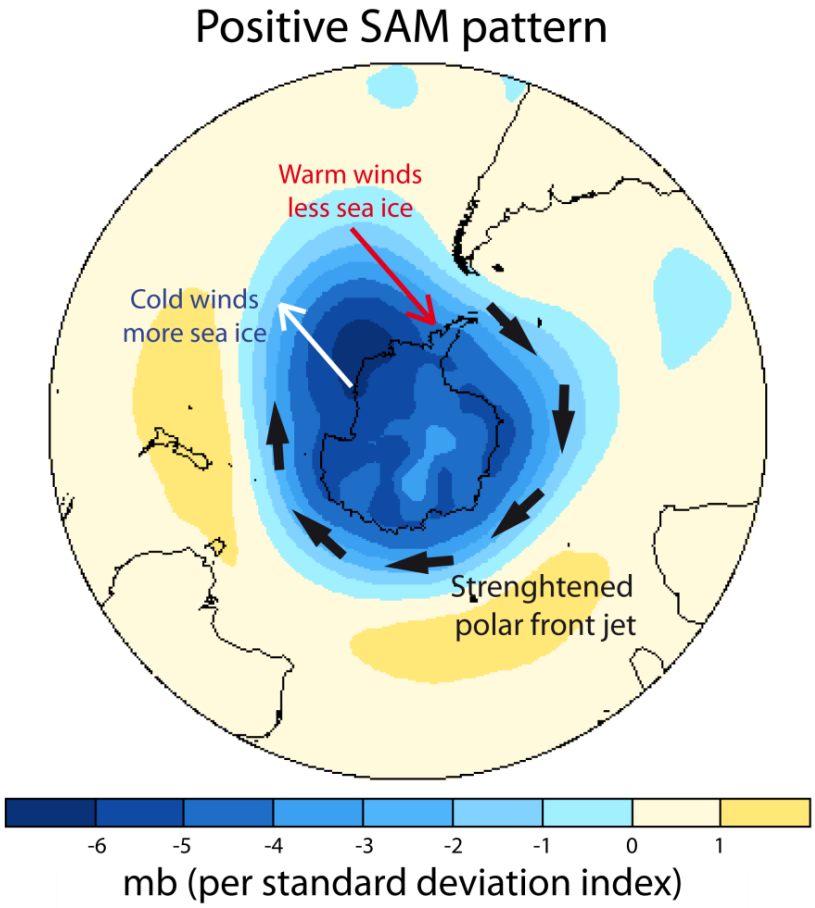

Figure 10. Carte des anomalies de pression et représentation schématique de la structure atmosphérique du SAM est positive (d'après Stammerjohn et al., 2008).

Plusieurs études suggèrent que le SAM a un impact important sur la glace de mer (Hall and Visbeck, 2002; Stammerjohn et al., 2008). En effet, il a été proposé que l'extension de banquise récemment observée dans les mers de Ross et d'Amundsen, ainsi que la diminution de glace enregistrée en PA et en Mer de Wedell seraient associées à des changements de vents et de températures, dûs à une anomalie de basse pression centrée en Mer d'Amundsen-Bellingshausen (Amundsen Sea Low-ASL) durant une phase positive du SAM (Fig. 11a) (Lefebvre et al., 2004; Stammerjohn et al., 2008). De récentes études tendent à montrer que la variabilité du SAM induit également une réponse océanique (et biologique), caractérisée par une intensification de l'AACC et de la pompe d'Ekman en phase positive (Hall and Visbeck, 2002; Marini et al., 2011). Ces variations se traduisent par l'augmentation des conditions d'upwelling à 65°S et de downwelling à 45°S (Hall and Visbeck, 2002; Lefebvre et al., 2004; Marini et al., 2011). Ainsi à proximité du plateau, la remontée de CDW, dont une partie est transportée en direction du continent, relativement plus chaude et riche en nutriment, peut favoriser la fonte de glace de mer ainsi que la PP en milieu côtier (Dinniman et al., 2012).

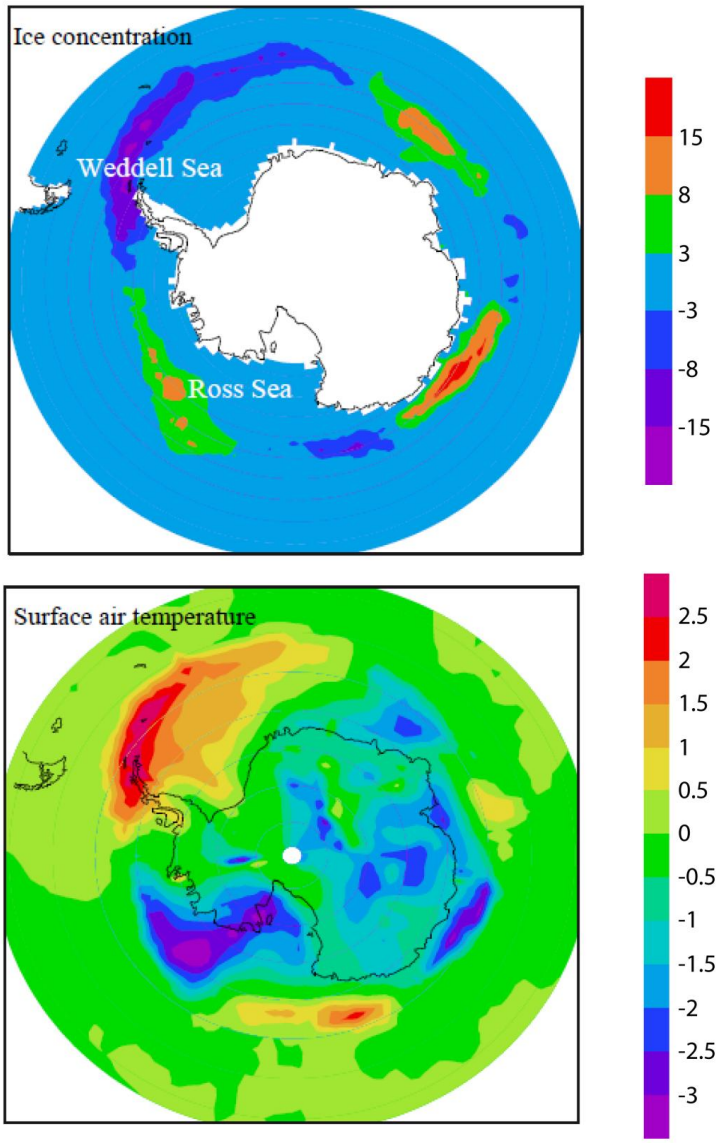

Figure 11. Régression entre l'indice SAM moyenné sur Juillet, Août, et Septembre pour la période 1980-1999 avec a) la concentration de la glace de mer (%), et b) la température de l'air en surface (°C), from http://wattsupwiththat.com/2011/02/05/some-interesting-thoughts-on-antarctic-peninsula-warming/.

Le SAM montre une tendance positive croissante depuis les années 50 (Fig. 12) (Marshall, 2003), attribuée à la diminution de l'ozone stratosphérique et à l'augmentation des gaz à effet de serre ces dernières décennies (Thompson and Solomon, 2002;Arblaster et al., 2006). Cette tendance pluri-décennale, considérée comme le changement majeur actuel aux hautes latitudes Sud, est plus marquée en été qu'en automne et hiver (Marshall, 2003).

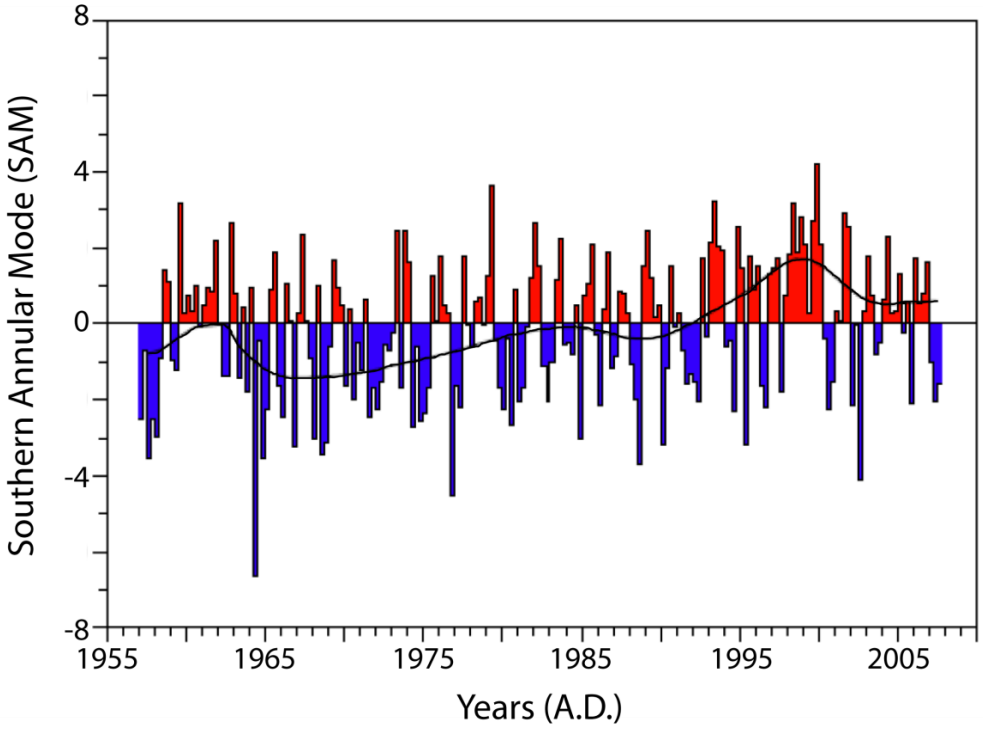

Figure 12. Valeurs saisonnières (histogramme) et moyenne décennale (courbe noire) de l'indice du SAM, mesurées à partir de stations météorologiques (Marshall, 2003).

b ENSO

La bascule interannuelle vers un état la Niña ou El Nino (Fig. 13) a été reliée à un cycle de variation de la pression atmosphérique globale entre l'Est et l'Ouest du Pacifique que l'on nomme Southern Oscillation, donnant le nom au phénomène ENSO (El Niño-Southern Oscillation). ENSO à été décrit pour la première fois par un scientifique britannique Sir Gilbert Walker, au début du XXe siècle. ENSO est une des plus grandes manifestations du système climatique global à l'échelle annuelle ou pluriannuelle, ayant notamment des impacts économiques (ex: exploitation des ressources halieutiques) et sociétaux majeurs (ex: mousson asiatique).

Le Pacifique équatorial contient les réserves d'eaux chaudes les plus importantes de la planète, constituant la *Warm Pool*. Les eaux chaudes en surface sont séparées des eaux plus froides par une thermocline dont la profondeur varie essentiellement en fonction de la taille du réservoir d'eaux chaudes. En surface, les Alizés (ou Trade Winds; Fig. 13) transportent ces eaux chaudes à l'ouest du Pacifique. L'accumulation de ces eaux caractérisées par des températures de surface (SST) élevées provoquent un approfondissement de la thermocline à l'Ouest du Pacifique équatorial. La circulation atmosphérique zonale qui en résulte en altitude,

appelée circulation de Walker, forme une boucle caractérisée par un régime dépressionnaire à l'Ouest, dû à une évaporation excédentaire dans cette région, et anticyclonique à l'Est, reliés en surface par les Alizés qui circulent d'Est en Ouest.

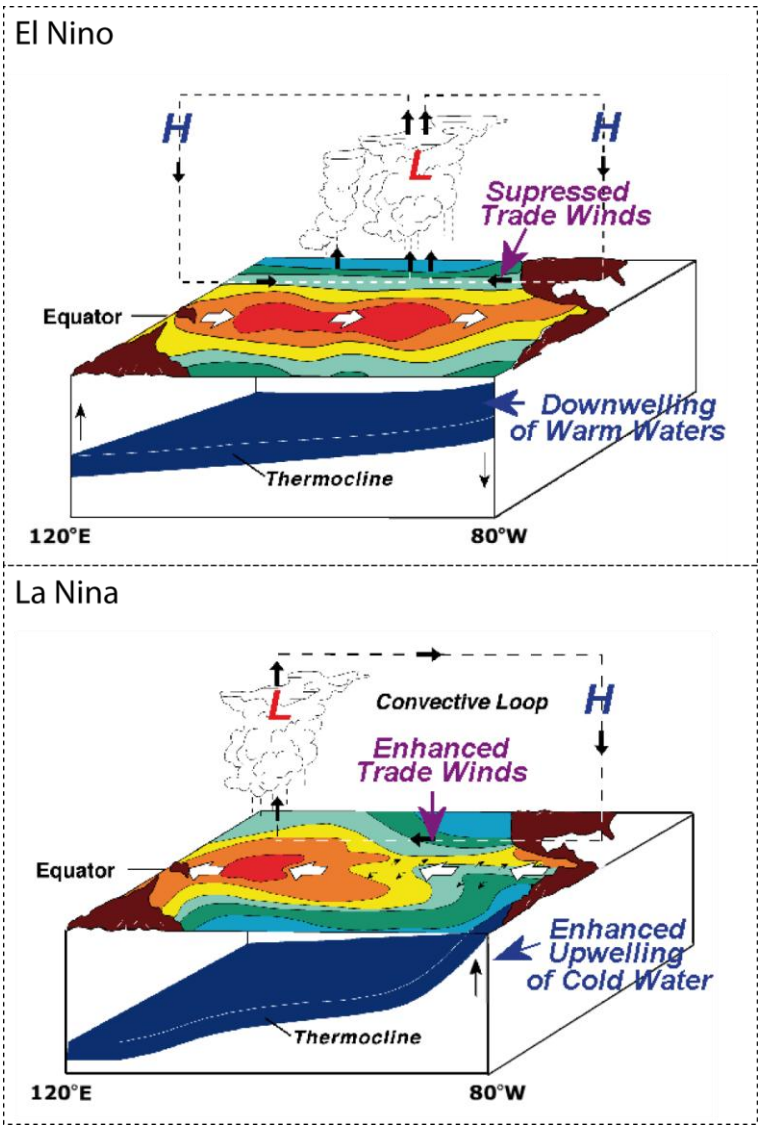

Figure 13. Vue schématique des conditions El Nino/La Nina dans le Pacifique, et des répercutions atmosphériques et océaniques dans la région du Pacifique (http://fr.wikipedia.org/wiki/El_Nino).

Cet état de référence du Pacifique équatorial peut basculer vers un état la Nina ou El Nino, dû à des variations zonales de pression atmosphérique dans le Pacifique, modifiant le trajet et l'intensité des Alizés. Ainsi, la Nina est définie par le renforcement des Alizés et donc de la cellule de Walker, qui contribuent au développement de la *Warm Pool* et à l'approfondissement de la thermocline à l'Ouest, augmentant le gradient de surface Est-Ouest

dans le Pacifique (Fig. 13) A l'inverse dans le Pacifique Est, l'épaisseur de le thermocline diminue (Fig. 13) rendant possible la remontée en surface des eaux froides chargées en nutriments, contribuant à une forte productivité dans cette région. En revanche, un état El Niño est associé à un affaiblissement des Alizés, qui permettent aux eaux chaudes à l'Ouest d'envahir le reste du bassin Pacifique conduisant à une double cellule de convection atmosphérique pour des épisodes de grande ampleur. Ainsi l'état El Niño n'est pas l'exact opposé de la Niña.

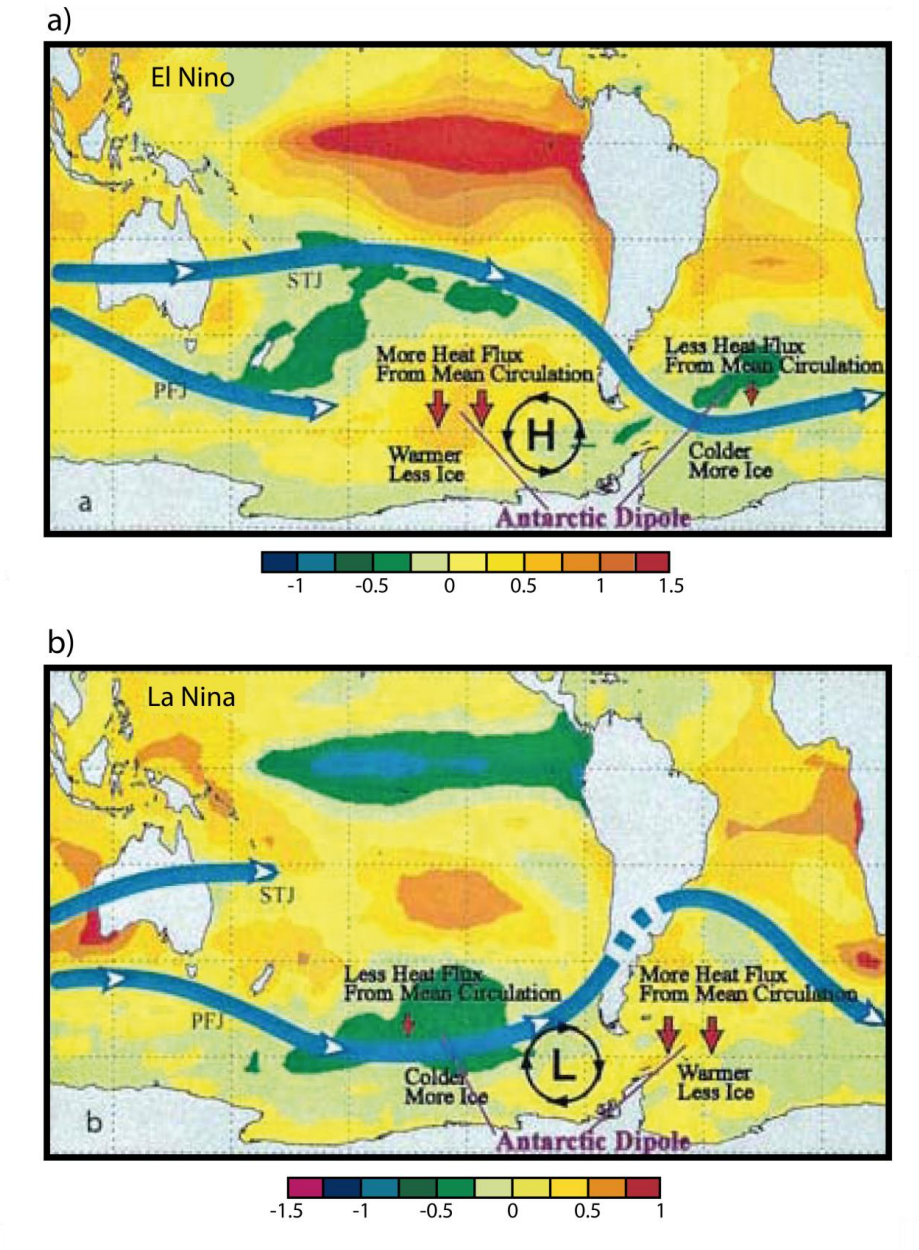

Figure 14. Anomalies de températures de surface (° C) pour les conditions a) El Niño et b) La Niña. Le jet subtropical (STJ), le jet du front polaire (PFJ), les anomalies de haute et de basse pression ainsi que les flux de chaleur ont été schématisés sur ces cartes d'anomalie (d'après Yuan et al., 2004).

Le Southern Oscillation Index (SOI) à été définie par Walker comme étant la différence de pression atmosphérique de surface entre l'Est (Tahiti) et l'Ouest (Darwin) du Pacifique. Utilisé pour représenter les phases et l'amplitude du phénomène ENSO , le SOI est d'autant plus important que le gradient de pression entre l'Est et l'Ouest est fort, c'est à dire que la circulation de Walker est intense (Yan et al., 2011). Ainsi, le Pacifique équatorial, siège d'une circulation atmosphérique et océanique intense, est relié à la circulation climatique générale. En effet, ENSO peut fortement influencer les autres régions du globe à travers les téléconnexions entre les basses et les hautes latitudes (Fig. 14). Ainsi, la réponse climatique

antarctique lors d'un évènement la Niña ressemble à la structure atmosphérique d'un SAM positif très prononcé, toutefois moins zonale. En revanche, l'inverse, un évènement El Nino ressemblant à un SAM négatif n'est pas nécessairement vrai (Stammerjohn et al., 2008). Lors d'un évènement El Niño, l'amplification de la convection atmosphérique au-dessus de la *Warm Pool* alimente également la cellule d'Hadley, qui se trouve renforcée et contractée dans le Pacifique Sud, induisant ainsi une intensification du jet subtropical et un déplacement vers le nord des cyclones extratropicaux (Fig. 14a). Conjointement, une anomalie de hautes pressions centrée en Mer d'Amundsen-Bellingshausen (ABS) permet l'entrée d'air chaud dans la région, ainsi qu'en Mer de Ross et l'export d'air froid à l'Est de l'AP et en Mer de Weddell (Fig. 14a) (Yuan, 2004). Un évènement la Niña génère les effets inverses (Fig. 14b).

2.4.2 Variabilité séculaire à pluri-décennale

Le climat Holocène à l'échelle globale est dominé par l'influence du forçage orbital estival. Dans l'HS, ce dernier a peu augmenté (environ 2 $W.m^2$ à 65°S; Wanner et al., 2011) au cours des derniers 2000 ans (Fig. 15), et n'explique pas la variabilité rapide pluri décennale a pluri centennale ainsi que les disparités régionales importantes qui caractérise le climat à l'Holocène tardif. A l'échelle des derniers 2000 ans qui nous intéresse ici, d'autres processus tels que les variations de l'activité solaire, de l'activité volcanique et de la circulation thermohaline sont donc responsables de la variabilité climatique rapide pluri-décennale et séculaire (Wanner et al., 2011; Bertler et al., 2011).

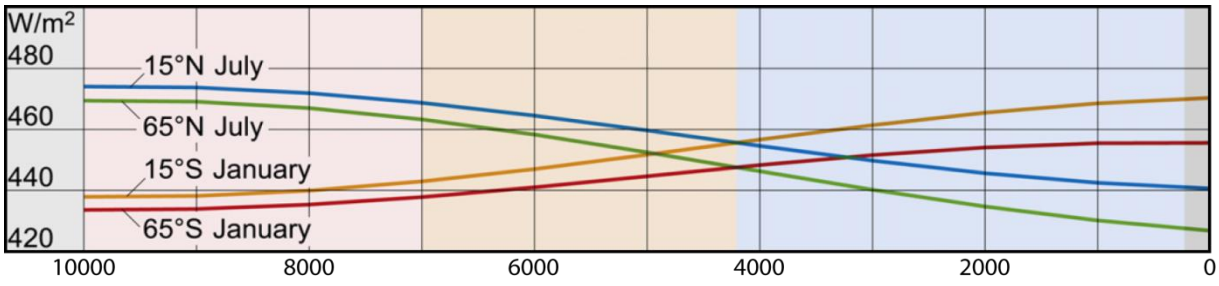

Figure 15. Insolation d'été due aux variations orbitales dans l'HN et dans l'HS (d'après Wanner et al., 2011).

a L'activité solaire

L'activité solaire, modulée par le nombre de taches solaires, semble faire varier l'irradiance solaire d'environ 0,1% (0,24 W/m2) arrivant à la surface de la Terre sur une période de 11 ans, période qui est amplifiée à l'échelle séculaire (Fig. 16). Une période d'activité solaire intense correspond à une augmentation du nombre de taches solaires (Fig. 16), et à un soleil plus lumineux . A l'inverse, le nombre de tache diminue pendant les phases d'activité moins intense. Il a été montré que les taches solaires étaient inexistantes au XVIIe siècle pendant le Minimum de Maunder du Petit Age Glaciaire et ont atteint un maximum en 1959 (Fig. 16) (Steinhilber et al., 2011).

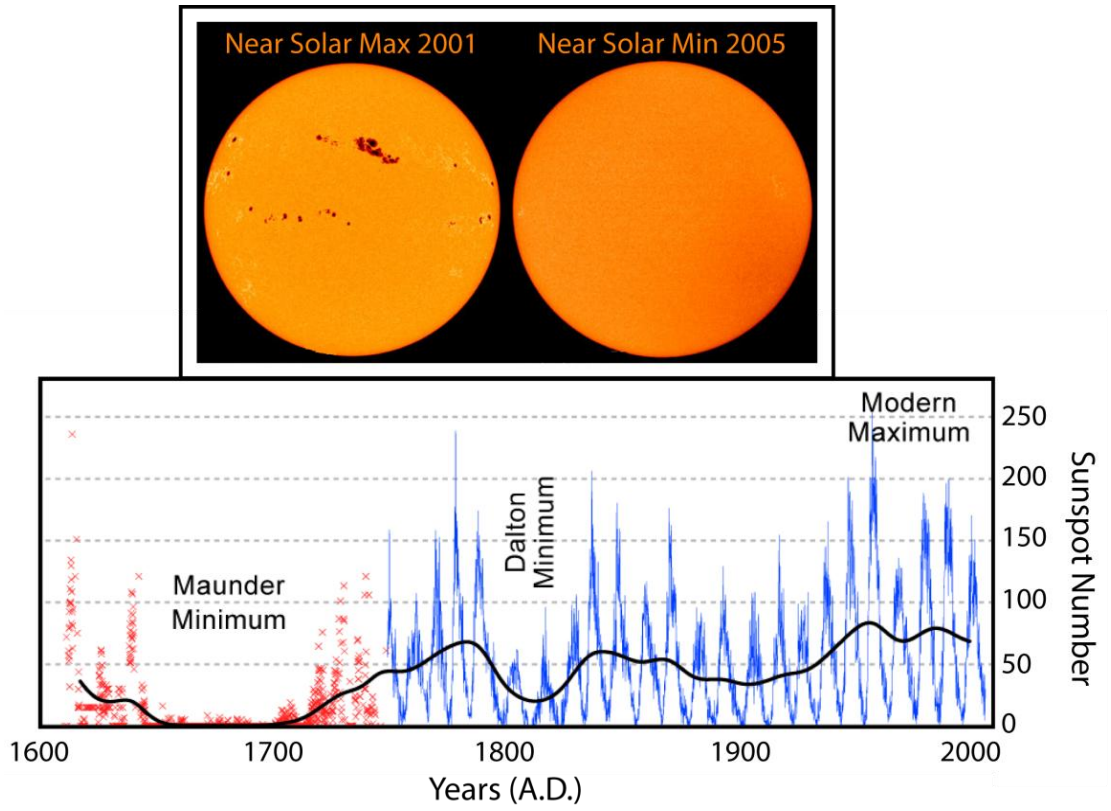

Figure 16. Le cycle solaire. La partie haute montre deux états moyens du soleil au cours d'un cycle solaire, du maximum en Mars 2001 (à gauche) au minimum (à droite) en Janvier 2005. Images tirées de la NASA/ESA. La partie basse montre les variations du nombre de tâches solaires au cours des derniers 400 ans avec, notamment, le Minimum de Maunder (en rouge).

Au cours des derniers 1000 ans, le Soleil a connu plusieurs périodes de faible activité (Fig. 16) (Steinhilber et al., 2009; Ljungqvist et al., 2010) : le minimum de Oort (1010-1050 C.E.), le minimum de Wolf (1280-1340 C.E.), le minimum de Spörer (1420-1530 C.E.), le minimum de Maunder (1645 - 1715 C.E.) et le minimum de Dalton (1790-1820 C.E.). L'irradiance solaire (Fig. 17) montre également des valeur de Be^{10} (isotope produit dans l'atmosphère sous

l'effet des rayons cosmiques liés à l'activité solaire; Beer et al., 2000) plus négatives autour du VIIe siècle, puis de nouveau entre le XIIIe et XIXe siècle, cohérente avec le refroidissement observé au cours des phases climatiques : Dark Age Cold Period (DACP) et Little Ice Age (LIA) (Wanner et al., 2011). Inversement, les anomalies positives de l'irradiance solaire coïncideraient avec les périodes plus chaudes: Roman Warm Period (RWP), Medieval Warm Period (MWP) et plus récemment le réchauffement climatique qui a débuté au début du XXème siècle (Wanner et al., 2011).

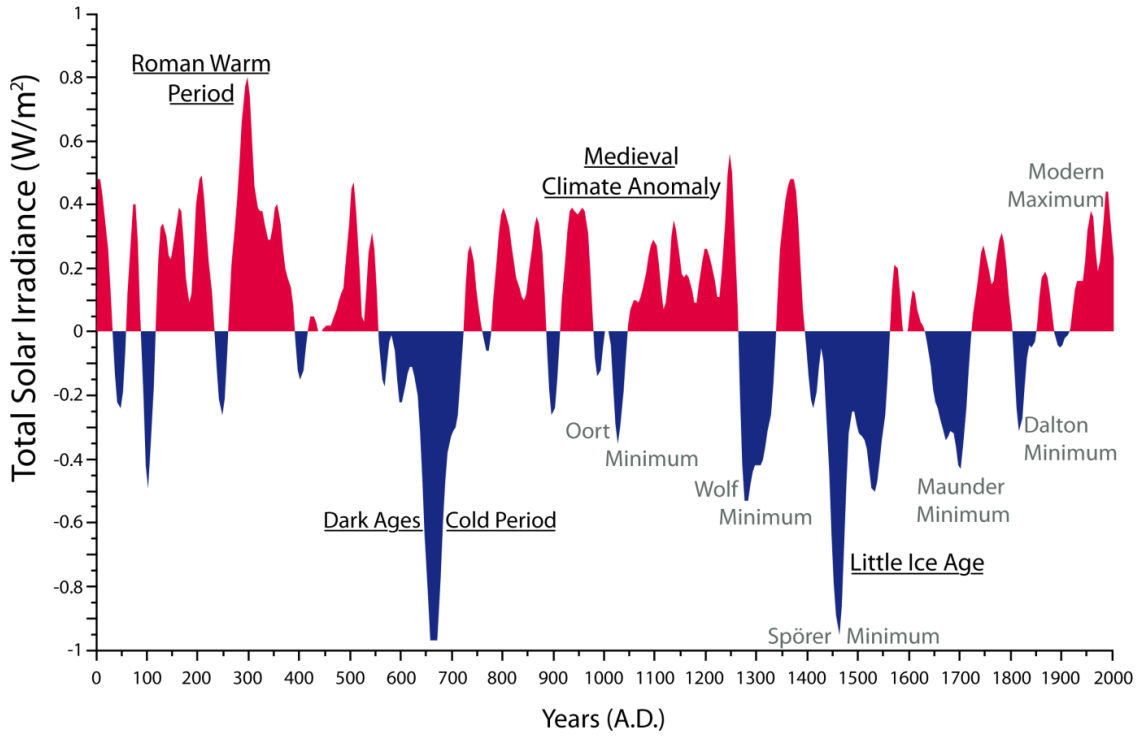

Figure 17. Variation de l'activité solaire reconstruite d'après les enregistrements de10Be mesurés dans la glace polaire (Steinhilber et al., 2009), indiquant les anomalies positive (aires rouges) et négatives (aires bleues), les pics reconnaissables (en gris) de l'activité solaire du dernier millénaire ainsi que les grande phases climatiques connues de l'Hémisphère Nord (surlignées).

b L'activité volcanique

Les éruptions volcaniques constituent un important forçage climatique, à n'importe quelle échelle de temps. Quasiment imprévisibles, on peut cependant avoir une idée des effets du volcanisme sur le climat à travers les archives géologiques et historiques qui montrent que l'activité volcanique a des implications environnementales et sociétales majeures, au cours des derniers millénaires. En effet, les éruptions volcaniques les plus importantes ont été

suivies d'une diminution d'ensoleillement et ainsi d'un refroidissement immédiat à grande échelle, comme par exemple l'éruption du Tambora (Indonésie) en 1815. Le refroidissement à court terme associé au volcanisme est dû à l'injection de dioxyde de soufre (SO_2) et de cendres jusque dans la stratosphère où ils peuvent résider plusieurs années et être redistribués à l'échelle du globe (Robock et al., 2002). Les cendres contribuent à augmenter le couvert nuageux et les précipitations dans l'atmosphère inférieure. Le SO_2, en se mélangeant avec la vapeur d'eau dans la stratosphère, forme un aérosol qui augmente l'albédo planétaire en absorbant et en réfléchissant vers l'espace le rayonnement solaire, provoquant ainsi un réchauffement stratosphérique et un refroidissement des basses couches de l'atmosphère (troposphère) et de la surface de la Terre, principalement pendant l'été lorsque les processus radiatifs dominent (Robock et al., 2002).De plus, à court terme, outre un impact direct sur la température de surface, à travers les variations d'ensoleillement, le volcanisme à également un impact indirect sur la configuration atmosphérique, à travers l'accentuation des gradients latitudinaux de température (Robock et al., 2002). En revanche, à long terme, le dégazage de CO_2 et d' H_2O, principaux gaz à effet de serre, contribuent au réchauffement planétaire. Des mesures précises des effets radiatifs des éruptions volcaniques ne sont disponibles que pour les trois dernières décennies. Cependant, la reconstruction du volcanisme au cours des derniers millénaires est possible grâce à l'enregistrement des aérosols volcaniques préservés, notamment, dans les calottes polaires (Fig. 18). Ainsi, au cours de l'Holocène, il apparaît que la période des 2000 dernières années est marquée par une activité volcanique accrue comprenant 33 éruptions enregistrées et identifiées, dont les deux tiers ont eu lieu au cours du dernier millénaire (Cole-Dai et al., 2000; McGregor et al., 2015). Des études suggérent des liens possibles entre l'apparition des phases climatiques froides au cours des derniers 2000 ans et le nombre d'éruption volcaniques ou leur intensité (ex: Crowley et al., 2000; Bertler et al., 2011). Récemment, des données issues de la modélisation ont également montré qu'une succession d'évènements volcaniques a pu impacter la variabilité naturelle de l'Atlantic Meridional Overturning Circulation (AMOC) au cours du XXe siècle, à travers le refroidissement des eaux de surface et donc la formation de glace aux hautes latitudes (Swingedouw et al., 2013).

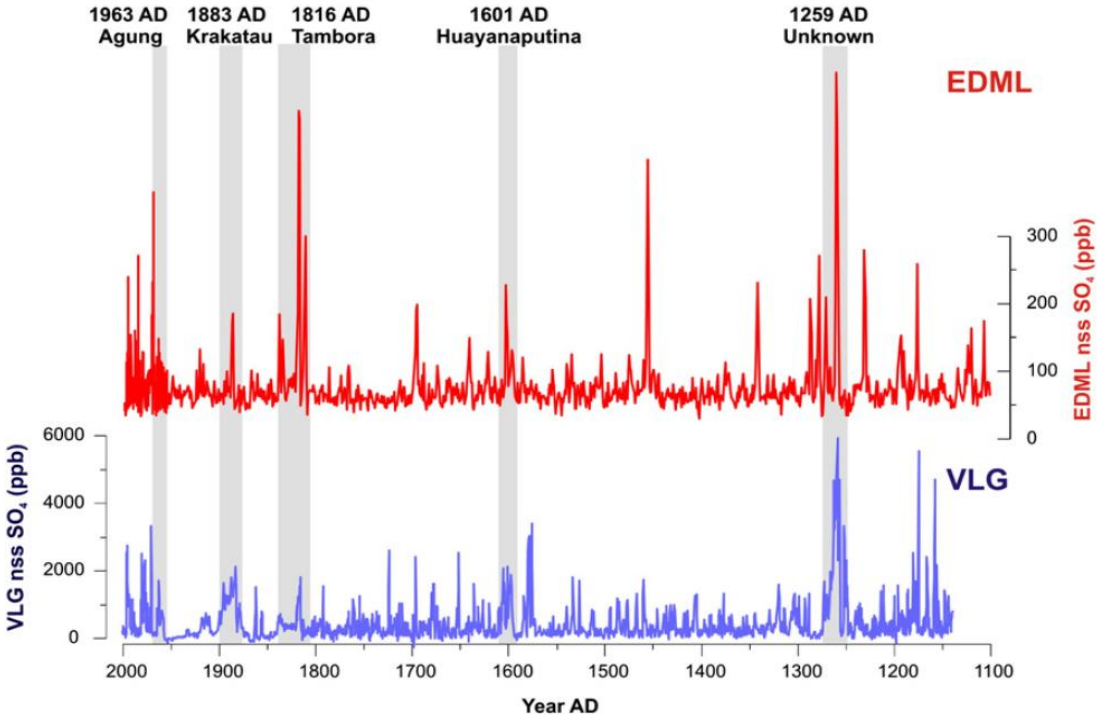

Figure 18. Enregistrements de SO4nns (non seasulphate) à EPICA Dronning Maud Land (EDML) et à Victoria Lower Glacier (VLG) pour les derniers 900 ans, indiquant les éruptions volcaniques sur cette période. Les aires en gris soulignent les éruptions volcaniques identifiées aux deux sites, EDML et VLG. D'après Bertler et al., 2011.

c La circulation thermohaline

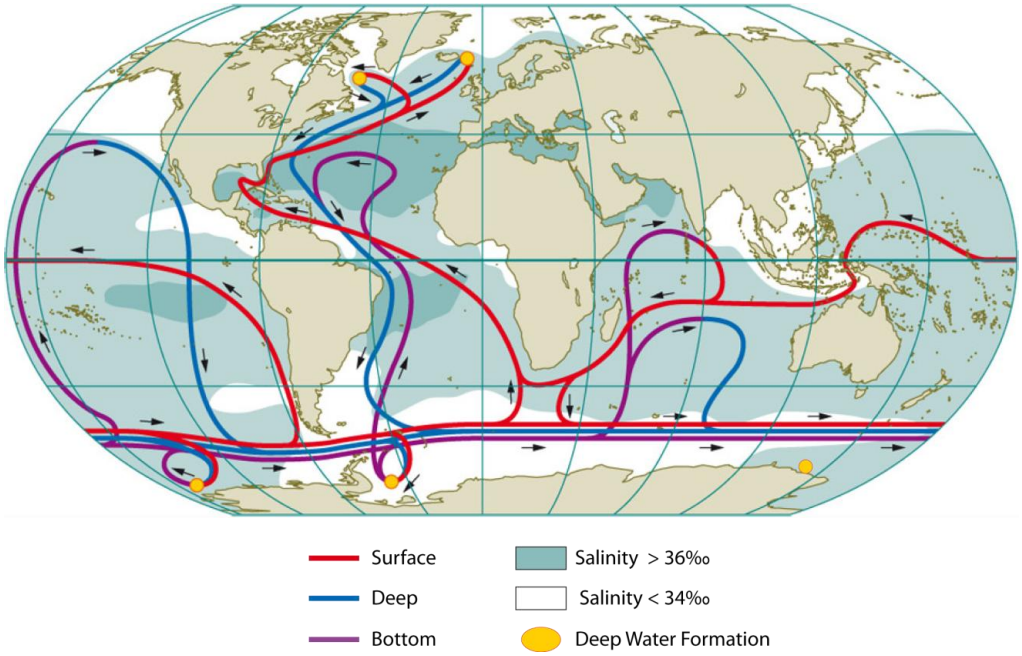

Figure 19. Circulation océanique mondiale montrant les principaux courants de surface et de fond, ainsi que les principaux sites de formation d'eau dense (d'après Rintoul et al., 1998).

La circulation thermohaline, est définie comme la circulation océanique à grande échelle générée par les gradients de température et de salinité des masses d'eau et qui participe au transport de chaleur de l'équateur vers les pôles. Aux tropiques, l'océan en surface est excédentaire en chaleur, alors qu'aux hautes latitudes les eaux atteignent la température de congélation de l'eau de mer (-2°C). Ces eaux de surface très denses (froides et salées), plongent par gravité sous les eaux chaudes moins salées, jusqu'à la profondeur où elles se trouvent en équilibre de densité avec les eaux voisines (vers 2000 m en région subarctique, 4000 m en Antarctique), formant les eaux de fond. Ainsi, les zones polaires constituent des régions de convection profonde (Fig. 19). Ces eaux profondes, moteur de cette circulation globale, entraîne ainsi un transport d'eaux en surface vers les hautes latitudes (Fig. 19). La plongée des eaux de surface qui a lieu principalement en Atlantique Nord, s'écoulent par le fond en vers le Sud, où vers 60° S, elle est reprise et distribuée par le courant circumpolaire Antarctique au sein duquel elles remontent progressivement vers la thermocline, puis et se répandent dans l'Atlantique sud, le Pacifique et l'océan Indien (Fig. 19). Le retour de cette grande circulation dans l'Atlantique nord s'effectue via des courants chauds, proches de la surface, dont la circulation est liée à la circulation atmosphérique. Ce brassage océanique a été schématisé sous la forme d'un «tapis roulant» à l'échelle du globe et peut durer environ 1000 ans environ (Fig. 19). L'intensité de la circulation thermohaline varie fortement entre périodes glaciaires et interglaciaires (Ballarotta et al., 2014). En effet, le développement aux hautes latitudes d'un couvert de banquise plus important pendant une période glaciaire limite la

formation d’eau profonde, dont les sites se décalent vers de plus basses latitudes, réduisant ainsi l'étendue et l'intensité de cette boucle océanique, et donc de la redistribution de chaleur entre les différentes régions du globe. En effet, diverses études suggèrent qu’un arrêt de la circulation thermohaline peut générer un refroidissement de plusieurs degrés, notamment en Atlantique Nord et en Europe. Ainsi, dans son étude, Lund (2006) estime que le débit total du Gulf Stream a diminué de 10% au cours du dernier millénaire, notamment entre 1250-1850 C.E. Cette cohérence avec l'évolution des températures de l'HN au cours du LIA suggère que la réduction du transport de chaleur océanique vers le nord peut avoir contribué à des températures plus basses caractérisant cette période. L’étude de la variabilité de la circulation thermohaline peut donc permettre de mieux appréhender la variabilité du climat.

En conclusion, il apparaît que les changements climatiques au cours de l'Holocène ne soient pas le résultat d'un seul forçage, mais au contraire soient issus de plusieurs mécanismes, eux mêmes interconnectés de façon non-linéaire et à plusieurs échelles de temps.

2.4.3 Disparités régionales en Antarctique

a Période instrumentale

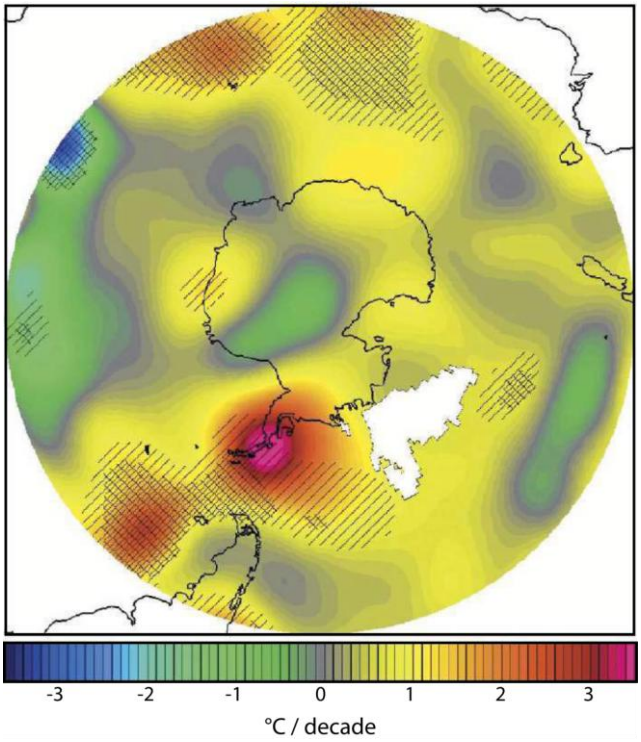

Figure 20. Estimation de la température moyenne annuelle de surface en Antarctique pour la période 1958-2002. Les tendances significatives sont indiquées par des hachures simples (95% de significativité) et double (99% de significativité) (Chapman et Walsh (2007).

Au cours des derniers 50 ans, l'Antarctique montre d'importantes disparités régionales climatiques (Fig. 20). En effet, alors que les tendances générales désignent la PA comme la région du globe la plus vulnérable face aux changements climatiques récents (+0.56°C/décennie à Faraday/Vernadsky station; Turner et al., 2005), le reste du continent montre des changements significatifs de plus faible amplitude (+0.1°/décennie en Antarctique de l'Ouest; Chapman and Walsh, 2007), et même un refroidissement (-0.7°C/décennie à McMurdo Dry Valleys; Doran et al., 2002). Toutefois, les rares stations situées à l'intérieur du continent Antarctique ne présente pas de changement significatif de température (ACCE report, 2009).

Des données historiques de l'étendue du couvert de banquise existent en certaines régions (baleiniers, expéditions etc.) depuis les XIX et XXe siècles, mais sont trop rares et irrégulières pour définir des tendances significatives de l'évolution de la glace mer et de la temperature sur cette période. Au cours des dernières 40 ans, grâce aux satellites, les observations montrent une légère augmentation des conditions de glace globale en Antarctique (0.96 à 1 %/décennie; Cavalieri et al., 2008; ACCE report, 2009). Cette tendance est cohérente avec le refroidissement observé par Kwok et Comiso (2002) en Antarctique durant cette période. Cependant, les tendances du couvert de banquise présentent de fortes disparités régionales

(Fig. 21) (Cavalieri et al., 2008; ACCE report, 2009). Ainsi, le secteur de la Mer de Ross connaît une augmentation du couvert de glace (+4.3 %/décennie), contre-balancée par une diminution importante dans la région d'ABS (-6.8 %/décennie). D'autres secteurs montrent une augmentation du couvert de glace plus modérée: l'Océan Indien (1.9 %/décennie), la Mer de Weddell (0.8 %/décennie) et le Pacifique Ouest (0.7 %/décennie) (ACCE report, 2009). Ces changements récents et notamment ce fort antagonisme, semblent être causés en partie par l'influence du régime des vents et d'une récente réorganisation atmosphérique dans l'HS, ayant pour conséquence un transfert de glace entre les secteurs de Ross et d'ABS, proches géographiquement (Thompson et al., 2002; Marshall 2003; ACCE report, 2009). En effet, l'augmentation de l'indice du SAM, positif depuis les années 80 et particulièrement à l'été-automne, en relation avec une diminution printanière d'ozone stratosphérique, est considérée comme le changement atmosphérique majeur aux hautes latitudes (Thompson et al., 2002; Marshall 2003; ACCE report, 2009). Kwok and Comiso (2002) ont montré qu'il existe un lien entre le SAM et les anomalies climatiques (température atmosphérique et océanique de surface, pression atmosphérique, couvert de glace) dans les secteurs de Ross et d'ABS. Ces résultats sont cohérents avec plusieurs autres études qui suggèrent que la contribution du SAM en Antarctique s'exprime par un refroidissement en surface le long de la côte Est, et un réchauffement en AP (Thompson and Solomon, 2002; Schneider et al., 2006; Thompson et al., 2011).

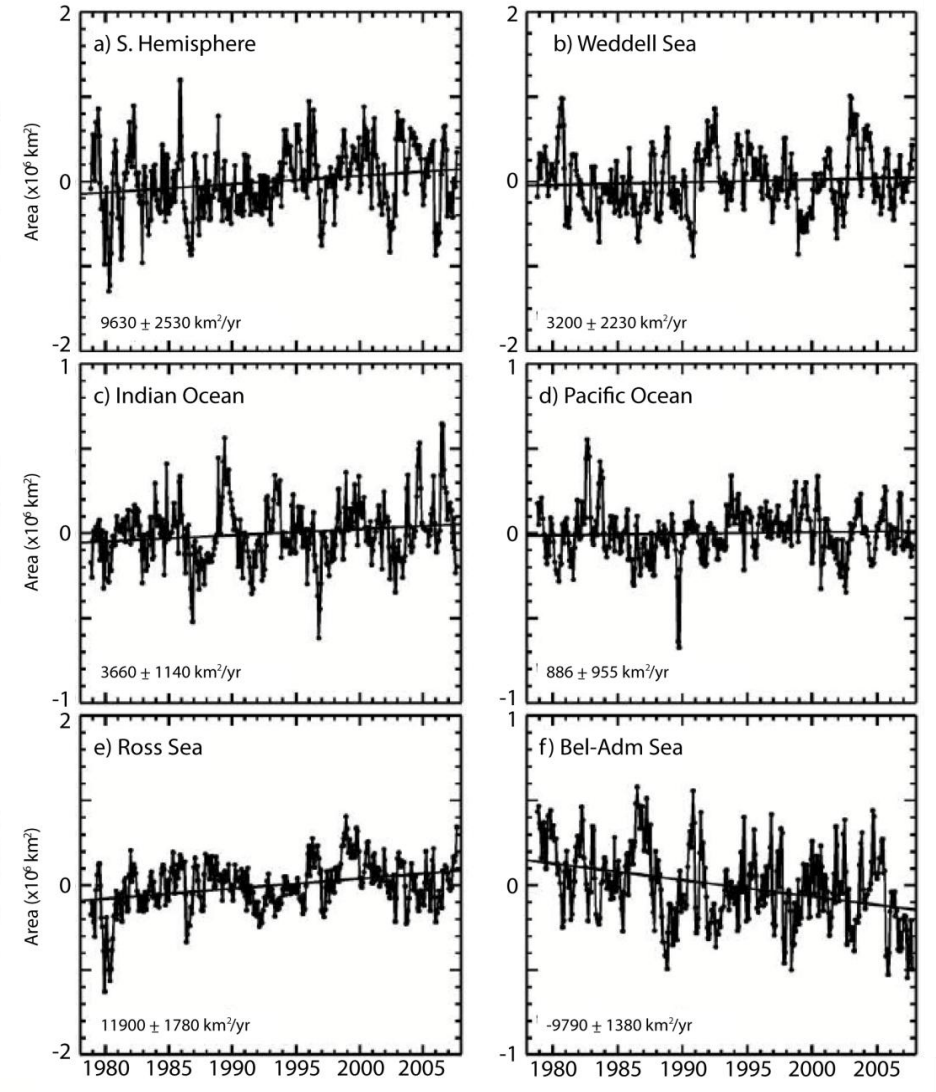

Figure 21. Anomalies mensuelles et tendances du couvert de glace pour (a) l'Hémisphère Sud, (b) la Mer de Weddell, (c) l'Océan Indien, (d) l'Océan Pacifique, (e) la Mer de Ross et (f) etla Mer de Bellingshausen-Amundsen (ACCE report, 2009).

b L'ère moderne

Les observations au cours de la période instrumentale ont permis d'étudier la variabilité climatique haute fréquence en Antarctique ainsi que de mettre en évidence les importantes disparités régionales du continent. Cependant, ces données issues des stations météorologiques sont incomplètes, la majorité des stations étant située le long de la côte et une minorité des mesures remontant au début du XX° siècle. Il apparaît ainsi nécessaire de travailler à partir d'enregistrements climatiques haute résolution allant au-delà de la période instrumentale. Le projet ITASE (International Trans Antarctic Science Expedition) permet ainsi le recoupement de l'ère instrumentale et de la période historique grâce à diverses carottes

de glace haute résolution, dont les données les plus récentes ont été calibrées avec les données instrumentales (Schneider et al., 2006).

Dans l'ensemble, la température de surface à augmenté de 0.2°C en Antarctique au cours des derniers 200 ans (Schneider et al., 2006). A l'échelle régionale, les reconstructions indiquent un réchauffement important depuis le début du XIXe siècle en Mer de Ross, à EDC, TyD, Taldice et SD, et depuis le XXe siècle à EDML (Mayewski et al., 2004; Bertler et al., 2011; Goosse et al., 2012).

Des contrastes régionaux importants apparaissent. En effet, le réchauffement s'accentue jusque sur la période instrumentale (Mayewski et al., 2004) en Antarctique de l'Ouest, en PA ainsi qu'en Mer de Ross (Taldice), peut être causé par l'augmentation de la fréquence d'événements El Nino au XIXe siècle (Mayewski et al., 2004). A l'inverse en Antarctique de l'Est (LD), les enregistrement pointent un refroidissement au cours de cette période (Mayewski et al., 2004), peut être associé à l'augmentation de l'index du SAM (Villalba et al., 2012).

Les mesures de températures issues de forages de glace qui couvrent les derniers siècle, fournissent des informations précieuses, qui cependant comportent des incertitudes à cette échelle de temps, due notamment au manque de données instrumentales pour calibrer ces enregistrements.

c Reconstruction climatique à l'Holocène tardif

L'étude de la variabilité climatique à l'Holocène tardif a pour objectif de déterminer la part de variabilité climatique naturelle et anthropique. L'obtention d'enregistrements récents et bien préservés est nécessaire afin de permettre la reconstruction climatique à haute résolution, et d'appréhender les forçages climatiques ainsi que les mécanismes sous jacents de la variabilité climatique. Les derniers 2,000 ans sont marqués par des changements rapides de température à l'échelle globale, dont les plus prononcés et les plus observés dans l'HN sont la Medieval Warm Period (MWP), le Little Ice Age (LIA) et le réchauffement récent observé depuis le XXe siècle (Mann et al., 2009). Bien que ces périodes soient très bien observés dans l'HN, dans l'HS, la réponse climatique et environnementale aux forçages climatiques (présentés plus haut) est fortement régionalisée aux hautes latitudes, et notamment en Antarctique, rendant ainsi complexe l'étude des changements climatiques.

- *Les grandes phases climatiques*

Les trois premiers siècle après J.C sont caractérisés par des conditions douces en Europe, de même intensité que le réchauffement observé au cours du XXe siècle (Ljungqvist et al., 2010). Cette période est connue sous le nom de Roman Warm Period (RWP), et est suivie par un refroidissement appelé Dark Age Cooling Period (DACP), entre 500 et 900 C.E (Fig. 22). La MWP (correspond à un réchauffement inscrit dans plusieurs régions, notamment dans l'HN, entre 900-1300 C.E. (Fig. 22). Cette période est mise en évidence notamment par des traces archéologiques témoignant de la colonisation Vikings aux hautes latitudes Nord.La MWP est suivie par un refroidissement très prononcé, le LIA, caractérisé par l'avancée des glaciers en Europe, ainsi que par des conditions climatiques plus fraîches dans l'hémisphère Nord entre 1300-1850 ans C.E. (Fig. 22) (Mann et al., 2008, 2009). Comme pour la MWP, les reconstructions montrent un refroidissement variable dans le temps et l'espace, avec des différences régionales très marquées (Mann et al., 1999). Enfin, depuis le XIXe siècle, l'HN connaît un fort réchauffement appelé Current Warm Period (CWP) (Fig. 22) (Ljungqvist et al., 2010).

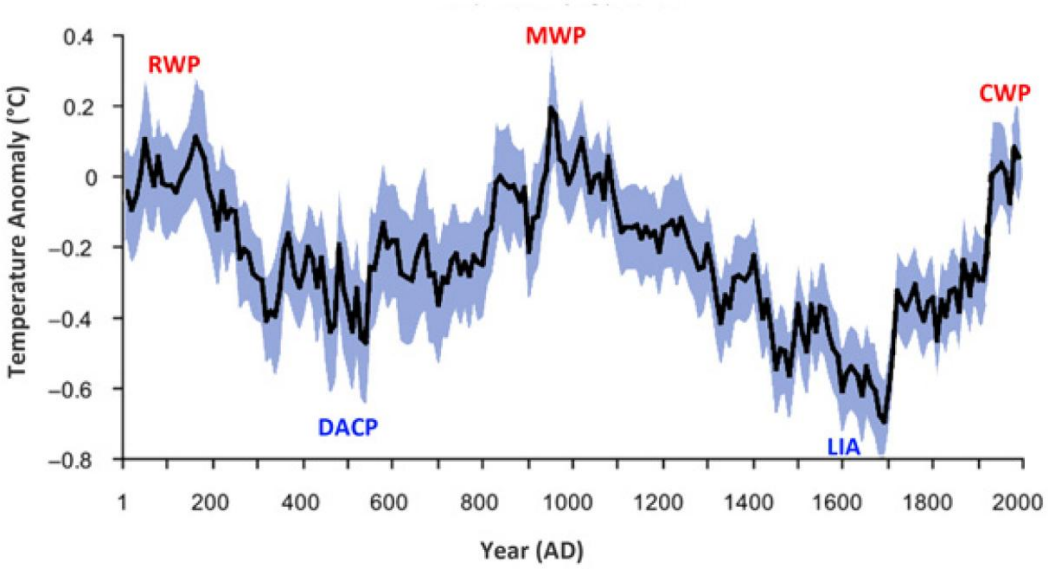

Figure 22. Les grandes phases climatiques de l'Hémisphère Nord basées sur les reconstructions de température (°C) entre 30-90°N (d'après Ljungqvist et al., 2010): Roman Warm Period (RWP), Dark Age Cold Period (DACP), Medieval Warm Period (MWP), Little Ice Age (LIA) et Current Warm Period (CWP).

- *Reconstruction climatique dans l'HS*

Dans l'HS, la compréhension de la variabilité climatique des derniers 2000 ans est encore très limitée en raison d'un manque important d'enregistrements paléoclimatiques aux hautes latitudes dû à l'éloignement, au climat extrême et à la présence quasi annuelle de banquise. En Antarctique, les reconstructions haute résolution de température existent grâce à un nombre important de carottes de glace. Cependant au niveau marin, il existe peu de d'enregistrements paléocéanographiques. Quelques enregistrements à relativement basse résolution existent dans la PFZ (ex: Nielsen et al., 2004) et dans les régions côtières antarctiques (Denis et al., 2010 ; Etourneau et al., 2013).

Globalement les reconstructions dans l'HS suggèrent un refroidissement au des derniers 2000 ans culminant entre 1500 C.E.-1800 C.E. (Fig. 23), suivit par un réchauffement au cours des derniers 200 ans (Mann et al., 2008 ; PAGES, 2013). Cependant, les reconstructions pointent une importante hétérogénéité spatiale et temporelle. Le Sud du continent américain connaît un réchauffement entre 900 et 1350, et est suivit par un refroidissement jusqu'en 1700 environ alors que la Nouvelle-Zélande, région très liée à l' Antarctique (Orsi et Whitworth, 2005), connaît un refroidissement entre le XIII-XIXe siècle environ, dont le paroxysme se situe autour de 1500-1650 C.E. (Lorrey et al., 2008). Ces tendances rappellent certaines grandes phases climatiques connues dans l'HN (Fig. 22). Malgré de nombreuses études, des incertitudes considérables persistent dans la compréhension de la réponse régionale dans l'HS, associée aux changements à grande échelle de la température (Mann et al., 2009), et notamment en Antarctique, où de récentes observations ont montré qu'une partie du continent connaît probablement un réchauffement des plus prononcés à la surface du globe (Turner et al., 2005; Schneider et al., 2006; Steig et al., 2009). Il semble que ces disparités entre l'Est et l'Ouest du continent ont également caractérisé la période tardive de l'Holocène.

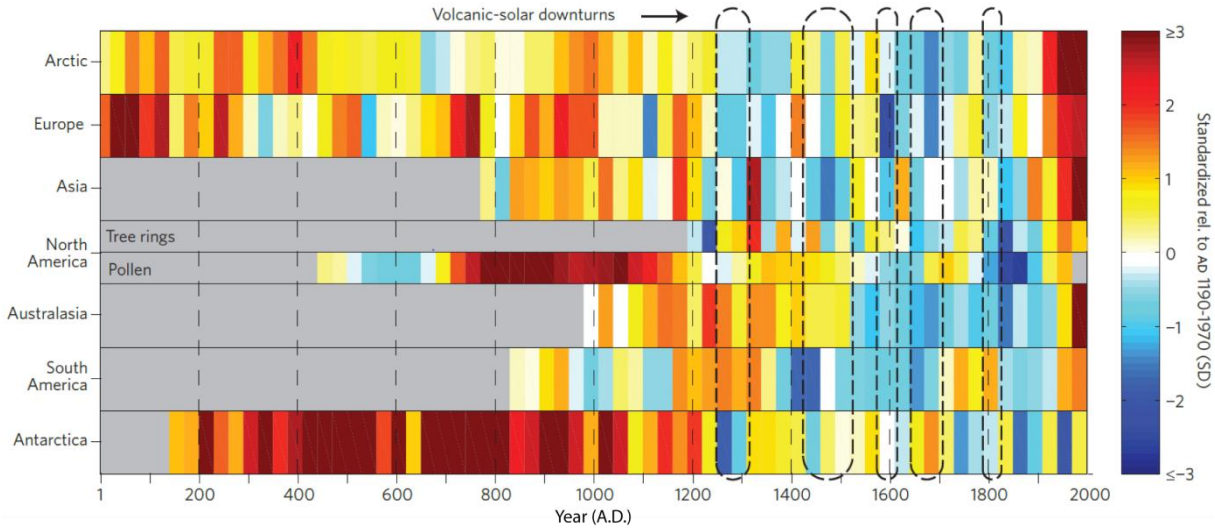

Figure 23. Reconstruction de température moyennée à 30 ans pour les sept régions du Projet PAGES 2k (2013), standardisée sur la période de recouvrement des enregistrements (1190-1970 C.E.).Les lignes en pointillés indiquent les intervalles d'activité volcanique prononcée et de forçage solaire faible à partir de 850 C.E. (d'après PAGES 2k Consortium, 2013).

- *Reconstruction climatique en Antarctique de l'Ouest*

Les enregistrements marins et continentaux indiquent un refroidissement néoglaciaire en Antarctique de l'Ouest (et particulièrement en Péninsule Antarctique-AP) au cours des derniers 3000 ans environ (Barcena et al., 1998; Taylor et al., 2001; Allen et al., 2010; Bentley et al., 2009). Cependant, cet intervalle est ponctué de période plus douces, où quelques enregistrements (marins et continentaux) indiquent un réchauffement similaire à la MWP (dont le commencement n'est pas synchrone selon les sites) qui se prolonge jusque vers le XIII-XIVe siècle (Domack et al., 2003; Mayewski et al., 2004). Les reconstructions dans le cadre du projet West Antarctic Ice Sheet (WAIS) Divide indiquent un refroidissement global au cours entre ~XIV-XIXe siècle en Antarctique de l'Ouest, cohérent avec la période LIA et qui atteint son maximum autour du XVIIe siècle (Orsi et al., 2012). A Siple Dome (SD) le paroxysme de ce refroidissement se situe entre 1350 C.E. et 1450 C.E. (Mayewski et al., 2004). Plus tard, les températures à SD diminuent entre 1700-1850 C.E. (Mayewski et al., 2004), L'AP enregistre également des conditions plus froides entre le XIV et le XVIIIe siècle (Domack et al., 2003; Shevenell et al., 2011).

- *Reconstruction climatique en Antarctique de l'Est*

En Antarctique de l'Est, les enregistrements continentaux (carottes de glace, lacs) montrent une période plus chaude qualifiée d'optimum climatique de l'Holocène tardif qui démarre entre 2000 et 4000 ans BP (selon les sites) et se poursuit jusqu'au premier millénaire après

J.C. (Verleyen et al., 2011). Dans les Wilkes Land, cet optimum climatique est marqué par des conditions plus humides et chaudes sur le continent et des conditions libres de glace à l'été en milieu côtier (Cremer et al., 2003; Verleyen et al., 2011). Plus à l'Ouest (Amery Oasis, Burger Hills, Larsemann Hills) des enregistrements en milieu côtier (terrestres et marins peu profond) témoignent d'un refroidissement néoglaciaire après 2-1 ka BP, suivit de conditions plus douces entre le V-Xe siècle (Cremer et al., 2003; Wagner et al., 2004, Hodgson et al., 2005; Verleyen et al., 2011). Au contraire, la plupart des enregistrements marins qui existent en Antarctique de l'Est montrent à l'inverse un refroidissement néoglaciaire net entre 4000-1000 ans BP (Presti et al., 2003; Denis et al., 2006; 2010). Une forte régionalisation du climat en Antarctique de l'Est peut être à l'origine de ces reconstructions contrastées. Cependant, de nombreux biais liés à l'enregistrement des variations climatiques notamment en milieu continental (enregistrement discontinu, faible résolution, erreurs de datation etc.) peuvent également être en cause. Au cours des derniers 2,000 ans, divers enregistrements (glaciaires et terrestres) dans la région de Ross suggèrent que ce secteur a connu un réchauffement tardif à la fin du premier millénaire, semblable à la MWP, et qui se prolonge jusque vers le XIII-XIVe siècle environ selon les sites, suivit par un refroidissement entre le VIII-XVIIe siècle (Bertler et al., 2011; Verleyen et al., 2011).

Au cours du dernier millénaire, de nombreuses reconstructions s'accordent sur une dégradation des conditions climatiques en Antarctique de l'Est et en Mer de Ross (Bertler et al., 2011; Verleyen et al., 2011). Une fois de plus, ce refroidissement survient de manière non synchrone entre les différents sites à Taldice, EDC, TyD et LD (Fig. 24; Morgan and Ommen, 1997; Stenni et al., 2002; Bertler et al., 2011). Les enregistrements indiquent que la région de Ross (Victoria Land Coast, Talos Dome, Taylor Dome) connait une diminution rapide des SST et des conditions plus venteuses entre les ~XVI/XVIIe-XIXe siècle selon les sites, suggérant un renforcement des vents catabatiques, une augmentation du couvert de banquise et/ou un raccourcissement de la saison de croissance, (Leventer et Dunbar, 1988; Stenni et al., 2002; Bertler et al., 2011). Ce refroidissement est également enregistré en Antarctique de l'Est (enregistrements glaciaires) à la même période (Masson et al., 2000). Cette dégradation des conditions climatiques s'apparente selon certaines études à évènement de type LIA en Antarctique de l'Est (Masson et al., 2000; Stenni et al., 2002; Bertler et al, 2011). Les températures côtières à LD enregistrent un refroidissement entre 1700-1850 C.E. (Mayewski et al., 2004),

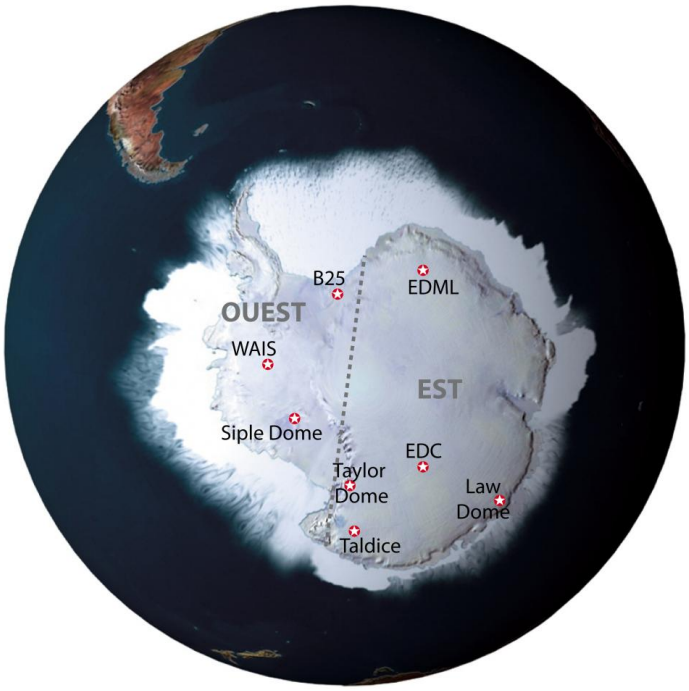

Figure 24. Localisation des principaux sites d'enregistrements glaciaires couvrant l'Holocène tardif en Antarctique.

En conclusion, la plupart des reconstructions de températures en Antarctique à l'Holocène tardif montrent des variations à l'échelle décennale et centennale, sans tendance commune précise. En raison de l'hétérogénéité spatiale et temporelle de l'expression de ces tendances climatiques, l'établissement de phase climatiques telles qu'observées dans l'HN apparait difficile. Cependant, le radoucissement aux alentours de l'an 1000 C.E. observé dans divers enregistrements pourrait constituer un homologue de la MWP (Mayewski et al., 2004; Bertler et al., 2011) (Goosse et al., 2004, Mayewski et al., 2004; Bertler et al., 2011). De même, il apparait que le continent Antarctique ait dans sa globalité connu un refroidissement au cours des derniers 700 ans apparu de manière non synchrone sur le continent, et qui pourrait s'apparenter à un évènement LIA (Masson et al., 2000; Roberts et al., 2001; Verleyen et al., 2011).

Des mécanismes ont été suggéré à l'origine de retards et/ou décalages possibles entre les deux hémisphères. En effet, dans son étude basée sur de la modélisation, Goosse et al. (2004) suggère que l'évolution des températures dans l'HS au cours de la MWP connaît un retard d'environ 150 ans par rapport à l'HN. Ainsi, lors d'un réchauffement dans l'HN, les anomalies positives de température de surface formées dans l'Atlantique Nord sont transportées par la circulation profonde de l'océan (NADW) vers l'Océan Austral. La chaleur est alors libérée aux

hautes latitudes Sud sous l'effet d'upwelling à grande l'échelle autour de l'Antarctique, maintenant ainsi des conditions plus douces avec un décalage par rapport à l'HN dû au temps de transport. Cette hypothèse expliquerait alors que réchauffement homologue à la MWP de l'HN débute un peu plus tardivement en Antarctique (autour et après l'an 1000 C.E.). Toutefois, de nombreuses évidences tendent à montrer que le climat entre les deux hémisphères au cours des derniers 2,000 ans n'a finalement été en phase que sur quelques périodes de temps, correspondant à des extrêmes climatiques (Tavernier et la., 2014; Neukom et al., 2014).

d Conclusion

Les données instrumentales indiquent que l'Océan Austral et le continent Antarctique connaissent d'importantes disparités régionales. Les dernières décennies dans l'HS sont caractérisées par des changements climatiques importants, de précipitations, de température atmosphériques et océanique de surface, ainsi que de vitesse et direction du vent (ACCE report, 2009). Bien que des données issues de modèles indiquent que la réponse environnementale récente en Antarctique s'inscrit dans la variabilité climatique naturelle (Polvani et al., 2013), les reconstructions paléoclimatiques indiquent que ces changements récents sont au contraire en dehors de cette variabilité naturelle climatique à l'échelle des derniers 2000 ans (ex: Mayewski et al., 2004).

Les reconstructions de température et de couvert de glace sur les derniers siècles et à l'Holocène tardif suggèrent que ces disparités régionales ont également caractérisé ces périodes. Les reconstructions de températures pour les derniers 200 ans montrent globalement un réchauffement important en PA et en Antarctique de l'Ouest depuis le XVIII-XXe siècle (ex: Mayewski et al., 2004; Orsi et al., 2012), alors que les tendances, moins claires, en Antarctique de l'Est pointent un refroidissement (Bertler et al., 2011; Goosse et al., 2012). Ainsi, des comportements contrastés ressortent entre l'Est et l'Ouest du continent Antarctique, à l'échelle séculaire mais aussi décennale. Par conséquent, détecter des phases et/ou des transitions climatiques, équivalentes à des évènements globaux tels que la MWP et la LIA, apparaît complexe. A cela s'ajoute le fait qu' il existe peu d'enregistrements paléoclimatiques, de haute résolution de surcroît, disponibles en Antarctique sur cette période (ACCE report, 2009; Verleyen et al., 2011). Ainsi, la plupart des reconstructions climatiques de l'Holocène tardif proviennent des quelques carottes glaciaires. Ces enregistrements de haute résolution

permettent les reconstructions de la variabilité atmosphérique (ex: Mayewski et al., 2004). En revanche, les reconstructions paléocéanographiques, basées sur les enregistrements sédimentaires marins, souffrent d'une résolution et d'une reproductibilité trop faible (Nielsen et al., 2004; Crosta et al., 2007; Denis et al., 2010) rendant peu robuste le dessin de tendances climatique globale, et notamment la compréhension de la dynamique du couvert de glace en Antarctique (Goosse et al., 2012). Particulièrement, en Antarctique de l'Est, les enregistrements sédimentaires marins ne couvraient pas jusqu'à présent le dernier millénaire, une période capitale afin d'appréhender les la part de variabilité climatique naturelle de la part anthropique.

Chapitre II: Matériels et Méthodes

Ce deuxième chapitre dresse dans un premier temps de manière synthétique l'état actuel des connaissances sur les caractéristiques environnementales à l'échelle de notre zone d'étude, la Terre Adélie-Georges V. Plus particulièrement, nous nous intéressons aux compartiments atmosphère/banquise/océan et à leurs interconnections. Ces informations serviront de base à l'élaboration ultérieure d'une vision, la plus complète possible, de la variabilité des conditions environnementales dans notre zone d'étude, capitale pour la compréhension de nos enregistrements récents. Dans un deuxième temps, nous présentons les caractéristiques des différents sites d'étude de cette thèse. Enfin dans un troisième temps nous nous sommes attachés à la présentation des différents outils utilisés dans les chapitres suivant (III, IV & V) pour la reconstruction des conditions environnementales récentes et passées dans la région.

1 La Terre Adélie - Georges V (TAGV)

1.1 Caractéristiques environnementales et enjeux

La Terre Adélie-George V (TAGV) est située à la transition des secteurs Indien et Pacifique de l'Océan Austral, le long de la marge Est antarctique (138°E to 158°E; Fig. 25). La région est localement influencée par des vents violents et des glaciers émissaires (ex: Glacier de l'Astrolabe, Glacier du Mertz). La TAGV est caractérisée par une forte productivité et export ainsi que par la formation d'eau profonde (Arrigo and van Dijken, 2003; Laccara et al., 2014).

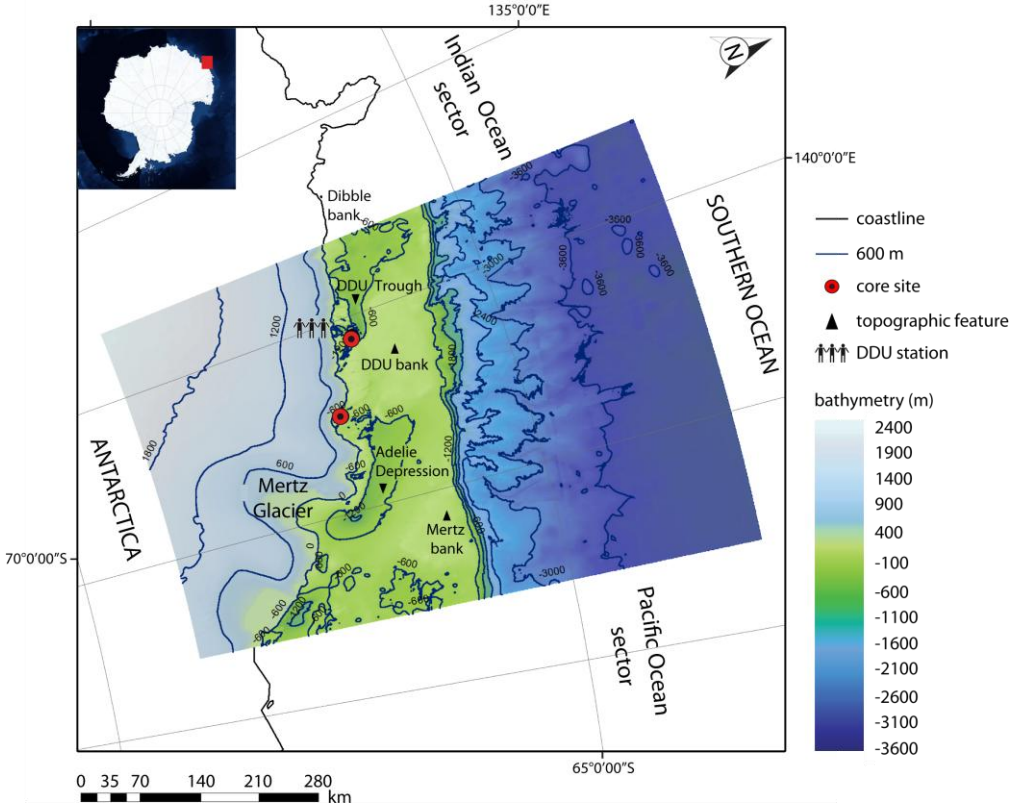

Figure 25. Localisation et carte topographique de la Terre Adélie Georges V (TAGV) en Antarctique, montrant les positions de la station de recherche française Dumont D'Urville (DDU) et des sites de carottages, et incluant les lignes topographiques ainsi que les structures topographiques remarquables, de relief positif (banc du Mertz, banc de DDU, banc de Dibble) et de relief négatif (Dépression Adélie et Dépression de DDU). Données tirées de Beaman (2011).

1.2 L'océanographie du plateau continental

Les conditions océanographiques de la TAGV sont influencées saisonnièrement par l'action conjuguée de plusieurs masses d'eau (Rintoul, 1998 ; Williams et al., 2008). La CDW qui remonte au niveau de la Divergence Antarctique plus au large, se divise en deux branches dont une qui s'écoule vers le Sud en sub-surface. Cette dernière pénètre le plateau de la TA–GV en été (Fig. 26). Plus localement, la répartition spatiale de la CDW semble être gouvernée par la présence de cellules de convection qui créent un 'rideau' le long de la colonne d'eau et limitent ainsi l'intrusion de la CDW ainsi que sa redistribution à différentes profondeurs (Williams et al., 2008; Dinniman et al., 2012). En hiver, les importants rejets de sel qui accompagnent la formation de glace, notamment dans les polynies côtières du plateau, conduisent à la formation et à la plongée d'une eau dense très salée et très oxygénée, la HSSW (High Salinity Shelf Water ; Fig. 26), dont la température se situe au point de congélation. Le taux de formation de HSSW dans le Dumont D'Urville Trough (DDUT) est beaucoup plus faible que dans la Dépression d'Adélie, où la présence d'une polynie récurrente (polynie du Glacier de Mertz ; Fig; 29) en hiver favorise la formation de banquise et le rejet de sel. La HSSW se mélange avec la CDW pour former l'eau dense appelée l'Adélie Land Bottom Water (ALBW ; Fig. 26) (Williams et al., 2008), qui s'écoule sur le fond vers l'Ouest de la marge continental, puis au Nord et s'accumule dans le bassin abyssal australien-antarctique, alimentant l'Antarctic Bottom Water (AABW). L'ALBW est considérée comme la troisième source d'eau de fond antarctique, contribuant environ au quart du réservoir d'AABW (Rintoul, 1998; Jacobs, 2004; Meredith et al., 2013).

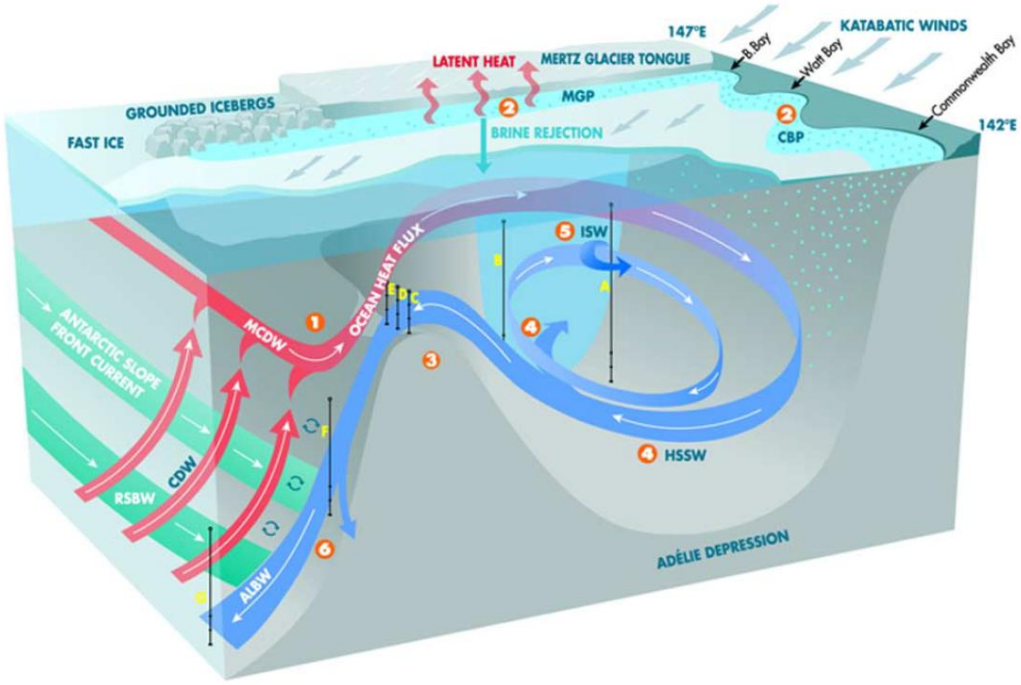

Figure 26. Schéma de la circulation océanique dans la Dépression Adélie et des processus impliqués dans la production d'ALBW, d'après William et al (2008). 1, Modified Circumpolar Deep Water (MCDW); 2, rejet de saumure dans la polynie du Glacier de Mertz (Mertz Glacier polynya-MGP). La MGP s'étend le long de la cote vers l'Ouest jusqu'à Commonwealth Bay et forme la Coastal Bay Polynya (CBP); 3, seuil de la Dépression Adélie ; 4, formation et export d'eau dense (High Salinity Shelf Water-HSSW)à travers la Dépression Adélie; 5, formation de l'Ice Shelf Water (ISW), issue de la fonte de la langue du Mertz;6, plongée de l'ALBW qui vient se mélanger avec la Ross Sea Bottom Water (RSBW), plus salée.

1.3 Les vents catabatiques: "The Home of Blizzard"

La région de la TAGV est exposée à des vents gravitaires les plus violents et persistants jamais enregistrés à la surface du globe, appelés vents catabatiques (Périard and Pettré, 1993), pouvant atteindre en moyenne 25 $m.s^{-1}$ à Cape Denison à Commonwealth Bay (CB) (Wendler et al., 1997). Le caractère exceptionnel de ces vents a été décrit dès les premières explorations de la région. Ainsi, durant l'Expédition Aurora (1911-1914) le long de la TAGV, Douglas Mawson qui bâtit son camp à CB appela cet endroit «The Home of the Blizzard». Dans la région, la présence de vallées glaciaires proche de la côte explique l'intensité de ces vents ainsi que leur direction Sud-Nord (Wendler et al.,1997). De nombreuses études ont montré l'impact des vents catabatiques sur les conditions de surface et l'océanographie de la région (Withworth et al., 2002; Vaillancourt et al., 2003; Massom et al., 2003; Massom et al., 2009). En effet, ces vents jouent un rôle majeur dans l'ouverture de zones libres de glace (Fig. 28)

appelées polynies (Massom et al., 1998 ; Arrigo and van Dijken, 2003), car leur vitesse élevée permet de maintenir un fort export de glace de mer jusqu'à 100 km de la côte (Adolphs and Wendler, 1995). L'air continental très froid provoque à la surface de l'océan la formation de glace et donc le rejet de saumure, ce qui contribue à la formation d'eau dense sur le plateau (Tamura et al., 2008 ; Arrigo and van Dijken, 2003). Ainsi en TAGV, la polynie du Mertz, troisième polynie la plus importante en Antarctique de l'Est, est annuellement récurrente et très dynamique en partie dû à la présence des vents catabatiques particulièrement forts dans la zone (Wendler et al., 1997 ; Arrigo and van Dijken, 2003; Tamura et al., 2008).

1.4 Dynamique du couvert de glace en Terre Adélie George V

1.4.1 Saisonnalité de la banquise

La banquise varie de manière saisonnière en TAGV. Elle se retire jusqu'au trait de côte en été et atteint une extension maximale jusqu'à 62°S en hiver (Fig. 27). Au niveau de DDU, le couvert de banquise est présent au-dessus du site de carottage entre février/mars et novembre/décembre, soit environ 9 mois/an (Arrigo and van Dijken, 2003; Denis et al., 2009). Généralement, la concentration de glace est supérieure à 80% d'Avril à Octobre, et la période libre de glace où la concentration est inférieure à 20%, est plus variable (0-4 mois/an) et survient entre Décembre et Mars (Fig. 27). La dynamique temporelle et l'extension du couvert de banquise sont limitées en TAGV par la proximité de l'ACC (Fig. 30) et l'intensité du couplage vents catabatiques/upwellings, qui accélèrent la destruction printanière et retarde la reformation automnale du couvert de banquise (Orsi et al., 1995 ; Arrigo and van Dijken, 2003).

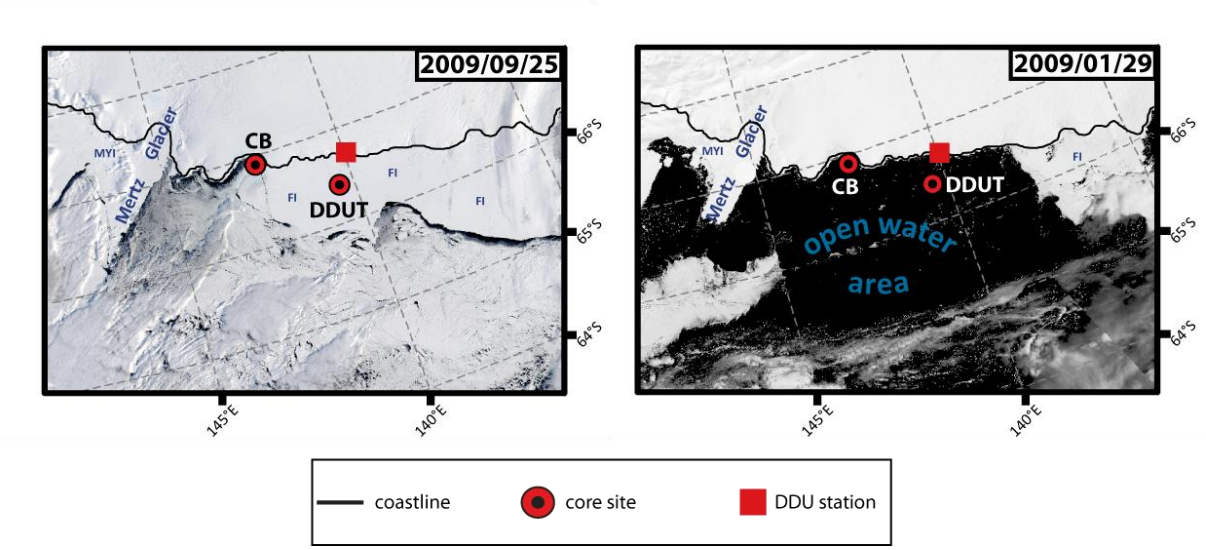

Figure 27. Images satellite MODIS de la TAGV pour la saison hivernale (à gauche) et estivale (à droite), montrant la relation entre les sites de carottage (Commonwealth Bay- CB; Dumont D'Urville Trough-DDUT) et la répartition spatiale des différentes structures géographique de la région (FI=fastice ; MYI=multi yearice ; glacier du Mertz) ainsi que le cycle saisonnier du couvert de banquise. Images disponible sur http://lance2.modaps.eosdis.nasa.gov.

1.4.2 Les polynies: 'sea ice factory'

- *Généralités*

Le terme polynie provient du russe « polynya » signifiant « clairière de glace». En 1970, l'organisation météorologique mondiale a défini les polynies comme étant des surfaces d'eau libre pendant l'hiver dans des régions où la banquise est présente. Ces structures constituent des zones clés pour la circulation thermohaline, par le biais de la formation d'eau dense (Fig. 28). De plus, les polynies sont caractérisées par des fortes biomasses de phytoplancton, et constituent ainsi zones capitales pour tous les niveaux trophiques de la chaine alimentaire (ex : les colonies de manchot Adélie sont co-localisées avec des polynies côtières en Antarctique; Arrigo and van Dijken, 2003).

En Antarctique, 37 polynies ont été identifiées autour du continent entre 1997 et 2002 (Arrigo and van Dijken, 2003). De taille variable (plusieurs dizaines à centaines de km^2), ces structures permettent d'importants échanges de flux d'énergie entre l'océan et l'atmosphère. En effet, au cours de l'hiver le flux de chaleur océanique des polynies vers l'atmosphère est estimé deux fois supérieur à celui du pack ice (Maykut et al.,1978). Ainsi, même les polynies

de taille réduite peuvent avoir un impact conséquent sur les flux de chaleur à l'échelle régionale (Adolphs and Wendler, 1995).

- *Formation des polynies*

Les polynies se forment grâce à la convergence de facteurs atmosphériques et/ou océaniques tels que la force, la direction et la fréquence du vent et des courants, la distribution des masses d'air et d'eau, mais aussi de paramètres géographiques comme la bathymétrie, le trait et le relief de la côte, la présence de langue de glace, etc. (Maqueda et al., 2004). Suivant la persistance/récurrence des mécanismes qui les engendrent, les polynies sont des phénomènes plus ou moins récurrents. On distingue généralement deux types de polynies (Fig. 28).

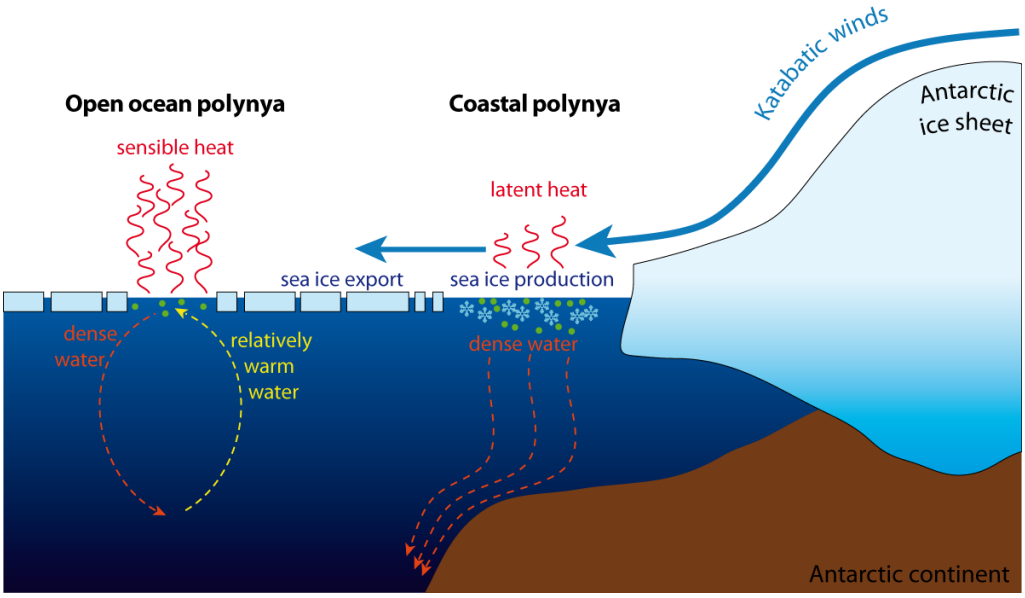

Figure 28. Caractéristiques et formation des polynies en Antarctique.

La polynie à chaleur sensible est liée à un apport de chaleur océanique (Maqueda et al., 2004), le plus souvent par upwelling (Fig. 28). Ces polynies sont généralement étendues etsont caractérisée par une faible production de glace de mer. Du fait de son origine (océanographique), une telle structure apparait souvent dans des régions profonde au large, où la couche de surface froide est séparée des eaux sous-jacentes plus chaudes par une faible pycnocline rendant possible les mouvements de convection verticale (ex: Weddell Sea Polynya ou Maud Rise Polynya; Comiso et al., 2000).

A l'inverse, les polynies à chaleur latente (Fig. 28) sont de taille plus réduite et généralement localisées en milieu côtier. Ces structures sont liées à l'action des vents de surface ou courants océaniques (Zwally et al. 1998 ; Maqueda et al., 2004). Ainsi, dans les zones littorales

l'impact des vents catabatiques permet la formation de glace en surface qui est continuellement formée et exportée plus au large, provoquant ainsi le maintien de conditions d'eau libre près de la cote (Fig. 28). Certaines polynies ont des taux de production de glace très élevés (ex : 390 km^3/an pour la polynie de Ross et 181 km^3/an pour la polynie de Darnley en Antarctique de l'Est; Tamura et al., 2008), et sont de ce fait qualifiées d'usines à glace. L'étendue de ces polynies peut également être liée de la présence de structures géographiques telles qu'une baie ou langue de glace, comme pour la polynie du Glacier de Mertz (Arrigo and van Dijken, 2003).

- *Les polynies en TAGV*

La polynie du Glacier de Mertz (MGP-Mertz Glacier Polynya), située dans la partie orientale de la TAGV entre 142 °E et 146°E (Fig. 29), est le résultat de l'action de vents catabatiques extrêmement violents et persistants dans la région, combinée à la présence de la langue de glace du Glacier de Mertz ou MGT (Mertz Glacier Tongue). En effet, la MGT agit comme une barrière en amont de la polynie aux courants côtiers de glace entrainés le long de la cote par les Easterlies, et permet ainsi l'extension de la polynie vers l'Ouest et le Nord (Frezzotti et al., 1998). L'addition de ces phénomènes confère à la MGP une dynamique importante (production de glace de mer, activité biologique, formation d'eau dense ; Arrigo and van Dijken, 2003 ;Tamura et al., 2008 ; Kusahara et al., 2011).

La MGP a une superficie de presque 6,000 km^2 en hiver (concentration de glace $\leq$ 10%; Arrigo and van Dijken, 2003), soit un facteur de près de quatre fois inférieur à la taille de la polynie de Ross, la plus importante en Antarctique. Toutefois, avec une production de glace annuelle d'environ 120 ± 11km^3, la MGP est la 3ème polynie la plus productive en Antarctique (Tamura et al., 2008). De plus, de récentes études montrent que la production d'eau dense et donc d'ALBW dans cette zone contribue à hauteur de 25% à l'AABW, ce qui en fait la troisième source après la Ross Sea Bottom Water (RSBW) et la Weddell Sea Bottom Water (WSBW) (Rintoul et al., 1998; Jacobs et al., 2004; Meredith et al., 2013). Egalement très productive, l'activité biologique dans la MGP peut se maintenir durant trois mois en hiver ce qui conduit à une productivité primaire (PP) annuelle d'environ 65 $g.C.m^{-2}$, soit globalement trois fois moins qu'en Mer de Ross ou d'Amundsen, deux des zones les plus productives en Antarctique (Arrigo and van Dijken, 2003).

Plus à l'Ouest le long de la cote, la polynie de Dumont D'Urville (DDUP-Dumont d'Urville Polynya) (66.11°S-139.31°E) est plus réduite (Fig. 29), avec une taille d'environ 1,000 km^2 (concentration de glace ≤ 10%; Arrigo and van Dijken, 2003). Contrairement à la MGP, la DDUP s'étend plutôt le long de la cote linéairement sous l'action de vents catabatiques, et peut être modulée saisonnièrement et localement par le développement et l'ancrage de fastice et d'icebergs au dessus des hauts fonds de la zone (Massom et al., 2009). Toutefois, la DDUP est très productive avec une PP annuelle d'environ 55 $g.C.m^{-2}$, mais à la différence de la MGP, l'activité biologique connait généralement deux pics de productivité fin Décembre et début Mars (Arrigo and van Dijken, 2003).

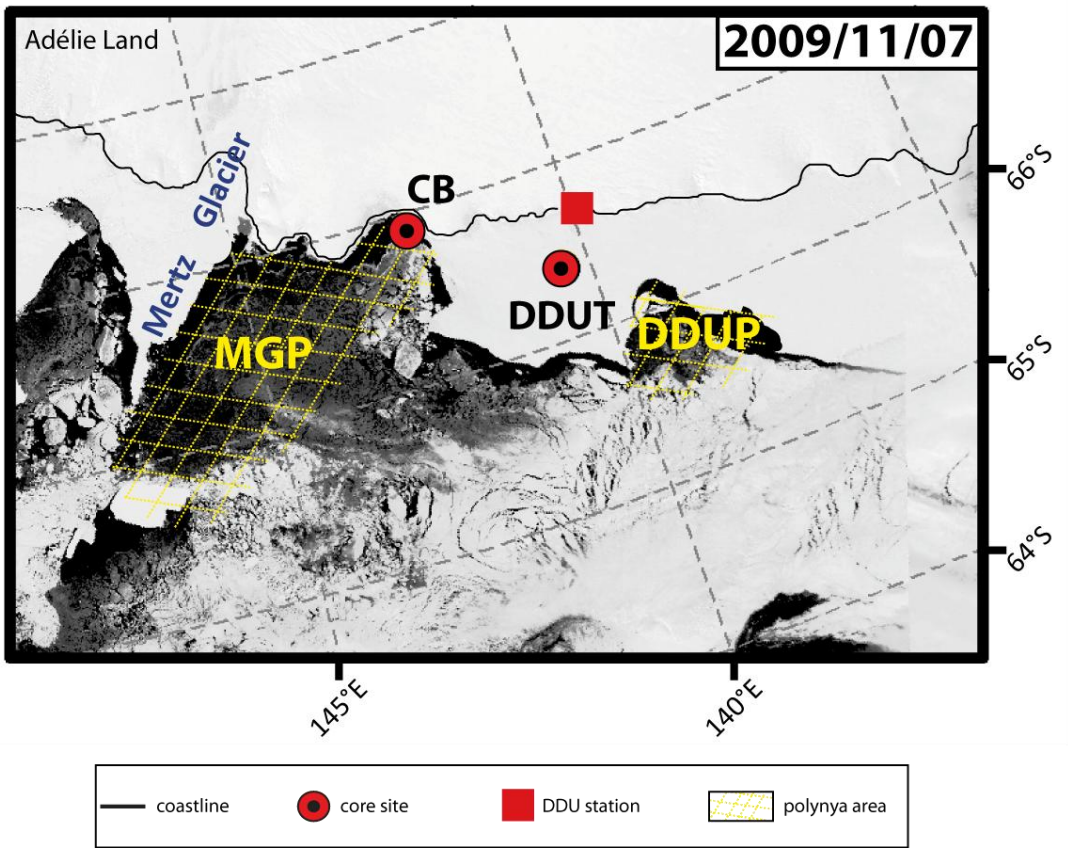

Figure 29. Image satellite MODIS montrant la relation entre les sites de carottage et la répartition spatiale de la polynie de Dumont D'Urville (DDUP) et de la polynie du Glacier de Mertz (MGP) en TAGV.

1.5 Productivité

La production phytoplanctonique est largement dominée par les diatomées en TAGV (plus de 80% du microplancton), dont les blooms sont très intenses au printemps (Wright and van den Enden, 2000 ; Beans et al., 2008). D'autres organismes phytoplanctoniques sont présents dans cette zone, tels que les Haptophytes, les Prasinophytes, les silicoflagellés et les coccolithophoridés.

L'augmentation de la luminosité au printemps engendre la production primaire, favorisée par la stabilité de la colonne d'eau liée à la fonte de la banquise (Leventer, 1992). La région est riche en macro- et micro- nutriments, approvisionnés par la fonte des glaces continentales et de la glace de mer (Vaillancourt et al., 2003), l'intrusion de la CDW (Williams et al., 2008), la mise en re-suspension du sédiment (Fitzwater et al., 2000). Les apports éoliens directs sont considérés comme négligeables dans la zone étude en raison de l'éloignement des sources continentales potentielles (Australie, Afrique etc.). Le déclin de la PP à la fin de la saison de croissance (automne) est dû à une co-limitation de la lumière et des métaux traces tels que le fer (Arrigo and van Dijken, 2003).

Au sein des eaux côtières de la TAGV, la PP et les types d'assemblages phytoplanctoniques associés sont assez variés, en fonction des conditions environnementales (Arrigo and van Dijken, 2003; Beans et al., 2008). De DDU au Glacier de Mertz, l'activité biologique de surface diffère. En effet, dans la région du Merz par rapport à la région de DDU, malgré de faibles taux de nutriments (respectivement), la biomasse phytoplanctonique et les abondances de diatomées (ex: 22,9 cell/L, chla ~0.79 µg/L et 3,3 cell/L, chla ~0.14 µg/L respectivement) sont plus importantes dues à une plus forte stratification à l'Est (Beans et al., 2008). Ceci est confirmé par des assemblages dominés par *Fragilariopsis spp* dans la région du Mertz, alors que la région de DDU connait des populations importantes de *Corethron pennatum* et *Rhizosolenia* spp qui réflètent des conditions de mélanges assez importantes (Beans et al., 2008). Globalement, bien que les eaux de la région soient très froides en TAGV, les abondances et biomasses de diatomées restent conséquentes (Beans et al., 2008). En effet, les eaux cotières antarctiques comptent parmi les régions les plus productives de l'Océan Austral. En TA, il a été récemment montré que la PP annuelle avoisinait les 60 g.C.m-2, alors qu'elle est de 0,156 g.C.m-2 en moyenne dans l'Océan Austral (Arrigo et al., 2008; Arrigo et al., 2003). Ces résultats sont à mettre en perspective avec la présence de deux importantes

polynies en Terre Adélie, la DDUP et la MGP qui maintiennent la production biologique à un niveau élevé durant la saison de croissance (Vaillancourt et al., 2003; Arrigo et al., 2008; Beans et al., 2008).

2 Matériel

Le plateau de la Terre Adélie s'étend sur environ 125 km de largeur depuis le talus jusqu'à la côte, où la profondeur est souvent plus importante. En effet, la région est caractérisée par plusieurs dépressions le long de la côte pouvant dépasser les 1000 m de profondeur (Fig. 30), dues à l'érosion glaciaire (Beaman et al., 2011). Ces dépressions, bordées par des bancs culminants entre 200 et 500 m sous le niveau marin (Fig. 30), sont caractérisées par de faibles courants de fond. Ces structures forment de véritables pièges à sédiment en permettant la concentration de matériel issu des plumes hyperpicnales (écoulements gravitaires) et de la production de surface (Denis, PhD, 2008). Ainsi, la région présente un grand intérêt pour les archives climatiques basées sur les enregistrements sédimentaires marins (Denis, PhD, 2008 ; Gregory, PhD, 2012) avec des zones d'accumulation pouvant atteindre 200 m d'épaisseur pour 12,000 ans (Escutia et al.,2010).

2.1 Sites d'étude

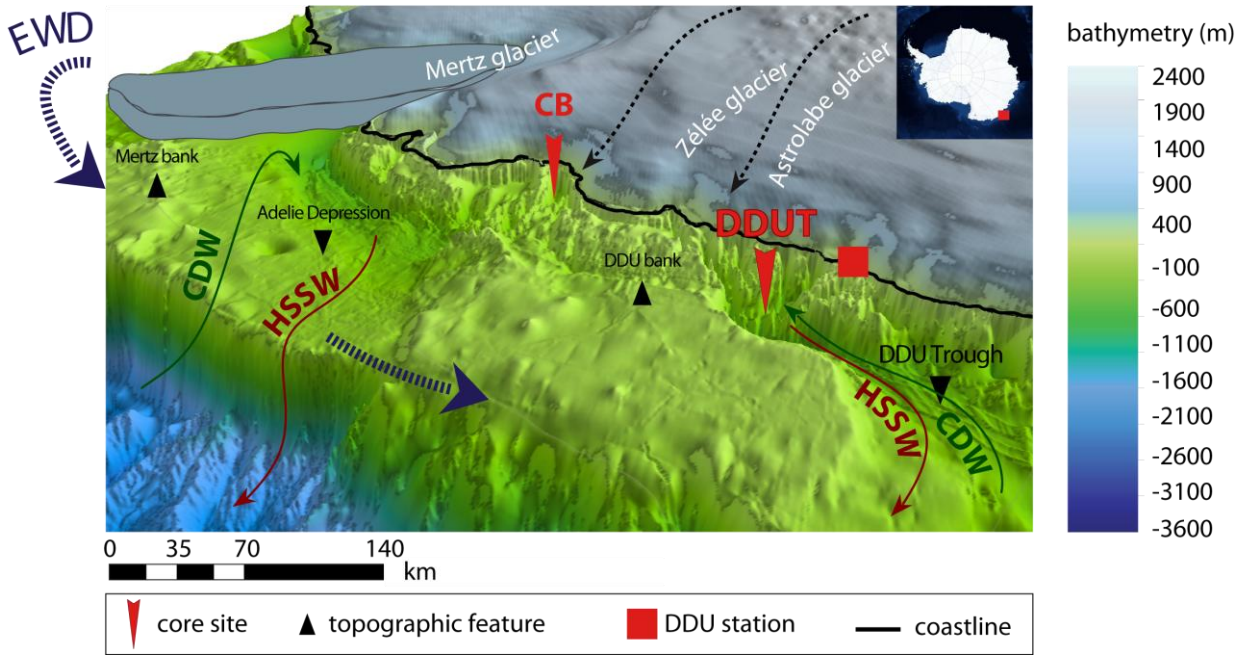

Figure 30. Vue topographique 3D de la TAGV, indiquant les structures topographiques remarquables (glaciers, hauts fonds etc.), les principales masses d'eaux et les principaux courants océaniques (ex: East Wind Drift - EWD), ainsi que la localisation des sites de carottage. Données topographiques issues de Beaman et al. (2011).

2.1.1 La Bassin de Dumont D'Urville (DDUT)

Le bassin de Dumont D'Urville (DDUT-Dumont D'Urville Trough) est orienté SE-NW et profond de 1000 m environ (Fig. 30). DDUT entaille le plateau depuis la station française Dumont D'Urville jusqu'au talus continental. Il est séparé de l'Adelie Depression plus à l'Est (également appelée Mertz-Ninnis Trough) par le DDU bank qui culmine à environ 200 m sous le niveau de la mer (Fig. 30), limitant ainsi les échanges océaniques sur le plateau. Le DDUT est bordé à l'Ouest par le banc de Dibble (Fig. 30; Beaman et al., 2011). Trois glaciers s'écoulent dans la mer de Dumont d'Urville (Fig. 30) et injectent de l'eau douce et des particules terrigènes (Denis et al., 2009): le Glacier de Zélée, le Glacier de l'Astrolabe qui est relié au DDUT au moyen d'un canyon, et le Glacier Français (Fig. 30).

Le site de carottage DDUT se situe au niveau de la dépression la plus proximale au continent et profonde d'environ 1300 m au maximum, non loin du Glacier de l'Astrolabe (Fig. 30). Les analyses sismiques dans la région du site ont révélé un dépôt sédimentaire saisonnier à annuel, probablement sans disconuité, sur environ 200 m d'épaisseur (Fig. 31), traduit par une

alternance de lamines claires (blanchâtre) et sombres (de teinte vert foncé à noire). Ce dépôt recouvre le diamicton glaciaire (Fig. 31), indiquant que les quelques 200 m de sédimentation couvrent la période Holocène (Escutia et al., 2010).

Basés sur les précédentes études sédimentaires en TAGV,et de manière plus large en Antarctique de l'Est, l'accumulation d'un couple de lamines claire/sombre se fait au cours d'une année durant la saison de croissance (été austral). Le reste de l'année l'ensoleillement trop faible ainsi que l'importante concentration de glace empêchent la production primaire et l'écoulement de terrigènes, ayant pour conséquence un hiatus de sédimentation (Stickley et al., 2005; Denis et al., 2006; Maddison et al., 2006). Ainsi, les lamines claires ou biogéniques sont le résultat de la production de surface printanière. Bien que contenant également du matériel biogène issue de la production estivale et automnale, les lamines sombres se distinguent par des teneurs en particules terrigènes plus ou moins conséquentes (probablement apportées par des plumes hyperpicnales), issues de la fonte de la banquise et des glaciers émissaires au cours de cette saison.

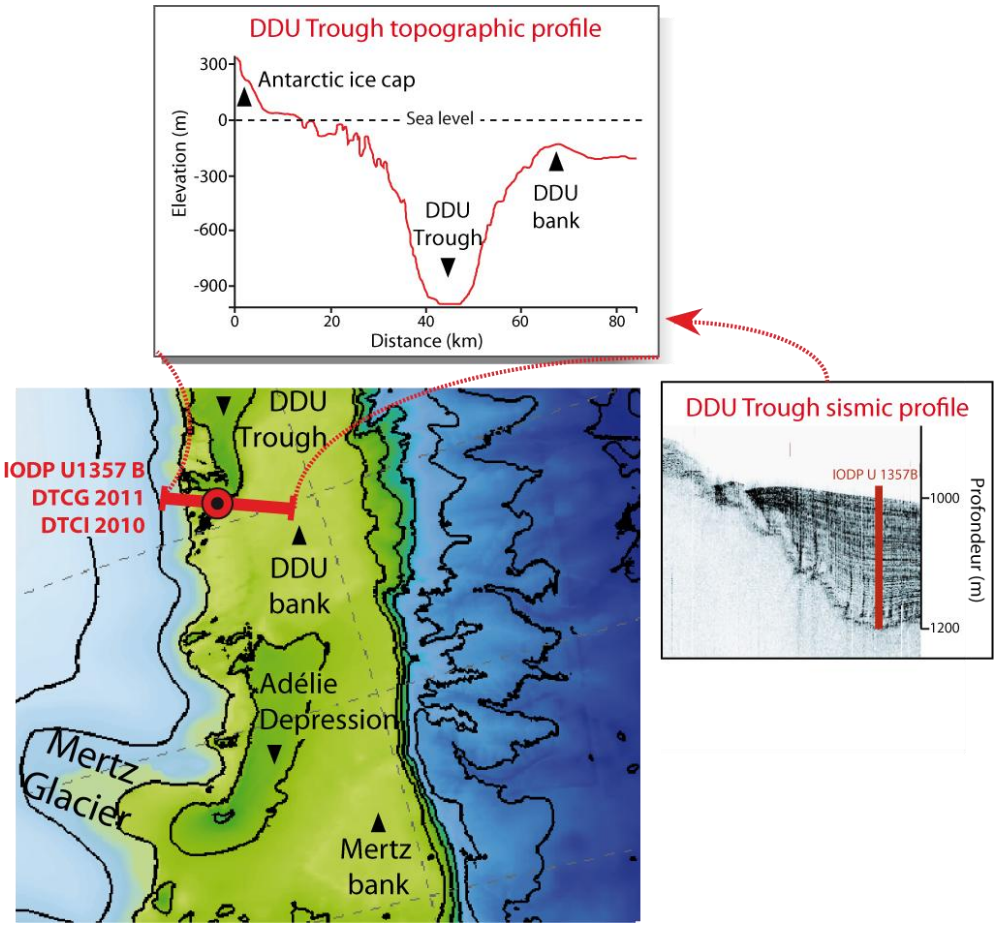

Figure 31. Carte topographique de la TAGV (données traitées d'après Beaman et al., 2011), montrant le profil topographique ainsi que le profil sismique (Escutia et al., 2010) du site DDUT.

- IODP U1357B

En Février 2010, l'Expédition 318 IODP (Integrated OceanDrilling Program) a permi de récupérer ~190 mètres de sédiments Holocène dans le Bassin de DDU, au point de coordonnées (66°24.79'S -140°25.57'E) par 1010 m de profondeur (Escutia et al., 2010) (Fig. 31). Trois forages ont été réalisés au site IODP, afin d'assurer un recouvrement complet ainsi qu'une importante quantité d'échantillons. La carotte IODP U1357B est composée de 19 carottes découpées en plusieurs sections (environ 6 à 7 par carotte). Le sédiment est majoritairement constitué de diatomites laminées, et occasionnellement de boues à diatomées. La carotte IODP U1357B mesure 172 m environ et est laminée sur tout le long, alternée de lamines claires et sombres. Il a été observé sur de nombreux intervalles que le nombre de couplets de lamines correspond à la différence d'âge entre les dates radiocarbone AMS, suggérant que beaucoup de couplets sont le résultat d'une production annuelle, en accord avec diverses études dans la zone. De plus, la perte de sédiment au site B du forage U1357 a été

réduite au minimum par rapport aux sites C et A. Ainsi, la carotte IODP U1357B constitue la plus importante et complète section sédimentaire holocène en Antarctique.

La lithostratigraphie du site IODP U1357 a été réalisée uniquement à partir des informations du site A. Trois unités lithostratigraphiques ont été établies de haut en bas: les 170 premiers mètres de boue à diatomées stratifiées correspondent à la période Holocène, suivie par une unité transitoire de 15 m composée de sable, de silts et de boues à diatomées, puis par un diamicton glaciaire. Notre étude porte sur les 40 premiers mètres de la carotte IODP U1357B, qui couvrent globalement les derniers 2,000 ans. La carotte IODP U1357B a été échantillonnée à bord du Joides à Victoria (Canada) tous les 5 cm, avec des tranches de 2 cm d'épaisseur par échantillon.

- DTCG2011

La carotte DTCG2011 (66°24.50'S -140°26.43'E) a été récoltée au site DDUT (Fig. 31) lors de la campagne ALBION-HOLOCLIP en Janvier 2011, au moyen d'un carottier gravité par 1030 m de profondeur. Cette carotte s'inscrit dans le cadre du projet HOLOCLIP (HOLOcene CLimate variability at High-southern latitudes: an Integrated Perspective) qui bénéficie du support logistique de l'IPEV (Institut Paul Emile Victor) et du programme ALBION (Adelie Land Bottom water formation and Ice Ocean iNteractions). La carotte DTCG2011 couvre une période plus récente que la IODP U1357B, allant de 1540 à 2002 ans C.E.

La carotte DTCG2011 est laminée tout le long, alternée de lamines claires et sombres. La carotte DTCG2011 a conservé l'interface (présence de la couche de mélange) et mesure 4.69 m de long, permettant l'étude des variations climatiques sur la période historique et jusque sur la période instrumentale. DTCG2011 a été découpée et échantillonnée tous les 1 cm à l'UMR EPOC (FRANCE).

- DTCI2010

La carotte interface DTCI2010 a été collectée en Janvier 2010 au moyen d'un carottier d'interface lors de la mission ALBION-HOLOCLIP à bord de l'Astrolabe. Tout comme la carotte DTCG2011, DTCI2010 a été récupérée dans le cadre de la collaboration entre le projet HOLOCLIP et le projet ALBION. La carotte DTCI2010 a été prélevée au moyen d'un carottier d'interface au point de coordonnées (66°24.68'S -140°26.67'E) par 1010 m de profondeur, dans le DDUT (Fig. 31).

La carotte DTCI2010 est longue de 72,5 cm. Elle a conservée l'interface, marquée par la présence de la couche de mélange. La carotte est constituée de boues à diatomées plus ou moins argileuses, comportant des lamines de teinte vert foncé à noire (fortes teneur en terrigènes), alternées par des lamines blanchâtres d'aspect cotonneux (matériel biogène), caractérisées par des contacts plus progressifs. Les images RX ne montrent pas de bioturbation. DTCI2010 a été découpée et échantillonnée tous les 0,5 cm à l'IFREMER de Brest (France).

2.1.2 La Dépression Adélie

Commonwealth Bay (CB) a été découverte au cours de l'Expédition Aurora entre 1911-1914 par Douglas Mawson, qui y installa sont campement près de Cap Denison. CB est connue pour ses conditions climatiques extrêmes, à savoir les vents les plus violents et les vents les plus persistants de la surface du globe (Wendler et al., 1997). Située à 142.5°E - 66.8°S (Fig. 30), CB forme une cuvette peu profonde de 850 m et étroite de 48 km à l'entrée de la baie. CB débouche sur la Dépression Adélie, où s'accumule l'eau dense formée sur le plateau. Cette vallée sous-marine linéaire parallèle à la côte est issue de l'érosion glaciaire des glaciers de Mertz et de Ninnis à l'Est. La Dépression Adélie connait de forts taux de sédimentation (Mertz Drift), cependant inferieurs par rapport au DDUT. CB est bordée à l'Ouest par le banc d'Adélie (Fig. 30), alors qu'à l'Est en amont, la langue du Glacier de Mertz (MGT) agit comme une barrière aux courants de glace transportés par l'ACC et, permettant le développement récurrent de la MGP au-dessus de la Dépression Adélie, jusqu'à la côte incluant le site de carottage à CB.

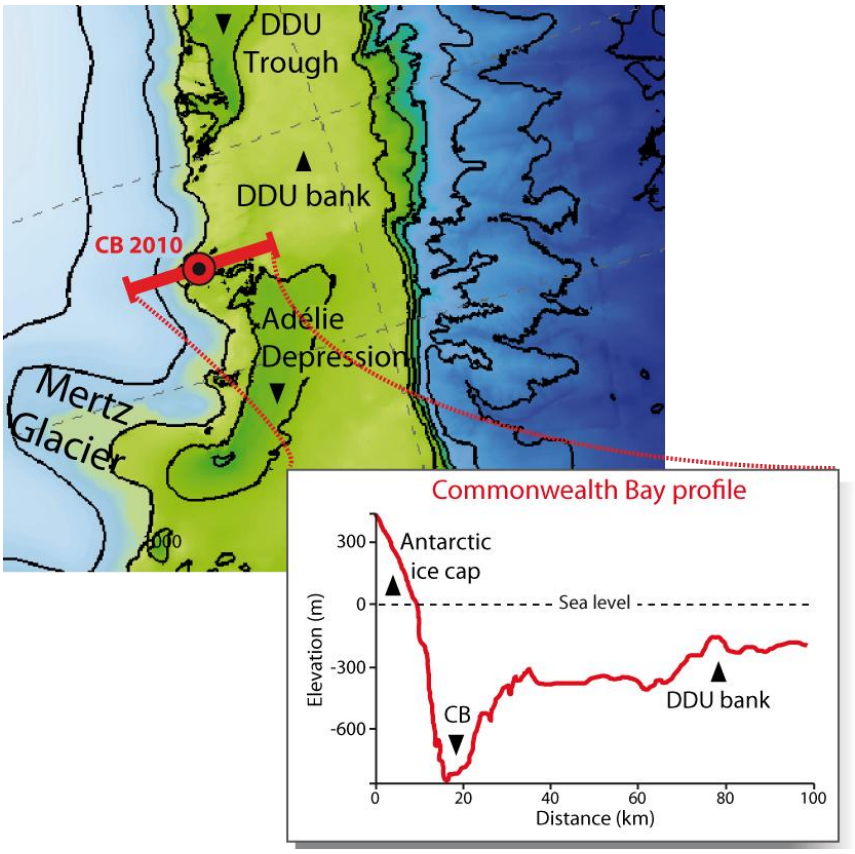

Figure 32. Carte topographique de la TA–GV (données traitées d'après Beaman et al., 2011), montrant le site de carottage CB2010 et le profil topographique de la baie du Commonwealth.

- CB 2010

La carotte CB2010 (66°54,38'S - 142°26,18'E), longue de 30.5 cm, a été prélevée au moyen d'un carottier d'interface dans CB (Fig. 32) à 775 m de profondeur, au cours de la mission COCA en 2010. L'analyse de la structure sédimentaire par images SCOPIX a révélé que la section CB2010 est composée de sédiment non-stratifié de boue à diatomées, contrairement à divers enregistrements sédimentaires de la TAGV (ex: IODP U1357B; JPC 10; Maddison et al., 2006). Le taux de sédimentation au site CB est bien inférieur à ceux observés dans la région, et particulièrement au site DDUT. La carotte CB a été échantillonnée tous les 0.5 cm à l'UMR EPOC (France). Les analyses des assemblages de diatomées et mesures XRS ont été traitées à l'UMR EPOC (France), et l'analyse de biomarqueurs au laboratoire LOCEAN (France).

2.2 Chronologie des carottes

Deux méthodes ont été utilisées pour dater nos enregistrements sédimentaires. Des datations radiocarbone AMS ont été réalisées sur la carotte IODP qui couvre les quelques derniers 2,000 ans (*cf.* Chap V), ainsi que sur la carotte DTCG2011 (*cf.* Chap IV), qui couvre les quelques 450 derniers ans. Des mesures de l'activité du ^{210}Pb en excès ($^{210}Pb_{xs}$; Appleby and Olfield, 1992) dans le sédiment ont également été réalisées sur le premier mètre et l'interface de la DTCG2011, qui couvre la période actuelle (*cf.* Chap IV). La datation au plomb a permis de corroborer ainsi les âges et le taux de sédimentation obtenu par datation ^{14}C. Le radio-isotope naturel du plomb (^{210}Pb) possède une courte durée de vie (t1/2=22,3 ans), permettant d'estimer les vitesses de sédimentation à l'échelle du siècle. Ainsi, pour les séquences sédimentaires DTCI2010 (*cf.* Chap III) et CB2010 (*cf.* Chap IV), couvrant la période récente, la chronologie est uniquement basée sur les mesures de l'activité du ^{210}Pb.

2.3 Synthèse

Table 1. Synthèse des enregistrements sédimentaires, de leurs caractéristiques ainsi que des analyses qui ont été réalisées au cours de la thèse.

LOCATION	**Bassin de Dumont d'Urville**	**Bassin de Dumont d'Urville**	**Bassin de Dumont d'Urville**	**Dépression Adélie**
CORES	IODP U 1357 B	DTCG 2011	DTCI 2010	CB 2010
COORDONNEES	66°24.79'S - 140°25.57'E	66°24.50'S - 140°26.43'E	66°24.68'S - 140°26.67'E	66°54,38'S - 142°26,18'E
LONGUEUR	3801 cm	469 cm	72.5 cm	30.5 cm
AGE	~-129-1907 C.E.	~1540-2000 C.E.	~1970-2010 C.E.	~1738-2004 C.E.
TAUX DE SEDIMENTATION	~ 1.8 cm/an	~ 1 cm/an	~ 1.2 cm/an	~ 0.11 cm/an

DIATOMEES	216 échantillons Résolution: ~ 9.4 an	118 échantillons Résolution: ~ 3.9 an	144 échantillons Résolution: ~ 0.3 an	50 échantillons Résolution: ~ 5.3 an
HBI	706 échantillons Résolution: ~ 3 an	235 échantillons Résolution: ~ 2 an	144 échantillons Résolution: ~ 0.3 an	62 échantillons Résolution: ~ 4.3 an
XRF		2306 échantillons Résolution: ~ 0.2 an	361 échantillons Résolution: ~ 0.1 an	146 échantillons Résolution: ~ 1.8 an

Des séquences sédimentaires holocènes très bien préservées (laminées avec un taux de sédimentation annuel allant jusqu'à plusieurs centimètres) ont été mises en évidence dans le DDUT, notre principal site d'étude. De telles archives sont dues à une topographie particulière de la région qui concentre l'apport sédimentaire et la production de surface, augmentant ainsi les conditions de préservation (Crosta et al., 2005). La compilation et le recoupement de trois enregistrements sédimentaires (IODP U1357B, DTCG2011 et DTCI2010) au site DDUT permet pour la première fois la reconstruction des variations passées du couvert de glace et des conditions environnementales en Antarctique de l'Est au cours de l'Holocène tardif et jusque sur la période instrumentale, à une résolution sans précédent. Ces sections sédimentaires permettent également la comparaison avec des enregistrements glaciaires en Antarctique à une résolution similaire. Bien que la résolution de CB2010 soit plus faible, la combinaison des diverses séquences sédimentaires aux deux sites offrent une vision régionale des changements passés océaniques et climatiques survenus en TAGV. De plus, le site CB constitue un point stratégique de la polynie du Mertz, permettant ainsi l'étude de la dynamique passée de l'ALBW, très liée à la dynamique du Glacier de Mertz (Lacarra et al., 2014).

3 Outils utilisés dans cette étude

3.1 Données sédimentaires

3.1.1 Diatomées

a Généralités

Les diatomées, ou Bacillariophyta, sont des algues unicellulaires eucaryotes microscopiques, de taille comprise entre 2-250µm dans notre zone d'étude (jusqu'à 2mm au maximum; *Thalassiothrix* sp), caractérisées par un frustule siliceux de forme très variée. Les diatomées sont représentées dans la plupart les milieux aquatiques : océans, lacs et rivières. Dans les régions polaires et sub-polaires, leur distribution est contrôlée par une combinaison de paramètres physico-chimiques tels que la lumière, la température et la salinité des eaux de surface, la disponibilité en macro et micro nutriments, la concentration de glace de mer et la stabilité de la colonne d'eau (Beans et al., 2008; Riaux-Gobin et al., 2011; Crosta, 2011). Dans l'Océan Austral, elle contribuent à plus de 75% de la productivité primaire, jouant ainsi un rôle important dans les cycles globaux du carbone et de la silice (Tréguer et al., 1995).

b Indicateur paléo-environnemental

Les boues à diatomées sont caractéristiques des milieux froids associés à une production quasi ou exclusivement siliceuse. Dans l'Océan Austral, cette sédimentation est largement représentée dans la bande comprise entre le Front Polaire et l'étendue maximale de glace ainsi que sur la marge continentale de manière localisée en fonction de la phyisographie du plateau continental et des courants de fond (Leventer et al., 2006). Dans ces régions, les assemblages de diatomées sont très diversifiés et bien préservés dans le sédiment (Leventer, 1991, 1992 ; Armand et al., 1995), permettant alors une identification précise jusqu'à l'espèce. Ainsi, les marges continentales constituent des zones clés pour la reconstruction des conditions passées environnementales et climatiques à très haute résolution.

L'utilisation des diatomées comme indicateurs paléo-environnementales en Antarctique comprend cependant plusieurs limites. En effet, une fraction relativement faible des valves produites dans la zone photique atteint le sédiment, entre 1-10%, pouvant aller jusqu'à 30% sur le plateau continental (Ragueneau et al, 2000). Divers processus tels que la dissolution préférentielle d'espèces faiblement silicifiées ou le broutage de certaines classe de taille d'espèces, des évènements de sédimentation massive ou bien le transport latéral peuvent induire un biais dans les pourcentages relatifs (Crosta, 2011). De plus, la taille du frustule

ainsi que son degré de silicification influent également sur la vitesse de sédimentation, l'enfouissement et la préservation des diatomées, et donc sur leur distribution dans le sédiment. Ainsi, pour identifier le degré de conservation dans le sédiment, on utilise les traces de dissolution sur certaines espèces dites sensibles telles que *Corethron pennatum* ou *F. cylindrus* par exemple (Pichon et al., 1992). Certaines espèces de diatomées sont sujettes à une dissolution préférentielle, notamment les espèces inféodées à la banquise (ex: *Amphiprora* spp.), et donc ne constituent pas de bon indicateur environnementaux en raison de leur faible représentation dans le sédiment (Riaux-Gobin et al., 2011). En revanche, d'autres espèces ayant une préservation plus importante, mais aussi des préférences écologiques marquées, telles que les les *Fragilariopsis* spp. ou *Thalassiosira* spp., plus siliciées, constituent de bon marqueurs pour reconstruire les variations environnementales (Leventer, 1998). C'est le cas dans nos échantillons.

Des études ont montré que la distribution des diatomées dans les sédiments des régions antarctiques reflète une moyenne des conditions de surface (Armand et al., 2005 ; Crosta et al., 2005; Gersonde et al., 2005). La variété des espèces ainsi que leurs préférences écologiques, appliquées aux assemblages fossiles selon le principe d'actualisme, font des diatomées un excellent proxy pour les reconstitutions océanographiques et climatiques, permettant d'appréhender les conditions de surface, ainsi que les conditions d'exportation et de préservation du sédiment en surface (Leventer, 1992; Zielinski and Gersonde, 1997 ; Armand et al., 2005; Crosta et al., 2005).

c Assemblages de diatomées

Sur le plateau continental, la dynamique du couvert de glace contrôle largement la PP ainsi que la diversité spécifique et l'enchainement saisonnier des assemblages de diatomées (Armand et al., 2005; Crosta et al., 2008; Arrigo et al., 2010), rendant ainsi distinct deux types d'environnements associés à des assemblages de diatomées. Les diatomées d'océan ouvert sont communes dans la zone libre de glace au delà de la limite hivernale du couvert de glace, ainsi que dans la PFZ (Crosta et al., 2005b) alors que les diatomées de glace sont présentes au Sud du PF dans la MIZ et dominent la SIZ (Sea Ice Zone) (Armand et al., 2005). D'autres diatomées sont présentées dans un troisième groupe et constituent plutôt des indicateurs de conditions environnementales autres que le couvert de banquise telles que la stratification/mélange, l'apport en nutriments etc. Dans notre nos échantillons entre 50-70 espèces environ ont été recensées. Les détails relatifs à l'écologie des espèces dominantes,

c'est-à-dire celles présentant des pourcentages significatifs dans nos échantillons et/ou ayant des conditions environnementales spécifiques sont présentés dans le Chapitre III. La synthèse de ces espèces est présentée Figure 33, en fonction de leur classification ainsi que de leur préférence écologique saisonnière.

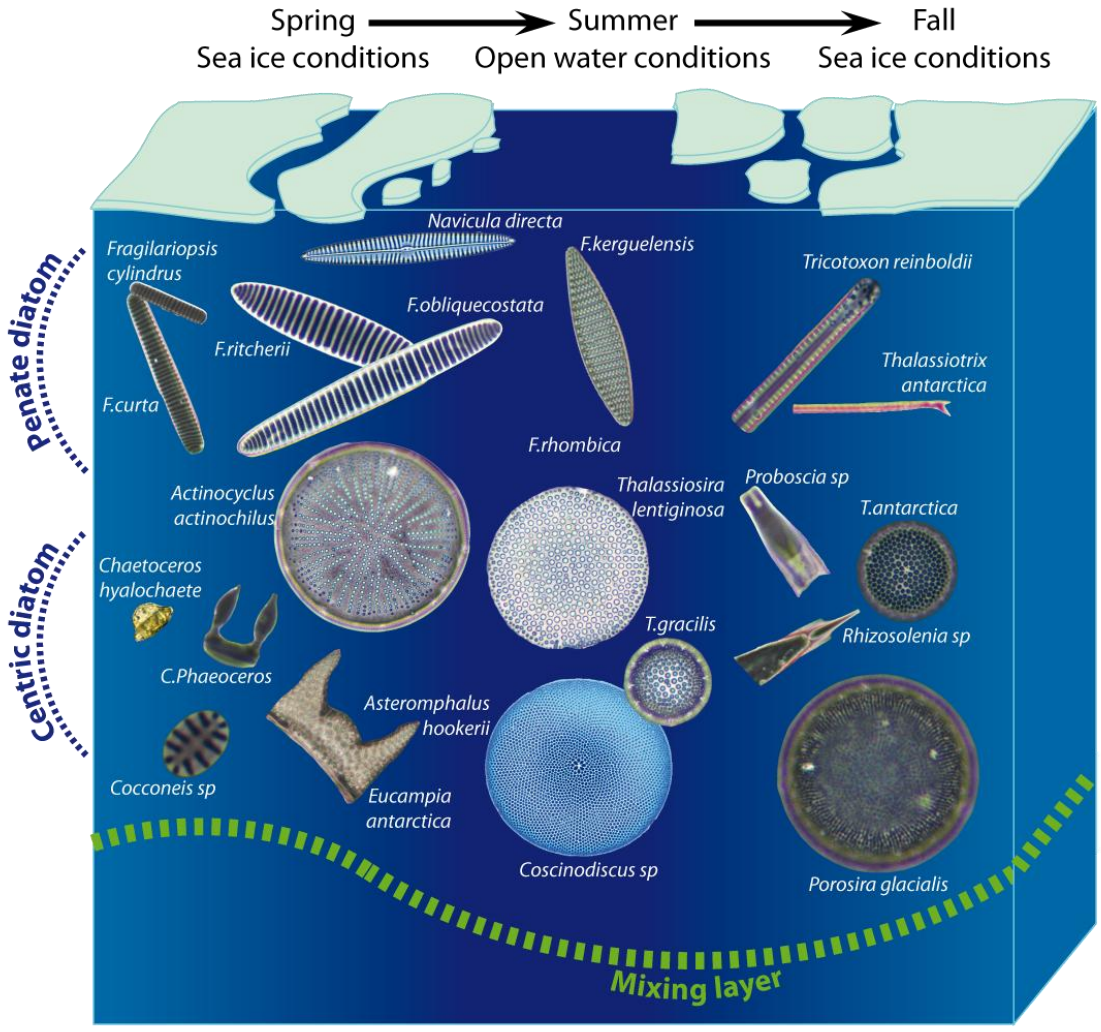

Figure 33. Principales espèces de diatomées de la zone côtière en Antarctique, en fonction de leur classification et de leur préférence écologique saisonnière.

- **<u>Diatomées de glace</u>**

Les diatomées associées/ accrochées à la banquise, dites cryophiliques, dominent la production siliceuse du plateau continental. Le type de banquise (*cf.* paragraphe banquise) ainsi que la dynamique du couvert de glace (fonte, reforme) jouent un rôle très important dans la composition des assemblages de diatomées (Arrigo et al., 2010). En effet, les blooms printaniers sont engendrés globalement entre Octobre et Décembre, dus à l'augmentation de la luminosité qui initie la fonte de la banquise, créant ainsi un environnement stable (stratifié),

caractérisé par des eaux froides peu salées, riche en nutriments (issus de la fonte de la banquise) nécessaire au développement phytoplanctonique (Moore et Abbott, 2000). Les « bloomers » ont un taux de croissance rapide et des besoins en nutriments assez élevés. Les blooms printaniers sont généralement monospécifique ou faiblement diversifié, largement représentés par le genre *Fragilariopsis*, particulièrement *Fragilariopsis curta* et *Fragilariopsis cylindrus*, et le genre *Chaetoceros Hyalochaete* (Kang and Fryxell, 1992; Beans et al., 2008; Riaux-Gobin et al., 2011). D'autres diatomées telles que *Amphiprora* spp., *Navicula* spp. and *Nitzschia* spp, sont également communes dans la fast ice. Toutefois, ces espèces, faiblement silicifiées, ne contribuent pas significativement aux assemblages fossiles en raison de leur faible préservation dans le sédiment (Riaux-Gobin et al., 2003) et sont donc anecdotiques dans notre étude.

- **Diatomées d'océan ouvert**

Le long des côtes antarctiques, les diatomées de printemps (associées à la présence de glace) sont remplacées à l'été/automne par les diatomées dites d'océan ouvert, dont certaines espèces sont communes dans la zone permanente libre de glace, au nord de la limite maximale d'extension de banquise hivernale (Crosta et al., 2005; Crosta et al., 2008). Ainsi, dans notre zone d'étude, les diatomées d'océan ouvert qui se développent à l'été/automne, rendent compte de l'apparition saisonnière de condition d'eau libre, plutôt que d'une compétition latitudinale entre diverses provinces écologiques (type PFZ etc.). L'apparition de telles espèces dans la zone côtière antarctique a lieu entre Décembre et Février, en lien avec la formation d'une couche stable, claire et relativement plus chaude sous l'effet de l'irradiance (Leventer, 2003). Nos assemblages d'été ou d'océan ouvert sont caractérisés par la présence de pennées du genre *Fragilariopsi* ssp, et notamment *F. kerguelensis*, ainsi que par la présence de larges centriques du genre *Thalassiosira* spp et *Porosira* spp, dont le taux de croissances et le besoin en nutriments est moins élevé que celui des pennées (Zielinski and Gersonde, 1997).

Bien que moins représentées dans nos assemblages, diverses autres espèces telles que *Rhizosolenia, Thalassiothrix antarctica, Tricotoxon reinboldii* et *Pseudonitzschia* (Froneman et al., 1995; Crosta et al., 2005) sont caractéristiques de la zone d'océan ouvert permanente.

- **Diatomées ubiquistes**

D'autres espèces peuvent se développer tout au long de la saison de croissance. Elles ont en effet des préférences écologiques davantage liées à la profondeur de mélange de la colonne

d'eau ou à l'abondance en nutriments, plutôt qu'à des conditions particulières et saisonnières de couvert de banquise. Ce troisième groupe comprend les *Chaetoceros Hyalochaete* (cellules végétatives et spores), qui constituent le groupe le plus abondant autour du continent Antarctique (Crosta et al., 1997), largement représentée dans la plupart des environnements côtiers. La stratification du milieu apparait comme le facteur dominant de la formation des CRS (Leventer et al., 1996). Sont également présents ici *Corethron* spp et, *Rhizosolenia* spp sont associées à aux conditions de nutriments ainsi que de stratification de la couche de surface (Crosta et al., 2005; Beans et al., 2008). Ces diatomées sont cependant faiblement abondantes dans nos échantillons. La présence des diatomées dites benthiques, attachées au substratum (rochers, macro-algues, vase, …) est fonction de plusieurs facteurs, dont la nature du substrat, la profondeur de la colonne d'eau, l'épaisseur de glace et l'énergie lumineuse incidente, indispensable à leur croissance (Crosta and Koç, 2007). Ces diatomées dites néritiques se développent après la débâcle de la banquise au printemps et à l'été, ou lors de la remise en suspension du sédiment par la houle et les tempêtes d'automne (Krebs et al., 1987). Bien que les diatomées benthiques sont très peu présentes dans nos échantillons en raison de leur faible conditions de préservation, le genre *Cocconeis* est le plus fréquemment observé.

d Comptage

Les techniques utilisées pour l'analyse des diatomées, le traitement du sédiment et la préparation des lames, sont celles décrites dans Rathburn et al. (1997). Le protocole permet la concentration et la dispersion des valves de diatomées par la dissolution des carbonates et l'oxydation de la matière organique. Les diatomées sont ensuite fixées entre lames et lamelles. Les méthodes d'identification et de comptage des diatomées sont celles de Schrader and Gersonde (1978) et Laws (1983), complétées par celles de Crosta and Koç (2007). Chaque lame (3 par échantillon) a été traversée horizontalement jusqu'à compter 300-350 valves de diatomées sur un microscope Olympus BH-2 avec une magnification de 1000. Seules les valves intactes à moitié ou plus sont comptées pour éviter de recenser le même spécimen deux fois. Pour les espèces allongées (ex: *Trichotoxon*, *Thalassiothrix*, *Pseudonitzschia*), seules les extrémités des valves ont été comptées puis divisées par deux, sachant que deux extrémités représentent une valve. Ainsi, les diatomées ont été identifiées au niveau de l'espèce ou du groupe d'espèces, et l'abondance relative de chaque espèce a été déterminée comme la fraction de l'espèce sur l'assemblage total de diatomées de chaque échantillon. Les comptages ont été réalisés à l'UMR EPOC (France).

3.1.2 Highly Branched Isoprenoids

Les Highly Branched Isoprenoids (HBI) sont des hydrocarbures insaturés (alcènes) caractérisés par une chaîne carbonée ouverte, et la présence d'au moins une double liaison covalente entre deux atomes de carbone. Ces composés lipidiques sont abondamment représentés dans la nature et particulièrement dans le phytoplancton. Probablement produits dans les chloroplastes (Massé et al., 2004) leur rôle dans la cellule est cependant méconnu.

Certains de ces alcènes sont présents dans la plupart des microalgues, alors que d'autres ont été identifiés comme spécifiques à une classe ou un groupe d'espèces. Notamment, les HBI de type C25 sont synthétisés par un nombre restreint de diatomées telles que *Haslea* sp., *Rhizosolenia* sp., *Pleurosigma* sp. et quelques *Navicula* sp. (Massé et al., 2004; Sinninghe-Damsté et al., 2004). Le nombre de doubles liaisons de la molécule co-varie avec la température et permet ainsi la présence dans la nature de plusieurs degrés d'insaturation de la chaîne carbonée C25 (Rowland et al., 2001). En effet, la culture en laboratoire de l'espèce *Haslea ostrearia* a montré que les formes di-, tri- et tétra-insaturée apparaissent en majorité à 5°C, 15°C et 25°C respectivement (Rowland et al., 2001).

De plus, certains HBI sont spécifiques à des espèces de diatomées, et donc à des conditions environnementales particulières. En effet, en Antarctique, alors que l'isomère mono-insaturé (IP25) n'ai jamais été détecté, les formes di- ([HBI:2]; Diène), tri- et tétra-insaturé ([HBI:3]; Triène) ont été identifiées respectivement dans la banquise et dans le phytoplancton dans des conditions d'océan ouvert (Fig. 34) (Belt et al., 2000; Massé et al., 2011). En effet, [HBI:2] est présent dans les sédiments de surface des régions expérimentant un balancement saisonnier de banquise, mais est absent dans les sédiments des régions où le couvert de glace est permanent ou totalement absent (Belt et al., 2007). De plus, [HBI:2] a une signature isotopique caractéristique de celle des diatomées vivant dans la glace de mer. A l'inverse, [HBI:3] est présent dans les sédiments des régions connaissant un faible (saisonnier) ou inexistant couvert de glace et possède une composition isotopique traduisant une origine planctonique (Massé et al., 2011).

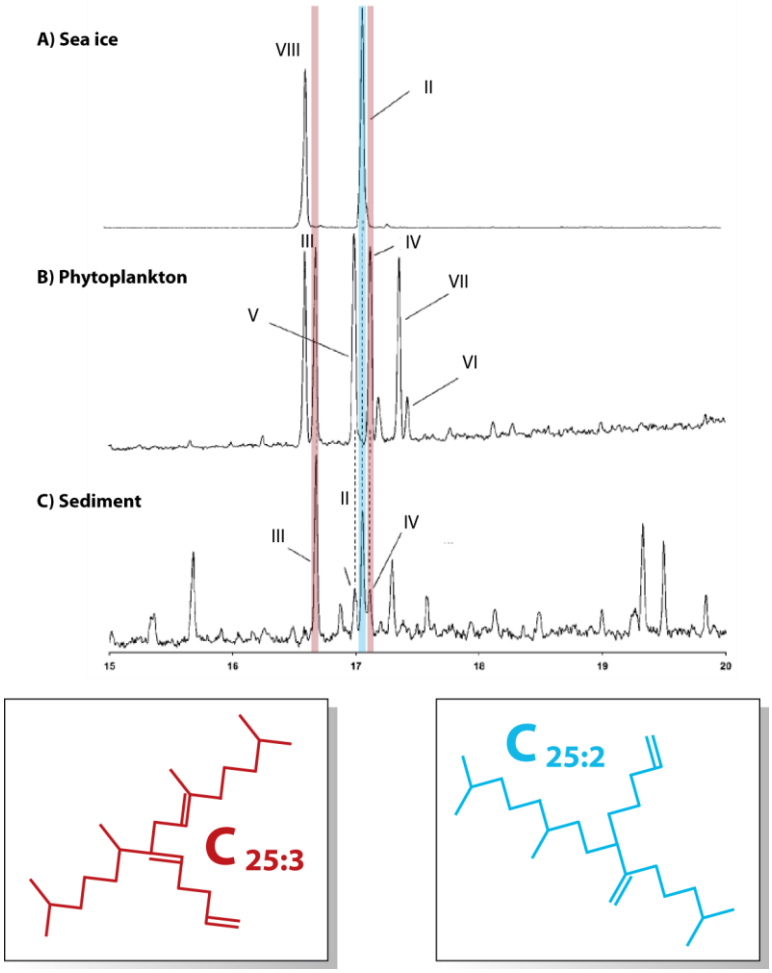

Figure 34. Partie supérieure: chromatogrammes des fractions d'hydrocarbure montrant les différents isomères HBIs de II à VI sur des échantillons de banquise, de phytoplancton et de sédiments antarctique (modifié d'après Massé et al., 2011). Le pic rouge correspond à [HBI:3] (Triène Z et E) et le pic bleu correspond à [HBI:2]. Partie inférieure: dessin des molécules de [HBI:3] (en rouge) et de [HBI:2] (en bleu).

Ainsi, la distribution de [HBI:2] et [HBI:3] dans des enregistrements sédimentaires marins Holocène montre une forte cohérence avec les proxies de banquise (Massé et al., 2007). Ces bio-marqueurs retraçant la présence/absence de glace, de récentes études sur des carottes marines d'Antarctique, notamment en Baie de Prydz et dans le bassin de DDU (Barbara et al., 2010; Denis et al., 2010), ont proposé d'utiliser le rapport [HBI:2]/[HBI:3] afin de reconstruire les variations du couvert de banquise et de sa saisonnalité (Belt et al., 2007).

La méthode d'analyse utilisée pour mesurer les HBI, décrite dans Belt et al. (2007), permet d'extraire les composées lipidiques du sédiment (1.5 g par échantillon), au préalablement lyophilisé, afin de conserver les molécules. On ajoute ensuite un standard interne puis les lipides sont récupérés par le biais d'une solution de Dichlorométhane/Méthanol, qui est ensuite purifiée par chromatographie sur colonne de silice. La fraction hydrocarbones est

analysée par chromatographie en phase gazeuse couplée à un spectromètre de masse (GC-MS). Enfin, les spectres sont traités avec le logiciel Hewlett-Packard *MS Chemstation*, et les abondances des isomères des HBIs sont calculées en fonction de leurs réponses relatives par rapport au standard interne. Les analyses ont été réalisées au Laboratoire LOCEAN (France) pour les carottes IODP U1357B, DTCI2010 et CB2010, ainsi qu'à l'UMI Takuvik (Canada) pour la carotte DTCG2011.

3.1.3 Fluorescence RX et radioscopie RX

La composition élémentaire des carottes DTCG2011, DTCI2010 et CB2010 a été analysée grâce à la spectrométrie par fluorescence X (XRF), technique d'analyse non destructive et semi-quantitative qui permet de déterminer la composition en éléments majeurs et mineurs dans le sédiment (Si, Al, Ti, Ca, Sr, etc.) (Jansen et al., 1998). Les analyses ont été réalisées au laboratoire EPOC/Université Bordeaux1, pour tous nos enregistrements à l'exception de la IODP U1357B, qui a été traitée à College Station/Texas (USA). Ces mesures ont été effectuées tous les 5 mm pour la carotte IODP U1357B, tous les 2 mm pour les carottes DTCG2011, DTCI201 et CB2010, grâce au même système, nommé XRF Core Scanner fabriqué par la société Aavatech.

De nombreuses études ont utilisé cette technique pour l'étude des variations environnementales à partir de carottes sédimentaires (ex. Denis et al., 2008; Milzer et al., 2013). Les éléments tels que le fer (Fe) et le titane (Ti) sont considérés comme les éléments les plus appropriés pour déterminer les apports terrigènes dans les bassins océaniques (Richter et al., 2006). Ces deux éléments permettent d'étudier les transferts sédimentaires continent-océan ainsi que le cycle saisonnier des apports terrigènes dans le sédiment, en lien avec les variations du couvert de glace en TAGV (Denis, PhD, 2008 ; Maddison et al., 2006 ; 2012). Les éléments rubidium (Rb) et Zirconium (Zr) permettent de mettre en évidence les variations structurelles du sédiment. En effet, le rapport Zr/Rb retrace les variations de la taille de grain dans le sédiment, Rb étant associé aux particules d'argile détritique, et Zr aux minéraux résistants lourds (Dypvik et al., 2001).

La structure du sédiment des carottes DTCG2011, DTCI2010 et CB2010 a été analysée par radioscopie RX, grâce au système SCOPIX. Cette technique non destructive permet de

radiographier le sédiment et ainsi de mettre en évidence la structure, la densité ou encore la bioturbation du sédiment (Migeon et al., 1999). Le SCOPIX est composé d'une source de rayon X couplée à un amplificateur de brillance et une camera CCD 16 bits.

3.2 Données instrumentales

3.2.1 Données météorologiques

La Publithèque est un service de Météo-France, permettant d'accéder à de nombreuses données climatologiques (précipitations, température, rayonnement etc.) à des pas de temps variables (horaire, quotidien etc.). Divers paramètres météorologiques de la région de DDU (-66°39'42"S, 140°00'00"E), issus de stations automatiques, ont ainsi été extraits à partir de la publithèque de Météo France (Table 2) pour la période du 14/02/1950 au 01/09/2013.

Table 2. Tableau récapitulatif des variables météorologiques utilisées, couvrant la période du 14/02/1950 au 01/09/2013.

	Libellé variable	**Unité**	**Pas de temps**	**Début série**	**Fin série**	**Données manquant**
FXY	VITESSE VENT QUOTIDIEN MAXI MOYENNE SUR 10 MIN	M/S ET 1/10	QUOTIDIEN	4/01/1956	1/09/2013	4033
DXY	DIRECTION VENT QUOTIDIEN MAXI MOYENNE SUR 10 MIN	ROSE DE 360	QUOTIDIEN	4/01/1956	1/09/2013	4034
TM	TEMPERATUREMOYENNE SOUS ABRI QUOTIDIENNE	DEG C ET 1/10	QUOTIDIEN	1/01/1957	1/09/2013	678

3.2.2 Données satellite

Les radiomètres micro-ondes mesurent les rayonnements émis par la terre, l'océan et l'atmosphère, dans des fréquences différentes, sous forme de Température de brillance (Tb).

La Tb dépend de l'émissivité de la surface du corps. Ainsi, dans les régions polaires, suivant l'âge de la glace et sa concentration, l'émissivité est différente pour une fréquence donnée.

Les concentrations quotidiennes de glace de mer (%) ont été extraites au Laboratoire LOCEAN pour la période 1978-2012, à partir de la base de données du National Snow and Ice Data Center. Les données satellitaires sont générées à partir de la valeur du rayonnement émis par la terre et mesurée par les capteurs Nimbus-7 SSMR (1978-1987), DMSP SSM/I (1987-2007) et SSMIS (2007-2012). Elles sont traitées grâce à l'algorithme de l'équipe de la NASA développé par la branche Ocean and Ice, au centre de la NASA Goddard Space Flight Center (GSFC) (Cavalieri et al., 1995). Les données sont fournies dans la projection stéréographique polaire avec une résolution spatiale (taille du pixel) de 25x25 km.

Les données ont été extraites pour la région de CB ainsi que pour la région de la Dépression Adélie, puis au site de carottage DDUT ainsi que pour la région de DDUT, de manière à avoir une vision plus globale des changements de glace en surface aux deux sites d'étude.

Chapitre III: Etude de la réponse sédimentaire aux variations océan/banquise/atmosphère en Terre Adélie durant la période récente

Les diatomées constituent une part importante de la production primaire dans les eaux côtières des marges continentales antarctiques. Les diatomées ont été longtemps utilisées du point de vue de la composition de leurs assemblages micropaléontologiques, et ont été plus récemment associées à des biomarqueurs spécifiques (HBI) afin de reconstruire les conditions de glace passées dans l'Océan Austral. Notre étude s'inscrit parmi les quelques études sédimentaires qui existent dans la zone marginale de glace en Antarctique, traitant de l'écologie et des conditions environnementales auxquelles sont associés les diatomées ainsi que les HBI. La zone marginale du plateau de la Terre Adélie a reçu peu d'attention jusqu'à présent et ce malgré la présence de sédiments laminés à forts taux d'accumulation, permettant de reconstruire à très haute résolution temporelle les variations climatiques et les processus sédimentaires associés.

Dans ce troisième chapitre, notre intérêt premier était de valider les divers proxies utilisés dans cette thèse afin de proposer des outils robustes pour la reconstruction paléoclimatique des conditions de surface au large de Terre Adélie. De plus, un des objectifs de ce chapitre était l'amélioration de la compréhension du système actuel. Nos enregistrements sédimentaires ont été analysés statistiquement et confrontés à des données météorologiques atmosphériques obtenues à partir de station terrestres automatiques, ainsi qu'à des données satellites de concentrations de glace. Cette démarche nous a permis d'affiner ainsi à l'échelle internannuelle les connaissances sur l'écologie des diatomées et sur les conditions environnementales auxquelles les biomarqueurs (HBI) sont associées, et enfin de documenter la réponse sédimentaire dans notre zone d'étude. Nos résultats suggèrent que l'action couplée de l'atmosphère et de l'océan en surface constitue le forçage principal de la variabilité de la productivité siliceuse ainsi que des conditions de glace à l'échelle interannuelle. Un article présentant les résultats de ce travail a été soumis au journal Biogeosciences.

Article I: Sedimentary response to sea ice and atmospheric variability over the instrumental period off Adélie Land, East Antarctica

Submitted to BIOGEOSCIENCES

Campagne, P.[1,2,3], Crosta, X.[1], Schmidt, S.[1], Houssais, M. N.[2], Ther, O.[1], and Massé, G.[2,3]

[1]EPOC, UMR CNRS 5805, Université de Bordeaux, Allée Geoffroy St Hilaire, 33615 Pessac, France

[2]LOCEAN, UMR CNRS/UPCM/IRD/MNHN 7159, Université Pierre et Marie Curie, 4 Place Jussieu, 75252 Paris, France

[3]TAKUVIK, UMI 3376 UL/CNRS, Université Laval, G1V 0A6 Quebec (Quebec), Canada

Diatoms account for a large proportion of primary productivity in Antarctic coastal and continental shelf zones. Diatoms, which have been used for a long time to infer past sea-surface conditions in the Southern Ocean, have recently been associated with diatom specific biomarkers (HBI). Our study is of the few sedimentary research projects on diatom ecology and associated biomarkers in the Antarctic seasonal sea ice zone. To date, the Adélie Land marginal ice zone has received little attention, despite evidence for the presence of high-resolution laminated sediment accumulation, allowing for finer climate reconstructions and sedimentary process studies. Here we provide a sequence of seasonally to annually laminated diatomaceous sediment from the DTCI2010 interface core retrieved on the continental shelf off Adélie Land, covering the 1970-2010 C.E. period. Investigations through statistical analyses of diatom communities, diatom specific biomarkers and major element abundances document the relationships between these proxies at an unprecedented resolution. Additionally, comparison of sedimentary records to meteorological data monitored by automatic weather station and satellite derived sea ice concentrations help to refine the relationships between our proxies and environmental conditions over the last decades. Our results suggest a coupled interaction of the atmospheric and sea surface variability on sea ice seasonality, which acts as the proximal forcing of siliceous productivity at that scale.

Key words: Instrumental period, Adélie Land, Sediment surface, Sea ice, Fast ice, Katabatic winds, Polar easterlies, Diatoms, HBIs, PCA.

1 Introduction

Diatoms have been used for a long time to infer past sea-surface conditions in the Southern Ocean on the basis of large-scale ecological studies from either plankton (e.g. Hasle, 1969) or surface sediments (DeFelice and Wise, 1981; Zielinski et al., 1997; Armand et al., 2005; Crosta et al., 2005). However, little is known about diatom ecology in the seasonal sea ice zone and, especially, in the coastal and continental shelf zone (CCSZ) off East Antarctica. To date, the Adélie Land region has received little attention, despite an abundance of evidence for the presence of high-resolution laminated sediment accumulation (e.g. Escutia et al., 2010). A very limited number of ecological studies have been performed at the species or species group level for plankton (Beans et al., 2008; Riaux-Gobin et al., 2013) or sediment (Leventer et al., 1992; Maddison et al., 2006, 2012; Denis et al., 2006), and even fewer studies have investigated their relationships with local or regional environmental conditions. As a result, paleoenvironmental reconstructions for this area that are using diatoms are based on large scale studies and do not take into account the regional specificities. The Adélie Land region is of further particular interest due to the presence of coastal polynyas in the vicinity of the Dumont d'Urville station (DDU) and the Mertz Glacier (MG), that are biologically very productive and where intense sea ice formation during winter leads to a large volume of dense water production (Arrigo and van Dijken 2003; Sambrotto et al. 2003; Laccara et al., 2014).

Investigations of diatom communities, diatom specific biomarkers and major element abundances at high resolution along a 72.5 cm long interface core retrieved in the Dumont d'Urville Trough (DDUT) allowed documentation of (1) the relationships between these proxies. The comparison of our proxy records to meteorological data inferred from either the automatic weather station (AWS) at DDU and satellite derived sea ice concentrations helped to determine (2) the relationships between environmental conditions and proxy data, and consequently, the sedimentary response to atmospheric and sea surface changes. Here, we refine our knowledge of diatom ecology at the regional scale and propose a robust tool to infer past sea-surface conditions off Wilkes Land.

2 Environmental settings

2.1 Geographic features

The Dumont d'Urville Trough (Fig. 35), located along the Adélie Land on the East Antarctica margin is composed of several glacial depressions. These topographic features, up to 1,000 meters deep, act as traps for sedimentary material (primary production and terrigenous particles) settling out from surface waters. The trough runs from the front of the Zélée and Astrolabe glaciers to the continental shelf break along a SE-NW orientation, and is bordered on its eastern side by the DDU Bank (Fig. 35), which culminates at 200 meters below the sea level and limit exchanges with the Adélie Depression. On the western side, the DDUT is flanked by the Dibble Bank where the Dibble Ice Tongue develops northward.

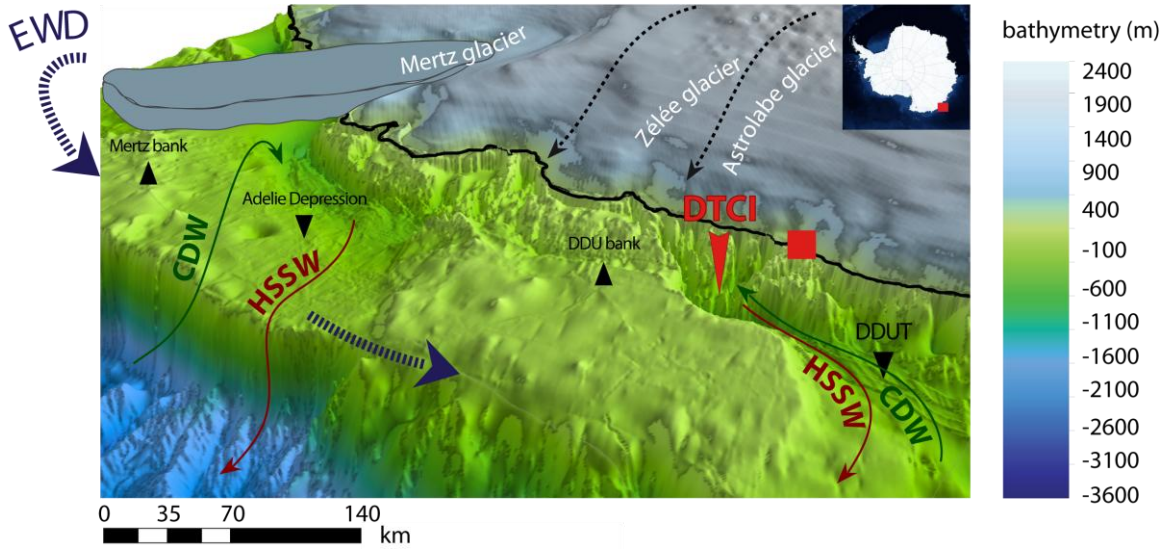

Figure 35. Study area. Map of the study area showing the location of sediment core DTCI 2010 (downward red arrow) in the Dumont D'Urville Through (DDUT), the Dumont D'Urville French station (red square), the main glacial (in white) and topographic (upward black triangle for high relief and downward for through) features, the East Wind Drift (EWD; blue dashed arrow), the principal water masses as Circumpolar Deep Water (CDW; green arrow) and the High Salinity Shelf Water (HSSW; brown arrow) (Williams et al., 2008), and katabatic winds (black dashed arrows; Massom et al., 1998). Bathymetry data were obtained from http://www.deepreef.org/publications/peer-review/82-gvdem.html.

2.2 Water masses

The Adélie Land is influenced by several water masses and currents (Rintoul, 1998; Williams and Bindoff, 2003; Williams et al., 2008). The wind-driven East Wind Drift (EWD) flows

westward at the surface, and the Antarctic Surface water constitutes the summer sub-surface water mass on the continental shelf. The Circumpolar Deep Water (CDW) upwells near the Antarctic Divergence and intrudes onto the plateau during summer. The high-salinity shelf water (HSSW), originates from the brine rejections during winter sea ice formation and from the cooling of the CDW (Fig. 35), and flows northward at the sea bottom as part of the dense shelf water that extrudes from the plateau. This Adélie Land Bottom Water ultimately sources the Antarctic Bottom Water (Rintoul et al., 1998; Jacobs et al., 2004; Meredith et al., 2013).

2.3 Wind conditions

The Adélie Land coast experiences the windiest conditions ever recorded on Earth through the presence of intense katabatic winds (Périard and Pettré, 1993) that are funneled by narrow glacial valleys close to the shoreline (Wendler et al., 1997). Although relatively strong winds (>10 m/s) blow widely between 65° and 225° at DDU, the station is characterized by a dominant and recurrent katabatic wind from 140°-180° (SE) coinciding with the maximum the wind speed (> 25 m/s) (Adolph and Wendler, 1995; Koning-Langlo et al., 1998). Such winds support the annual occurrence of polynyas in the region, such as the DDU Polynya (DDUP; 66.11°S–139.31°E), and are important in sea ice production leading to dense water formation in winter (Adolphs and Wendler, 1995; Massom et al., 1998; Arrigo and van Dijken 2003).

2.4 Sea ice conditions

In general, the sea ice melts every year between November/December and February/March, with sea ice concentrations greater than 80% in winter and dropping below 20% in summer (Arrigo and van Dijken, 2003). The Adélie Basin, and notably the core site (DDUT), experiences fast ice during the winter months that largely melts back to the coast during the summer season (Massom et al., 2003; 2009; Smith et al., 2011; Wang et al., 2014). At its maximum extent, the fast ice develops ~100 km offshore between the Dibble Ice Tongue in the west to the Adélie Bank in the east (Massom et al., 2009; Smith et al., 2011). From the early spring to autumn, unstable fast ice conditions, characterized by several fast ice breakouts and re-formations as a result of lack of anchor points, generally occur in the DDUT (Massom

et al., 2009; Smith et al., 2011), whereas the fast ice persists later in the season over the banks. A key factor of the formation, recurrence and persistence of this fast ice buttress, is the numerous grounded small icebergs on the Adélie and Dibble Banks that trap the passing pack ice and act as anchor points for fast ice formation (Massom et al., 2001; Giles et al., 2008; Smith et al., 2011), growing two ice promontories from either side of the core site. The presence of the fast ice buttress is therefore closely associated to the intense sea ice formation in the Mertz Glacier Polynya and westward advection within the EDW (Massom et al., 2009).

2.5 Atmospheric impacts on sea surface conditions

Sea ice cover in the area is subject to a strong interannual variability in terms of formation and retreat (Massom et al., 2009; Smith et al., 2011). Recent studies suggest the sea ice conditions are closely linked to fast-ice dynamics over the DDUT, which is largely depending to synoptic scale wind fields (Adolph and Wendler, 1995; Massom et al., 2003; 2009). Few studies have focused on the impacts of atmospheric and oceanic conditions on the regional sea ice. Most of these studies are either limited in time (Adolph and Wendler, 1995; Massom et al., 2009; Wang et al., 2014) or are too low in resolution to appropriately cover the Adélie Land region (Massom et al., 2013). In order to refine the relationships and response of sea-surface conditions to atmospheric forcing, Principal Component Analyses (PCA) were performed between seasonal meteorological parameters (Fig. 36; see section 3.4), recorded from AWS in the vicinity of DDU and satellite data over the core site (Fig. 37). Studying the seasonal lagged response between meteorological parameters is beyond the scope of this study, and would necessitate higher frequency analyses. We therefore restricted our investigations to the statistical relationships between parameters at the intra-seasonal scale.

2.5.1 Case A: Westerly winds dominated years

Overall, our observations suggest that years characterized by more westerly winds during spring-summer are associated with a delayed sea ice retreat over the DDUT (Suppl. Table 1; Suppl. Note 1). Heavier sea ice conditions and late sea ice retreat in the area are related to the southward migration of the Antarctic Circumpolar Trough, which induces a prevalence of a

westerly wind component (Heil et al., 2006; Parish and Bromwich, 2007; Massom et al., 2003; 2009; Wang et al., 2014). Westerly winds promote larger swells, advect pack ice into the region, and decrease the open water fraction (Massom et al., 2003; Heil et al., 2006; Smith et al., 2011; Wang et al., 2014; Zhai et al., 2015). However, while a more westerly wind regime retards the ice break-up, these warmer winds also delay sea ice formation and advance in autumn (Suppl. Table 1; Suppl. Note 1; Fig. 36). Heil et al. (2006) suggested that annual fast-ice duration will drastically reduce in the context of an increased cyclonicity. This phenomenon is particularly evident in autumn, as the young thin ice is easily removed during storms, delaying the sea ice advance and fast ice formation. Repeated removal of fast ice under strong cyclonic warm winds would further lead to thinning the ice cover and an overall increase in sea ice production and northward export (Heil et al., 2006).

2.5.2 Case B: Easterly winds dominated years

In contrast, during years that are characterized by stronger easterly winds during the spring-summer period, we observe a sea ice retreat earlier in the season (Suppl. Table 1; Suppl. Note 1). Massom et al (2009) have suggested that easterly winds promote the presence of pack ice in the region but also contribute to building a fast ice buttress over the banks. Persistence of fast ice promontories during the summer over the Dibble and the DDU banks, can in turn act as a barrier to westward sea ice advection and lead to the establishment of open water conditions over the DDUT, as observed in several locations off East Antarctica (e.g. MGP and Terra Nova Bay polynyas) (Arrigo and van Dijken, 2003; Massom et al., 2001; 2009; Campagne et al., 2015). In autumn, we observe colder easterly winds, which promote an early sea ice advance. In contrast to westerly winds (Heil et al., 2006), easterly winds tend to increase ice advection and icebergs in the area as observed for the spring-summer period, providing favorable conditions for the formation of thick fast ice and buttress earlier in the autumn.

2.5.3 Case C: The role of katabatics

Although our PCA suggest that sea ice concentration increase with an increasing wind direction, from southerly-dominated to westerly-dominated wind fields (see above), the relationship between atmospheric and sea surface conditions is not linear. Indeed, strong and persistent southerly (katabatic) winds break the fast ice and promote the formation of a coastal polynya despite a sizably reduced buttress (Massom et al., 2009; Riaux Gobin et al., 2013). Such polynya regime is however constrained to the coastline (Vaillancourt et al., 2003), implying that open conditions may not extent over the core site, where the pack ice would be present due to a reduced fast ice buttress.

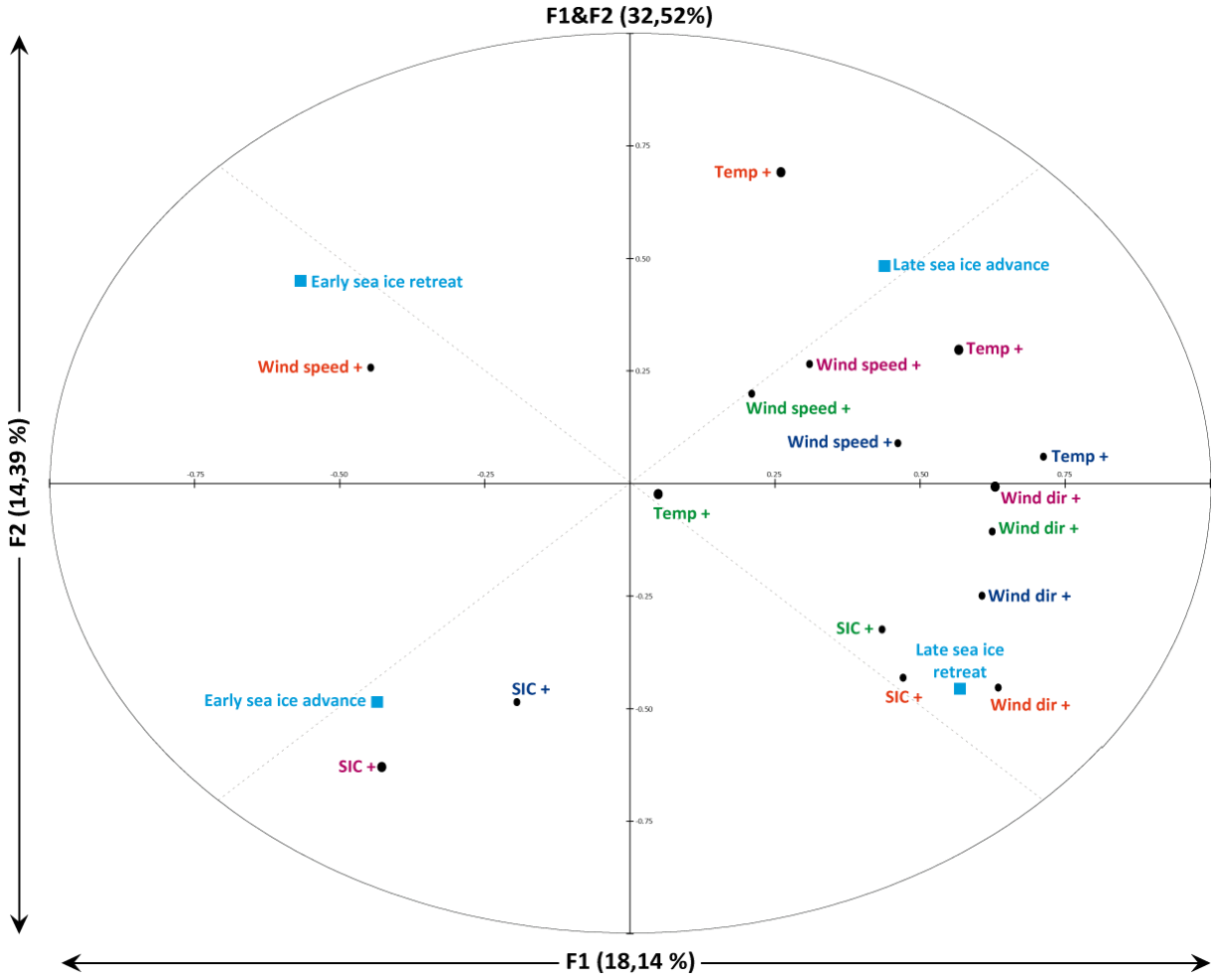

Figure 36. PCA seasonal data of weather forecast parameters. PCA on weather forecast and satellite data, that were previously seasonally averaged from June to August (dark blue), September to November (green), December to February (orange) and March to May (violet). Sea ice dynamics are

represented (in light blue): early/late-sea ice retreat and early/late-sea ice advance. A (+) or (-) symbols indicate the increase/decrease of the environmental parameters.

3 Material and methods

3.1 Core description and ^{210}Pb chronology

A 72.5 cm long interface core, DTCI2010, was retrieved aboard the R/V Astrolabe (66°24.68' S; 140°26.67' E; 1010 m water depth) during the 2010 ALBION-HOLOCLIP cruise. Positive X-ray images performed on the SCOPIX image-processing tool (Migeon et al., 1999) gave detailed information about sediment density and structure. SCOPIX images revealed laminations along the entire sedimentary section. The core was sampled continuously at 0.5 cm resolution and its chronological framework was determined based on ^{210}Pb excess ($^{210}Pb_{xs}$; $T_{1/2}$ = 22.3 years). The activities of ^{210}Pb and ^{226}Ra were measured on dried sediments by non-destructive gamma spectrometry using a well-type, high efficiency low background detector equipped with a Cryo-cycle (CANBERRA) (Schmidt and De Deckker, 2015). Activities are expressed in mBq g^{-1} and errors are based on 1 standard-deviation counting statistics. $^{210}Pb_{xs}$ was determined by subtracting the activity supported by its parent isotope, ^{226}Ra, from the total ^{210}Pb activity in the sediment. In the interface core DTCI2010, there is a general downcore trend in decreasing $^{210}Pb_{xs}$ activities, from 242 to 74 mBq g^{-1}, as expected due to the decay of the unsupported ^{210}Pb (Fig. 37). However, the observation of a layer where activities decrease slowly between 10 and 40 cm led us to retain the Constant Initial Concentration model (CIC; Robbins and Eglington, 1975) to calculate the age (t) of each measured horizon as: $t= (1/\lambda) \ln (A_0/A_z)$ where t and A_z are the age of the sediment and the excess ^{210}Pb activity at the depth z, A_0 is the activity at the surface and λ is the decay constant of ^{210}Pb. This choice is supported by the almost constant activities measured in the uppermost sediments of cores collected in 2003 (240 ± 13 mBq g^{-1}; Massé et al, 2011) and 2011 (253 ± 13 mBq g^{-1} in DTCI2011; Schmidt S., unpublished data). A second-order polynomial function was calculated from the 11 ^{210}Pb-dates obtained over the entire core to build the age model (Fig. 37).

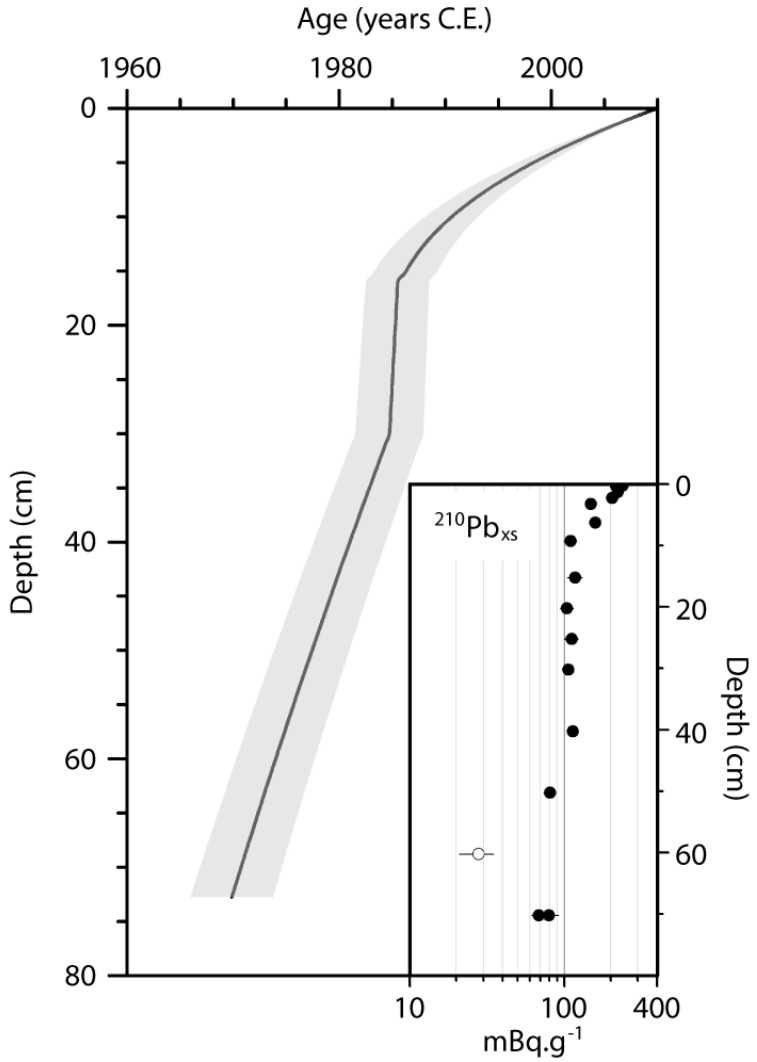

Figure 37. DTCI 2010 chronology. DTCI 2010 age model (dark line) based on 210Pb excess (210Pbxs) and associated age-model errors (grey area). The inset corresponds to the down core profile of 210Pbxs (error bars correspond to 1 SD).

3.2 Diatom analyses

Micropaleontological analyses were performed according to the methodology described in Crosta and Koç (2007) at a ~0.25 year resolution (every 0.5 cm) in core DTCI2010. Diatom slides were prepared from ~0.5 g of dry sediment. A few drops of the resulting residue suspended in distilled water were evaporated onto a coverslip, which was subsequently mounted on a glass slide with NOA61. Counts were performed under a microscope Olympus BH-2 at a magnification of x1000. For each sample, 300-350 diatom valves were counted and

data are presented as species relative abundances. Diatom identification was performed to the species or species group level. More details about slide preparation and diatom identification are available in Crosta et al. (2004). Nearly 70 diatom species were identified in down-core assemblages, from which 25 presented abundances higher than 2% of the total diatom assemblages.

3.3 Biomarker analyses

Biomarker analysis followed the technique described by Massé et al. (2011) and were also performed at a ~0.25 year resolution (every 0.5 cm) in core DTCI 2010. Briefly, an internal standard was added to 1g of the freeze-dried sediments, lipids were extracted using a Dichloromethane/Methanol mixture to yield a total organic extract (TOE), which was then purified using open column chromatography (silica). Hydrocarbons were analyzed using a Gas Chromatograph coupled to a Mass Spectrometry detector (GC-MS). More details about analytical parameters are available in Massé et al. (2011).

3.4 Instrumental data

Daily sea ice concentrations (SIC) for the time period 1978-2012 were obtained from the National Snow and Ice Data Center data repository. The dataset is based on passive microwave observations from the Nimbus-7 SSMR (1978-1987) and DMSP SSM/I (1987-2007) and SSMIS (2007-2012) radiometers processed with the NASA Team algorithm (Cavalieri et al., 1995) at a spatial resolution of 25x25 km. Averaged sea ice concentrations (SIC) were calculated over the core site in the central part of the DDUT (Suppl. Fig. 35). Daily measurements of wind direction (from 0 to 360°), velocity (m/s) and temperature (°C) for the time period 1956-2011 were obtained from the METEO France publithèque. The dataset is based on AWS at the DDU French station (66.7° S, 140° E), established on Petrel Island approximately 2 km offshore (Wendler et al., 1997) and 30 km from the core site. The dataset provides monthly statistics based on 6-hourly *in-situ* observations at 10 meters. Wendler et al. (1997) showed that from Penguin Point (east of the Mertz Glacier) to DDU

stations, meteorological parameters displayed similar variations, leading to the conclusion that measurements from AWS were relatively robust. For both, satellite and AWS datasets, monthly anomalies are expressed relative to the mean value calculated for each month over the 1979-2009 period. PCA between meteorological parameters (Fig. 36) were performed at seasonal scale, spring (September to November), summer (December to February), autumn (March to May) and winter (June to August), while PCA between sedimentary data and meteorological parameters were averaged over the November to March period (Fig. 40).

The sea ice retreat date was determined as the Julian day when the SIC (7 day average) dropped below 40%, while the sea ice advance corresponds to the day when SIC increased to above 40%. The duration of the ice-free season corresponds to the number of days per year during which SIC<40 %. Wind direction represents the origin of the wind over 360°. East/South/North/West -erly wind components indicate the number of days between November and March during which the wind blows from a selected direction. A ratio between easterly and southerly wind components (hereafter noted E/S; Fig. 42), and a ratio between northerly and westerly wind components (hereafter noted N/W; Fig. 42), were also calculated and used to account respectively of the dominant and the secondary wind directions in the region.

3.5 Principal Component analyses

Statistical analyses were run using the statistical software XLStat (Addinsoft). PCA and Pearson correlation tests (significance level α=0.05) were performed on 67 diatom species, 2 diatom specific biomarkers along with their associated ratio and on major elements to first (1) determine the relationships between species and identify potential diatom cluster (in order to increase the statistical weight of minor species) and (2) investigate the relationships between the different proxies in our study. The statistical analyses performed on all diatom species are presented in section 4.1 and in Supplementary Note 2, which includes the species accounting for less than 1% of the total diatom assemblage. In a second PCA, significant sedimentary data, in terms of population and ecological preferences, were interpolated at one year and compared with meteorological data to determine how phytoplankton was associated with selected environmental parameters. In parallel, PCA and the Pearson correlation test were

performed on seasonally averaged meteorological and satellite data, to support previous oceanographic and atmospheric observations about climate forcing and their environmental response in the area.

4 Results and Discussion

Several diatom species in polar and sub-polar marine environments exhibit a narrow range of environmental preferences, especially in terms of sea ice conditions. Diatom assemblages are therefore commonly used in association with geochemical proxies to infer past sea-surface conditions. The distributions of these proxies have been studied and validated at synoptic scale throughout the Southern Ocean (e.g. Gersonde et Zielinksi, 2000; Crosta et al., 2005; Armand et al., 2005) but less is known about the Antarctic Coastal and Continental Shelf Zone (CCSZ). Off the Adélie-Georges V Land, it has been suggested that diatom communities primarily respond to water column stability and sea ice conditions and dynamics which in turn respond to atmospheric and oceanic forcing (e.g. Beans et al., 2008; Riaux Gobin et al., 2005; 2013). In section 4.1, we refine the use of diatoms and geochemical proxies off Adélie Land by statistically comparing their downcore abundances in DTCI2010. In section 4.2, we study their relationships and response to regionally monitored environmental parameters. In section 4.3, we discuss the relevance of our proxies as potential environmental indicators for paleoclimate reconstructions, by interpreting the evolution of our results over 40 years of instrumental records.

4.1 Relationship between sedimentary proxies

The first PCA (Fig. 38) includes all diatom species and geochemical proxies in order to observe their relationships and identify diatom clusters as groups of species having similar records in core DTCI2010. Cluster composition is based on significant coefficient correlation between the diatom species (see section 3.5) combined to their known ecological preferences in the literature. Clusters allow the use of low abundance species (<2%; represented in grey on the first PCA; Fig. 38) that may bear important ecological signatures but cannot be used

alone as environmental indicators. Only significant Pearson correlation coefficients are detailed in the following section. High level but non-significant Pearson coefficients are mentioned as strong relationships. Hereafter, we focus on the main proxies, in terms of abundances and ecological preferences. Results are summarized and presented in Table 1, and information on secondary proxies can be found in Supplementary Note 2.

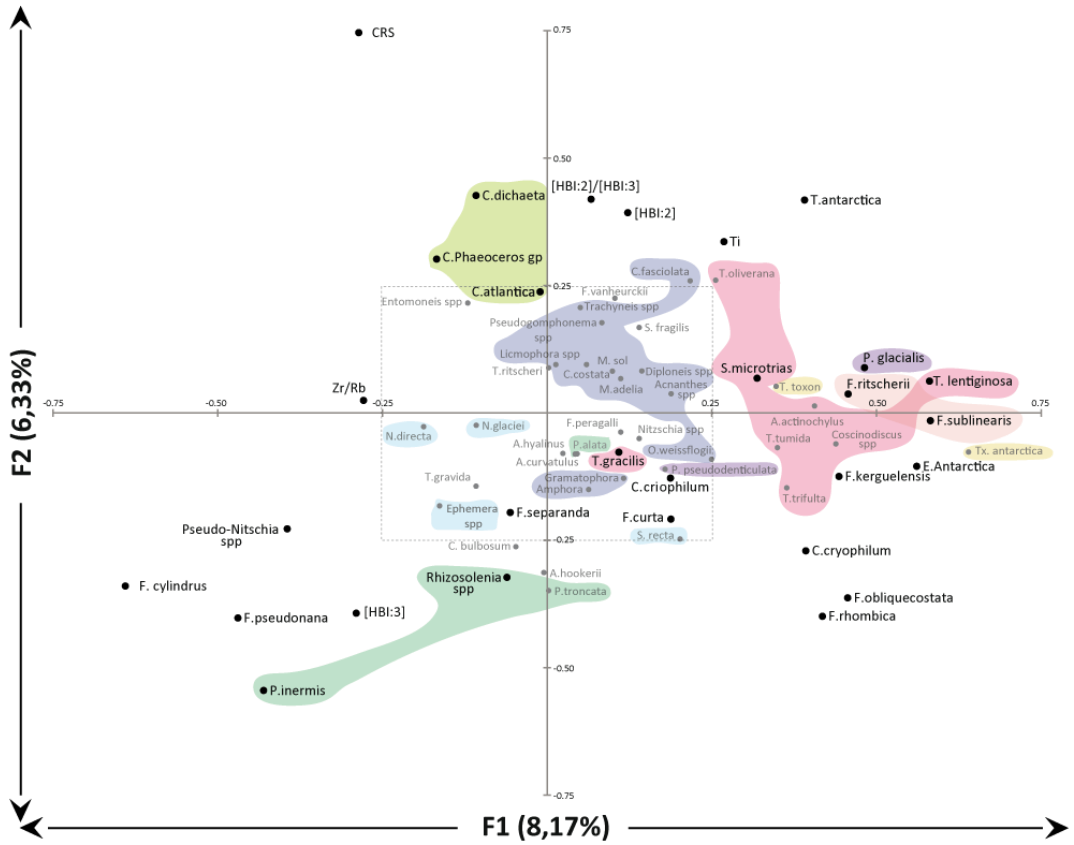

Figure 38. PCA on sedimentary raw data from the DTCI 2010 core. Shaded areas represent diatom clusters, based on significant correlation between species (Suppl. Table 2): open water gp (red); benthic diatom group (dark blue); sea ice diatom group (light blue); *Porosira* gp (violet); *Rhizosolenia* gp (dark green); *Thalassiothrix* gp (yellow); *Fragilariopsis* summer group (orange); *Chaetoceros Phaeoceros* gp (light green). Abundant species (relative abundance>2%) are written in black, unrepresentative species (relative abundance<2%) are written in grey.

4.1.1 Sea ice related proxies

Antarctic sea ice diatom assemblages are largely represented by *Fragilariopsis* species with *F. curta* and *F. cylindrus* being the dominant taxa. Sediment trap studies indicate that relative

abundances of the two species in the phytoplankton increase southward with increasing sea ice cover and decreasing temperature (Gersonde and Zielinski, 2000) with highest occurrences in stratified, ice melt influenced waters (Kang and Fryxell, 1992). This distribution is reflected in surface sediments. Highest abundances of *F. curta* occur in locations that experience 9–11 months/yr of sea ice cover, with highly consolidated ice conditions (65– 90%) during winter, while *F. cylindrus* optimum is at 8.5 months/yr and 70-90% of winter sea ice concentration (Armand et al., 2005). In the study area, investigation of the sediment microstructure demonstrates highest abundances of *F. curta* and *F. cylindrus* at the beginning of the annual couplet indicating an early growth phase and subsequent deposition (Maddison et al., 2006; Denis et al. 2006). As such, *F. curta* and *F. cylindrus* along with *F. vanheurckii* were often considered as indicators of heavy sea ice cover in several paleoclimate studies (Barcena et al., 2002; Barbara et al., 2010), notably in our region (Crosta et al., 2007; Denis et al., 2010). *Fragilariopsis cylindrus* and *F. curta* are among the most abundant species in DTCI2010, while *F. vanheurckii* is not significant in our dataset and is not discussed hereafter (Fig. 38; Suppl. Table 2). *Fragilariopsis cylindrus* is located in the F1-&F2- quarter (Fig. 38), and displays a significant negative correlation with *F. kerguelensis* (-0.432; Suppl. Table 2) and diatoms of clusters 4 and 6 (e.g. *T. lentiginosa*, -0.378; Suppl. Table 2). However, *F. cylindrus* is also negatively and significantly correlated with *F. curta* (-0.306; Suppl. Table 2). *Fragilariopsis curta* is located on F1+&F2- axes and is not significant (<0.25) neither on F1 nor F2, suggesting this species is poorly sensitive to changes in the main environmental parameters at that timescale (Fig. 38). Large changes in environmental conditions are probably necessary to induce a sedimentary response of *F. curta*.

Few marine and freshwater diatoms belonging to *Haslea*, *Navicula*, *Pleurosigma* and *Rhizosolenia* genera were recently found to be synthesizing Highly Branched Isoprenoids (HBI) (Sinninghé et al., 2004; Massé et al., 2011). A di-unsaturated isomer [HBI:2] has been identified in Antarctic sea ice and isotopic analyses provide evidence for that this isomer is synthesized by sea ice dwelling diatoms, while a tri unsaturated isomer [HBI:3] is synthesized by phytoplankton diatoms (Collins et al., 2013). In Adélie Land, relatively high concentrations of [HBI:2] have been found to occur during the spring sea ice melt (Massé et al., 2011). Recent studies have proposed the use of [HBI:2] and/or [HBI:2]/[HBI:3] to reconstruct variations of Holocene Antarctic sea ice duration as a complementary approach to diatom counts (Denis et al., 2010; Collins et al., 2013). More regionally, Campagne et al.

(2015) built on the co occurrence of [HBI:2] and *F. cylindrus* to infer periods of heavier sea ice conditions over the last 250 years in Commonwealth Bay. [HBI:2] and [HBI:2]/[HBI:3] are both located in the F1+&F2+ quarter, opposite [HBI:3] (Fig. 38), which agrees with the literature. However, [HBI:2] is significantly correlated with Ti (0.372; Suppl. Table 2) and *T. antarctica* (0.218; Suppl. Table 2), and does not show any relationships with the *Banquisia* gp or *F. cylindrus*, unlike observations at longer timescales (e.g. Denis et al., 2010; Etourneau et al., 2013; Collins et al., 2013; Campagne et al., 2015). These results may suggest that [HBI:2] respond to different sea ice conditions than sea-ice related diatoms at the seasonal-annual scale, possibly because of different origin of production. However, differential export towards the sediment may also account for the observed differences (Collins et al., 2013).

Thalassiosira antarctica is mainly present in stratified Antarctic inshore waters (Johansen and Fryxell, 1985). In the Weddell Sea, *T. antarctica* blooms are observed in newly formed platelet ice in polynyas and in crack pools formed by disintegrating sea ice during summer (Gleitz et al., 1996). *Thalassiosira antarctica* is closely related to sea ice formation and/or breakup, as it blooms in open waters during summer-autumn, and produces resting spores (RS) at the end of the growing season when sea ice returns (Cunningham and Leventer, 1998; 1999). Taylor (1999) suggests that the formation of *T. antarctica* spores could be triggered by the low light intensities that occur beneath developing pack and platelet ice. Reduced wind mixing below the sea ice may also induce spore formation (Taylor et al., 2001). *Thalassiosira antarctica* RS, the main form encountered in sediments, is most abundant in regions where sea ice is present for at least 6 months/year, and is believed to be induced under nutrient-stressed conditions or low light intensities (Armand et al., 2005). To note that the lower threshold of 6 months/yr is attributable to the warm variety thriving in the northern Antarctic Peninsula (Taylor and McMinn, 2001), whereas the cold variety occurs mainly in southern Antarctic Peninsula and coastal Antarctic zones where sea ice duration is above 8 months per year (Denis et al., 2006; Maddison et al., 2012). In DTCI2010, most valves were thus *T. antarctica* RS variety T1. In the Holocene sediment in the region, *T. antarctica* RS were found to co-occur with several large centric diatom species and *F. kerguelensis* (e.g. Denis et al., 2006). *Thalassiosira antarctica* were found to share globally similar sea surface temperature, sea surface salinity, sea ice proximity preferences and similar seasonal occurrences with *Porosira glacialis* (Pike et al., 2009). On the PCA, *T. antarctica* (here as RS of the cold form) is located in the F1+&F2+ axes (Fig. 38). The species shows significant

positive correlation with large centric diatoms (e.g. *Thalassiosira lentiginosa*: 0.266; *Thalassiosira oliverana*: 0.280; Suppl. Table 2) and higher correlation with *P. glacialis* (0.356; Suppl. Table 2), in line with previous studies.

The *Porosira* group is composed of *P. glacialis* and *P. pseudodenticulata*. *Porosira glacialis* is associated to cold coastal waters adjacent to sea ice (Taylor et al., 1997; Zielinski and Gersonde, 1997). It has been observed in waters with high concentrations of slush and wave-exposed shore ice (Krebs et al., 1987). *Porosira pseudodenticulata* is commonly observed in pack ice and fast ice. *Porosira* spp are known to survive environmental stress (nutrient depletion, prolonged periods of darkness) by forming resting spores (RS) at the end of the ice-free season (Taylor and McMinn, 2001; Cremer et al., 2003; Pike et al., 2009). These spores can be incorporated into waxing sea ice. As such, *Porosira* spp can be directly seeded from the sea ice during spring of the following year (Gleitz et al., 1996). *Porosira glacialis* is abundant in regions that experience at least 7.5 months per year of sea ice cover (slightly longer than *T. antarctica*), with 30% of summer sea ice concentration and highly compacted winter sea ice (65–85% concentration) (Armand et al., 2005). As for *T. antarctica*, *P. glacialis* RS sublaminae have been interpreted in Holocene laminated sediments in Adélie Land, indicating a late summer/autumn rapid deposition that is linked to early sea ice return (Maddison et al., 2006). *Porosira glacialis* and *P. pseudodenticulata* are respectively situated on the F1+&F2+ and F1+&F2- axes (Fig. 38). Pearson coefficient correlation between these two species is significant (0,252; Suppl. Table 2), arguing that both species can be grouped together in our study and confirming previous observations.

Other sea ice related proxies, the Banquisia gp (*Navicula directa*, *N. glaciei*, *Synedra* spp and *Ephemera* spp), *Fragilariopsis obliquecostata*, *Eucampia antarctica*, and the *Fragilariopsis* summer gp (*Fragilariopsis ritscheri* and *F. sublinearis*) are sometime used in the literature to infer past sea ice conditions but are not significant in our study and therefore are only discussed in Supplement Note 2.

4.1.2 Open ocean proxies

Fragilariopsis kerguelensis dominates phytoplankton assemblages of the open ocean zone south of the Polar Front where sea ice is absent during summer (Halse et al., 1969; Froneman et al., 1995) and thus characterizes open water conditions during summer. *Fragilariopsis kerguelensis* is observed in recent sediments of areas experiencing up to 8 months/yr of sea-ice cover (Crosta et al., 2005). In several paleoclimate studies (e.g. Crosta et al., 2008), notably from the area, *F. kerguelensis*, present an inverse relationship to sea ice and cold-water species. Summer-autumn laminae were found to present high occurrences of *F. kerguelensis*, along with *T. antarctica* and large centric species (Denis et al., 2006; Maddison et al., 2006). On the PCA, *F. kerguelensis* is located on the F1+&F2- (Fig. 38), and displays a significant positive correlation with several large centric diatoms (e.g. *T. lentiginosa*, 0.507; *T. antarctica*: 0.184; *P. glacialis*: 0.235; Suppl. Table 2), and a strong negative correlation with *F. cylindrus* (-0.432; Suppl. Table 2) and *Chaetoceros* RS (-0.248; Suppl. Table 2), in agreement with previous studies.

The Open Water group is composed of large centric diatoms. In general, species belonging to the genus *Thalassiosira* are most commonly found in areas experiencing open water conditions during the growing season (Johanssen and Fryxell, 1985). *Thalassiosira lentiginosa* and *T. oliverana* commonly occur in the Southern Ocean, south of the Polar Front, in areas characterized by permanent open ocean conditions (Johanssen and Fryxell, 1985). Relative abundances in sediment of *T. lentiginosa* show an inverse relationship with sea ice cover with high occurrences in areas experiencing between 0 and 4 month/yr of sea ice presence and a decline towards prolonged sea ice duration (Crosta et al., 2005). *Thalassiosira oliverana* is clearly dominant in locations where open ocean conditions occur close to the sea ice edge during summer (Crosta et al., 2005). For *Thalassiosira gracilis*, the distinction between the two varieties (*T. gracilis* var. *gracilis* and *T. gracilis* var. *expecta)* has not been performed in this study as this species presents low abundances in Antarctic coastal areas (Armand et al., 2005). In summer, the species appears most highly associated with conditions related to open-ocean conditions and its population diminishes in regions of unconsolidated sea ice (<40% concentration, SST below 2°C) (Crosta et al., 2005). *Actinocyclus actinochilus* has been observed with abundances over 2% (which is not the case in our study area) in regions where sea ice cover persists more than 7 month/yr (Armand et al., 2005). *Actinocyclus actinochilus* can be considered as a cold-water Antarctic species, and increasing sedimentary

abundances of this species are in line with an ice-free region during summer (<40% concentration) and a strongly compact sea ice covered region in winter (70–90% concentration) (Armand et al., 2005). *Coscinodiscus* is generally considered as an open water genus (Garrison and Buck, 1989; Moisan and Fryxell, 1993). High abundances of *Coscinodiscus* spp over the shelf were related to a southward influx of warm surface water (Taylor and Sjunneskog, 2002). *Stellarima microtrias* is reported as restricted to the Antarctic Zone south of the Polar Front (Zielinski and Gersonde, 1997). The species has been observed attached to sea ice in waters influenced by the ice (Hasle, 1988). *Stellarima microtrias* is rarely used in paleoenvironmental studies as its ecology is poorly documented, its ecological affinity is uncertain and its abundances are generally low (Taylor et al., 2001). *Thalassiosira tumida* has maximum occurrences south of the Polar Frontal Zone, and is most abundant during the austral summer (Cunningham and Leventer, 1998; Armand et al., 2005). Armand et al. (2005) indicate that maximum abundances of *T. tumida* occur in regions with low sea-ice cover during summer (open water conditions). Finally, Armand et al. (1997) have suggested that *Thalassiosira trifulta* thrives in the coldest waters amongst the *Thalassiosira spp*. However, its overall low abundance precluded any use downcore alone. *Thalassiosira lentiginosa*, *T. oliverana*, *A. actinochilus* and *S. microtrias* are localized on F1+&F2+, and *T. trifulta*, *T. gracilis*, *Coscinodiscus* spp, *T. gracilis* and *T. tumida* are localized on F1+&F2- (Fig. 38). *Thalassiosira lentiginosa* exhibits significant positive correlation with *Coscinodiscus spp* (0,190; Suppl. Table 2), *T. oliverana* (0.251; Suppl. Table 2), *S.microtrias* (0.186; Suppl. Table 2), *A. actinochilus* (0.330; Suppl. Table 2) and *T. gracilis* (0.266; Suppl. Table 2). *Thalassiosira oliverana* also displays significant positive correlation with *A. actinochilus* (0.166; Suppl. Table 2), *T.trifulta* is significantly correlated with *Coscinodiscus spp* (0.174; Suppl. Table 2) and *T. gracilis* is correlated with *A. actinochilus* (0.218; Suppl. Table 2). *Coscinodiscus spp* exhibits a significant coefficient correlation with *A. actinochilus* (0.244; Suppl. Table 2) and *S. microtrias* (0.211; Suppl. Table 2). Strangely, *T. tumida* does not display a significant correlation with the species mentioned above despite being close to them in the PCA (Fig. 38). This species was therefore not included in the Open water group despite its distribution on the PCA and its documented ecological preferences. Our results show a significant positive correlation between *T. gracilis* (0.485; Suppl. Table 2) and *T. lentiginosa* (0.507; Suppl. Table 2) with *F. kerguelensis*, confirming grouping in previous studies (e.g. Crosta et al., 2008). As with other clusters cited above (e.g. cluster 4 & 5), it seems that the Open Water gp is also closely linked to the F1+ area in our analyses. We

thereby decided to not include *Asteromphalus hookeri* in the group despite the few correlations (Suppl. Table 2), as it seems to rather depend on F2 (Fig. 38). Additionally, *Thalassiosira ritscheri*, *Actinocyclus curvatulus* and *Asteromphalus hyalinus* are insignificant in the F1+ area (Fig. 38) and, since they do not present any significant positive correlation with the other species (Suppl. Table 2), we decided to remove them from the Open Water gp. *Thalassiosira gavida* also does not appear in this cluster as it is uncorrelated and positioned on the F1- area (Fig. 38). *Eucampia antarctica*, which is significantly correlated to species of the Open Water gp, was separated given its high abundance.

[HBI:3] is positioned in the F1-&F2- axes, opposite to [HBI:2] and [HBI:2]/[HBI:3] (Fig. 38). This suggests that the [HBI:2] and [HBI:3] are produced in contrasting environments, in agreement with previous studies that proposed the use of [HBI:2] and [HBI:3] to reconstruct variations of past sea ice cover as complementary sea ice proxy to diatom counts (Denis et al., 2010; Collins et al., 2013). Strangely, the Pearson correlation between [HBI:3] and [HBI:2] does not show any relationships in our PCA, (Suppl. Table 2). This could be caused by the variability of the sea ice seasonality in our study area whereby Collins et al. (2013) suggested that [HBI:3] and [HBI:2] showed that these biomarkers correlate most positively and, consequently, co-occurred during a period of low seasonal sea ice change, and were less positively correlated during a period characterized by high seasonal change. Therefore, it seems that both biomarkers have to be considered carefully when they are taken separately. PCA show [HBI:3] is significantly correlated with *Rhizosolenia* spp and *Proboscia inermis* (0.491 and 0.635 respectively; Suppl. Table 2), in agreement with Sinninghé et al. (2004) that found the [HBI:3] to be synthesized by the *Rhizosolenoids*. While the analysis of the hydrocarbon content of several temperate species belonging to the genus *Proboscia* did not reveal the presence of HBIs, the polar species *P. inermis* may be able to synthesize these compounds.

Titanium (Ti) is considered as an indicator of terrigenous inputs (Denis et al., 2006; Presti et al., 2011). In Antarctic coastal areas, delivery of terrigenous particles is possible via several dominant modes such as meltwater discharge, ice rafting, runoff from outlet glaciers, and although, considered negligible in coastal East Antarctic regions, eolian transport (Presti et al., 2003; Escutia et al., 2003; Denis et al., 2006). In the literature, Ti content is used to infer past changes in terrigenous supply to the ocean and associated to open conditions (Denis et al., 2006; Campagne et al., 2015). Therefore, Ti is an indicator of enhanced melting period

over the ice-free season. In our data, Ti is located in the F1+&F2+ area (Fig. 38), and displays high significant positive correlation with some open water taxa, e.g. *F. kerguelensis* (0.248; Suppl. Table 2), *P. glacialis* (0.228; Suppl. Table 2) and *T.antarctica* (0.238; Suppl. Table 2), in line with previous studies. In the same way, Ti presents significant negative correlations with *F. cylindrus* (-0.283; Suppl. Table 2). Unexpectedly, Ti also shows significant negative correlations with [HBI:3] (-0.218; Suppl. Table 2) and positive correlations with the [HBI:2] (0.372; Suppl. Table 2).

Variations in the relative abundances of Zirconium (Zr) and Rubidium (Rb) content provide an estimate of the variations in sediment grain size, where Zr represents the coarsest sediment fraction and Rb the finest (Dypvik et al., 2001). In the Weddell Sea and in the Mertz Depression, recent studies have proposed the Zr/Rb ratio as an indicator for enhanced bottom water formation and increased (coarser) sediment transport due and intensification of convective current during periods of intense sea ice formation and brine rejection (Sprenk et al., 2014; Campagne et al., 2015). Zr/Rb is located on F1-&F2+ axes (Fig. 38), and displays highly significant negative correlations with some open water taxa, e.g. *P. glacialis* (-0.193; Suppl. Table 2), *T. antarctica* (-0,188; Suppl. Table 2) and *F. kerguelensis* (-0,176; Suppl. Table 2), coherent with the use of the ratio.

Other open water related proxies, the *Rhizosolenia* gp (*Rhizolenia* spp and *Proboscia* spp), the *Thalassiothrix* gp (*Thalassiotrix antarctica* and *Trichotoxon reinboldii)* and *F. rhombica*, are discussed in Supplement Note 2.

4.1.3 Surface water stratification and wind conditions related proxies

Vegetative cells of *Chaetoceros Hyalochaete* are often observed in high abundances within the surrounding pack ice waters (Gleitz et al., 1998) and are abundant in Adélie Land surface waters (Beans et al., 2008). High nutrient content in surface waters, surface water stratification by sea ice meltwater and stabilization by low wind intensity appear to be the most important factors for the development of *C. Hyalochaete* blooms (Leventer, 1991; Leventer, 1998). It has been suggested that resting spore formation occurs when the bloom begins to decline as a response to decreasing nutrient levels, low light levels during vertical

mixing of the water column or as a result of reduced seasonal insolation during the autumn (Hollibaugh et al., 1981). Nutrient depletion in highly stratified surface waters, as a result of both meltwater input and thermal warming (Leventer, 1991), is probably the main trigger for spore formation. Highest sedimentary abundances of CRS (>80%) occur in the Antarctic Peninsula with ~7 months/year sea ice cover (Armand et al., 2005). In Holocene sediment, high relative abundances of CRS are commonly used to track high productivity events and strongly stratified surface waters at the receding sea-ice edge (Leventer et al., 1996; Denis et al., 2006; Leventer et al., 2006). *Chaetoceros Hyalochaete* vegetative cells were here counted with CRS, as they are generally present in low abundance in Antarctic sediments. CRS is significantly located on the F1-&F2+ area in our PCA, strongly separated from other diatom species (Fig. 38). CRS display numerous negative significant correlation with both sea ice associated and open ocean associated species (e.g. *F. curta, F. cylindrus, F. rhombica, F. kerguelensis, Chaetoceros cryophilum;* Suppl. Table 2).

Other wind and stratification condition related proxies such as the *Chaetoceros Phaeoceros* (*Chaetoceros dichaeta and C.cryophilum*), the Benthic gp (*Cocconeis* spp, *Grammatophora* spp, *Trachyneis* spp, *Licmophora* spp, *Melosira sol* and *M. adelia*, *Achnantes brevipes*, *Amphora* spp, *Diploneis* spp, *Pseudogomphonema* spp, *O. weissflogii* and *Corethron* spp are discussed in Supplement Note 2.

4.2 Relationship between sedimentary proxies and instrumental data

Environmental parameters were averaged over the ice-free season (from November to March) to allow a direct comparison of the impact of atmospheric and sea surface conditions on sedimentary response, and by inference, biological surface response. Although the standardization partially hid the variability of our sedimentary signals (Suppl. Fig. 36), the main characteristics are preserved and allow for interannual comparisons. Results are summarized and presented in Table 3. Hereafter, we use the main diatom species and species groups along with geochemical proxies identified in the previous PCA (Fig. 38).

4.2.1 Axis interpretation

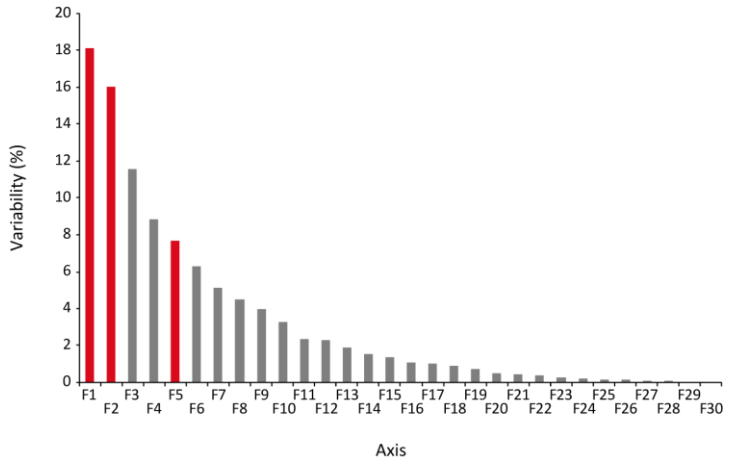

Figure 39. Axis contribution to the total variability, from PCA on standardized sedimentary and meteorological parameters.

On both PCA (Fig. 40) enhanced sea ice concentrations (SIC) and late sea ice retreat are located on F1-, along with late sea ice advance, which is insignificant (Fig. 40). In contrast, a longer ice-free season is significantly located on F1+ (Fig. 40). F1 axis, which represents the highest variance of 18.09 % (Fig. 39), represents sea ice conditions from November to March. As expected, the length of the ice-free season and SIC are strongly linked with sea ice cover dynamics. Pearson correlations indicate that early sea ice retreat and delayed sea ice advance are associated with decreasing SIC and a longer ice-free season, and *vice versa* (Suppl. Table 3). The easterly wind direction is significant on F1+ while the southerly wind component is significantly located on F1- (Fig. 40a; Suppl. Table 3), indicating that sea ice conditions off Adélie Land respond to the dominant wind field. Indeed, our data indicate that more easterly winds are associated to both earlier sea ice retreat and earlier sea ice advance, whereas more southerly winds are linked to later sea ice retreat and later sea ice advance (Suppl. Table 3), in line with section 2.5 (Cases B and C respectively). The length of the ice-free season does not show any relationship with atmospheric parameters but mainly depends on the timing of sea ice retreat (Suppl. Table 3), whereby earlier opening would lead to longer open season.

F2 axis accounts for 16 % of the total variance (Fig. 39). Westerly and northerly wind directions are significantly located on F2- and F2+, respectively, with very low scores on F1 (Fig. 40a; Suppl. Table 3). Westerly and northerly winds further display high positive

relationships with the timing of the closing date, but show no links with the opening date. They also show negative relationships with the wind speed (Fig. 40b; Suppl. Table 3). These results indicate that westerly and northerly wind fields generate delayed sea ice advance in autumn. The westerly wind component is associated with southerly winds and low temperatures (Suppl. Table 3). Increasing wind direction (southerly to westerly winds) or weak onshore (northerly winds) circulation is of cyclonic origin in our study area (section 2.5, Case A). This result suggests that storm forcing on sea ice conditions are represented by the F2 axis. Additionally, the wind speed parameter seems to be closely associated to the F5 axis (Fig. 40b) and represents a lower contribution of 7.65 % (Fig. 39).

These results agree well with the PCA between seasonal atmospheric forcing and sea ice conditions over the core site depicted in section 2.5, and with several studies at larger spatial scales (Massom et al., 2003; 2009; Smith et al., 2011; Wang et al., 2014; Campagne et al., 2015) which argue that wind conditions, and particularly wind direction, exert a strong impact on sea surface conditions off Adélie Land.

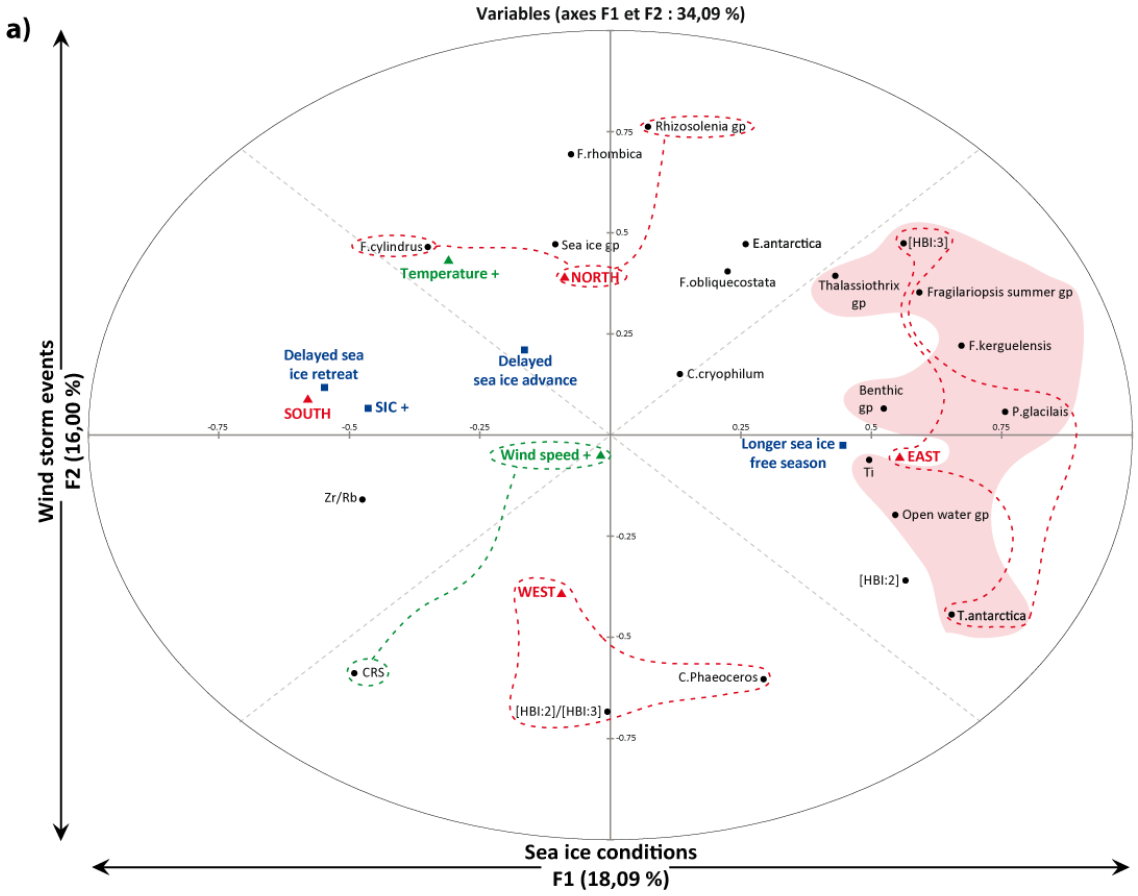
a)
Variables (axes F1 et F2 : 34,09 %)
Wind storm events
F2 (16,00 %)
Sea ice conditions
F1 (18,09 %)
Rhizosolenia gp
F.rhombica
F.cylindrus
Sea ice gp
E.antarctica
[HBI:3]
Temperature +
NORTH
F.obliquecostata
Thalassiothrix gp
Fragilariopsis summer gp
Delayed sea ice retreat
Delayed sea ice advance
F.kerguelensis
C.cryophilum
Benthic gp
P.glacilais
SOUTH
SIC +
Longer sea ice free season
EAST
Wind speed +
Ti
Zr/Rb
Open water gp
[HBI:2]
WEST
T.antarctica
CRS
C.Phaeoceros
[HBI:2]/[HBI:3]

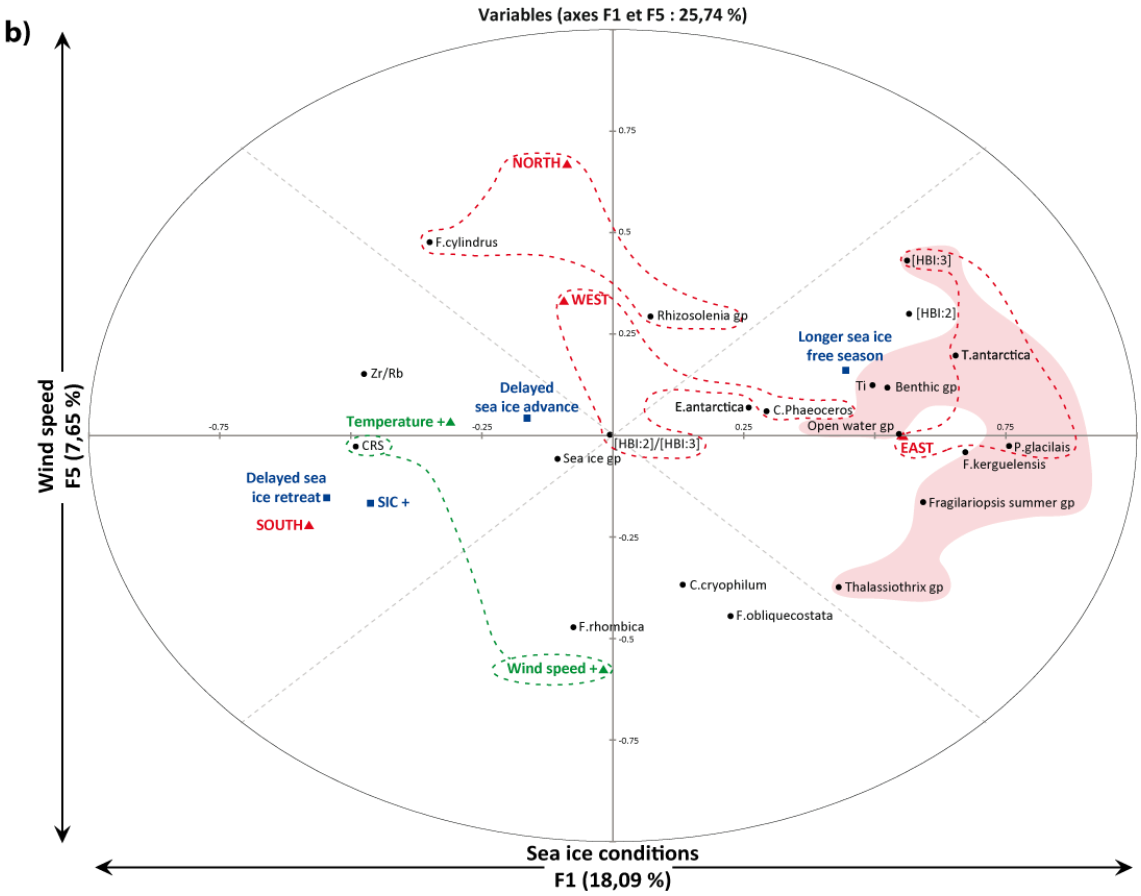
b)
Variables (axes F1 et F5 : 25,74 %)
Wind speed
F5 (7,65 %)
Sea ice conditions
F1 (18,09 %)
NORTH
F.cylindrus
[HBI:3]
WEST
[HBI:2]
Rhizosolenia gp
Longer sea ice free season
T.antarctica
Zr/Rb
Ti
Benthic gp
Delayed sea ice advance
E.antarctica
C.Phaeoceros
Temperature +
Open water gp
[HBI:2]/[HBI:3]
EAST
P.glacilais
CRS
Sea ice gp
F.kerguelensis
Delayed sea ice retreat
SIC +
Fragilariopsis summer gp
SOUTH
C.cryophilum
Thalassiothrix gp
F.obliquecostata
F.rhombica
Wind speed +

Figure 40. PCA on standardized sedimentary and meteorological parameters. PCA on sedimentary standardized data from the DTCI 2010 core, combined with environmental parameters. The yearly standardized data sedimentary data representing the ice-free season of the related year, and weather forecast/satellite data were averaged between November and March. a) F1 axis represents the sea ice conditions (blue square): opening, closing and SIC linked to the main wind direction (in red triangle): East and South winds. F2 axis represents the secondary wind direction in the study area (in red triangle): North and West winds. Additional parameters such as wind speed and temperature (green triangle) are also represented. Red shaded areas represent the open water diatom assemblages, based on significant correlation between species (Suppl. Table 3). Dotted lines represent a positive correlation between sediment proxies and environmental parameters. b) F1 axis represents the sea ice conditions (blue square): opening, closing and SIC linked to the main wind direction (in red triangle): East and South winds. F5 axis represents the wind speed (green triangle). Secondary wind directions such as North and West winds (in red triangle) and temperature (in green) are also represented. Red shaded areas represent the open water diatom assemblages, based on significant correlation between species (Suppl. Table 3). Dotted lines represent positive correlation between sediment proxies and environmental parameters.

4.2.2 Sedimentary response

a Westerly winds increase spring sea ice conditions (Case A; section 2.5)

A dominant westerly wind component originating from enhanced cyclone activity conducts to lower temperatures and wind speed in our data (Suppl. Table 3). Westerly winds have been observed to promote pack ice or thinner sea ice lasting longer in spring (see section 2.5) and delayed sea ice advance in autumn in our study area (Suppl. Table 3). Under such conditions, the sedimentary response shown by the PCA indicates increased an abundance of [HBI:2]. Indeed, [HBI:2]/[HBI:3] (0.398; Suppl. Table 3) is significantly correlated with westerly winds and presents a strong negative relationship with low temperature in our data (Fig. 40). Similar environmental relationships are observed for [HBI:2] (Fig. 40), agreeing with the environmental interpretation of [HBI:2] as a sea ice indicator.

b Northerly winds increase spring sea ice conditions (Cases A or B; section 2.5)

At the Antarctic scale, northerly winds promote early spring sea ice retreat and late autumn sea ice advance (Stammerjohn, et al., 2008). Northerly winds in our study area have been observed to decrease northward transport of sea ice (Holland et al., 2012). Our PCA results (Fig. 40) indicate that the northerly wind component is associated with lower wind speeds

conducive to delayed sea ice advance at the core site (see section 4.2.1), but relationships with SIC and sea ice retreat date are not clear in our data. We propose that northerly winds have two opposite impacts on sea ice conditions off Adélie Land. First, they tend to increase spring sea ice presence in the area, likely by pushing the offshore pack ice toward the coast. Secondly, they contribute to increased summer melting and limit ice growth in autumn by transporting warm air from the north and by enhancing the swell. Under such environmental conditions, the sedimentary response shown by the PCA indicates concomitant increasing abundances of the *Rhizosolenia* gp, [HBI:3], *F. cylindrus* and *E. antarctica*, that have high scores on F2+ (Fig. 40a). The concomitant presence of sea ice related proxies and open ocean proxies indicate a marked seasonal cycle. *Fragilariopsis cylindrus* displays a strong association with high temperature in our study area, but present a non-significant positive relationship with SIC (Suppl. Table 3). These results may indicate that this species would respond to heavier pack ice conditions in spring and subsequent melting. Similarly, *E. antarctica* is strongly related to northerly winds through later sea ice retreat and shorter ice free season in our data (Fig. 40; Suppl. Table 3). The presence of [HBI:3], a marker of open water related productivity, along with *Rhizosolenia* gp, an indicator of warmer conditions and of a long diatom productivity season (see section 4.1.1), would support the presence of stable sea surface conditions due to longer melting conditions during spring-summer and with enhanced open water conditions in autumn.

c Easterly winds induce open conditions (Case B; section 2.5)

A dominant easterly wind component yields to earlier sea ice retreat and earlier sea ice advance, less SIC from November to March, and in some extent to a longer ice free season in the study area. Under such environmental conditions, the PCA indicates that the sedimentary response consists of higher abundances of several proxies strongly linked to F1+, *Thalassiotrix* gp, *T. antarctica*, *P. glacialis*, *F. kerguelensis*, *Fragilariopsis* summer gp, the Benthic gp, [HBI:3] and Ti (red shaded area on Fig. 40). As they are closely positioned on F1+, these diatom species/gp and geochemical proxies display a strong positive intercorrelation (Suppl. Table 3) as well as being correlated with the easterly wind component. The Ti signal is also highly linked to the northerly wind component (Suppl. Table 3), suggesting that this proxy is tied to onshore/westward wind circulation and probably responds to longer ice–free season. *Thalassiotrix* gp, *T. antarctica*, *P. glacialis*, *F. kerguelensis* and Ti are strongly linked to low SIC over the ice free season in our study area

(Suppl. Table 3). Similarly, [HBI:3], *P. glacialis* (-0.431; Suppl. Table 3), *F. kerguelensis* (-0.360) and *T. antarctica* are strongly associated with earlier open water conditions, and *F. kerguelensis* is linked to a longer ice-free season. Open water gp, *C. cryophilum*, *F. kerguelensis*, Ti and [HBI:3] are highly associated with ice free seasons characterized by weak winds, suggesting that these species prefer more stable environments. However some differences also appear in the environmental response of these proxies. While the *Thalassiotrix* gp is strongly linked with more open conditions in autumn, *P. glacialis* and *T. antarctica* are, contrastingly, associated with an earlier sea ice advance and lower temperature (Fig.40; Suppl. Table 3). These results agree well with ecological preferences of *P. glacialis* and *T. antarctica*, which are considered as biological indicators of early sea ice conditions in autumn. However, in our study *P. glacialis* is linked to a longer ice free season, contrary to *T. antarctica (*(Fig.40; Suppl. Table 3). These results contradict paleoecological inferences on these species whereby *P. glacialis* has been associated with areas experiencing a slightly longer annual sea ice cover relative to *T. antarctica* (Armand et al., 2005; Pike et al., 2009), maybe because these studies did not separate the two varieties of *T. antarctica*.

Our results are generally in line with the known ecology of this geochemical and diatom assemblage (section 4.1.1). Several of these proxies are associated with enhanced open conditions during the ice free season in the area. Indeed, increasing abundances of *T. antarctica*, *F. kerguelensis, P. glacialis*, large centric diatoms that constitute the Open water gp, [HBI:3] and Ti have been attributed to more open conditions in the Mertz Glacier Polynya area, during periods with reinforced easterly wind conditions (Campagne et al., 2015). This sedimentary assemblage that is associated to an easterly wind promoting open water conditions may therefore reflect the development of the DDU polynya (Arrigo et al. 2003) during the early spring-summer period in the study area.

d Katabatic winds and coastal polynya (Case C; section 2.5)

A dominant southerly wind component is conducive to a delayed spring sea ice retreat and late autumn freezing, higher SIC from November to March, and to some extent, a shortened ice free season in the study area (section 4.2.1). Strong southerly winds (katabatic) produce open water conditions near the coast but not necessarily at the core site. Southerly winds allow more fast ice to be transported northward of the core site (section 2.5) by restoring the eastward drift of the pack ice. Under such environmental conditions, the sedimentary response

shown by the PCA indicates increasing abundances of CRS and Zr/Rb that are strongly linked to F1- (Fig. 40a). Their response to katabatic wind events is probably through the opening of the coastal polynya (section 2.5). In addition, although CRS shows no relation with SIC parameters, this group is associated to a strong wind speed (0,364; Suppl. Table 3) over the ice-free season, in agreement with the environmental interpretation of the species (section 4.1). In contrast, Zr/Rb is closely associated with increasing SIC over the ice-free season in addition to a delayed sea ice retreat (Suppl. Table 3).

Enhanced polynya activity along the coast has been shown to coincide with deep mixed layer and high Chl a levels (Vaillancourt et al., 2003; Riaux Gobin et al., 2013). Stronger vertical mixing may increase nutrient availability; favoring the rapid development of *Hyalochaete* spp. Spore formation may occur through deep mixing of vegetative cells under the photic zone or nutrient depletion when winds weaken. Northward lateral advection of surface production from the coast to the study area may explain the occurrence of CRS along with more sea ice at the core site. Continuous sea ice formation in the coastal polynya may have favored brine production and subsequently, stronger bottom currents, leading to the observed Zr/Rb values.

4.3 Which proxies and environmental interpretations for long term reconstructions

We here discuss the relevance of our results as proxies for long term reconstructions, by commenting on their co-occurrence with environmental parameters over the last 40 years.

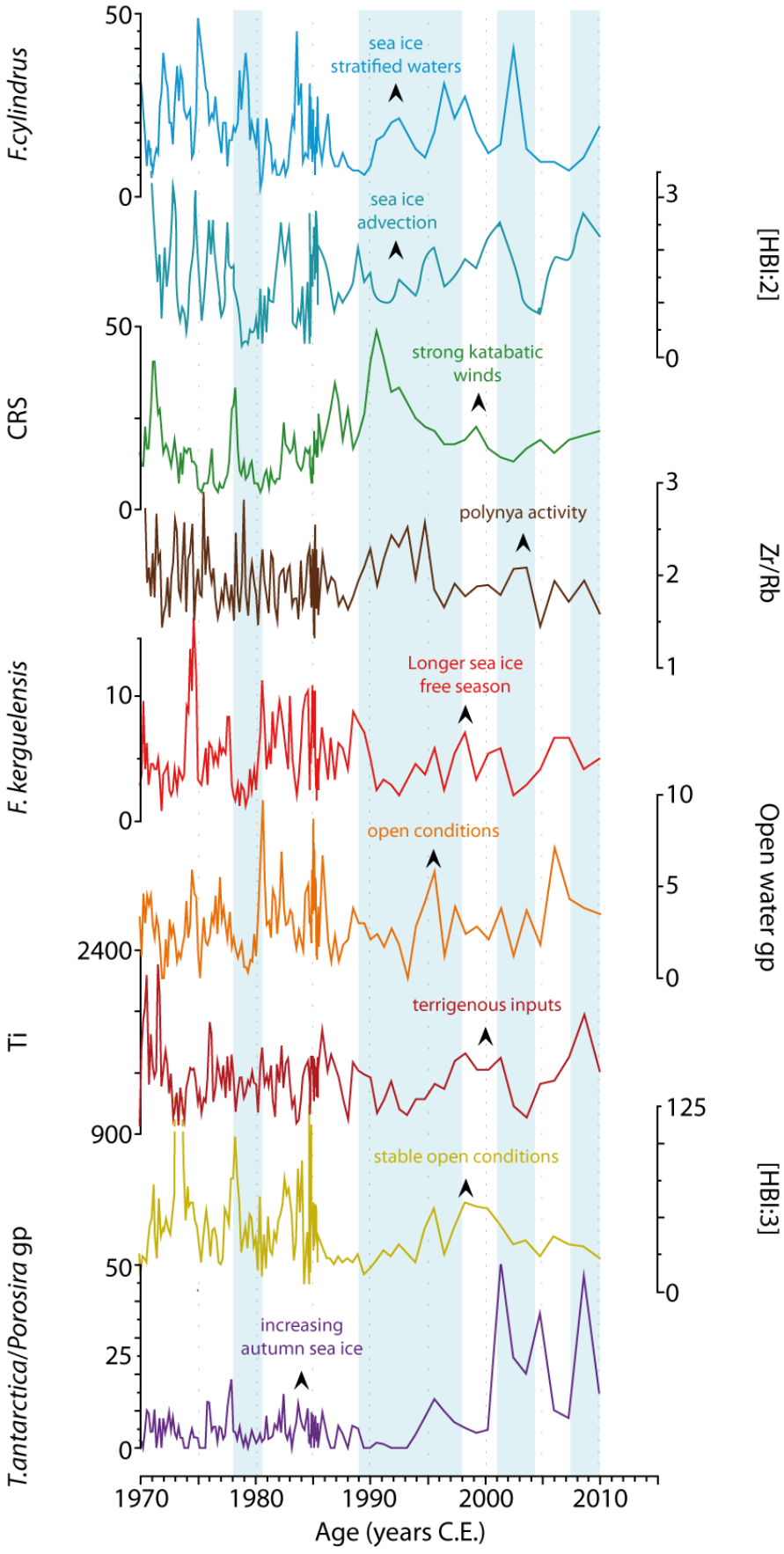
F.cylindrus
sea ice
stratified waters
sea ice
advection
[HBI:2]
CRS
strong katabatic
winds
polynya activity
Zr/Rb
F. kerguelensis
Longer sea ice
free season
open conditions
Open water gp
Ti
terrigenous inputs
stable open conditions
[HBI:3]
T.antarctica/Porosira gp
increasing
autumn sea ice
Age (years C.E.)

Figure 41. Raw sedimentary records from DTCI 2010 interface core over the 1970-2010 period. Relative abundances of *Fragilariopsis cylindrus* (blue), concentrations of [HBI:2] (greenish blue), relative abundances of *Chaetoceros Hyalochaetes* resting spores (CRS; green), the Zirconium/Rubidium ratio (Zr/Rb; brown), *Fragilariopsis kerguelensis* (red), open water group (orange), Titanium levels (Ti; reddish brown), concentrations of [HBI:3] (yellow) and *Thalassiosira antarctica/Porosira* gp ratio (violet). The blue shadings indicate periods marked by increasing sea ice concentration at the core site.

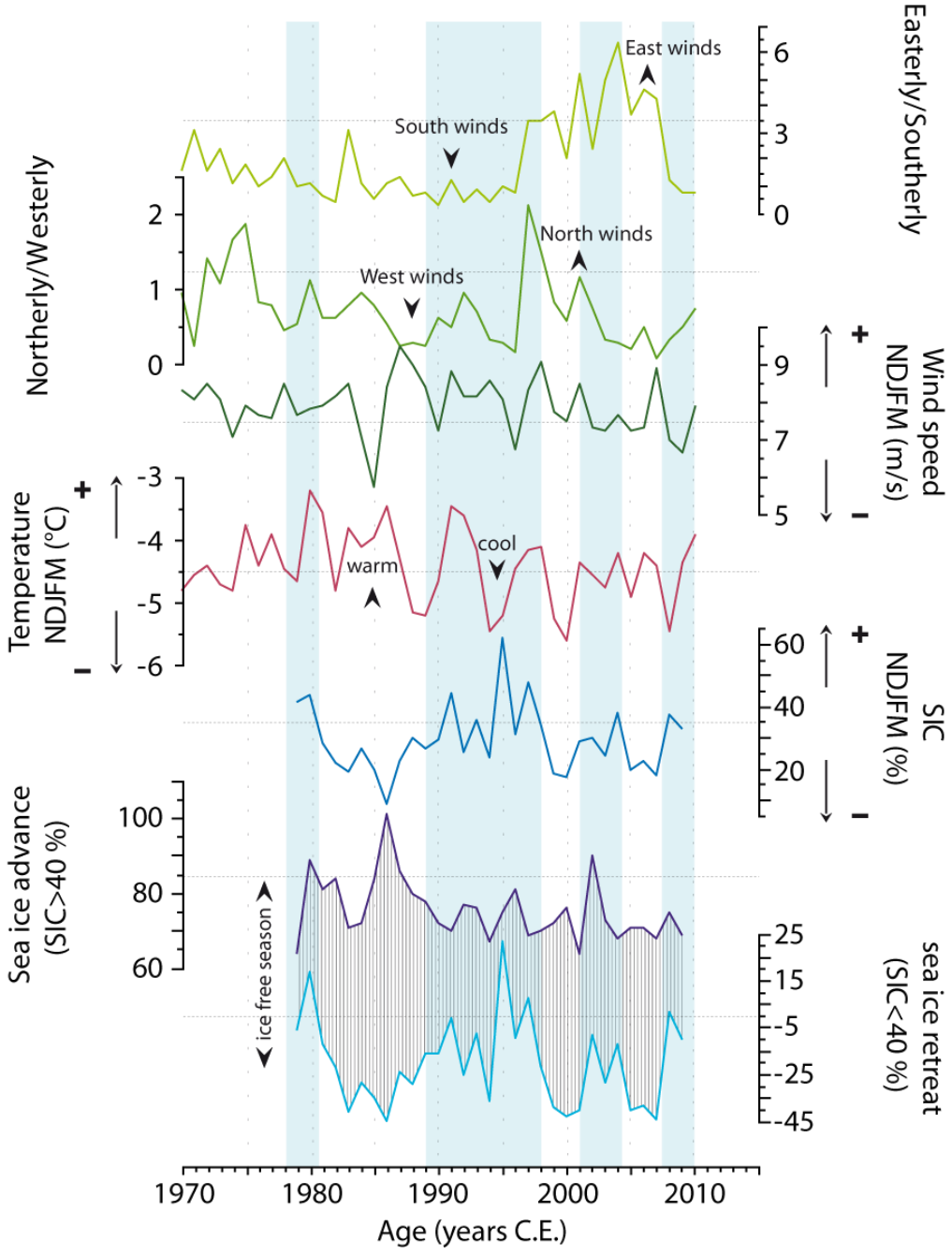

Figure 42. Meteorological parameters and climate index over the 1970-2010 period. Daily meteorological parameters were averaged over the November to March period. E/S (light green) represents the amount of days over the ice free season where the wind blew from the easterly (45° to

135°) versus southerly (135° to 225°) wind component; N/W (green) represents the amount of days over the ice free season where the wind blows from the northerly (315° to 45°) versus westerly (225° to 315°) wind component; wind speed (dark green); sea ice concentrations (SIC; blue); the sea ice advance (violet) accounts for the day of the year (DOY) where the sea ice concentrations increase over 40%; the sea ice retreat (light blue) accounts for the DOY where the sea ice concentrations drop below 40%; the length of the ice-free season from the sea ice retreat to the sea ice advance is marked by the hatched area. Blue shaded areas mark increases of SIC.

4.3.1 Sea ice conditions

Highest abundances of *F. cylindrus* cells in sediments are observed during the ~1972-1979, 1983-1984 C.E., 1996-1998 C.E. and 2002-2003 C.E. periods (Fig. 41). At the same time, analysis of the satellite data reveals the presence of heavier sea ice conditions in the area during spring, summer and autumn in the 1979-1981 C.E., 1990-1998 C.E. and 2001-2004 C.E. periods (Fig. 42). Although these intervals broadly coincide with those characterized by higher abundances of *F. cylindrus*, ice concentration during the productive season does not satisfactorily explain the variability of species abundance during the last 40 years. Since this species has previously been reported as favouring environments characterized by the presence of sea ice in spring (Kang and Fryxell, 1992; Armand et al., 2005), cell abundances were compared with the timing of the sea ice retreat. Again, both records displayed only a weak (or non-existent) relationship (Fig. 42). Interestingly, a strong relationship is observed between *F. cylindrus* abundances and wind origins. The increasing occurrence of relatively weak northerly winds (N/W ratio >0.9), bringing warmer water masses and somewhat advecting pack ice into the area during 1971-1975 C.E., 1979-1980 C.E., 1984 and 1992 C.E. and in the 1996-2001 C.E. period (Fig. 42), would contribute to the stratification of surface waters with large amounts of sea ice meltwater that have also been identified as promoting the development of this species. The [HBI:2] concentrations increased in 1971-1978 C.E., ~1982 C.E., 1985-1986 C.E., ~1989 C.E., 1995-2002 C.E., and since 2006 C.E. (Fig. 41). As observed for *F. cylindrus*, [HBI:2] concentrations do not closely follow SICs and the sea ice dynamics at interannual scale over the last 40 years. Rather, high concentrations of this biomarker co-occur with more westerly winds, as the N/W ratio is low between 1975-1979 C.E., 1981-1982 C.E., 1985-1991 C.E., 1993-1996 C.E., 2000 C.E. and since 2002 C.E. (Fig. 42), suggesting [HBI:2], and sea ice dwelling diatoms, would have greater affinities with pack ice conditions relative to fast ice. Our results therefore attest to the importance of the origin and nature of the sea ice in the sedimentary distribution of sea ice proxies in our study area.

Distinction of the two sea ice structures through finer satellite study in the region (e.g. MODIS satellite imagery) would help to assess and better constrain such relationships. Although [HBI:2] and *F. cylindrus* are both associated with increasing pack ice in our study area, the biomarker record lags the diatom record by ~2 years in core DTCI2010. This may suggest that one species (*F. cylindrus*) responds better to warmer (melted) conditions relative to the other species ([HBI:2]). However, time series studies on the formation, export and burial of HBIs and diatoms are necessary to fully understand this decoupling. We note that the two proxies present similar trends at sub-decadal scale, supporting their use as complementary sea ice indicators for paleoclimate studies.

The *T. antarctica/Porosira* gp ratio increased slightly over the 1976-1978 C.E., 1982-1985 C.E. and ~1995-1996 C.E. periods, reaching highest values between 2000-2010 C.E. (Fig. 41). As already observed for previous sea ice related proxies, the distribution of autumnal bloom species does not closely follow SICs variability in our study area. However, the large *T. antarctica/Porosira* gp increase over the last decade coincides with the earliest sea ice advance in the last 30 years, occurring in March, which resulted from the prevalence of easterly winds (Fig. 42). A significant shift to more easterly winds in Adélie Land was concomitant to a southward migration of the mid-latitude Westerlies and to positive Southern Annular Mode (SAM) values since 1960 C.E. (Campagne et al., 2015), the latter being the principal mode of atmospheric variability over the Southern Ocean (Thompson and Solomon, 2002). Enhanced easterly winds have been observed to weaken the northward transport of sea ice in the region, increasing sea ice conditions (Massom et al., 2003; 2009). This suggests that *T. antarctica* and *Porosira* spp are likely good indicators for autumnal sea ice dynamics forced by atmospheric variability.

4.3.2 Open ocean conditions

At the opposite of the sea ice related proxies, open ocean proxies seem to follow sea ice conditions in our study area relatively well, regardless origin, structure and nature. Indeed, the Open Water gp and *F. kerguelensis* assemblages display similar patterns, increasing in 1972-1977 C.E., in 1980-1986 C.E., in 1995-2001 C.E. and at ~2007 C.E. (Fig. 41), which coincides with periods of low SICs, earlier sea ice retreat and enhanced ice free season (Fig. 42). Similarly, [HBI:3] exhibits high values in ~1973 C.E., ~1978 C.E., 1983-1985 C.E., and moderate increase in 1995-2001 C.E. (Fig. 41), supporting a strong relationship with ice- free

conditions. The maximum occurrence of [HBI:3] between the mid 1970s to the mid 1980s coincides well with positive temperature anomalies and lower wind speed anomalies at that time (Fig. 42), arguing for a strong relationship between biomarker development and surface conditions forced by atmospheric variability. The open ocean proxies discussed above further present a similar long term trend in core DTCI2010, supporting their use as indicators of the lengthening of ice free conditions in paleoclimate studies. Additionally, these proxies are relatively coherent with the Ti increasing values in 1975-1978 C.E., 1985-1987 C.E., 1996-2001 C.E. and ~2008-2010 C.E. (Fig. 41). However, highest Ti values occurred in 1970-1972 C.E., concomitant to a slight increase of open ocean proxies and no particular warming trend in monitored temperatures (Fig. 42). This suggests that Ti content can be impacted by rapid terrigenous events that are independent of the length of the ice-free season (Fig. 42). Therefore, downcore differences between Ti and open ocean proxies may help in identifying episodic events such as local glacial discharge or ice rafted material derived from the Mertz Glacier Tongue basal melting (Maddison et al., 2006; Dinniman et al., 2012; Campagne et al., 2015).

4.3.3 Polynya activity

Chaetoceros RS and Zr/Rb exhibit contrasting trends during the 1970s to the mid 1980s, with decreasing (increasing) CRS (Zr/Rb) values during the 1973-1976 C.E. and the ~1977-1978 C.E. periods, and are then relatively in phase with concomitant increasing values in 1984/1985-1987 C.E., and in 1989-1995 C.E. (Fig. 41). Zr/Rb follows SIC variability relatively well whereas CRS relative abundances follow spring sea ice dynamics (Fig. 42). It is also worth noting that both proxies coincide well with prevalence of southerly winds in our study area between 1983-1996 C.E. (Fig. 42). Such a change in their relationships during the 1970s-1980s may highlight a decoupling between polynya activity and katabatic winds. While CRS are strongly linked to katabatic wind pulses and rapid stratification/mixing events, polynya activity (and bottom water velocity) may respond to windy conditions, whatever the wind origin. In Adélie Land, maximum wind speeds have been found for prevalent south to easterly winds (section 2.5). This, combined with increases of Zr/Rb between 1970-1985 C.E. and highest open ocean proxies values, suggests a balance between easterly and southerly winds over the ice free season during this period, promoting early spring polynya activity and summer open conditions. Subsequently, strong and persistent easterly winds, along with

increasing onshore wind circulation, may have softened polynya activity since the mid 1990s (Figs 41 & 42).

Table 3. Summary of our results. Summary of the statistical relationships of geochemical proxies, diatoms and the species association downcore (left column), of their known ecological preferences and utilization (middle column), and presentation of their relationships with meteorological parameters over the 1970-2010 period off Adélie Land (right column).

PROXY/GROUP IN DTCI 2010 (PEARSON AND PCA)	**KNOWN ECOLOGY (LITTERATURES)**	**ENVIRONMENTAL/METOROLOGICAL RELATIONSHIPS OFF ADÉLIE LAND**
F. cylindrus	Spring sea ice covered/sea ice stratified waters	Onshore wind circulation increase spring melted (relative warm conditions) pack ice conditions
[HBI:2], [HBI:2]/[HBI:3]	Spring sea ice environment	Westerly winds increase spring compacted (cold conditions) pack ice conditions
Banquisia gp (*N. directa N. glaciei, Synedra* spp, *Ephemera* spp)	Spring sea ice conditions	No clear pattern
F. obliquecostata	Surface melt pools, sea ice covered waters	No clear pattern
E. antarctica	Ubiquist, open conditions	Onshore wind circulation increase spring-summer sea ice conditions (short ice free season, delayed sea ice retreat)
Fragilariopsis summer gp (*F. ritscheri, F. sublinearis*)	Summer sea-ice edge environment, melted waters	No clear pattern

T. antarctica	Open water conditions in summer-autumn, slush and wave-exposed shore ice environment	Easterly wind induce summer open conditions but icy autumn conditions (early sea ice advance)
Porosira gp (*P. glacialis, P. pseudodenticulata*)	Relative open water conditions in summer, slush and wave-exposed shore ice environment, icy autumn and early sea ice advance	Easterly wind induce summer-autumn open conditions (long ice free season, relatively early sea ice advance)
F. kerguelensis	Open water-ice free conditions during summer	Easterly wind induced summer open conditions (earlier sea ice retreat, long ice free season)
Open water gp (*T. lentiginosa, T. oliverana, T. trifulta, T. gracilis, T. tumida, Coscinodiscus* spp, *A. actinochilus, S. microtrias*)	Open water-ice free conditions during summer	Easterly wind induced summer open conditions (earlier sea ice retreat, long ice free season)
[HBI:3]	Open water-ice free conditions during summer	Easterly-onshore wind circulation induced summer open conditions (early sea ice retreat)
Rhizosolenia gp (*Rhizolenia* spp, *R. antennata semispina, Proboscia* spp, *P. truncata* and *P. inermis*)	Open conditions in autumn, highly stable and nutrient poor waters	Onshore wind circulation induce stable surface waters, no clear trend with sea ice conditions
Thalassiotrix gp (*Tx. antarctica, T. reinboldii*)	Open conditions in autumn, highly stable and nutrient poor water column	Easterly wind induce summer-autumn open conditions (low SIC, long ice free season, early sea ice

		retreat-later sea ice advance)
F. rhombica	Spring-summer ice free-less icy conditions	Spring-summer warm conditions, delayed ice free season (late sea ice retreat-late sea ice advance)
Ti	Summer open conditions, melted conditions	Onshore wind circulation increase spring melted (warm conditions) sea ice and summer open conditions (low SIC)
Zr/Rb	Polynya environment	Katabatic winds induce coastal polynya and sea ice formation (high SIC)
CRS (*Chaetoceros Hyalochaetes* spp)	Rapid changes in stratification, decreasing nutrient levels	Katabatic winds pulses induce coastal polynya or turbulent surface layer events (high wind speed)
Phaeoceros gp (*C. Phaeoceros* spp, *C. atlantica, C. dichaeta*)	Open water environment	No clear pattern
Benthic gp (*Cocconeis* spp, *Grammatophora* spp, *Trachyneis* spp, *Licmophora* spp, *Melosira solenia, Achnantes brevipes, Amphora* spp, *Diploneis* spp, *Melosira adelia, Pseudogomphonema* spp, *O. weissflogii*)	Spring wind (storm) induced mixing conditions	Ambiguous pattern: cold conditions, open conditions (low sea ice concentrations, early sea ice retreat, long ice free season)
Corethron gp (*C. criophilum, C. pennatum*)	Open ocean conditions, surface mixed waters	No clear pattern

5 Conclusion

Investigation of annual to interannual relationships between diatom communities, diatom specific biomarkers and major element abundances in connection with meteorological parameters show that the relevance and use of some proxies (1) may be characteristic of the study area (e.g. CRS assemblage), or (2) differ slightly from previous long term studies (e.g. *F. cylindrus*). Indeed at such a fine scale, the distribution of the sea ice related proxies in sediment highlights complex relationships of the biota with sea ice concentration, sea ice dynamics, sea ice cover structure and origin, constrained by the wind pattern. However, we note that the complex relationship between winds and sea ice should be alleviated at longer time scales if larger atmospheric and ocean temperatures changes become more preponderant. Open ocean related proxies seem to primarily respond to the lengthening of the growing season in our study area, agreeing well with previously published regional to large scale studies. Polynya activity may be inferred from variations in the Zr/Rb ratio values. Monitoring the sedimentary signal formation in surface water, through the water column and its export and burial in deep-sea sediments is necessary to understand the local behaviour of the proxies commonly constrained via synoptic studies. Other high-resolution and longer timescale reconstructions are required to refine our understanding of the ice-ocean-atmosphere interactions and system feedbacks.

AUTHOR CONTRIBUTIONS

X. Crosta and G. Massé designed the study and P. Campagne carried it out. O. Ther performed diatom and XRF analyses; P. Campagne performed diatom sensus counts and PCA analyses; M-N. Houssais extracted daily sea ice concentrations; S. Schmidt performed ^{210}Pb analyses and developed the age model of the core; P. Campagne prepared the manuscript with contributions from all co-authors.

ACKNOWLEDGMENTS

This research was funded by the ERC StG ICEPROXY project (203441), the ANR CLIMICE project and FP7 Past4Future project (243908). The French Polar Institute provided logistical

support for sediment and data collection (IPEV projects 452 & 1010). This is ESF PolarClimate HOLOCLIP contribution n°24 and Past4Future contribution n°83.

SUPPLEMENTARY INFORMATIONS, FIGURES AND TABLES are available in Annexe 1.

Chapitre IV: La période historique en Terre Adélie-Georges V - identification des forçages climatiques et de leurs mécanismes associés

Au cours des dernières décennies, les observations satellites ont montré une augmentation des conditions de banquise en Antarctique de l'Est, qui contraste avec le réchauffement observé en Antarctique de l'Ouest (Cavalieri et de Parkinson, 2008). Les quelques enregistrements sédimentaires marins qui existent dans l'Océan Austral, généralement de faible résolution, suggèrent néanmoins que cette asymétrie a également caractérisé la période de l'Holocène en Antarctique, avec notamment des conditions de glace présentant une réponse régionale forte (Denis et al., 2011; Shevenell et al, 2011; Etourneau et al, 2013). Cette forte hétérogénéité spatiale en Antarctique complexifie la compréhension des mécanismes climatiques sous-jacents agissant à l'échelle décennale et centennale.

Dans ce quatrième chapitre, l'objectif était d'identifier les forçages locaux, régionaux et synoptiques ainsi que leurs mécanismes associés aux échelles pluri décennale à inter annuelle au cours de l'Holocène tardif. Grâce à deux archives sédimentaires complètes couvrant la période historique, notre intérêt portait sur la caractérisation des conditions océanographiques et climatiques en Antarctique de l'Est au cours des derniers siècles, là où d'autres enregistrements manquaient. Nous avons également tenté de mettre en avant d'éventuels schémas répétitifs au cours de l'Holocène tardif grâce à l'analyse par ondelettes des signaux sédimentaires. Dans la première partie de ce chapitre, nous nous sommes focalisés sur l'étude de la carotte CB2010 afin de documenter les variations des conditions de surface au cours des derniers 250 ans dans la polynie du Mertz en TAGV, en relation avec la dynamique du glacier de Mertz. Le but étant de déterminer les mécanismes contrôlant les changements locaux environnementaux à l'échelle pluri décennale. Ce travail a fait l'objet d'un article scientifique publié dans *Nature communications*. Dans la deuxième partie de ce chapitre, nous nous sommes attachés à reconstruire les changements environnementaux au cours des derniers 500 ans grâce à la carotte DTCG2011 au large de Dumont D'Urville, pour ensuite les comparer à ceux documentés dans la première partie de ce chapitre, afin d'identifier la variabilité climatique associée aux forçages locaux, régionaux et synoptiques aux échelles pluri décennale à inter annuelle au cours de l'Holocène tardif. Les résultats sont également présentés sous la forme d'un article scientifique, en préparation. Dans ce quatrième chapitre,

nos résultats montrent trois intervalles climatiques séculaires au cours des derniers 500 ans, caractérisés par des changements de la dynamique saisonnière du couvert de banquise et des conditions de polynie. Des variations décennales à pluri décennales relativement stationnaires ont également été mises en évidence à travers nos enregistrements, et ont été associées à la variabilité atmosphérique et océanique régionale, ainsi qu'à la dynamique glaciaire locale.

Article II: Glacial ice and atmospheric forcing on the Mertz Glacier Polynya over the past 250 years

Article in NATURE COMMUNICATIONS · MARCH 2015

Impact Factor: 10.74 · DOI: 10.1038/ncomms7642 · Source: PubMed

Campagne, P.1,2,3, Crosta, X.1, Houssais, M. N.2, Swingedouw D.1, Schmidt, S.1, Martin, A.2, Devred, E.3, Capo, S.1, Marieu, V.1, Closset, I.2 and Massé, G.2,3

1EPOC, UMR CNRS 5805, Université de Bordeaux, Allée Geoffroy St Hilaire, 33615 Pessac, France

2LOCEAN, UMR CNRS/UPCM/IRD/MNHN 7159, Université Pierre et Marie Curie, 4 Place Jussieu, 75252 Paris, France

3TAKUVIK, UMI 3376 UL/CNRS, Université Laval, G1V 0A6 Quebec (Quebec), Canada

The Mertz Glacier Polynya off George V Land, East Antarctica, is a source for the Adélie Land Bottom Water, which contributes up to ~25% of the Antarctic Bottom Water. This major polynya is closely linked to the presence of the Mertz Glacier Tongue, which traps pack ice upstream. In 2010, the Mertz Glacier calved a massive iceberg, deeply impacting local sea ice conditions and dense shelf water formation. Here we provide the first detailed 250-year long reconstruction of local sea ice and bottom water conditions. Spectral analysis of the datasets reveals large and abrupt changes in sea surface and bottom water conditions with a ~70-year cyclicity, associated with the Mertz Glacier Tongue calving and re-growth dynamics. Geological data and atmospheric reanalysis however suggest that sea ice conditions in the polynya were also very sensitive to changes in surface winds in relation to the recent intensification of the Southern Annular Mode.

1 Introduction

Antarctic Bottom Water (AABW) is considered as the great ventilator of the world deep ocean and is a critical component of the global climate system[1,2]. AABW is sourced by dense saline shelf waters, locally produced in several polynyas, where low sea ice concentrations and open water conditions are maintained during winter and favour local sea ice and brine production[3,4]. Coastal polynyas are usually associated with the presence of local topographic or glacial features and synoptic-scale gravity winds[4]. Although they only represent a small fraction of the area covered by sea ice, polynyas are considered of key importance for the Earth climate system[3,5]. Indeed, while the 13 major Antarctic coastal polynyas only represent ~1% of the maximum ice area, they are responsible for the production of 10% of the Southern Ocean sea ice[3]. Recently, it has been shown that approximately 25% of the AABW is sourced from the export of Adélie Land Bottom Water (ALBW) produced in the George V Land polynyas[2,6]. ALBW mainly originates from the Adélie Depression off the coast of George V Land[3,6,7], where the Mertz Glacier Polynya (MGP) develops in winter along the western flank of the Mertz Glacier Tongue (MGT) and further extend to the West in the adjacent coastal bays (Commonwealth, Watt and Buchanan Bays; Fig. 43b)[8,9]. The MGP constitutes the third most productive polynya in Antarctica, with a winter area of up to 6,000 km^2 and an annual sea ice production of 120 km^3 over the 1992-2001 period[3,4].

Early in 2010, the Mertz Glacier (MG) underwent massive calving and lost half its tongue after collision with the B09B iceberg. The generation of an 80 km long iceberg and subsequent retreat of the MG front had a profound impact on both regional icescape and ocean conditions[9,10,11]. S*atellite* passive microwave data show that sea ice concentration (SIC) increased by 50% (relative to the 1979-2009 period) in the MGP area after the calving (Fig. 43e). Advection of thick consolidated sea ice and presence of fast ice downstream the MG *in the MGP* (Fig. 43c,d) led to a large reduction in sea ice production in the MGP, which in turn affected dense water formation[9,10,11]. Within 2 years following the calving, bottom water salinity decreased by over 0.30 psu in Commonwealth Bay (CB)[9].

Located in the southern part of the polynya, CB is ideal for studying past dynamics of the MGP and dense water formation[9]. Indeed, mooring observations and satellite data showed that oceanic and sea ice conditions (Fig. 43e) over the CB and MGP areas have experienced similar and synchronous pre- and post-calving changes over the recent years[9]. Additionally, recent observations highlighting the presence of the saltiest waters of the Adélie depression in

CB suggest that large production rates of dense shelf water occur in the bay[9,13]. Based on past expeditions, it has been suggested that the MG previously underwent similar calving events in the early part of the 20th century[12]. However, these sporadic observations are insufficient to reconstruct past MGT dynamics with a high level of confidence. In the present study we provide a detailed reconstruction of surface and bottom oceanic conditions in the MGP over the last 250 years. This reconstruction is based on high-resolution analyses of diatom assemblages, diatom-specific biomarkers and major element abundances along a well-dated interface sediment core retrieved in January 2010 at CB (Fig. 43a; 66°54,38'S - 142°26,18'E; 775 m depth). This study represents the first detailed assessment of the MG-MGP system dynamics over the last centuries, and therefore provides essential information on how the system recovers after major perturbations such as calving events. Here, we also evaluate the impact of the recent positive shift in the Southern Annular Mode (SAM) on MGP surface conditions through a century-long atmospheric reanalysis.

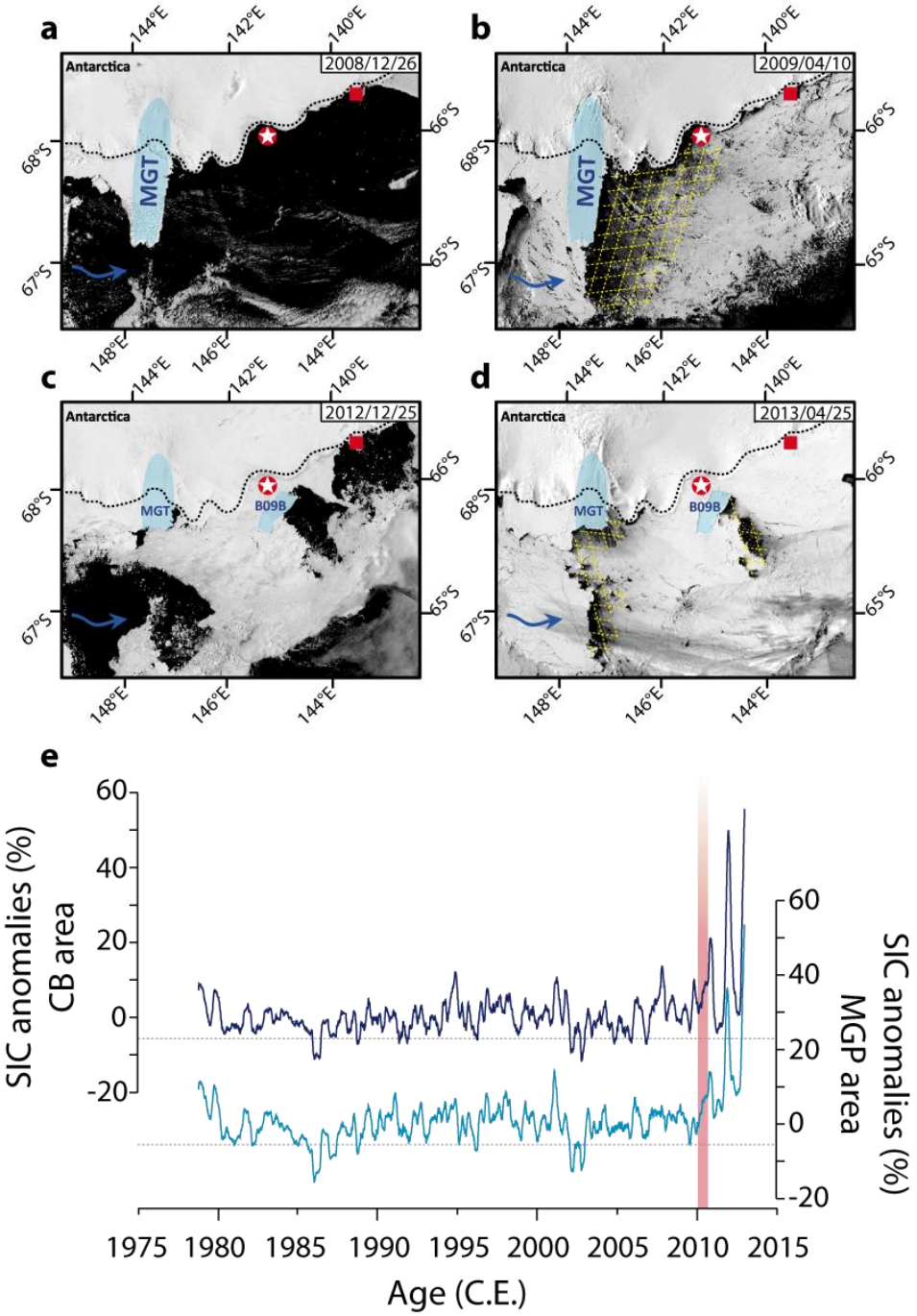

Figure 43. Pre- and post-calving sea ice conditions in the George V Land. Aqua MODIS satellite images showing sea ice conditions in the study area during summer a, and winter b, before the 2010 calving event, and during summer c, and winter d, after the 2010 calving event. The white star in a red circle indicates the core location; the Dumont D'Urville station is indicated by a red square; blue shadings indicate glacial features, the Mertz Glacier Tongue (MGT) and the B09B iceberg; the Mertz Glacier Polynya area in winter before and after the calving is designated by the yellow grid on b, and d; the blue arrow indicates the general direction of the East Wind Drift; coastline is marked by the black dotted line e, three-month averaged SSM/I time series of daily sea ice concentration (SIC) anomalies in Commonwealth Bay (CB - dark blue) and in the Mertz area (MGP - light blue), for the

1978-2012 period using 1978-2009 as the reference period (for the exact grid points locations see Fig. 49). The red shading indicates the 2010 calving event.

2 Results

Multi decadal trends of sea surface conditions. Variations of *Fragilariopsis cylindrus* populations and di-unsaturated highly branched isoprenoid lipid [HBI:2] abundances characterize spring sea ice occurrence[14,15], while summer open-ocean conditions are inferred from high abundances of open water diatoms[16] (see Methods). Ti content is used here to infer changes in terrigenous supply to the ocean[17], thus reflecting the variability of the terrigenous delivery by glacial melting, the dominant process in Antarctic coastal areas at such timescale[18,19]. High (low) relative abundances of open water diatoms are concomitant with high (low) contents of Ti and, conversely, with low (high) relative abundances of *F. cylindrus* and low (high) concentrations of [HBI:2] (Fig. 44). Minimum abundances of [HBI:2] and *F. cylindrus* associated with maxima of open water diatoms and Ti during 1740-1760, 1800-1845 and 1880-1915 periods (Fig. 44) therefore indicate the presence of a well-developed polynya characterized by low sea ice concentration during the winter, early spring sea ice retreat and long summer season. The presence of a well-developed MGP promoted intense sea ice formation during winter and enhanced brine-induced convection. Variations in bottom current velocities were estimated from changes in sediment grain size inferred from Zirconium *versus* Rubidium (Zr/Rb) relative abundances[20]. Assuming that greater deep-reaching convection is associated with intensified bottom currents, the high Zr/Rb ratios *(Fig. 44)* recorded during periods of well-developed MGP suggest enhanced bottom currents favouring a coarse sedimentation at the core location. In contrast, the 1760-1800, 1845-1880 and 1915-1960 periods are characterized by maxima in [HBI:2] and *F. cylindrus* relative abundances and minima in open water diatoms, Ti and Zr/Rb records *(Fig. 44)*. This reflects the presence of heavier sea ice conditions in spring, leading to shorter growing seasons and cooler summers, associated with reduced inputs from glacial runoffs and melting. During these intervals, a reduction of the MGP area and sea ice production coincided with a weaker bottom circulation, as revealed by the presence of finer (low Zr/Rb) sediments. Our records therefore suggest that since the mid-18th century, surface ocean conditions and MGP activity alternated between periods of high sea ice presence and periods of prolonged open-ocean conditions.

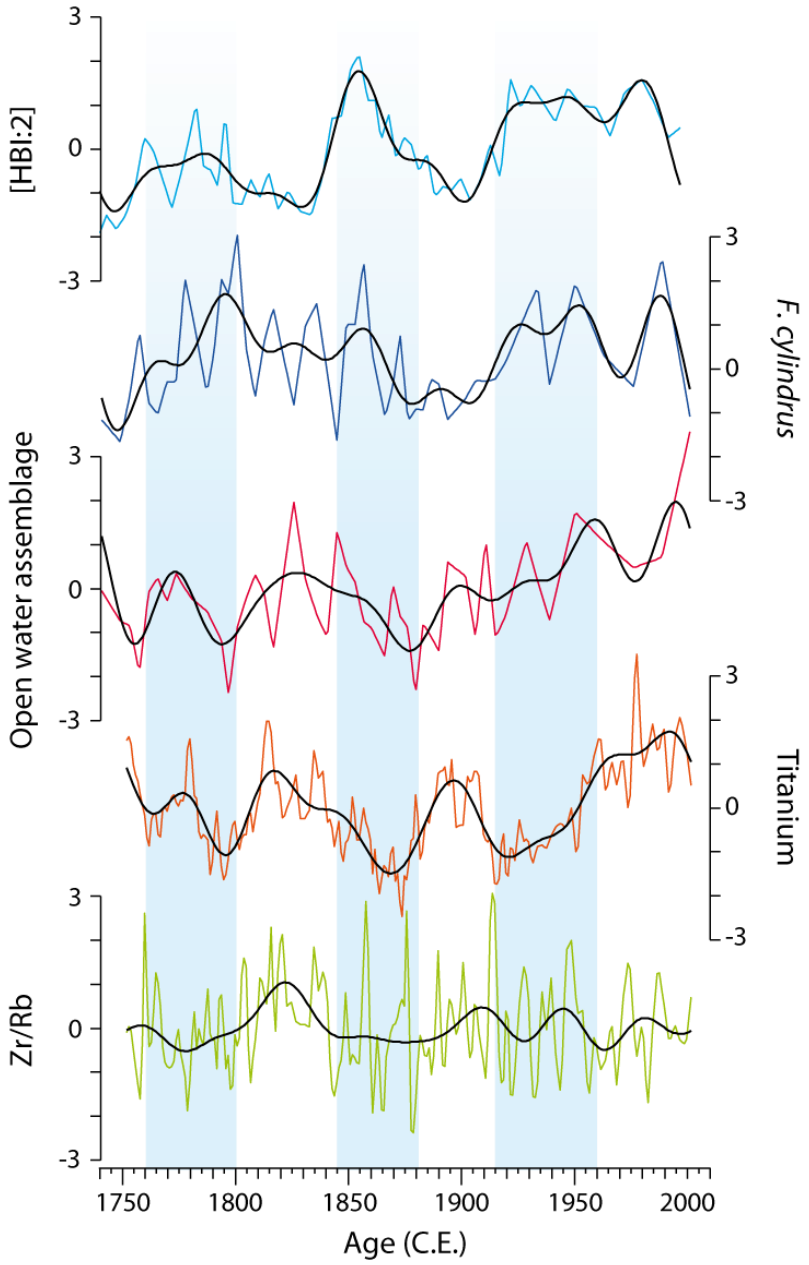

Figure 44. Sea ice and ocean conditions in Commonwealth Bay over the last 250 years. Sea ice proxies: standardised concentrations of HBI:2 (light blue) and relative abundances of *Fragilariopsis cylindrus* (dark blue). Open water proxies: standardised relative abundances of open water diatom group (red) and Titanium content (orange). Bottom current variability: standardised Zr/Rb ratio (green). Black curves represent the low pass filtered data, with a cut-off frequency at 1/32 (in year). The blue shadings indicate decades following each calving event with marked increase in sea ice concentration in the CB area.

Cyclic pattern. These multi decadal trends of the MG-MGP system are further characterized by a strong asymmetric evolution with sharp increases in sea ice concentration at ~1760,

~1845 and ~1915, followed by a slow decrease over the subsequent decades (Fig. 44). A similar sharp increase observed after the 2010 calving event (Fig. 43e) suggests that, at least for the past 250 years, these asymmetric oscillations (~70 years periodicity) are related to a series of large calving events. Each of these events probably induced a rapid closing of the MGP as the loss of the ice tongue allowed for sea ice transported within the East Wind Drift (EWD) to enter the area.

This scenario is further supported by the wavelet analysis of our dataset, which shows that all variables exhibit a common high power in the 60-80 year band, throughout the entire record (Fig. 45). Although such periods (60-80 years) are close to the limit of detection (the bottom of the cone influence), they are characterized by a high statistical significance level of the period (95%, according to [21]). Additionally, in the 60-80 year band a positive correlation, characterized by rightward pointed arrows, is shown by cross wavelet analyses (see Methods) between sea ice proxies (Fig. 45a) and between open water proxies (Fig. 45b). In contrast, as indicated by leftward pointed arrows, negative correlations occur in the 60-80 year band when comparing sea ice *versus* open water proxies (Fig. 45c,d,e,f). Interestingly, continuous wavelet transforms indicate that open water and sea ice diatom signals (Supplementary Fig. S1) exhibit an additional ~20-25 year cyclicity which is absent from the geochemical proxies. Although the causes remain unclear, differences in the spectral pattern of diatom and geochemical records may be attributed to the origin of the proxies themselves. The [HBI:2] is synthesized by diatoms living within or attached to sea ice. As such we expect a direct response of [HBI:2] to sea ice concentration and the timing of ice waning[14]. Sea ice related diatoms such as *F. cylindrus* thrive at the sea ice margin while open water diatoms thrive in the water column. Therefore, we believe that diatoms respond to both the timing of sea ice waning and oceanic biotic and abiotic factors such as stratification, upwelling, and the injection of warmer waters[15,16,17] which are expressed at shorter timescales[22,23].

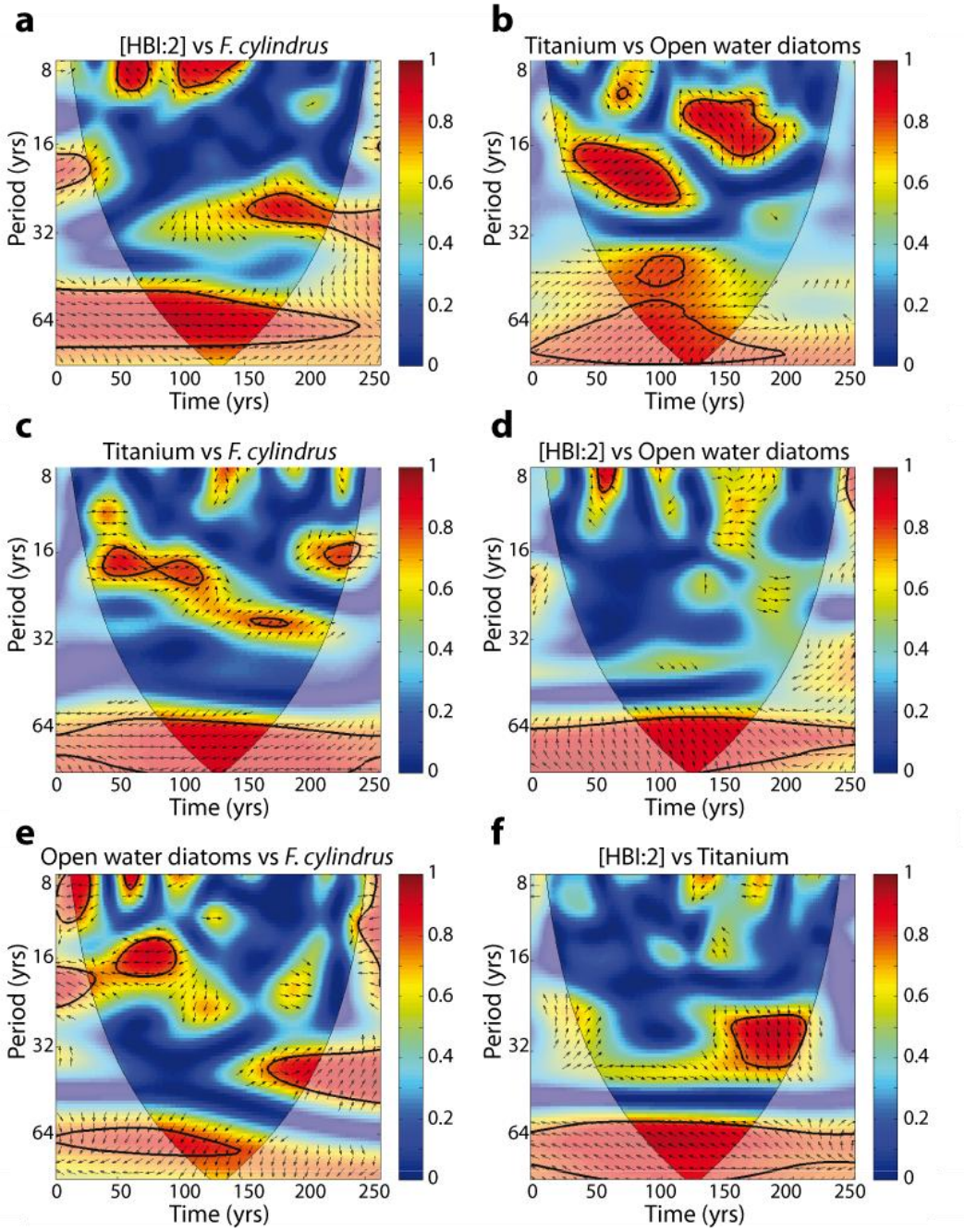

Figure 45. Relationship between proxies and cyclicity of sea surface conditions in the Mertz Glacier Polynya area. Cross wavelet transform (CWT) on the sedimentary proxies (using Morlet wavelet and Monte Carlo methods) between a, [HBI:2] *vs Fragilariopsis cylindrus*; b, Titanium vs open water diatoms; c, Titanium vs *Fragilariopsis cylindrus*; d, [HBI:2] vs open water diatoms; e, Open water diatoms *vs Fragilariopsis cylindrus*; and f, [HBI:2] vs Titanium. Statistically significant periods are identified by the black circled red zones. Rightward pointed arrows indicate positively correlated signals while leftward pointed arrows indicate negatively correlated signals.

Barrier effect of the Mertz Glacier. Each calving event is characterized by relatively elevated abundances of the sea ice proxies for a couple of decades, followed by a slow decrease of the sea ice proxies and a concomitant increase of the open water proxies. These results suggest that each event was followed by a slow and constant re-advance of the glacier

but that a few decades are necessary for the tongue to reach a sufficient length to prevent sea ice advection in the area. As such, during few decades after 1800, 1880 and 1960 (Fig. 44), the tongue probably acted as a barrier and deflected the EWD pack ice northward, thus restoring favourable conditions for the establishment of the polynya. Although only limited observations exist to reconstruct the recent history of the MGP, it is clear that at least one major calving event occurred between 1912, when the Australasian Antarctic Expedition led by Mawson (1911-1914) measured a 150 km long tongue from the grounding line, and 1958, when the Soviet Antarctic Expedition reported a 113 km long tongue[12]. The sharp increase in sea ice proxies in 1915 strongly suggests that this event occurred only a few years after Mawson's expedition. Given the mean growth rate of the tongue of ~1 km/yr[24], the glacier had presumably reached ~150-160 km at that time when it calved. This length is similar to the one reached by the glacier prior to the 2010 calving[25,26] and is in line with Mawson's observations in 1912. If the MGT lost half (80 km) of its length, similar to the 2010 calving event, it would have taken ~40 years for the tongue to grow back from ~80 km in 1915 to 113 km, based on the Soviet Antarctic Expedition in 1958. These results suggest that from the 1960s, the ice tongue was then long enough to effectively act as a barrier for drifting ice. In the 1990s, signs of imminent calving were already detected with the formation of two major rifts near the glacier grounding line and the front of the glacier grounding on the Mertz Bank to the north[12,25]. The shallow bathymetry of the bank (Supplementary Fig. S2) enhances local tidal currents exerting lateral stress on the tip of the glacier, likely impacting the tongue along-flow velocity[26]. In addition, the presence of several icebergs released by upstream glaciers and grounded onto the Mertz bank[12,26] probably further increases the lateral distortion of the tongue. As such, it appears that beyond a threshold of ~150-160 km, lateral stresses exerted on the sides and at the lie of the tongue lead to its rupture.

Recent changes in seasonality. Interestingly, the analysis of the upper sediment section show that while the MGT was sufficiently long to promote open water conditions in the lie of the glacier during the last 50 years, both [HBI:2] and *F. cylindrus* remained relatively abundant in the sediments (Fig. 44). Additionally, Zr/Rb values did not show a marked increase as expected during this phase (Fig. 44). This suggests that, in contrast to previous cycles, pre-calving conditions over recent decades were characterized by a more persistent sea ice cover during spring and were associated with weaker bottom water circulation than observed during previous cycles. We also note higher Ti contents (terrigenous inputs) along with greater abundances of open water diatom species (and in particular large centric diatoms; Fig. 46)

suggesting strong glacial melting and more persistent open water conditions led by warmer surface waters during summer over the recent decades. Warmer open water conditions during the summer are further confirmed by the large peak of a specific HBI isomer [HBI:3] during the past 40 years (Supplementary Fig. S3). High abundances of [HBI:3] in sediments reflect the contribution of phytoplanktonic-derived organic matter[14] and thus indicate a higher phytoplankton productivity during the summer (Supplementary Note 1). Overall, these results therefore provide strong evidence for changes occurring over the growing season in recent decades. From our records, this apparent shift in seasonality is characterized by cooler and icier springs, warmer and more open summers in line with recent atmospheric and oceanic observations from other areas in the Southern Hemisphere[22,27].

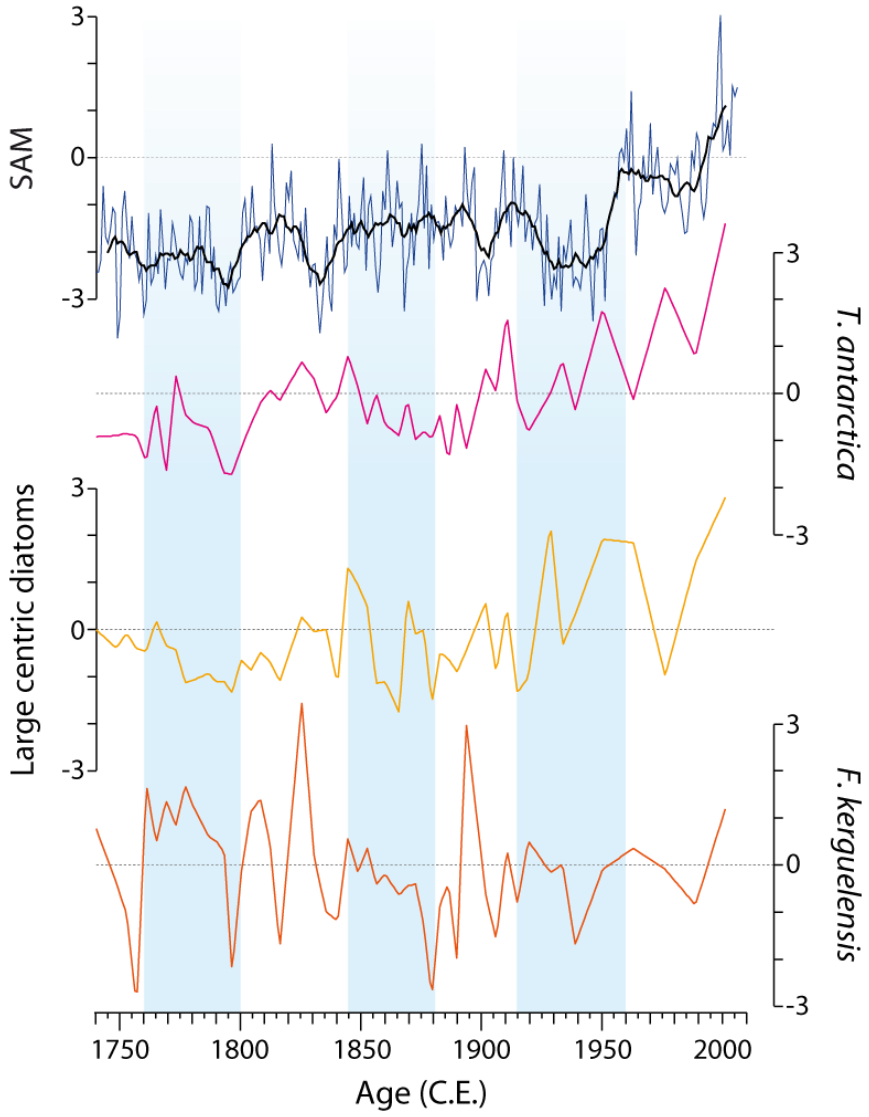

Figure 46. Atmospheric forcing and impacts on the sea ice free season during the instrumental period in the Mertz Glacier Polynya area. Evolution of the Southern Annular Mode (SAM) according to the reconstructed Marshall index (blue, annual values and black, 11 years moving average) over the last 250 years31. Open water proxies: standardised relative abundances of *Thalassiosira antarctica* sp

(pink), large centric diatom group (yellow; see Methods for species composition) and *Fragilariopsis kerguelensis* (orange). The blue shadings indicate decades following each calving event with marked increase in sea ice concentration in the CB area.

3 Discussion

Our results strongly suggest that surface oceanic conditions and dense shelf water production are closely related to the MGP presence and activity. Reasons for the ~70 years cyclicity of the MGP are still not fully understood but, given the major constraints of the local topography, it is likely that these cycles are set by the rate of advance and along-flow velocity of the Mertz Glacier. However, according to several studies[12,25], icebergs released from upstream outlet glaciers (*e.g.* Ninnis Glacier) could have impacted the stability of the MGT when they grounded and/or passed through the area. Additionally, when the tongue is too short to constitute a barrier, these icebergs can impact the regional oceanography for several years, leading to a temporary increase in sea ice conditions, as observed since 2010 with the presence of the B09B iceberg in front of CB (Fig. 43c,d). The resolution of our records however does not allow us to capture such phenomena, if they ever occurred in or around CB in the past. Our data also indicates a close relationship between the MG history and MGP dynamics between 1740 and 1960. However, since the 1960s our records suggest unexpectedly cool and icy springs at a time where the MG tongue should have reached a sufficient length to promote the presence of a well-established MGP.

We propose that, superimposed on the large multi-decadal oscillations generated by the MG dynamics, additional factors contributed to modulating sea surface conditions in the area. The Southern Annular Mode (SAM), principal mode of atmospheric variability over the Southern Ocean[28], has shown a steadily increasing index over the last 50 years[27,29] (Figs 46 and 47a), with a more positive trend in summer[27,30]. Reconstructions indicate that this increase is unprecedented over the last few centuries[31] possibly due to ozone depletion and a rise in greenhouse gases[29,32], and recent investigations have argued that such trend had a direct influence on sea surface conditions in several regions around Antarctica through modulation of the wind pattern[22,23,29,33,34,35]. The recent positive trend in the SAM index is indeed associated with an intensification of the polar vortex[32] leading to a southward shift of enhanced circumpolar westerlies[28]. This, in turn, led to a more intense Antarctic Circumpolar Current[35] and associated ocean eddy activity[36]. We postulate that such large-scale changes

impacted the sea ice distribution in spring, modified the summer off-shelf ocean circulation due to changes in the large-scale wind stress pattern and are the dominant cause for the contrasted response of the Adélie Land continental shelf over the last fifty years.

Indeed, several studies have evidenced a close link between the planetary circulation in the southern polar atmosphere and the katabatic wind regime, the latter being part of the large-scale meridional tropospheric circulation over Antarctica[37,38,39,40]. Observations in East Antarctica revealed that an intensified tropospheric vortex was associated with weakened katabatic winds over the Antarctic margin[40] and analysis of the atmospheric wind fields during the last 140 years from the 20CR reanalysis[41] confirms a significant westward shift of the wind pattern in the George V Land over recent decades (Fig. 47a, green curve; Supplementary Note 2). A weakening of the meridional wind circulation and thus, increasing zonal circulation over the last decades as suggested by [40;42] has also been observed in the region[34,43]. Indeed, at seasonal to inter-annual time scales, sea ice conditions in the MGP area have been shown to be sensitive to the latitudinal location of the Antarctic Circumpolar Trough and associated to more along shore wind transport[34,43]. In the present scenario, reduction of katabatic winds intensity over the MGP area would weaken the northward transport of sea ice, resulting in the retention of more ice within the area. The latter would delay the onset of sea ice melt in spring in agreement with higher sea ice proxies in our record since 1960. Although based on a restricted number of data points, a reduction of sea ice proxies in the uppermost sediment sections suggests a recent tendency toward a more reduced sea ice cover in spring, in line with the recent analysis of the sea ice seasonality in the area using the satellite records[44].

Our data also indicate warmer sea surface conditions during summer over recent decades. As recently observed in several Antarctic regions, it is argued here that intrusions of warm Circumpolar Deep Water (CDW) onto the continental shelf promoted open water conditions and higher sea surface temperatures[7,23,33,45]. Increasing CDW contribution onto the Antarctic Peninsula shelf was linked to the recent changes in the strength of the SAM[46]. Indeed, modeling studies have shown that advection of CDW onto the Antarctic continental shelf is linked to enhanced upwelling southward of the Antarctic Circumpolar Current (ACC), promoted by a southward shift and strengthening of the Southern Ocean Westerlies[35,47]. Surface wind stress curl calculated from the 20CR reanalysis indeed suggests long periods of strong positive trend in upwelling-favorable vertical velocities with positive values starting

roughly after 1950, concomitant with the SAM trend (Supplementary Fig. S4; Supplementary Note 2). In the Mertz region, in contrast with West Antarctica, flooding of the shelf by the CDW occurs as synoptic weather time scale intrusions rather than as a continuous flow[7]. However the proximity of George V Land continental shelf to the southern ACC boundary facilitates transport of CDW into the Mertz region[48], as suggested in other Antarctic areas[23], providing that adequate dynamical forcing exists to drive this water mass on the shelf. According to [49], a number of mechanisms involving interaction of the zonal flow with the topographic troughs disseminated along the Antarctic shelf break are likely to favor such transport. While some of these may be linked to the internal variability of the flow[50], some would be the result of enhanced wind-driven zonal flow. We note that, off the Adélie Land shelf, a more zonal wind pattern in the 20CR reanalysis (Fig. 47) over recent decades was concomitant to the southward shift (Supplementary Fig. S5) and the strengthening[35,47] of the Westerlies at mid latitudes. Increasing zonal wind circulation poleward may have contributed to accelerate the westward flowing Antarctic Slope Current, the southern branch of the Australian Antarctic Basin cyclonic circulation[51,52], thus favoring the inflow of CDW through non-linear momentum advection onto the shelf trough. Recent observations suggest that a weaker and more zonal circulation promote uplift and enhanced onshore intrusion of CDW[45] and studies attributed an increased abundance of terrigenous particles in the sediments to enhanced melting of both continental and sea ice during periods of increased advection of warm CDW onto the shelf[17,18,19,53]. The high terrigenous content recorded in CB2010 since 1960 (Fig. 44) can therefore be interpreted as a result of enhanced melting of regional glaciers in response to increased advection of warm CDW onto the shelf. This enhanced melting of glacial ice could also be contributing to further freshening the ALBW as reported by [9] and co-workers.

Our results demonstrate that, in response to glacial dynamics and local physiography, recurrent massive calving events of the Mertz glacier occurred over the last 250 years. These events had profound impacts on ocean surface conditions and dense water production of the downstream polynya. Taking into consideration that many of these glacier-polynya systems are disseminated around Antarctica[4] and that dense shelf water is ultimately a precursor of AABW, whose impact on large-scale ocean circulation is well-known[1,2], our study provides evidence that local processes may contribute to alter global ocean and climate systems. In contrast to previous cycles, our data indicate that during the last 50 years, the region was experiencing a more compact sea ice cover, a larger supply of glacial melt water and a

slowdown of bottom currents. These results suggest a reduction of dense water production and are consistent with the long-term freshening of the ALBW observed in the Australian Antarctic Basin since the late 1960s[54,55]. This contrasted response of the MGP region during the last Mertz cycle may just be a transitory phenomenon as the SAM increase over that period is thought to be partly due to ozone depletion in the polar vortex. Since studies are predicting that the ozone hole will replenish in the future decades[56], natural pluri decadal glacier cycles such as those identified in our records are likely to take over.

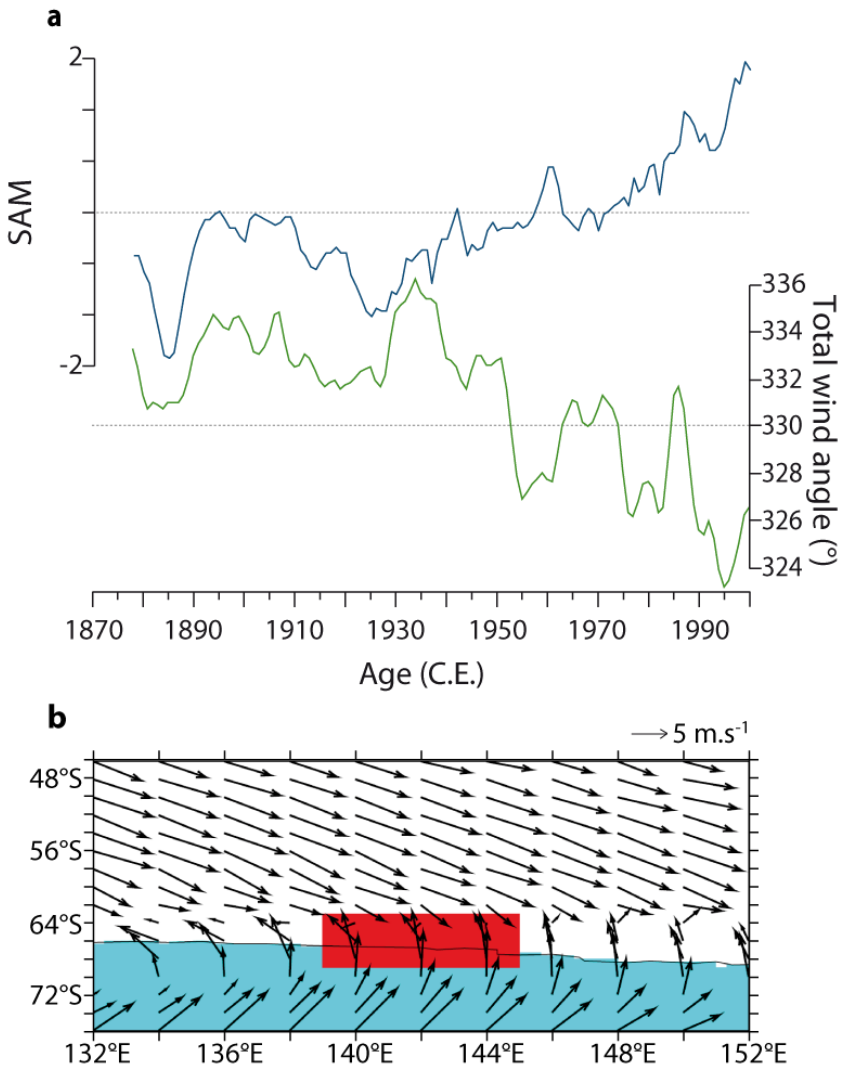

Figure 47. Evolution of the Southern Annular Mode and of the wind pattern over the Adélie-George V Land since the 19th century. a, Standardized values of SAM index (5 yr running mean; blue), computed in the 20CR reanalysis following [70], and the total wind direction angle at 2 meters (green; °) computed in the red box of the lower panel using the same reanalysis. The North direction indicates the 0° modulo 360° and the angle is counted positively clockwise; b, Annual mean wind speed from

20CR reanalysis averaged over the period. 1871-2010. The red box indicates the study area where the wind have been computed in panel a.

4 Methods

Sediment material and chronology. A 30.5 cm long interface core was retrieved aboard the R/V Astrolabe (66°54.38' S; 142°26.18' E; 775m water depth) during the 2010 COCA cruise. Positive X-ray images performed on the SCOPIX image-processing tool[57] gave detailed information on sediment density and structure. SCOPIX images revealed that, in contrast to high accumulation sites from Dumont d'Urville Trough, sediments from Commonwealth Bay were massive with no signs of laminations. The core was sampled continuously at 0.5 cm resolution and its chronological framework was determined based on ^{210}Pb excess ($^{210}Pb_{xs}$; $T_{1/2}$ = 22.3 years), which is rapidly incorporated into the sediment from atmospheric fallout and water column scavenging. The activities of ^{210}Pb and ^{226}Ra were measured on dried sediments by non-destructive gamma spectrometry using a well-type, high efficiency low background detector equipped with a Cryo-cycle (CANBERRA). Activities are expressed in mBq g^{-1} and errors are based on 1 standard-deviation counting statistics (Fig. 48). $^{210}Pb_{xs}$ was determined by subtracting the activity supported by its parent isotope, ^{226}Ra, from the total ^{210}Pb activity in the sediment. Mass accumulation rate (MAR, 0.025 g cm^{-2} y^{-1}) was calculated from the sedimentary profiles of $^{210}Pb_{xs}$, plotted against cumulative mass. The deposition time (in years) was obtained by dividing the cumulative dry mass per unit area by MAR. The deposition year for each sediment layer was subsequently estimated based on the 2010 sampling date for the sediment-water interface.

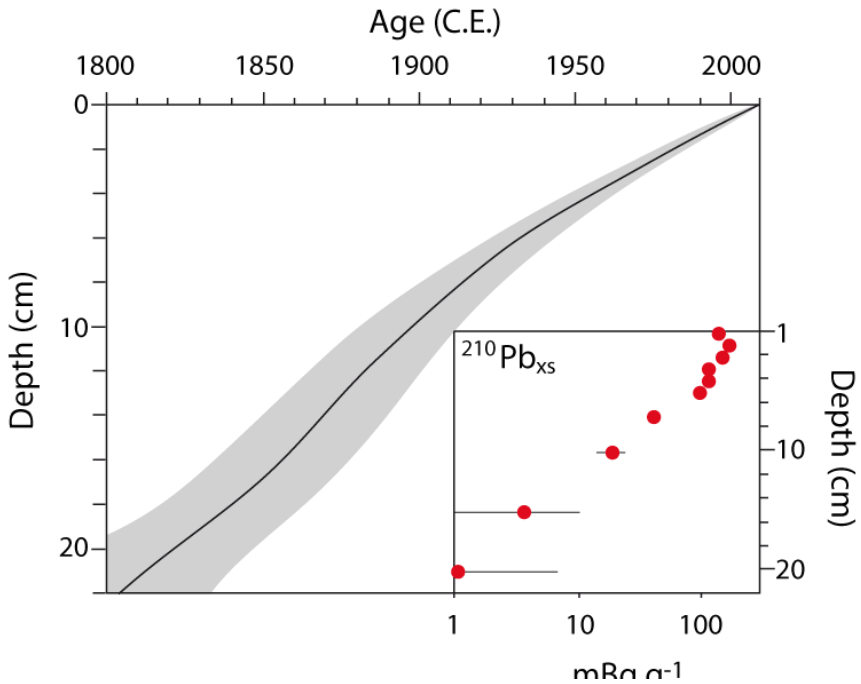

Figure 48. CB2010 chronology. CB2010 age model (dark line) based on 210Pb excess (210Pbxs) and associated age-model errors (grey area). The inset corresponds to the down core profile of 210Pbxs (error bars correspond to 1 SD).

Diatoms. Micropaleontological analyses were performed according to the methodology described in [58]. For each sample, 300-350 diatom valves were counted and data are presented as species relative abundances. Briefly, diatom identification was performed to the species or species group level at a ~5 year resolution. Sixty-eight diatom species were identified in down-core assemblages, from which only a dozen species presented abundances higher than 2% of the total diatom population. Only these species were considered relevant for reconstructing environmental changes. Diatom species or species groups we confront here experience similar ranges of variability in CB2010, ~2.5-13% for *F. cylindrus*, ~1-9% for *F. kerguelensis*, ~0%-7% for the large centric group and *Thalassiosira antarctica* abundances, respectively (Supplementary Fig. S6).

Fragilariopsis cylindrus is one of the most common diatoms found along the Adélie Land margins[59] as it thrives within stratified sea ice covered waters[15]. Large abundances of *F. cylindrus* in sediments indicate the presence of a sea ice cover persisting over 7.5 months per year[15]. In contrast, the open water diatom assemblage, composed by *Fragilariopsis kerguelensis* and large centric diatoms, characterizes open water conditions during summer[16].

Fragilariopsis kerguelensis dominates assemblages of the open ocean zone south of the Polar Front where sea ice is absent during summer[60]. Similarly, high abundances of large centric

diatom species, like *Thalassiosira lentiginosa* or *Thalassiosira oliverana*, commonly occur in the Southern Ocean south of the Polar Front in areas characterized by permanent open ocean conditions[16,61]. Relative abundances of *T. lentiginosa* show an inverse relationship with sea ice cover with high occurrences between 0 and 4 months of sea ice presence per year and a decline towards prolonged sea ice duration[16]. *Thalassiosira oliverana* is clearly dominant in locations where open ocean conditions to sea ice edge during summer occur[16]. *Thalassiosira antarctica* has been described as a dominant species within diatom assemblages in non-stratified or weakly stratified Antarctic surface waters[62]. *Thalassiosira antarctica* blooms in open waters during summer-autumn, and produces resting spores (RS) at the end of the growing season when sea ice returns[63]. *Thalassiosira antarctica* RS, the main form encountered in sediments, is most abundant in regions where sea ice is present for at least 6 months per year, and is believed to be induced under nutrient-stressed conditions or low light intensities[15].

Geochemical data. Few marine and freshwater diatoms belonging to *Haslea, Navicula, Pleurosigma* and *Rhizosolenia* genera were recently found to be synthesizing Highly Branched Isoprenoids (HBI)[14,64]. A di-unsaturated isomer [HBI:2] has been identified in Antarctic sea ice and isotopic analyses provide evidence for that this isomer to be synthesized by sea ice dwelling diatoms. In contrast, tri-unsaturated HBI isomers [HBI:3] have been identified in water column phytoplankton[14]. Recent studies have proposed the use of [HBI:2] and [HBI:3] to reconstruct variations of Holocene Antarctic sea ice duration as complementary sea ice proxy to diatom counts[65]. Biomarker analysis followed the technique described by [14] and were performed every 0.5 cm through the core. Briefly, an internal standard was added to the freeze-dried sediments, lipids were extracted using a Dichloromethane/Methanol mixture to yield a total organic extract (TOE), which was then purified using open column chromatography (silica). Hydrocarbons were analyzed using a Gas Chromatograph coupled to a Mass Spectrometry detector (GC-MS).

Titanium (Ti) and zirconium (Zr) are considered to be direct indicators of terrigenous inputs as these elements are not involved in biological cycles[17]. In the literature, variations in Ti content are largely used to infer past changes in terrigenous supply to the ocean[17]. Microfabric analysis of sediment in the Mertz-Ninnis and Adélie troughs show that both terrigenous content and Ti content are low in spring laminae and increase over the growing season (when open water diatoms dominate the siliceous assemblage) and during which the summer glacial

melting is high[17,53,66]. Indeed, in Antarctic coastal areas, delivery of terrigenous particles is possible via several dominant modes as meltwater discharge, ice rafting, runoff from outlet glaciers, and eolian transport, although this latter source is considered negligible in coastal East Antarctic regions[17,18,19]. Variations in Zr to Rubidium (Rb) content ratio track changes in sediment grain size, where Zr represents the coarsest sediment fraction and Rb the finest[20]. Titanium, Zirconium and Rubidium contents were measured on slab sections at a 2 mm resolution along the entire core using an AAVATECH XRF core-scanner[67].

Satellite data. Daily sea ice concentrations (SIC) for the time period 1978-2012 were obtained from the National Snow and Ice Data Center data repository. The dataset is based on passive microwave observations from the Nimbus-7 SSMR (1978-1987) and DMSP SSM/I (1987-2007) and SSMIS (2007-2012) radiometers processed with the NASA Team algorithm[68] at a spatial resolution of 25x25 km. Averaged concentrations were calculated over two specific domains, Commonwealth Bay and the entire Mertz Glacier Polynya domain (Fig. 49). Daily anomalies were calculated using the average of the pre calving 1978-2009 period and then low-pass filtered using a 3-month moving average (Fig. 43e). SIC data were standardized. Anomalies represent differences between the daily value and the mean daily value calculated over the reference period.

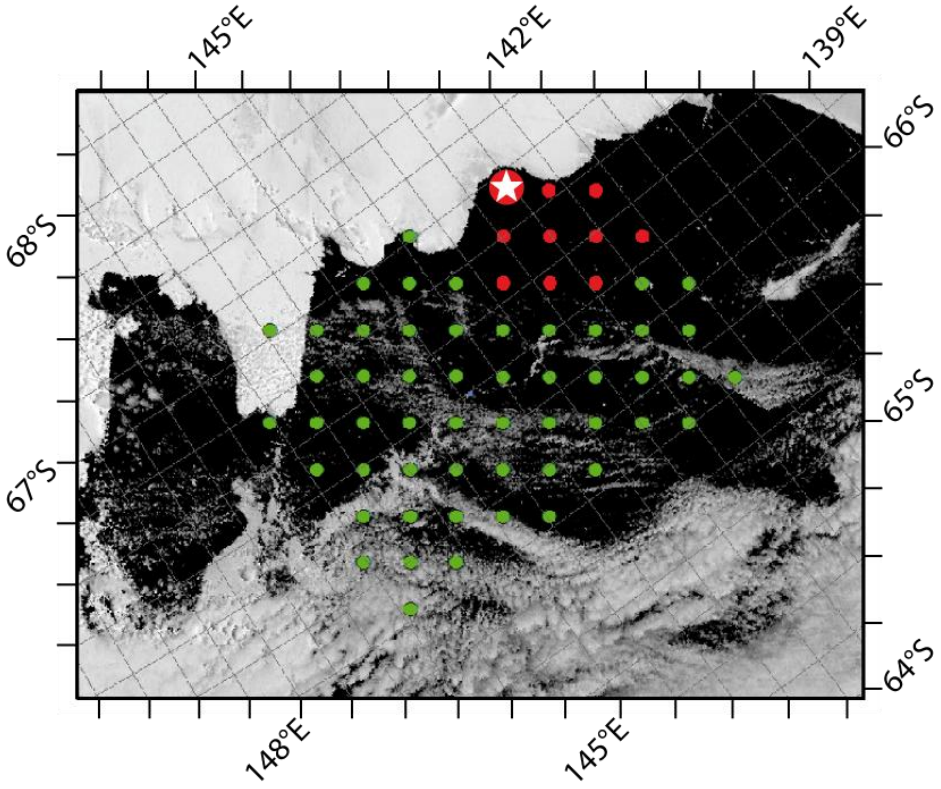

Figure 49. Pixels locations for extraction of sea ice concentration. MODIS satellite image (2008/12/26) of the George V Land indicating the grid points used for the extraction of the daily sea ice concentration values: white star in a red circle indicates the core location; red spots correspond to the CB area; green spots represent the MGP area.

Spectral analysis. Unlike many traditional mathematical methods (*e.g.* Fourier analysis), the wavelet approach can be used to analyze time series that contain non-stationary spectral power at many different frequencies[21]. For geological time series, although visual comparison of plots is commonly used, cross-wavelet analysis permits detection, extraction, and reconstruction of relationships between two non-stationary signals simultaneously in frequency (or scale) and time (or location)[69]. The continuous wavelet transform (CWT; Supplementary Fig. S1) of time series is its convolution with the local basis functions, or wavelets, which can be stretched and translated with flexible resolution in both frequency and time. The principle of cross wavelet analysis and the complete method we used are described in [21]. We used the MATLAB package for Cross-wavelet analysis written by [21] and applied the Morlet wavelet as the mother function on our dataset. This method provides a good balance between time and frequency localization, and we used Monte Carlo simulations to provide frequency-specific probability distribution (Global wavelet spectrum) that can be tested against wavelet coefficients. Statistical significance was estimated against a red noise

model[21]. In this study, to test the relevance of our proxies, their statistical relationships and to examine periodicities in a frequency domain, we compared the two time series by their CWTs, which we hypothesized are linked in some way. The resulting Cross Wavelet Transform (XWT; Fig. 45) exposed their common power and relative phase in time-frequency space of the two signals. Data were previously standardised, which did not introduce any change in the shape of the records but normalized the amplitude of the variations (Supplementary Fig. S6).

Atmospheric reanalysis. To analyse the Southern Hemisphere atmospheric circulation during the last 140 years, we used the recent twentieth century reanalysis (20CR) Project version 2 [41], consisting of an ensemble of 56 realisations with 2° x 2° gridded 6-hourly weather data from 1871 to 2010. Each ensemble member was performed using the NCEP/GFS atmospheric model, prescribing the monthly sea surface temperature and sea ice changes from HadISST as boundary conditions, and assimilating sea level pressure data from the International Surface Pressure Databank version 2 (http://rda.ucar.edu/datasets/ds132.0). We used the ensemble mean to perform our analysis. An important caveat concerns the fact that few data were assimilated at the beginning of the reanalysis in the Southern Hemisphere, due to the lack of available observations. Nevertheless, this product is one of the best datasets available for the evaluation of atmospheric circulation changes at a large scale in the Southern Hemisphere. Wind speed products were plotted over the Terre Adélie-George V Land (Fig. 47) and the offshore region around 55-60°S (Supplementary Fig. S5).

REFERENCES

1 Johnson, G. C. Quantifying Antarctic Bottom Water and North Atlantic Deep Water volumes. *J. Geophys. Res*. **113,** C05027 (2008).

2 Jacobs, S. Bottom water production and its links with the thermohaline circulation. *Antarctic Science* **16**(4), 427-437 (2004).

3 Tamura, T., Ohshima, K. I. & Nihashi, S. Mapping of sea ice production for Antarctic coastal polynyas. *Geophys. Res. Lett.* **35,** L07606 (2008).

4 Arrigo, K. R. & van Dijken, G. L. Phytoplankton dynamics within 37 Antarctic coastal polynya systems. *J. Geophys. Res*. **108**(C8), 3271 (2003).

5 Barber, D.G. & Massom, R.A. The role of sea ice in Arctic and Antarctic polynyas. In *Polynyas: windows to the world*, Smith Jr., W.O. *et al.* (Ed.), Elsevier Oceanography Series, **74**, 1-54 (2007).

6 Rintoul, S. R. On the Origin and Influence of Adélie Land Bottom Water. In *Ocean, Ice, and Atmosphere: Interactions at the Antarctic Continental Margin*, Jacobs, S. & Weiss, R. (Ed.), Antarctic Research Series **75**, 151–171 (1998).

7 Williams, G. D., Bindoff, N. L., Marsland, S. J. & Rintoul, S. R. Formation and export of dense shelf water from the Adélie Depression, East Antarctica. *J. Geophys. Res.* **113**, C04039 (2008).

8 Massom, R. A., Harris, P. T., Michael, K. J. & Potter, M. J. The distribution of formative processes of latent heat polynyas in East Antarctica. *Ann. Glaciology* **27**, 420-426 (1998).

9 Lacarra, M., Houssais, M. N., Herbaut, C., Sultan, E. & Beauverger, M. Dense shelf water production in the Adélie Depression 2004-2012: Impact of the Mertz glacier calving. *J. Geoph. Res.* **119**(8), 5203-5220 (2014).

10 Tamura, T., Williams, G. D., Fraser, A. D. & Ohshima, K. I. Potential regime shift in decreased sea ice production after the Mertz Glacier calving. *Nat. Commun.* **3,** 826 (2012).

11 Kusahara, K., Hasumi, H. & Williams, G. Impact of Mertz Glacier Tongue calving on dense shelf water. *Nat. Commun.* **2,** 159 (2011a).

12 Frezzotti, M., Cimbelli, A. & Ferrigno, J. G. Ice-front change and iceberg behavior along Oates and George V coasts, Antarctica, 1912–96. *Ann. Glaciol*. **27,** 643–650 (1998).

13 Williams, G.D. & Bindoff, N.L. Wintertime oceanography of the Adélie depression. *Deep-Sea Res. Part II* **50**, 1373-1392 (2003).

14 Massé, G. *et al*. Highly branched isoprenoids as proxies for variable sea ice conditions in the Southern Ocean. *Ant. Sci.* **23,** 487-498 (2011).

15 Armand, L. K., Crosta, X., Romero, O. & Pichon, J.-J. The biogeography of major diatom taxa in Southern Ocean sediments: 1. Sea ice related species. *Palaeogeog., Palaeoclim., Palaeoecol.* **223**, 93-126 (2005).

16 Crosta, X., Romero, O., Armand, L. K. & Pichon, J.-J. The biogeography of major diatom taxa in Southern Ocean sediments: 2. Open ocean related species. *Palaeogeog., Palaeoclim., Palaeoecol.* **223,** 66-92 (2005).

17 Denis D. *et al*. Seasonal and sub-seasonal climate changes recorded in laminated diatom ooze sediments, Adélie Land, East Antarctica. *The Holocene* **16,** 1137-1147 (2006).

18 Presti, M., De Santis, L., Busetti, M. & Harris, P.T. Late Pleistocene and Holocene sedimentation on the George V Continental Shelf, East Antarctica. *Deep-Sea Res. Part II* **50**, 1441-1461 (2003).

19 Escutia, C. *et al*. Sediment distribution and sedimentary processes across the Antarctic Wilkes Land margin during the Quaternary. *Deep Sea Research Part II* **50**, 3225-3226 (2003).

20 Dypvik, H. & Harris, N. B. Geochemical facies analysis of fine-grained siliciclastics using Th/U, Zr/Rb and (Zr+Rb)/Sr ratios. *Chem. Geol.* **181**(1–4), 131–146 (2001).

21 Grinsted, A., Moore, J.C. & Jevrejeva, S. Application of the cross wavelet transform and wavelet coherence to geophysical time series. *Nonlin. Process. Geophys.* **11,** 561-566 (2004).

22 Stammerjohn, S. E., Martinson, D. G., Smith, R. C., Yuan, X. & Rind, D. Trends in Antarctic annual sea ice retreat and advance and their relation to El Niño–Southern Oscillation and Southern Annular Mode variability. *J. Geophys. Res.* **113**, C03S90, doi: 10.1029/2007JC004269 (2008).

23 Dinniman M. S., Klinck, J. M. & Hofmann, E. E. Sensitivity of Circumpolar Deep Water Transport and Ice Shelf Basal Melt along the West Antarctic Peninsula to changes in the winds. *Amer. Meteor. Soc*. **25**(14), 4799-4816 (2012).

24 Wuite, J. Spatial and Temporal Dynamics of Three East Antarctic Outlet Glaciers and Their Floating Ice Tongues. Ph.D. thesis, Ohio State Univ., Columbus, pp. 190 (2006).

25 Lescarmontier, L. *et al*. Vibration of the Mertz Glacier ice tongue, East Antarctica. *J. Glaciol.* **58**(210), 665-676 (2012).

26 Legresy B., Wendt A., Tabacco I., Remy F. & Dietrich R. Influence of tides and tidal current on Mertz Glacier, Antarctica. *J. Glaciol.* **50**(170), 427-435 (2004).

27 Marshall, G. J. Trends in the Southern Annular Mode from observations and reanalyzes. *J. Clim.* **16,** 4134–4143 (2003).

28 Thompson, D. W. J. & Wallace, J. M. Annular Modes in the Extratropical Circulation. Part I: Month-to-Month Variability. *J. Climate* **13**, 1000–1016 (2000).

29 Thompson, D. W. J. & Solomon, S. Interpretation of recent Southern Hemisphere climate change. *Science* **296,** 895-899 (2002).

30 Fogt, R. L., Perlwitz, J., Monaghan, A. J., Bromwich, D. H., Jones, J. M. & Marshall, G. J. Historical SAM Variability. Part II: Twentieth-Century Variability and Trends from Reconstructions, Observations, and the IPCC AR4 Models. *J. Climate* **22**, 5346–5365 (2009).

31 Villalba, R. *et al*. Unusual Southern Hemisphere tree growth patterns induced by changes in the Southern Annular Mode. *Nat. Geosci*. **5,** 793–798 (2012).

32 Arblaster, J. M. & Meehl, G. A. Contributions of External Forcings to Southern Annular Mode Trends. *J. Climate* **19**, 2896–2905 (2006).

33 Jacobs, S. Observations of changes in the Southern Ocean. *Phil. Trans. R. Soc. A.* **364,** 1657-1681 (2006).

34 Massom, R. A. *et al*. Fast ice distribution in Adélie Land, East Antarctica: Interannual variability and implications for Emperor penguins (*Aptenodytesforsteri*). *Mar Ecol. Progr. Ser*. **374,** 243–257 (2009).

35 Hall, A. & Visbeck, M. Synchronous variability in the Southern Hemisphere atmosphere, sea ice, and ocean resulting from the Annular Mode. *J. Clim.* **15,** 3043-3057 (2002).

36 Meredith, M. P. & Hogg, A. M. Circumpolar response of Southern Ocean eddy activity to a change in the Southern Annular Mode. *Geophys. Res. Lett.*, **33**, L16608 (2006).

37 Parish, N. J. P. & Bromwich, D. H. Continental-scale simulation of the Antarctic katabatic wind regime. *J. Climate* **4,** 135–146 (1991).

38 Van der Broeke, M. R., van Lipzig, N. P. M. & van Meijgaard, E. Momentum Budget of the East Antarctic Atmospheric Boundary Layer: Results of a Regional Climate Model. *J. Atmos. Sci.* **59**, 3117–3129 (2002).

39 Egger, J. Slope winds and the axisymmetric circulation over Antarctica. *J. atmos. sci.* **42**, 1859-1867 (1985).

40 Yasunari, T. & Kodama, S. Intraseasonal variability of katabatic wind over east Antarctica and planetary flow regime in the southern hemisphere. *J. Geophys. Res.* **98**(D7), 13063–13070 (1993).

41 Compo, G. P. *et al*. The Twentieth Century reanalysis Project. *Q.J.R. Meteor. Soc.* **137,** 1–28 (2011).

42 Van der Broeke, M. & van Lipzig, N. P. M. Changes in Antarctic temperature wind and precipitation in response to Antarctic Oscillation. *Ann. Glaciology* **39**, 119-126 (2004).

43 Massom, R. A. *et al*. An anomalous late-season change in the regional sea ice regime in the vicinity of the Mertz Glacier Polynya, East Antarctica. *J. Geophys. Res.* **108**(C7)**,** 3212 (2003).

44 Massom, R. A. *et al*. Change and variability in East Antarctic sea ice seasonality, 1979/80–2009/10. *PLoS ONE* **8**(5), e64756 (2013).

45 Schmidtko, S., Heywood, K. J., Thompson, H. & Shigeru, A. Multidecadal warming of antarctic waters. *Science* **346**, 1227-1231 (2014).

46 Martinson, D. G., Stammerjohn, S. E., Iannuzzi, R. A., Smith, R. C. & Vernet, M. Western Antarctic Peninsula physical oceanography and spatio-temporal variability. *Deep-Sea Res. Part II* **55,** 1964–1987 (2008).

47 Marini, C., Frankignoul, C. & Mignot, J. Links between the Southern Annular Mode and the Atlantic Meridional Overturning Circulation in a Climate Model. *J. Climate* **24,** 624–640 (2011).

48 Orsi, A. H., Whitworth III, T. & Nowlin, W. D. Jr. On the meridional extent and fronts of the Antarctic Circumpolar Current. *Deep-Sea Res. Part I* **42,** 641–673 (1995).

49 Klinck, J. M. & Dinniman, M. S. Exchange across the shelf break at high southern latitudes. *Ocean Sci*., **6**, 513-524 (2010).

50 St-Laurent, P., Klinck, J.M. & Dinniman, M.S. On the Role of Coastal Troughs in the Circulation of Warm Circumpolar Deep Water on Antarctic Shelves. *J. Phys. Ocean.* **43**(1), 51-64 (2013).

51 Bindoff, N. L., Rosenberg, M. A. & Warner, M. J. On the circulation and water masses over the Antarctic continental slope and rise between 80 and 150°E. *Deep-Sea Res II* **47**, 2299-2326 (2000).

52 Aoki, S., Sasai, Y., Sasaki, H., Mitsudera, H. & Williams, G. D. The cyclonic circulation in the Australian Antarctic basin simulated by an eddy resolving general circulation model. *Ocean Dyn.* **60**(3), 743-757 (2010).

53 Maddison, E. J. *et al*. Post-glacial seasonal diatom record of the Mertz Glacier Polynya, East Antarctica. *Mar. Micropal.* **60**(1), 66–88 (2006).

54 Rintoul, S. R. Rapid freshening of Antarctic Bottom Water formed in the Indian and Pacific oceans. *Geophys. Res. Lett.* **34**, L06606 (2007).

55 Aoki, S., Rintoul, S., Ushio, S. & Watanabe, S. Freshening of the Adélie Land Bottom Water near 140°E. *Geophys. Res. Lett*. **32,** L23601 (2005).

56 Previdi, M. & Polvani, L. M. Climate system response to stratospheric ozone depletion and recovery. *Q.J.R. Meteorol. Soc.* **140**, 2401–2419 (2014).

57 Migeon, S., Weber, O., Faugères, J.-C. & Saint-Paul, J. SCOPIX : a new X-ray imaging system for core analysis. *Geo-Mar. Lett.* **18,** 251-255 (1999).

58 Crosta, X. & Koc, N. Diatoms: From micropaleontology to isotope geochemistry. In *Methods in Late Cenozoic Paleoceanography*, Hilaire-Marcel, C. & de Vernal, A. (Ed.), Elsevier, Amsterdam, The Netherlands, 327-369 (2007).

59 Kang, S.-H. & Fryxell, G. A. *Fragilariopsis cylindrus* (Grunow) Krieger: The most abundant diatom in water column assemblages of Antarctic marginal ice edge zones. *Pol. Biol.* **12,** 609–627 (1992).

60 Froneman, J. W., McQuaid, G. D. & Perissinotto, R. Biogeographic structure of the microphytoplankton assemblages of the south Atlantic and Southern Ocean during austral summer. *J. Plankton Res.* **17,** 1791-1802 (1995b).

61 Johansen, J.R. & Fryxell, G.A. The genus *Thalassiosira* (Bacillariophyceae): Studies on species occurring south of the Antarctic Convergence Zone. *Phycologia* **24**(2), 155-179 (1985).

62 Gregory, T. Holocene sea ice-ocean-climate variability from Adélie Land, East Antarctica. Ph.D. thesis, Cardiff University, UK., pp. 237 (2012).

63 Cunningham, W. L. & Leventer, A. Diatom assemblages in surface sediments of the Ross Sea: Relationship to present oceanographic conditions. *Ant. Sci.* **10**(2), 134-146 (1998).

64 Sinninghé Damsté, J. S. *et al*. The rise of the Rhizosolenoid diatoms. *Science,* **304**(5670), 584-587 (2004).

65 Collins, L. G. *et al*. Evaluating highly branched isoprenoid (HBI) biomarkers as a novel Antarctic sea-ice proxy in deep ocean glacial age sediments. *Quat. Sci. Rev.* **79**, 87-98 (2013).

66 Maddison, E. J., Pike, J. & Dunbar, R. Seasonally laminated diatom-rich sediments from Dumont d'Urville Trough, East Antarctic Margin: Late-Holocene Neoglacial sea-ice conditions. *The Holocene* **22**(8), 857-875 (2012).

67 Jansen, J. H. F., Van der Gaast, S. J., Koster, B. & Vaars, A. J. CORTEX, a shipboard XRF-scanner for element analyses in split sediment cores. *Mar. Geol.* **151,** 143-53 (1998).

68 Cavalieri, D. J., St. Germain, K. & Swift, C. T. Reduction of weather effects in the calculation of sea ice concentration with the DMSP SSM/I. *J. Glaciol.* **41,** 455-464 (1995).

69 Prokoph, A. & El Bilali, H. Cross-Wavelet Analysis: a Tool for Detection of Relationships between Paleoclimate Proxy Records. *Math. Geosc.* **40**(5), 575-586 (2008).

70 Gong, D. & Wang, S. Definition of Antarctic Oscillation Index, *Geophys. Res. Lett.* **26,** 459-462 (1999).

ACKNOWLEDGMENTS

This research was funded by the ERC StG ICEPROXY project (203441), the ANR CLIMICE project and FP7 Past4Future project (243908). P.C. is supported by a CNRS studentship. The French Polar Institute provided logistical support for sediment and data collection (IPEV projects 452 & 1010). This is ESF PolarClimate HOLOCLIP contribution n°24 and Past4Future contribution n°83.

AUTHOR CONTRIBUTIONS

X. C., G. M. & M-N. H. designed the study; P.C. performed diatom and XRF analyses; I. C. performed the biomarker analysis; D.S. performed atmospheric reanalysis; M-N. H. and A. M. extracted daily sea ice concentrations and provided modern oceanographic insights; S. S. performed ^{210}Pb analyses and developed the age model of the core; S. C., E. D. and V. M. helped with satellite images and spectral analyses; All the authors contributed to the redaction of the manuscript.

ADDITIONAL INFORMATION

The authors declare no competing financial interests. Supplementary information accompanies this paper on www.nature.com. Reprints and permissions information is available online at http://www.nature.com/reprints. Correspondence and requests for material should be addressed to X.C (x.crosta@epoc.u-bordeaux1.fr) or G.M. (guillaume.masse@takuvik.ulaval.ca).

Suppementary information

Supplementary Figures

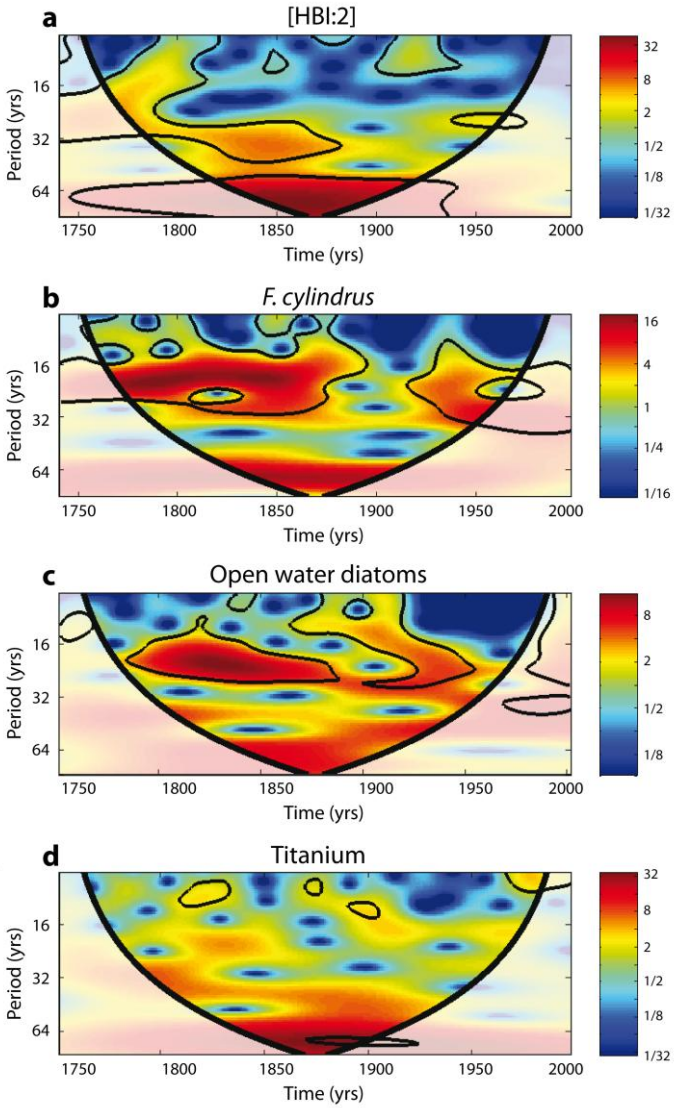

Supplementary Figure 1 | Spectral analysis on individual sedimentary records. Continuous wavelet transform applied on **a**, [HBI:2], **b**, *Fragilariopsis cylindrus*, **c**, Open water diatom assemblage and **d**, Titanium, using Morlet wavelet according to [1] (see Methods).

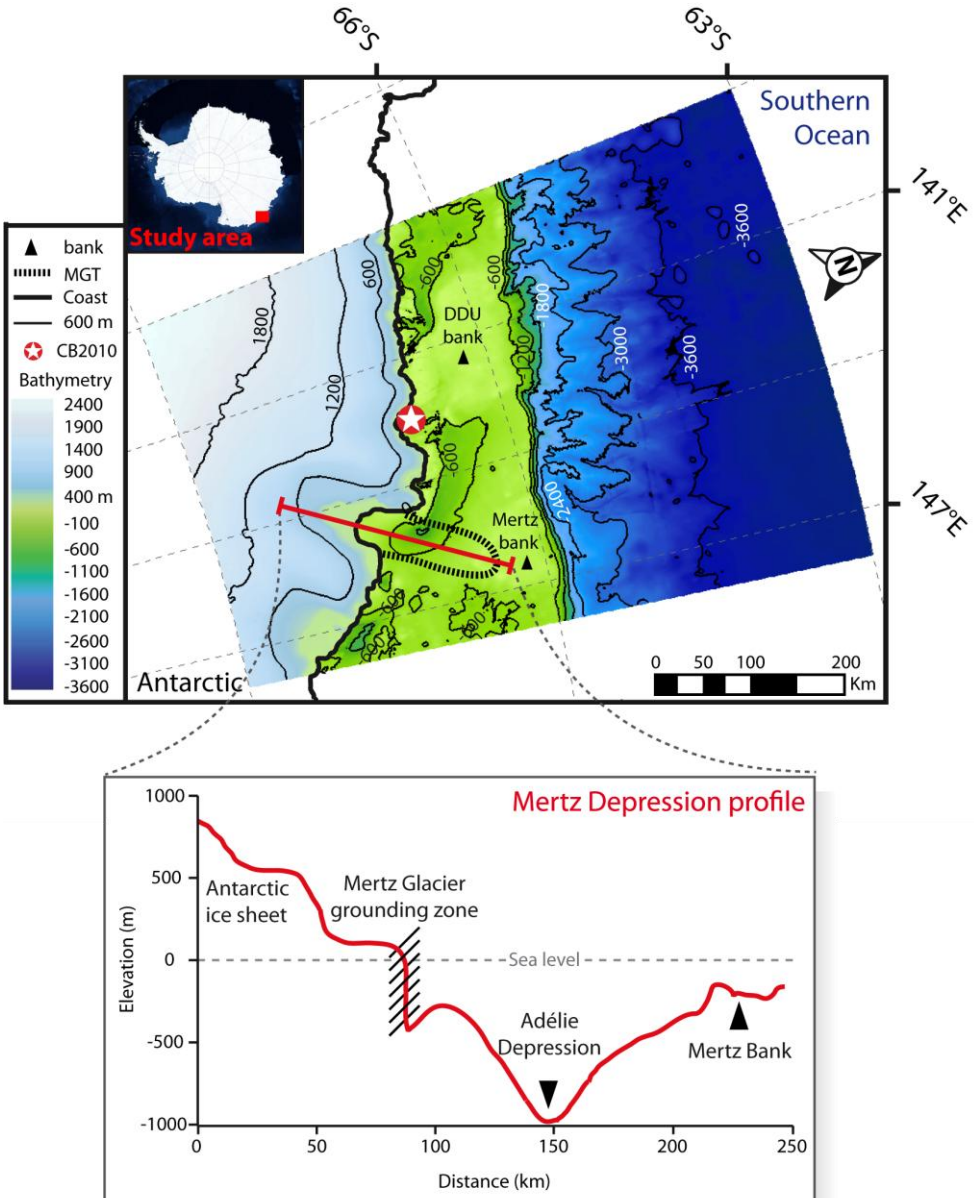

Supplementary Figure 2 | Bathymetry model of the Georges V Land. Data obtained from http://www.deepreef.org/publications/peer-review/82-gvdem.html.

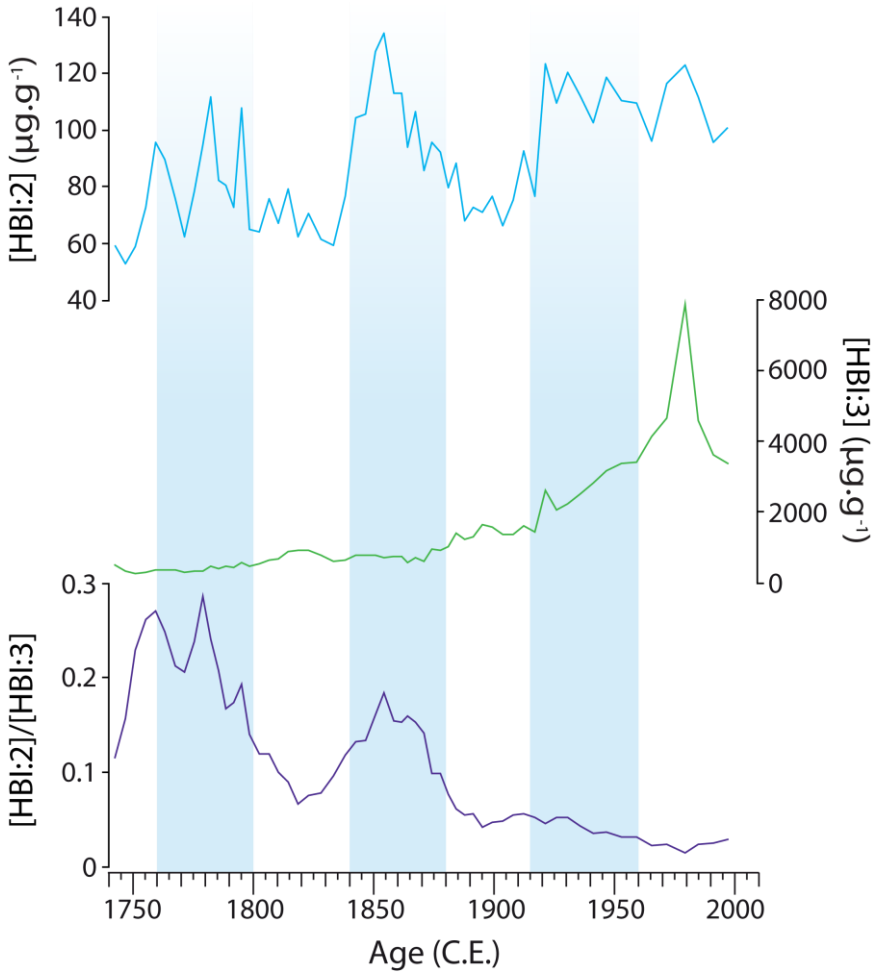

Supplementary Figure 3 | Relative contributions of sea ice *versus* phytoplanktonic-derived organic matter over the last 250 years, inferred from Highly Branched Isoprenoids records. Relative concentration (in µg.g^{-1}) of [HBI:2] (blue)**,** [HBI:3] (green) and [HBI:2]/[HBI:3] (dark blue). The blue shadings indicate decades following each calving event with marked increase in sea-ice concentration in the CB area.

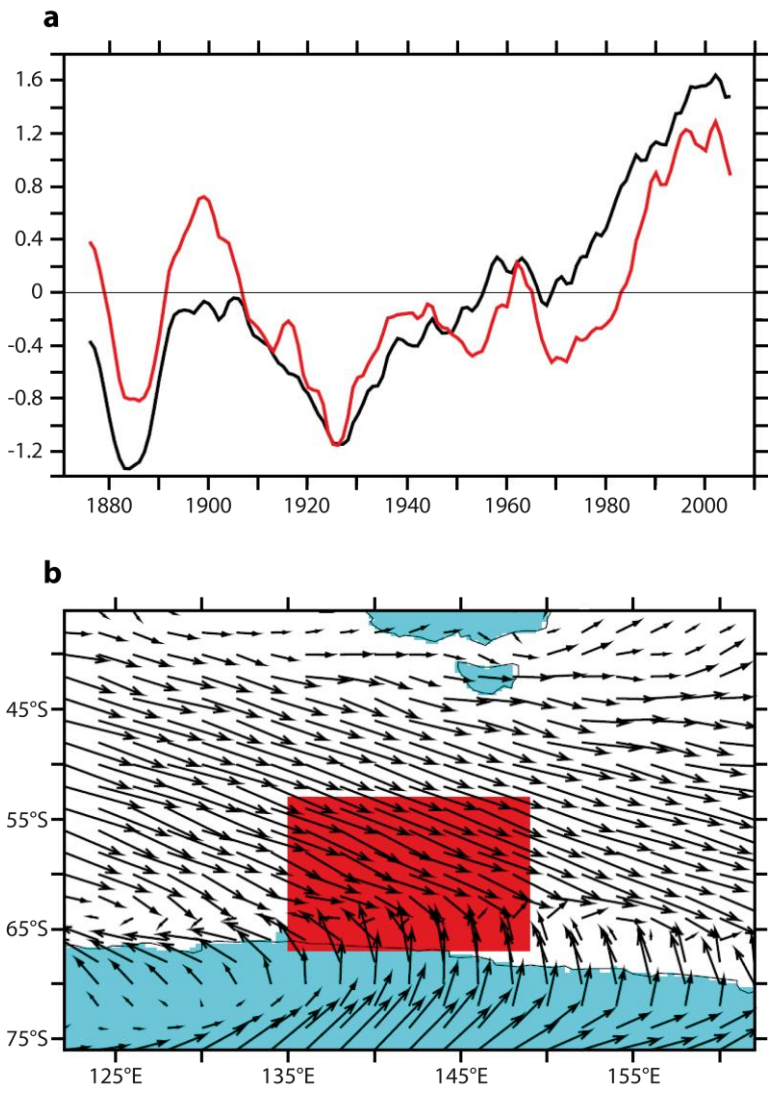

Supplementary Figure 4 | Evolution of the Southern Annular Mode (SAM) and its impacts on the Ekman pumping through changes in the wind stress, offshore Georges V Land since the XIX century. Wind speed at 2 meters from 20CR reanalysis over the last 140 years. **a**, Annual standardised values of SAM index (black), computed in the reanalysis following [2], and the surface wind stress curl (red); **b**, Wind mean speed and vector, red box indicates the study area where the winds have been computed in panel **a**.

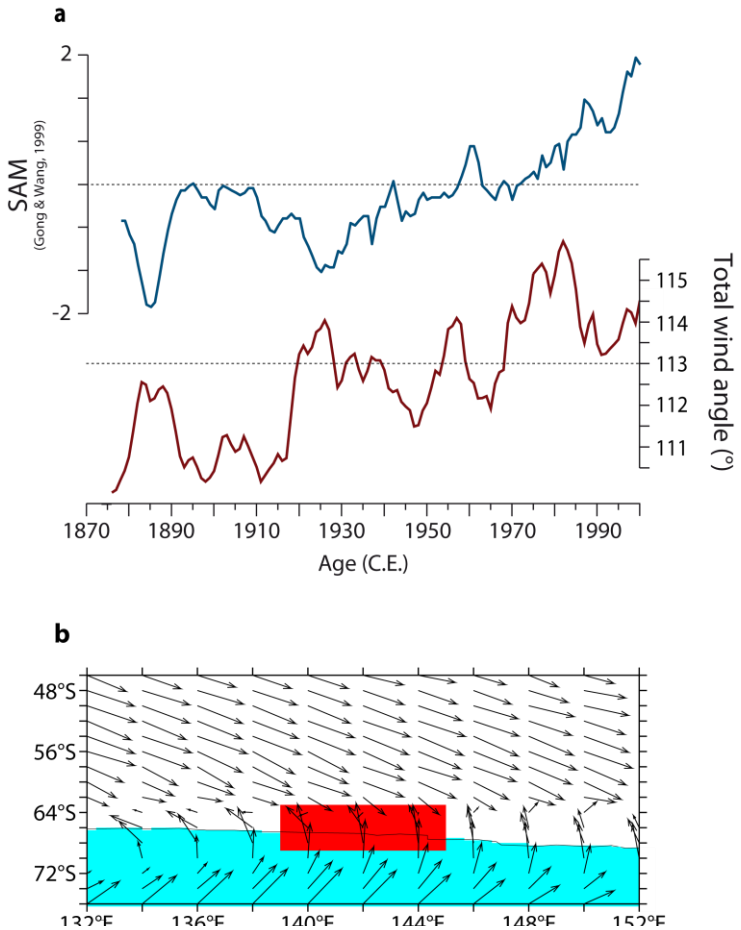

Supplementary Figure 5 | Evolution of the Southern Annular Mode (SAM) and its impacts on the wind pattern, offshore Georges V Land since the XIX century. Wind speed at 2 meters from 20CR reanalysis over the last 140 years. **a**, Standardised values of SAM index (5 yr running mean; blue), computed in the reanalysis following [2], and the total wind direction angle (brown; °) respective to the North direction indicating the 0° or 360° and counting positively clockwise; **b**, Mean wind speed and vector, red box indicates the study area where the wind have been computed in panel **a**.

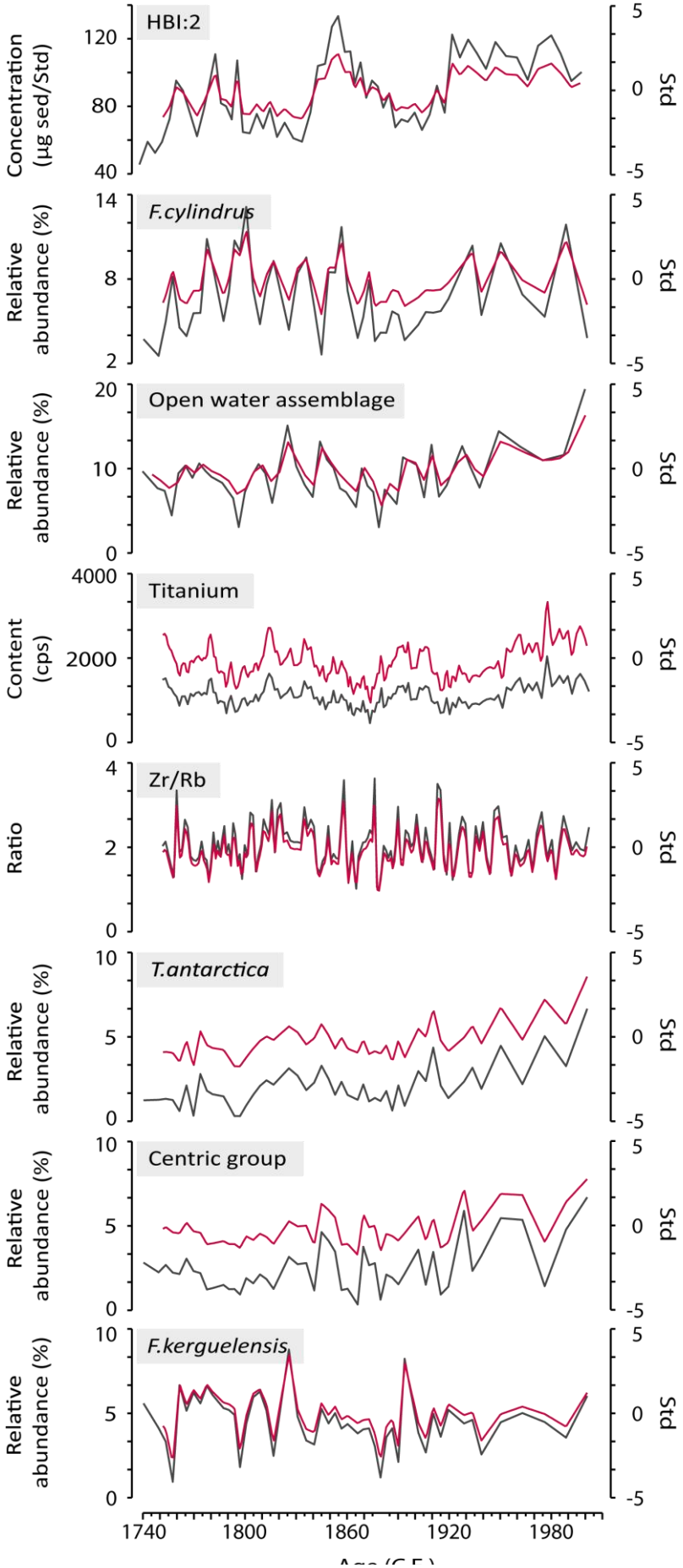
HBI:2
Concentration (µg sed/Std)
120
80
40
F.cylindrus
Relative abundance (%)
14
8
2
Open water assemblage
Relative abundance (%)
20
10
0
Titanium
Content (cps)
4000
2000
0
Zr/Rb
Ratio
4
2
0
T.antarctica
Relative abundance (%)
10
5
0
Centric group
Relative abundance (%)
10
5
0
F.kerguelensis
Relative abundance (%)
10
5
0
Std
5
0
-5
1740
1800
1860
1920
1980

Supplementary Figure 6 | Raw versus standardised data. Raw data (grey) and standardised data (red) obtained from the sediment core CB2010.

Supplementary Note 1

Supplementary Fig. 3 shows the evolution of the [HBI:2] and [HBI:3] abundances, along with their ratio, through the sediment core CB2010. Although [HBI:3] show increased abundances during 'open water' periods throughout the last 250 years, the very large peak centered in the 1980s reduces the amplitude of past cycles. The overall shape of the record does not result from early diagenesis with an increase in degradation of HBIs with time since we observe a decrease in abundances in the most recent sediments. The increase in [HBI:3] over recent decades reflects greater productivity at the sea ice edge during late spring-early summer as observed in the Scotia Sea[3]. Although the signal is perturbed by a large peak, [HBI:3] presents an opposite trend to that of [HBI:2]. Indeed, increasing values of [HBI:3] are concomitant to low values of [HBI:2] (Supplementary Fig. 3). This is further confirmed by the [HBI:2]/[HBI:3] ratio, which agrees with the [HBI:2] cyclic pattern, although the signal is blurred over the last century, owing to high values of both [HBI:3] and [HBI:2] (Supplementary Fig. 3). An increase in both [HBI:2] and [HBI:3], concomitant to an increase in sea ice diatoms and open water diatoms, reflects a shift towards more contrasted seasonal conditions in the last 65 years, with longer sea ice persistence in springtime and warmer surface waters during the summer. Model re-analyses (Fig. 47; Supplementary Fig. 4; Supplementary Fig. 5) and recent studies suggest that positive SAM may be the trigger for stronger seasonal contrasts[4,5] that result from atmospheric reorganization[6,7] and influence both sea ice duration and CDW intrusion around Antartica[4,8,9] and possibly in our study area.

Supplementary Note 2

Wind fields from 20CR reanalysis over the George V Land (Fig. 47) show that the wind pattern deviates toward more zonal component since the 1950s (indicating a stronger westward stress, Fig. 47a) resulting in a significant shift of ~10° towards more easterly winds. Interestingly, this shift is concomitant with the SAM increasing trend.

Wind fields from 20CR reanalysis offshore George V Land show that since 1950, the total wind angle has increased toward more meridional component (indicated a southward stress; Supplementary Fig. 5a, brown curve) resulting in a more southern position of the Westerlies (Suppplementary Fig. 5b). Interestingly, the Westerlies record from 20CR reanalysis is positively correlated to the reanalyzed SAM pattern (Supplementary Fig. 5a, blue curve). Such observations agree with several studies suggesting that the increasing positive trend of the SAM led to reinforcing the Westerlies and pushing them southward[6].

This atmospheric configuration, with more zonal winds along the East Antarctic coast, and a southward migration of the Westerlies since 1950 promoting the southward migration of the Antarctic Circumpolar Current (ACC), lead to enhance CDW upwelling close to the continent[10,11] due to the increase in the wind stress shear leading to a stronger Ekman drift and ocean surface current divergence. This scenario is supported by the surface wind stress curl calculated from the 20CR reanalysis (Supplementary Fig. 4, red curve), which suggests a good correlation with the SAM pattern over the reanalysis period, and shows strong positive trend in upwelling-favorable vertical velocities starting roughly at 1950, traducing an enhanced Ekman pumping over the last decades, concomitant with increasing open water signals in our geological data.

Supplementary References

1. Grinsted, A., Moore, J.C. & Jevrejeva, S. Application of the cross wavelet transform and wavelet coherence to geophysical time series. *Nonlin. Process. Geophys.* **11,** 561-566 (2004).

2. Gong, D. & Wang, S. Definition of Antarctic Oscillation Index, *Geophys. Res. Lett.* **26,** 459-462 (1999).

3. Collins, L. G. *et al*. Evaluating highly branched isoprenoid (HBI) biomarkers as a novel Antarctic sea-ice proxy in deep ocean glacial age sediments. *Quat. Sci. Rev.* **79**, 87-98 (2013).

4. Stammerjohn, S. E., Martinson, D. G., Smith, R. C., Yuan, X. & Rind, D. Trends in Antarctic annual sea ice retreat and advance and their relation to El Niño–Southern

Oscillation and Southern Annular Mode variability. *J. Geophys. Res.* **113**(C03), (2008).

5. Marshall, G. J. Trends in the Southern Annular Mode from observations and reanalyzes. *J. Clim.* **16,** 4134–4143 (2003).

6. Thompson, D. W. J. & Wallace, J. M. Annular Modes in the Extratropical Circulation. Part I: Month-to-Month Variability. *J. Climate*, **13**, 1000–1016 (2000).

7. Arblaster, J. M. & Meehl, G. A. Contributions of External Forcings to Southern Annular Mode Trends. *J. Climate*, **19**, 2896–2905 (2006).

8. Dinniman M. S., Klinick, J. M. & Hofmann, E. E. Sensitivity of Circumpolar Deep Water Transport and Ice Shelf Basal Melt along the West Antarctic Peninsula to changes in the winds. *Amer. Meteor. Soc*. **25**(14), (2012).

9. Martinson, D. G., Stammerjohn, S. E., Iannuzzi, R. A., Smith, R. C. & Vernet, M. Western Antarctic Peninsula physical oceanography and spatio-temporal variability. *Deep-Sea Res. Part II* **55,** 1964–1987 (2008).

10. Hall, A. & Visbeck, M. Synchronous variability in the Southern Hemisphere atmosphere, sea ice, and ocean resulting from the Annular Mode. *J. Clim.* **15,** 3043-3057 (2002).

11. Marini, C., Frankignoul, C. & Mignot, J. Links between the Southern Annular Mode and the Atlantic Meridional Overturning Circulation in a Climate Model. *J. Climate* **24,** 624–640 (2011).

Article III: Sea ice variability and potential related forcing in the Adélie-Georges V Land over the last 500 years

in preparation

Campagne, P.1,2,3, Massé, G.2,3, Schmidt, S.1 and Crosta, X.1

1EPOC, UMR CNRS 5805, Université de Bordeaux, Allée Geoffroy St Hilaire, 33615 Pessac, France

2LOCEAN, UMR CNRS/UPCM/IRD/MNHN 7159, Université Pierre et Marie Curie, 4 Place Jussieu, 75252 Paris, France

3TAKUVIK, UMI 3376 UL/CNRS, Université Laval, G1V 0A6 Quebec (Quebec), Canada

Over the past decades, satellite observations indicate increasing sea ice conditions off East Antarctica at the opposite of the relatively strong warming monitored in the western Antarctic region (Cavalieri and Parkinson, 2008). The few existing marine records in the Southern Ocean, generally at low resolution and missing the last millennium, indicate that this opposition may have lasted for the whole Holocene with an out-of-phase sea ice variability between East Antarctica (Denis et al., 2011) and West Antarctica (Shevenell et al., 2011; Etourneau et al., 2013). Such a complex and highly heterogeneous regional climate trends in Antarctica therefore complicate the understanding of underlying mechanisms at decadal to centennial timescales. Here, we provide a sub-decadal resolution record of sea ice dynamic off Adélie Land (East Antarctica) over the last 500 years based on diatom census counts and diatom-specific lipid biomarkers (HBIs) in the laminated core DTGC2011. Three climate intervals, characterized by changes in sea ice seasonality and polynya activity, can be distinguished over the last 500 years. Stationary decadal to pluri-decadal climate variations were present in all three climate intervals. Comparison of the new datasets with previous findings in the Mertz Depression off Adélie-Georges V Land (AGVL) through wavelet analyses revealed that synoptic scale atmospheric and oceanic reorganization coupled to local glacial dynamics drove the sub-decadal to centennial scales variability of sea surface and polynya conditions in our study area.

Key words: Late Holocene, Adélie Land, Sea ice, diatoms, HBIs, decadal variability, Mertz glacier, forcing, atmospheric variability, SAM, SOI.

1 Introduction

The late Holocene period is characterized by large scale climate changes at decadal to centennial timescales (e.g. Mayewski et al., 2004; Mann et al., 2008), which have been mainly related to changes in the thermohaline circulation and solar activity (Debret et al., 2010; Whirth et al., 2013) and volcanic activity (McGregor et al., 2015; Sigl et al., 2015). Much less is known for the Southern Ocean (SO) where there is an evident lack of paleoclimate records covering this period of time. Although an extensive network of ice cores in Antarctica is revealing much about the nature of late Holocene atmospheric variability, the few paleoclimate reconstructions in the Southern Hemisphere (SH) further highlight complex and high heterogeneous regional variations in atmospheric temperatures and sea ice cover (e.g. Masson et al., 2000; Stenni et al., 2002; Mayewski et al., 2004; Denis et al., 2010; Bertler et al., 2011; Etourneau et al., 2013), complicating the understanding of underlying mechanisms. Additionally, the few marine records available tend to be short and low resolution. Indeed, most of the published marine records lack the last millennium (Cremer et al., 2007; Crosta et al., 2007; Denis et al., 2010), present a too low resolution (Leventer et al., 1993; Allen et al., 2010; Shevenell et al., 2011) or, conversely, are too short in time (Barbara et al., 2013; Campagne et al., 2015). For these reasons, only few paleoclimate studies have focused on decadal to pluri-decadal scale variability in the Antarctic region (Leventer et al., 1996; Warner and Domack, 2002; Nielsen et al., 2004; Crosta, et al., 2007). However, documenting climate changes over the last centuries and understanding their forcing mechanisms is pivotal to replace the current observed changes into the most proximal natural context and, hence, whether the recent changes are unique and externally forced or they are within the range of decadal-to-centennial natural climate variability.

We here present the first marine-based paleoclimate record covering the ~1540-2000 C.E. period at interannual resolution, retrieved on the Antarctic Continental Shelf off AGVL. The high sediment rates at the core site allow for assessing the evolution of sea surface conditions off East Antarctica over a period spanning from the middle of the Little Ice Age (~1300-1850 C.E.) to the Modern Era (~1850 C.E.-onward; Mann et al., 2008). We use sea ice-related and open-ocean associated diatom assemblages, along with diatom specific biomarkers and major/minor element content to reconstruct past sea ice variations and polynya activities in our study area. Achieving pluri-annual resolution allows for assessing the forcing factors of long- and short-scale sea ice variations in terms of amplitudes and frequencies through spectral analyses on sedimentary signals from the DTCG2011. Our results will be compared

to previous observations from Commonwealth Bay (CB) over the last 250 years (Campagne et al., 2015), in order to assess the homogeneity of regional sea ice fields over the last centuries or, conversely, understand the mechanisms conducting to local responses under common large scale forcing.

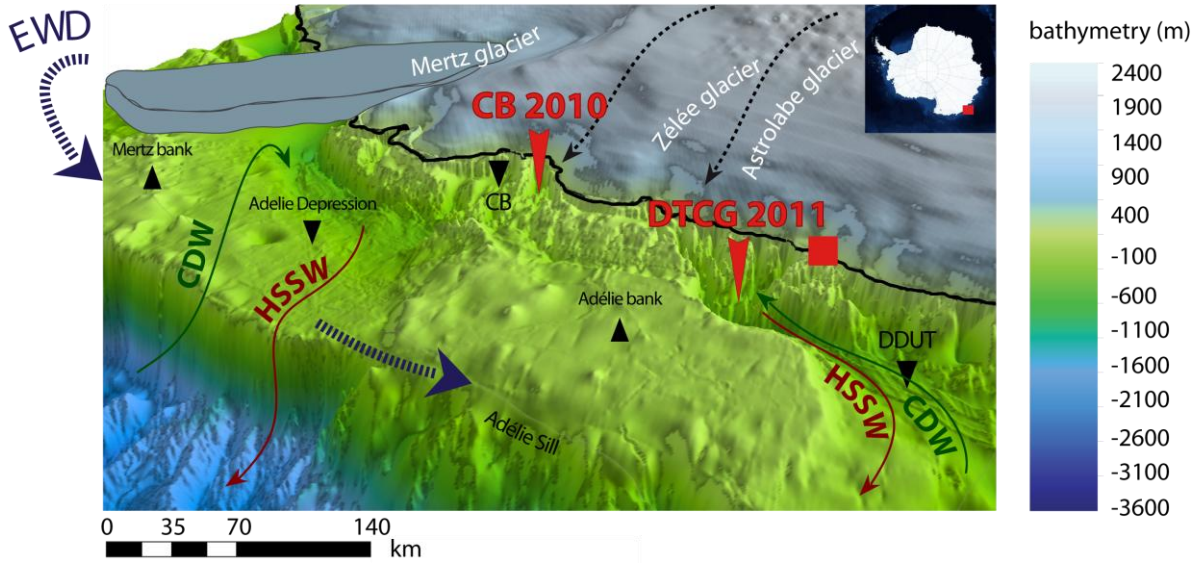

Figure 50. Study area. Map of the study area showing the location of sediment core DTGC2011 and the core CB2010 (downward red arrows) in the Dumont D'Urville Through (DDUT) and in Commonwealth Bay (CB). Are also mentioned the Dumont D'Urville (DDU) french station (red square), the main glacial (in white) and topographic (upward black triangle for high relief and downward for troughs) features, the East Wind Drift (EWD; blue dashed arrow), the principal water masses as Circumpolar Deep Water (CDW; green arrow) and the High Salinity Shelf Water (HSSW; brown arrow) (Williams et al., 2008), and the katabatic winds (black dashed arrows; Massom et al., 1998). Bathymetry data were obtained from http://www.deepreef.org/publications/peer-review/82-gvdem.html.

2 Environmental settings

The Dumont d'Urville Trough (DDUT; Fig. 50), in AGVL along the East Antarctica margin, is composed of several glacial depressions. These topographic features, beyond 1000 meters deep, act as natural sediment traps by focusing the sedimentary material in the area. The trough runs from the front of the Zélée and Astrolabe glaciers to the continental shelf break along a SE-NW orientation and is bordered on its eastern side by the Dumont d'Urville (DDU) Bank (Fig. 50), and on its western side by the Dibble Bank.

The AGVL is influenced by several water masses and currents (Rintoul, 1998; Williams and Bindoff, 2003; Williams et al., 2008). At the surface, the wind-driven East Wind Drift

(EWD), also called Antarctic Coastal Current, flows westward. Near the surface, the Antarctic Surface water (AASW) constitutes the summer sub-surface water mass on the continental shelf while the Circumpolar Deep Water (CDW) upwells near the Antarctic Divergence and intrudes onto the plateau during summer. At the bottom, the high-salinity shelf water (HSSW), formed by brine rejection during winter sea ice formation and cooling of the CDW (Fig. 50) flows northward as part of the dense shelf water that extrude the plateau. These Adélie Land Bottom Water (ALBW) ultimately source the Antarctic Bottom Water (AABW; Rintoul et al., 1998; Jacobs et al., 2004; Meredith et al., 2013).

The coastal area of AGVL experiences the strongest katabatic winds ever-recorded on Earth (Périard and Pettré, 1993). This is in part due to the presence of narrow glacial valleys close to the shoreline exerting a funnelling effect (Wendler et al., 1997). These winds blow from the south-east and support the annual occurrence of polynyas in the region, such as the DDU Polynya (DDUP; 66.11°S–139.31°E) and the Mertz Glacier Polynya (MGP), where important sea ice production leads to the formation of large amounts of dense water during winter (Adolphs and Wendler, 1995; Massom et al., 1998; Arrigo and van Dijken 2003; Tamura et al., 2012).

In the region, the sea ice rises above 80% in winter and melts below 20% in summer (Arrigo and van Dijken, 2003), with a mean sea ice duration of 8-10 months per year. However, recent studies suggest the sea ice cover strongly varies interannually both in extent and timing (formation and retreat) in our study area, as sea ice conditions are closely linked to the fast-ice dynamics over the DDUT which is, in turn, largely related to synoptic scale wind (Adolph et al., 1995; Massom et al., 2003; 2009; Smith et al., 2011; Chap III). Indeed, the DDUT experiences fast ice conditions during the freezing months, which extend up to ~100 km offshore between the Dibble Tongue in the west and the Adélie Bank in the east (Massom et al., 2003; 2009; Smith et al., 2011; Wang et al., 2014). In summer, this fast ice buttress is characterized by a succession of several breakouts and re-freeze in the DDUT as a result of a lack of anchor points (Massom et al., 2009; Smith et al., 2011). In contrast over the banks, the fast ice buttress remains more stable and persists generally later in the season. A key factor for the formation, recurrence and persistence of this fast ice buttress, is the presence of numerous icebergs grounded on the banks that trap the passing pack ice and act as anchor points for the formation of larger floes (Massom et al., 2001; Giles et al., 2008; Smith et al., 2011). As a result, two ice buttresses usually develop on both side of the trough. The presence of the fast

ice buttress is therefore closely associated to the intense sea ice formation from the MGP and westward advection within the EWD (Massom et al., 2009).

3 Material and methods

3.1 Core description and chronology

A 4.69 m long gravity core (DTGC2011) was retrieved aboard the R/V Astrolabe (66°24.50'S -140°26.43'E; 1030 m water depth) during the 2011 ALBION-HOLOCLIP cruise. Positive X-ray images performed on the SCOPIX image-processing tool (Migeon et al., 1999) provided detailed information on sediment density and structure. SCOPIX images revealed a succession of dark (olive-brown; summer season) and lighter (greenish brown; spring season) laminations throughout the entire archive. These laminations, characterized by color changes between lighter greenish brown versus darker brown intervals, were shown to result from the alternating high productivity deposition during spring (greenish and lighter lamination) and less organic-rich sedimentation during summer (darker and denser lamination) (Denis et al., 2006; Maddison et al., 2006, 2012).

Six radiocarbon dates (Table 4) were performed on acid insoluble organic matter fraction (AIOM) of the DTGC2011 at the Center for Accelerator Mass Spectrometry from the Lawrence Livermore National Laboratory, Livermore, USA. Two radiocarbon dates at 0 cm and 275 cm were discarded (in red; Suppl. Table 1) due to inversion values. The age of the sediment surface in DTGC2011 was therefore dated from both the top section of interface core DTCI2010 and a deep sediment trap (LOW B1) deployed at the core site, which provided a similar ^{14}C age of 1735 yrs (Suppl. Table 1). In order to confirm the robustness of the ^{14}C dating, $^{210}Pb_{xs}$ analyses were done on the first meter of core DTGC2011 (Fig. 51), at EPOC Laboratory, Bordeaux, FRANCE. $^{210}Pb_{xs}$ activities of the top DTCG2011 were similar to the top section of the interface core DTCI2010 retrieved in January 2010 (Fig. 51b; Table 4), indicating that only a very limited amount of sediment (less than 4-5cm) was lost from the surface of the gravity sediment core during collection. At the same site, a total reservoir (TR) correction of 1200 +/- 100 years (with a Delta R of 800 years) combined to a dead carbon fraction (DCF) correction of 425 years are generally applied to calibrate the AIOM ^{14}C dates (Costa et al., 2007). These corrections proved however unable to reconcile the core top ^{14}C date and $^{210}Pb_{xs}$ activities in DTCG2011. An additional DCF of 250 years was then applied. Radiocarbon dates were calibrated (Fig. 51a) to calendar ages using BACON (Blaauw and

Christen, 2011) and using a total correction of 1875 years (TR of 1200 years and DCF of 675 years). Although the reason remains unclear, such discrepancy between interface and long cores may result from that the DCF for the long cores has been inferred and averaged from Holocene sediments and might not be appropriate for the Late Holocene and the recent sediments.

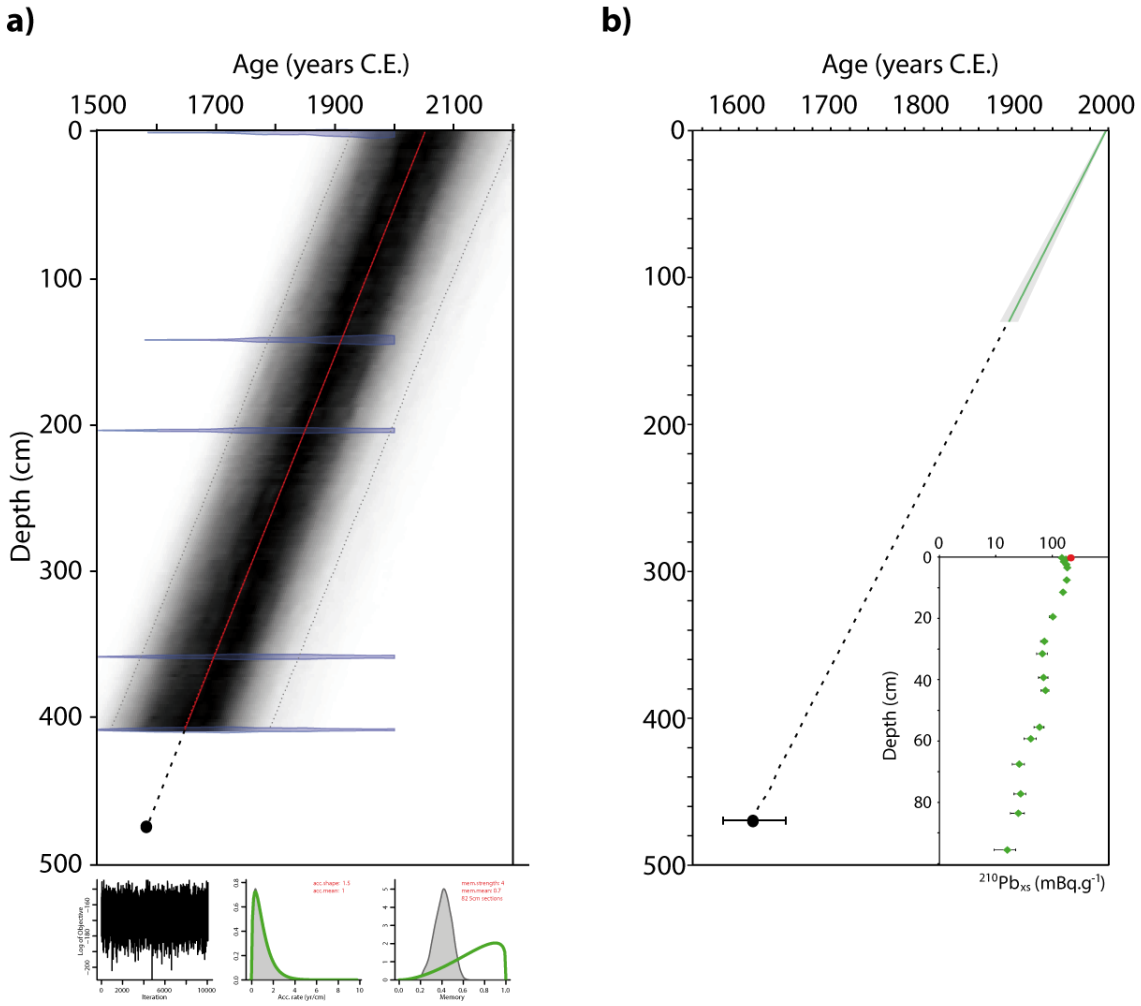

Figure 51. Chronology of the DTGC2011 based on AMS 14C dates, controlled by 210Pbxs. a) 14C ages (Suppl. Table 1) were calibrated to calendar ages (expressed in C.E.) using BACON (Blaauw and Christen, 2011), and were extrapolated to 469 cm (black dotted line), using a linear regression of Y = -0,982X + 2000. Blue points represent the age ranges corresponding to each radiocarbon measurement. The red line corresponds to the age model used by BACON to estimate the age of each sample. The error range in age estimations is represented by the grey shaded area. b) DTCG2011 age model (green line) based on 210Pb excess (210Pbxs) from the first meter of the DTCG2011 core, and associated age-model errors (grey area; 1 s.d.). 210Pbxs ages were extrapolated to 469 cm (black dotted line), using a linear regression of Y = -0,807X + 1997. The 210Pbxs bottom age (black spot) and error bars associated (black line) indicate relative good reproducibility between the 14C and 210Pbxs ages. The inset corresponds to the down-core profile of 210Pbxs of the DTCG2011 (green markers) and to the top profile of the interface core DTCI2010 (red marker), with error bars associated (black line).

Table 4. Accelerator Mass Spectrometry 14C ages and 210Pbxs activities from the core DTGC2011. Raw 14C ages were corrected with a total reservoir (TR) correction of 1200 and a DCF correction of 425+208 years, to fit the top with 2010 C.E. Ages were calibrated to calendar ages using BACON (Blaauw and Christen, 2011), and were extrapolated to 469 cm using a linear regression of Y = -0,982X + 2000.

Sample origin	depth (cm)	14C age (yr)	14C age AO corrected DCF (yr)	14C age calibrated 1 sigma (yr BP)	Value used 1 SD (yr BP)	14Cc age (1 SD) corrected to 2010
sed trap LOW B1	-	1735	1310	54-242	148	-60
DT-CI2	0	1735	1310	54-242	148	-60
DT-CG1	142	1835	1410	122-374	248	40
DT-CG1	204	2025	1600	321-505	413	205
DT-CG1	359	2070	1645	359-548	453,5	245,5
DT-CG1	409	2125	1700	440-614	527	319
DT-CG1	0	8145	-	-	-	-
DT-CG1	275	2170	-	-	-	-

Sample origin	depth (cm	210Pbxs
DT-CI2	0-3	216
DT-CG1	0-0,5	150

The 4,69 m long DTCG2011 sediment archive span the 1540–2000 years C.E. period with a mean sedimentation rate of ~1 cm/yr (Fig. 51a) in agreement with the mean sedimentation rate calculated from the $^{210}Pb_{xs}$ (~1,2 cm/yr; Schmidt, S., personal communications) activities in the upper one meter (Fig. 51b), leading to a maximum discrepancy between the two dating techniques of ~78 years at 4.69m, when Pb-based mean sedimentation rate is extrapolated along the whole core.

3.2 Diatom proxies

Micropaleontological analyses were performed every 4 cm according to the methodology described in Crosta and Koç (2007) providing a ~4 years resolution. Diatom slides were prepared from ~0.5 g of dry sediment. Few drops of the sediments previously suspended in distilled water were evaporated onto a coverslip, which was subsequently mounted on a glass slide with NOA61. Identifications and cell counts were done under an Olympus BH-2 at a magnification of x1000. For each sample, 300-350 diatom valves were counted and data are presented as species relative abundances. Diatom identification was performed to the species or species group level. Details about slide preparation and diatom identification are available

in Crosta et al. (2004). Approximately 70 diatom species were identified in the assemblages, from which 17 presented abundances higher than 2% of the total diatom population.

Fragilariopsis curta and *F. cylindrus* constitute the FCC group, indicating the presence of sea ice cover in several paleoclimate studies including our study area (Crosta et al., 2007; Denis et al., 2010). *Fragilariopsis cylindrus* in recent sediments at the core site (Chap III) was shown to co occur with relatively heavy pack ice conditions pushed southward by northerly winds. High percentages of *Chaetoceros Hyalochaete* resting spores (CRS) in Holocene sediment from AGVL have been associated to strong siliceous productivity supported by intermittent mixing of melting ice-induced stratified surface waters (Maddison et al., 2006). Intense katabatic winds through the growing season (Périard and Pettré, 1993) lead to intermittent thickening of the mixed layer allowing for nutrient replenishment but sink *Chaetoceros* to depth triggering spore formation (Hargraves, 1972; Hargraves and French, 1975). Similarly, highest CRS relative abundances in surface sediment off Adélie Land have been found to coincide with strong dominant southerly winds (Chap III). In sediments off AGVL, *Fragilariopsis kerguelensis* present an inverse pattern to sea ice and cold water species (Crosta et al., 2008; Campagne et al., 2015), and were found to dominate the summer-autumn laminae along with large centric species (Denis et al., 2006; Maddison et al., 2006). Similarly, diatom investigation in surface sediments in our study area (Chap III) reveals that high abundances of large centric diatoms (e.g. *Thalassiosira lentiginosa, T. oliverana, T. trifulta, T. gracilis, T. tumida, Actinocyclus actinochilus, Stellarima microtrias* and *Coscinodiscus* spp) record a lengthening of the open water season and a warming of sea-surface waters in summer. These large centric diatoms constitute the Open Water group. *Thalassiosira antarctica* resting spores (RS) of the cold variety were also observed as co-occurring with several large centric diatom species and *F. kerguelensis* in Holocene sediments collected in the area (Denis et al., 2006). The *Porosira* group is composed by *P. glacialis* and *P. pseudodenticulata*. *Thalassiosira antarctica* and *P. glacialis* were found to share similar seasonal occurrences, although with slightly colder and icier conditions for *P. glacialis* (Pike et al., 2009), and both species groups have thus been interpreted in Holocene sediments to indicate a late summer/autumn rapid deposition, linked to early sea ice return (Denis et al., 2006; Maddison et al., 2006, 2012). However, comparison of *T. antarctica* and *P. glacialis* relative abundances in modern sediments off AGVL and instrumental data suggest that *T. antarctica* slightly prefers icy environment than the *Porosira* gp in our study area (Chap III).

3.3 Biomarker proxies

Biomarker analyses followed the technique described in Massé et al. (2011) and were performed every 4 cm (~4 years resolution) in core DTGC2011. Briefly, an internal standard was added to the freeze-dried sediments, lipids were extracted using a Dichloromethane/Methanol mixture to yield a total organic extract (TOE), which was then purified using open column chromatography (silica). Hydrocarbons were analyzed using a Gas Chromatograph coupled to a Mass Spectrometry detector (GC-MS). More details about analyses are available in Massé et al. (2011).

Few marine and freshwater diatoms belonging to *Haslea*, *Navicula*, *Pleurosigma* and *Rhizosolenia* genera were recently found to be synthesizing Highly Branched Isoprenoids (HBI) (Sinninghé et al., 2004; Massé et al., 2011). A di-unsaturated isomer [HBI:2] has been identified in Antarctic sea ice and isotopic analyses provide evidence that this isomer is synthesized by sea ice dwelling diatoms, while a tri-unsaturated isomer [HBI:3] has been identified in water column phytoplankton (Massé et al., 2011). Recent studies have proposed the use of [HBI:2] and [HBI:3] to reconstruct variations of Holocene Antarctic sea ice duration as complementary sea ice proxy to diatom counts (Denis et al., 2010; Collins et al., 2013). In recent sediments at CB, Campagne et al. (2015) have found that [HBI:2] and *F. cylindrus* abundances were correlated to increasing sea ice conditions. As suggested by Collins et al. (2013), [HBI:3] was found to increase off AGVL along with increasing sea ice seasonality (Campagne et al., 2015).

3.4 Major and minor element proxies

Titanium (Ti), Zirconium (Zr) and Rubidium (Rb) contents were measured on slab sections every 0,2 cm (~0,2 years resolution) along the entire core using EPOC AAVATECH XRF core-scanner (Jansen et al., 1998). Variations in Ti content are linked to changes in terrigenous supply to the ocean (Presti et al., 2011). In Antarctic coastal areas, the delivery of terrigenous particles can occur *via* several modes such as meltwater discharge, ice rafting, runoff from outlet glaciers, and eolian transport, although this latter source is considered negligible in coastal East Antarctic regions (Presti et al., 2003; Escutia et al., 2003). Variations in Zr to Rb content ratio track changes in sediment grain size, where Zr represents the coarsest sediment fraction and Rb the finest (Dypvik et al., 2001). In the Weddell Sea and

in the Adélie Depression, recent studies have proposed that higher Zr/Rb ratio values record enhanced bottom water formation and increased (coarser) sediment transport due to strong brine rejection, increased of convection and intense polynya activity (Sprenk et al., 2014; Campagne et al., 2015).

3.5 Wavelet analyses

We used cross wavelet analysis and applied the Morlet wavelet to our dataset, using the MATLAB package and Grinsted et al. (2004) methodology. This method provides a good balance between time and frequency localization, and we used Monte Carlo simulations to provide frequency-specific probability distribution (Global wavelet spectrum) that can be tested against wavelet coefficients. Statistical significance was estimated against a red noise model (Grinsted et al., 2004). In this study, to test the relevance of our proxies, their statistical relationships and examine periodicities in a frequency domain, we compared the two time series by their continuous wavelet transform, which we hypothesized are linked in some way. The resulting Cross Wavelet Transform exposed their common power and relative phase in time-frequency space of the two signals. Data were resampled at a 4 years constant step. Data were then standardised by subtracting to each values the mean of the dataset and then by dividing it with the standard deviation. Given the interanual resolution of our analyses, we do not take in consideration cyclicities in the ~0-15 years band that could result from the noise.

4 Results

All results are presented as standardized anomalies, allowing a direct and statistical comparison between different signals and with other standardized sedimentary dataset (see Discussion). Raw results are presented in Suppl. Fig. 1. Use of standardized anomalies does not change the wavelet results and interpretations. Our data indicate that diatom, biomarker and major/minor element exhibit large variations in their relative abundances along the sediment archive.

Large centennial oscillations in the relative abundances of the FCC group are observed (Fig. 52). The FCC gp abundances increase rapidly in the sediments deposited between ~1544 C.E. and 1580 C.E. where they reach their highest values of the whole record. After 1580, the FCC

gp gradually decreases to reach its lowest values at ~1870 C.E. even if a slight rebound is observed at ~1800 C.E. During the most recent period (1870-2000 C.E.), relative abundances of FCC gp generally increase to values observed during the 16th century with however two events with low abundances at ~1940 C.E. and ~1990 C.E.

The [HBI:2]/[HBI:3] ratio exhibits relatively similar variations (Fig. 52), with increasing values between ~1544-1665, when it reaches a maximum, followed by a relatively abrupt decrease to low abundances between ~1680-1885 C.E., with two slight increasing periods around ~1710 and 1800 C.E. A large increase is then observed at the top of the core, with maximum values around 1900 C.E. and 1955 C.E. followed by an abrupt decrease during the last decades.

In contrast, relative abundances of the CRS gp exhibit an opposite record to both the FCC gp and [HBI:2]/[HBI:3] ratio (Fig. 52), with steady low values during the ~1544-1730 period, a sharp increase toward high values between ~1730-1870 (with two maxima at ~1755 and ~1835 C.E. and a minima at ~1800) followed by a decrease toward its lowest values near the top of the core.

The Zr/Rb ratio presents a similar trend to the CRS record with overall lower values during the 1544-1730 C.E. and 1880-2000 C.E. periods and higher values during the 1730-1880 C.E. period (Fig. 52). Pluri-decadal variability is observable with higher values in the 1570-1585 C.E. period and at 1625 C.E., 1635 C.E., 1710 C.E., 1740 C.E and 1990 C.E and minimum values at ~1600 C.E., ~1670 C.E., ~1750 C.E., ~1800 C.E., ~1860 C.E. and ~1990 C.E.

Fragilariospsis kerguelensis relative abundances exhibit a short scale variability throughout the record, with rapid oscillations between maximum and minimum abundances (Fig. 52). Despite these large and abrupt oscillations, we observe periods when *F. kerguelensis* abundances are generally more abundant *(e.g.* between ~1544-1645 C.E. with a peak around 1610 C.E., between 1765-1815 period, with three peaks at ~1765 C.E., ~1790 C.E. and ~1810 C.E and during the 1840-1955 period, with three maxima at ~1865 C.E., ~1890 C.E. and ~1945 C.E., and a minima at ~1910 C.E). The short intervals between these periods are characterised by low *F. kerguelensis* relative abundances.

As *F. kerguelensis*, relative abundances of the Open Water gp display pervasive large amplitude variations at short timescale (Fig. 52). However, higher relative abundances can be observed between ~1550 C.E. and 1700 C.E. followed by lower values until 1810 C.E and a subsequent increase.

The Ti signal exhibits high values between ~1550-1715 C.E., with maximum values at ~1665 C.E (Fig. 52). Lower values are found over the ~1665-1870 C.E. period with minima at ~1730 C.E., ~1740 C.E., ~1790-1795 C.E. and ~1850-1870 C.E. The Ti signal subsequently increases again over the ~1870-1910 C.E. and ~1950-1965 C.E. periods, with maxima around 1900 C.E. and 1965 C.E., and decreases between ~1915-1945 C.E. and ~1970-1980 C.E.

The *T. antarctica* record shows a singular trend compared to other proxies (Fig. 52). Highest values are encountered at ~1550 C.E., followed by an abrupt decrease until ~1660 C.E. *Thalassiosira antarctica* relative abundances then gradually increase over the ~1660-1885 C.E. period when it reaches its highest values at ~1885 C.E. Subsequently, *T. antarctica* abundances strongly decrease over the top of the core, notably with minima during ~1960-1995 C.E. period. Similarly, the *Porosira* gp displays its highest relative abundances at ~1550 C.E. and 1565 C.E., and then decrease rapidly until ~1655 C.E. Relative abundances of the *Porosira* gp subsequently increase between ~1660-1685 C.E. with a maximum at ~1680 C.E., and then decrease abruptly until ~1765 C.E. The *Porosira* gp slightly increases over the ~1765-1970 C.E. period as per several pluri-decadal oscillations.

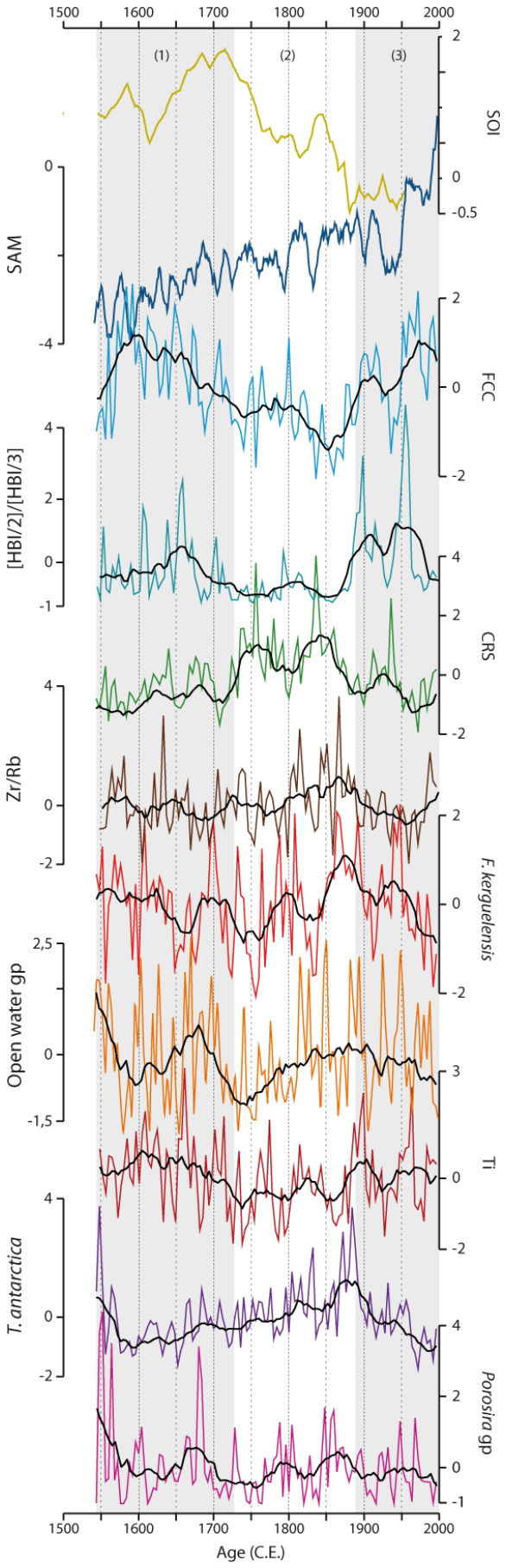
1500
1600
1700
1800
1900
2000
(1)
(2)
(3)
SOI
SAM
FCC
[HBI/2]/[HBI/3]
CRS
Zr/Rb
F. kerguelensis
Open water gp
Ti
T. antarctica
Porosira gp
Age (C.E.)

Figure 52. Variations of the diatom assemblage, sea ice related biomarkers, major and minor element content from the DTGC2011 covering the last 500 years in relation with climate modes of the Southern Hemisphere. The Southern Oscillation Index (SOI; yellow) precipitation-based reconstruction inferred from Yan et al. (2011); the Southern Annular Mode ~90 years running mean (SAM; dark blue), inferred from Villalba et al. (2012). Standardized and resampled sedimentary signals from DTGC2011: sea ice diatoms group composed of *Fragilariopsis curta* and *F. cylindrus* (FCC; light blue), [HBI:2]/[HBI:3] ratio (greenish blue), *Chaetoceros* resting spores group (CRS; green), the Zr/Rb ratio (dark brown), *F. kerguelensis* (red), Open Water gp (orange), Titanium (Ti; light brown), *Thalassiosira antarctica* (violet), and *Porosira* group (pink curve). (1) to (3) and grey shading areas indicate climate phases indentified. Black curves indicate the ~90 years running mean of the sedimentary signals.

5 Discussion

All the records in core DTGC2011 indicate a succession of abrupt and large amplitude changes that were firstly quantified by wavelet analysis. In a second step, the possible related forcing mechanisms are discussed by decreasing timescales.

5.1 Centennial scale variability

Variations of the diatom relative abundances, diatom specific biomarkers and of the major and minor element contents display centennial scale variability that allow to delineate three climatic periods characterized by significant changes in seasonal sea ice dynamics and polynya activity over the last 500 years.

- *(1) The 1540-1725 C.E. period*

High abundance values of the FCC gp along with relatively important [HBI:2]/[HBI:3] ratio (Fig. 52) probably indicate heavy sea ice presence in the form of increasing pack ice during the spring season over that period. Such conditions are inferred from modern validation of the proxy whereby sedimentary data from the core site were compared to meteorological data over the instrumental period (Chap III). The simultaneous high occurrences of the open water proxies, i.e. *F. kerguelensis* and the Open Water gp along with high Ti levels (Fig. 52), however, strongly suggest the presence of open water conditions during the summer-to-autumn season. This is further supported by high abundances of the *Porosira* gp and low values of *T. antarctica* (Fig. 52), which, when taking together, suggest the presence of light sea ice conditions during autumn as observed over the recent period (Chap III). Low CRS abundances along with relatively low Zr/Rb ratio values (Fig. 52) indicate that the DDUT

polynya was reduced during this interval, conducting to overall weak dense water formation and bottom water circulation, since both proxies were previously linked to intense coastal polynya activity in the region (Campagne et al., 2015; Chap III).

Combined observations from the sedimentary proxies therefore indicate that although the 1540-1725 C.E. period is characterized by increasing spring sea ice presence and surface stratification due to sea ice melting, the area also experience a relatively long ice-free season, with sporadic sea ice conditions during the summer-autumn season. Over the instrumental period, a similar scenario was observed to occur under dominant onshore wind circulation (northerly to easterly wind fields), contributing to increase pack ice conditions in spring. However, northerly winds also contribute to increase summer melting and limit ice growth in autumn by transporting warm air from the north and by enhancing the swell (Chap III). These interpretations are supported by previous studies that suggested a southward migration of the Southern Westerly Winds (SWW) and Circumpolar Trough during the ~1400-1700 C.E. period, which brought moisture to high southern latitudes via increased cyclone activity (Mayewski et al., 2004; Saunders et al., 2012; Goodwin et al., 2014). More regionally, several positive anomalies of snowfall were recorded at Law Dome (DSS) during the ~1500-1700 C.E. interval (van Ommen and Morgan, 2010). Greater snowfall precipitations were associated with more east to north-easterly flow at DSS and along the East Antarctic coast. Such scenario is in agreement with our results and is likely consistent with increasing SAM trends (Sinclair et al., 1997). Although paleo-reconstructions indicate a negative SAM (SAM-) at that time (Fig. 52), the SAM index has been gradually and continuously increasing over the previous centuries and the 1450-1725 C.E. period (Villalba et al., 2012; Abram et al., 2014). At the opposite, paleoreconstructions indicate a strong positive Southern Oscillation Index (SOI+; la Nina-like conditions) during the 1450-1725 C.E. period (Fig. 52; Yan et al., 2011). Recent observations around Antarctica suggest that La Nina conditions (similar to SAM+ and/or SOI+) would causes divergent sea ice motion and thus increased sea ice extent in some places (Jacobs et al., 2006; Stammerjohn et al., 2008; Dinniman et al., 2012), along with warm air advection to coastal Antarctica (Thompson and Solomon, 2002). Recent SAM+ trends would also cause anomalous upwelling of the relative warm and saline CDW onto the continental shelf, there increasing summer open water conditions and melting of continental ice (Jacobs et al., 2006; Williams et al., 2008; Dinniman et al., 2012; Schmidtko et al., 2014). In the Adélie Depression, increasing sea ice conditions were tied to a westward shift of the wind circulation onto the shelf (and decreasing katabatic winds) coinciding with the recent

SAM+ trend (Campagne et al., 2015). Keeping in mind that exporting modern relationships between climate mode forcing and environmental parameters to paleo records may not be completely suitable due to the recent unprecedented positive trend of the SAM (Villalba et al., 2012), the greater spring sea ice presence and reduced katabatic winds over the 1540-1725 C.E. period inferred from our sedimentary data, and further supported by regional glacial records, suggest that a La Nina like atmospheric pattern characterized the 1450-1725 C.E. interval despite the opposite phasing between the two climate modes.

- *(2) The 1725-1890 C.E. period*

Low values of the FCC gp and [HBI:2]/[HBI:3] ratio during that period suggest a reduced sea ice cover during the spring season (Fig. 52). Concomitant high CRS and Zr/Rb ratio values, low abundances of *F. kerguelensis* and Ti content during the 1730-1870 C.E. period, along with low Open Water gp assemblages in sediments in the 1725-1810 C.E. interval (Fig. 52), likely indicate the presence of a large coastal polynya and cool summer conditions, as suggested by our previous findings on recent sediments (Chap III). However, the 1850-1890 C.E. period is characterized by decreasing CRS population, while highest values of Zr/Rb and relative abundances of *T. antarctica*, *F. kerguelensis* and the Open Water gp (Fig. 52) suggest enhanced polynya activity and concomitant open conditions during summer, with however pronounced sea ice conditions in autumn.

The sedimentary assemblage indicate a progressive increase of the ice free season due to an early spring sea ice retreat and presence of a recurrent polynya over the 1725-1890 C.E. period. However, it seems that the polynya regime changed around 1850 C.E. from coastal polynya conditions to seaward spreading polynya system over the DDUT, as response to a shift from dominant southerly to easterly wind fields since 1850 C.E. Similarly at CB, 200 km eastward, high relative abundances of CRS were found between 1800-1890 C.E. and high Zr/Rb between 1800-1870 C.E. (Fig. 53; Campagne et al., 2015), suggesting that the entire area experienced enhanced polynya activity during the 1725-1890 C.E. period, maybe with maximum extent or activity during the 1750-1890 C.E period. Prevalent easterlies since 1850 C.E. also conducted to icier autumns as evidenced by higher abundances of *T. antarctic*a RS (Fig. 52). More regionally, precipitation reconstructions at DSS and Taldice point to negative snowfall anomalies roughly between the 18th and the 19th centuries (van Ommen and Morgan, 2010) probably in response to a reversal in the wind pattern relative to (1) characterized by increasing katabatic winds in East Antarctica (Stenni et al., 2002; Ommen

and Morgan, 2010). Regional reconstructions suggest that increasing Na levels at ~1850 C.E. imply less sea-ice extent and duration in the region (Mayewski et al., 2004). The SAM index continuously increases over this period (Villalba et al., 2012) while the SOI index decreases in a stepwise pattern (Yan et al., 2011) (Fig. 52). This configuration (less negative SAM and less positive SOI; more El Nino-like conditions) results in opposition to (1) to an equatorward migration of the SWW, which would reinforce katabatic winds at high latitudes. We however note that the inferred shift in polynya nature at ~1850 C.E. (as traced by CRS and Zr/Rb downcore records) falls in line with a drastic drop in SOI values, which may have conducted to a more easterly wind fields during spring, despite the equatorward migration of the SWW.

- *(3) The 1890-2000 C.E. period*

High values of the FCC gp and [HBI:2]/[HBI:3] ratio, along with low CRS assemblage suggest increasing sea ice conditions in spring (Fig. 52). Particularly, highest [HBI:2]/[HBI:3] ratio values are found during this interval, and according the study of recent sediments over the instrumental period (Chap III), suggest that amongst the coolest conditions occurred at 1895 C.E. and 1955 C.E. (Fig. 52). Highest values of *F. kerguelensis*, Open Water gp and Ti coincide with lowered Zr/Rb values and a strong decrease of *T. antarctica* (Fig. 52), suggesting an increase in the duration of the ice free season, and probably warmer surface waters, in summer-autumn months. Polynya efficiency seems to decrease at that time besides the presence of open conditions over the DDUT, as previously seen over the instrumental period (Chap III).

The sedimentary assemblage in (3) therefore indicate a delayed ice free season, characterized by longer sea ice duration in spring, but warmer and less icy conditions during the summer-autumn season. It also argues for reduced polynya activity off DDU. Increasing sea ice seasonality and variability in (3) may traduce enhanced zonal wind pattern in our study area, characterized by preponderant easterly winds alternating with westerly wind events, and so overall decreasing katabatic winds as previously suggested (Chap III; Campagne et al., 2015). Indeed, a strong decrease of polynya markers is observed in CB over the 20th century (Fig. 53; Campagne 2015), likely supporting the idea that polynya activity was regionally reduced over the last 150 years. Such scenario may be triggered by decreasing wind velocity associated to easterly wind circulation over the shelf, as demonstrated by atmospheric reanalyses over the last 140 years and meteorological data from the DDU station over the last 50 years (Fig. 54). Reduced polynya activity and lengthening of summer-autumn open water

conditions in interval (3) is in line with higher precipitations at DSS since 1880 C.E. and culminating since the 1970s, which were associated with east to north-easterly flow anomalies along the East Antarctic coast (van Ommen and Morgan, 2010). Since the 19th century, the SOI gradually decreases while the SAM increases toward its millennial highest values (Fig. 52; Villalba et al., 2012). Although relationships between the occurrence of easterly winds and climate modes is not fully assessed over the instrumental period, it has been suggested in the region that such SAM+ trends have promoted a more zonal atmospheric circulation onto the shelf (Chap. IV; Massom et al., 2009; Campagne et al., 2015). As such, wind pattern changes in (3) may have responded to preponderant SAM increase, relative to SOI.

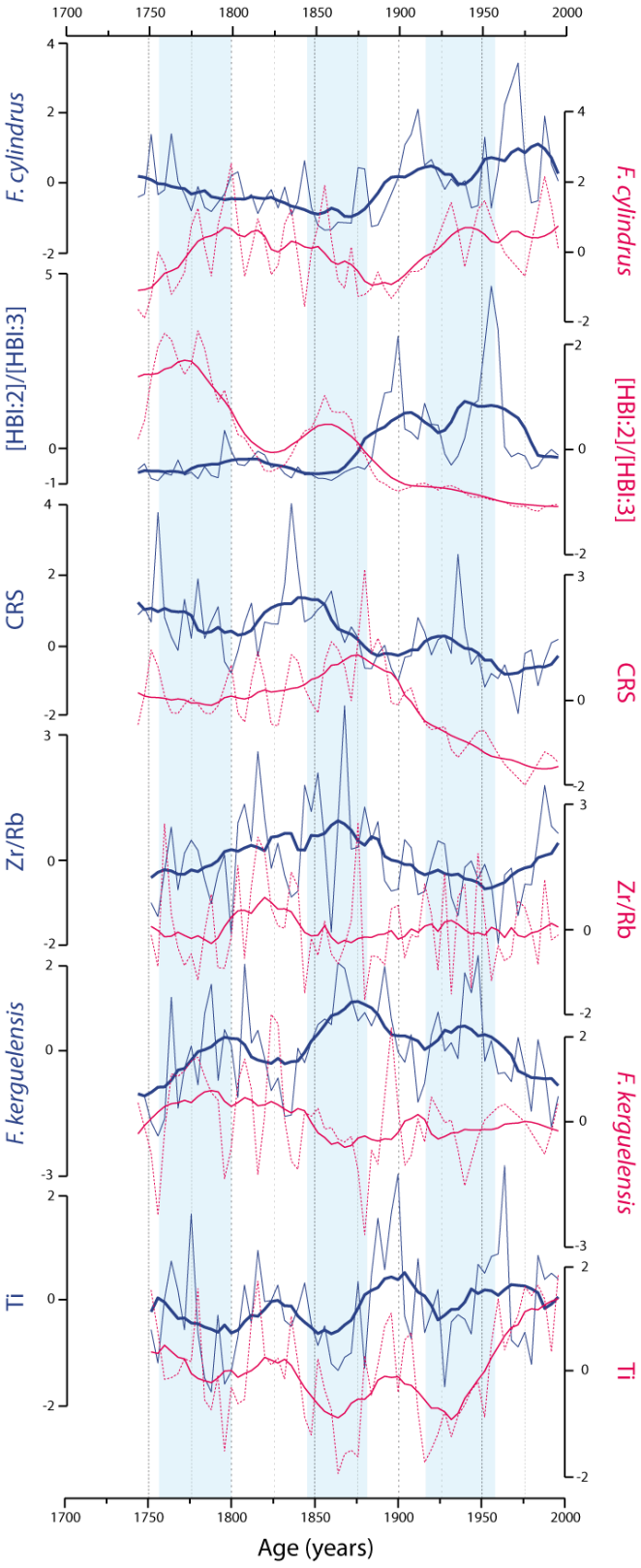

Figure 53. Variations of the diatom assemblage, sea ice related biomarkers, major and minor element content from the DTGC2011 versus CB2010 over the last 250 years. *Fragilariopsis cylindrus* over the DDUT (blue) and at CB (pink), [HBI:2]/[HBI:3] ratio over the DDUT (blue) and at CB (pink), *Chaetoceros* resting spores group (CRS) over the DDUT (blue) and at CB (pink), the Zr/Rb ratio over the DDUT (blue) and at CB (pink), *F. kerguelensis* over the DDUT (blue) and at CB (pink), Titanium over the DDUT (blue) and at CB (pink). Blue shading area indicate sea ice phases following calving

events of the MG (Campagne et al., 2015). Coarser curves indicate the ~90 years running mean of the sedimentary signals.

5.2 High frequency climate variability off AGVL

Our records further display decadal to pluri-decadal variability over the last 500 years. Spectral and wavelet analyses were performed to determine periodicities of the sedimentary signals recorded in core DTGC2011. In addition, we compared our results with previous findings from CB over the last 250 years in order to assess the origin and the regional *versus* synoptic scale pattern of the forcing impacting oceanic conditions in AGVL. To this effect, *F. cylindrus* (as for the CB records) and [HBI:2]/[HBI:3] ratio were used to track sea ice cover variability, *F. kerguelensis* relative abundances were used to record open ocean conditions, Zr/Rb ratio and CRS content were used to infer variations of DDU polynya activity, and Ti levels to assess the potential sources of terrigenous inputs onto the shelf. Wavelet analyses highlight the presence of non-stationary significant cyclicities at 10-30 years and 50-100 years in DTGC2011 sedimentary signals (Fig. 55), which origin and associated mechanisms are discussed hereafter.

5.2.1 Wind circulation and atmospheric variability

In the Southern Ocean and in Antarctica, decadal periodicities have generally been attributed to atmospheric teleconnexions between the southern mid- and high-latitudes (Cook et al., 1996; Souney et al., 2002; Enomoto et al., 1991; Thomas et al., 2008; Zitto et al., 2015). Enomoto (1991) and van Ommen and Morgan (2010) evidenced a pluri-decadal inverse relationship over the past centuries in precipitations and SLP between East Antarctica (e.g. Wilkes Land) and the mid-latitudes through changes in the Westerly Winds pattern, with a variability ranging from ~20-30 years and ~40-60 years. Similarly, quasi 20-year and quasi-50 year cyclicities were observed in the temperature and precipitation records of Base Orcadas at South Orkney Islands and of the Gomez ice core in southern Antarctic Peninsula over the past centuries and attributed to SAM and SOI forced atmospheric reorganisations (Thomas et al., 2008; Zitto et al., 2015). Recent studies have demonstrated that atmospheric changes, and notably modification of the wind pattern have important impacts on sea surface conditions, polynya activity and terrigenous inputs in AGVL (Chap III; Massom et al., 2009; Campagne

et al., 2015). Enhanced easterly winds pack ice and increased sea ice presence in the MGP region, decreasing the polynya activity, whereas southerly winds would have the opposite effects along the AGVL coast. As such, the significant decrease in polynya activity between 1950-1990 C.E., inferred from higher Zr/Rb values, may be attributed to the significant westward shift of the wind pattern (more easterly winds) at that time, which has been monitored and is supported by atmospheric reanalysis (Fig. 54; Campagne et al., 2015). However, wavelet analyses indicate no clear statistical relationships between our sedimentary records and SAM/SOI reconstructions and are thus not presented here. Absence of clear trends could be possibly due to the smoothed impacts at pluri decadal scale of the climate modes over the last centuries, relative to longer timescale forcing mechanisms. In addition, the short decadal periodicities in our records might result from the expression of the interannual fluctuations of the AAO and El Nino indices (Stenseth et al., 2003; Jevrejeva et al., 2003), that can increase noise in the signal.

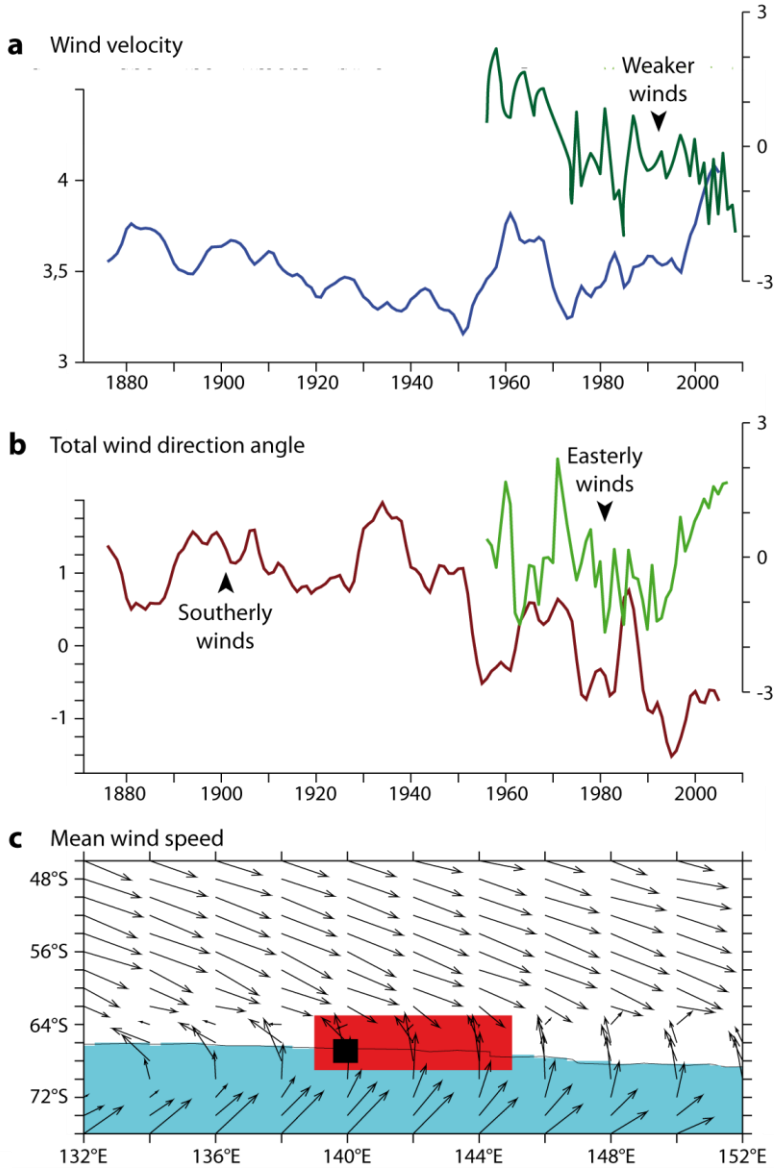

Figure 54. Changes in the wind pattern over the Adelie-Georges V Land since the 19 century. a) Standardized values of the wind magnitude (blue) inferred from the wind speed at 2 meters from 20CR reanalysis over the last 140 years for the A-GV Land; standardized yearly average values of wind speed (dark green) for the 1956-2007 period measured at the Dumont D'Urville (DDU) station. b) Standardized total wind direction angle (brown) respective to the inferred from the wind speed at 2 meters from 20CR reanalysis over the last 140 years for the A-GV Land; standardized yearly average values of wind direction (dark green) for the 1956-2007 period measured at the DDU station. c) Wind mean speed and vector, red box indicates the study area where the wind have been averaged in the 20CR reanalysis over the last 140 years, black box indicates the location of the DDU station.

In addition, direct influence of solar activity on the wind pattern over the SH has been suggested at decadal (Zhao et al., 2014) to centennial scales (e.g. Varma et al., 2011). Periodicities of 10-20 years have already been observed in previous studies in Antarctica throughout the Holocene and linked to solar activity (Warner and Domack, 2002; Crosta et

al., 2007) as they also occur in the ^{14}C and ^{10}Be records (Vonmoos et al., 2006). However, no stable and significant relationships between solar activity, using Total Solar Irradiance (TSI) reconstruction (Steinhilber et al., 2009), and sedimentary records from the DTGC2011 were observed (Fig. 55). The only significant relationship is observed with the Open Water gp (Suppl. Fig. 1), which sedimentary presence tracks warmer summer-autumn conditions and lengthening of the growing season. This likely suggests that, if solar activity was to modulate summer conditions off Adélie Land over the last centuries, the mechanisms involved remain unclear.

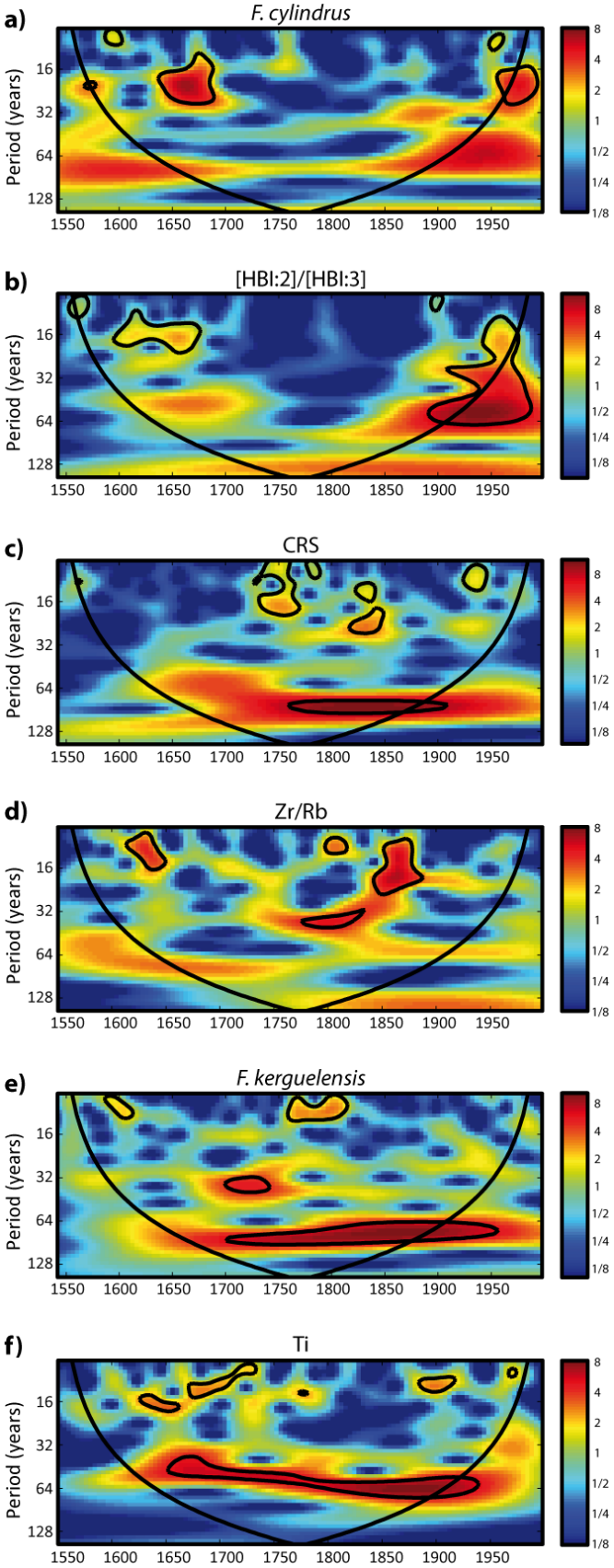

Figure 55. Continuous wavelet transform (CWT) of the sedimentary signals from the core DTGC2011 over the last 500 years. a) CWT of *Fragilariopsis cylindrus*; b) CWT of [HBI:2]/[HBI:3]; c) CWT of *Chaetoceros Hyalocaete* resting spores (CRS); d) CWT of Zr/Rb; e) CWT of *F. kerguelensis*; f) CWT

of Titanium. Data has been resampled every 4 years. CWT analyses were done using Morlet wavelet and Monte Carlo methods according to Grinsted et al. (2004). Statistically significant periods are identified by the black circled red zones. Data has been resampled every 4 years.

5.2.2 CDW pumping onto the shelf in Adélie Land

The Ti records in core DTGC2011 and CB2010 are perfectly synchronized and correlated in the 40-80 years band between 1750 C.E. and 1950 C.E. (Fig. 56) and exhibit large decreases during the 1760-1800 C.E., 1845-1880 C.E. and 1915-1960 C.E. periods (Fig. 53). Since the 1960s, both Ti signals present opposite trends, with low Ti values during the 1970s at DDUT and high Ti values at CB during the 1980s and (Fig. 53). Similar Ti records at both sites, whereas CB and DDUT experience opposite past sea-surface conditions, support the fact that a common and dominant forcing controlled the terrigenous inputs in AGVL. The upwelling and intrusion of warm CDW (Orsi et al., 1995) have been shown to increase sea surface temperatures onto the shelf (Williams et al., 2008), and promote the basal melting of regional glaciers (Miles et al., 2013), which contribute to higher release of bedrock and dirty ice particles that can sink to depth as subglacial meltwater plumes (Finocchiaro et al., 2005). Studies have suggested that increasing CDW onto the Antarctic continental shelf is driven by atmospheric variability over the SH. Indeed, modelling studies have shown that advection of CDW onto the Antarctic continental shelf is linked to enhanced upwelling southward of the ACC, promoted by a southward shift and strengthening of the Southern Ocean Westerlies (Hall and Visbeck, 2002; Marini et al., 2011), caused by a strengthening of the SAM pattern (Martinson et al., 2008). More locally, CDW inflow onto the shelf was found to be linked to stronger katabatic winds and enhanced polynya activity (Williams et al., 2008), likely suggesting that the northward transport of dense water would promote the southward intrusion of CDW in the region. In addition, pluri decadal periods of increasing terrigenous inputs at CB and DDUT are well correlated with phases of higher MGP activity over the last 250 years linked to the MG dynamics (Campagne et al., 2015), suggesting the potential role of the coupled MGP-MG system. In the Adélie depression, a general clockwise circulation results from the subsurface inflow of the CDW southeast into the depression and along the MG, and from a westward return flow of dense saline shelf water along the coast and out *via* the Adélie Sill (Williams et al., 2008). Mooring observations further indicate that the major incursion of CDW occurs east of the Adélie Sill into the Adélie Depression (Fig. 50), relative to the sill off the DDU Bank (Williams et al., 2010), likely due to a more intense formation and export of

dense shelf water in the Adélie depression (Arrigo et al., 2003; Tamura et al., 2012; Lacarra et al., 2014). The out-of-pattern of terrigenous inputs signals observed over recent decades suggest a punctual asymmetric inflow of CDW between both regions that is unexplained yet. The paucity of hydrological data in Adélie Land does not allow to firmly assess potential oceanic and glacial processes behind such decoupling between both regions.

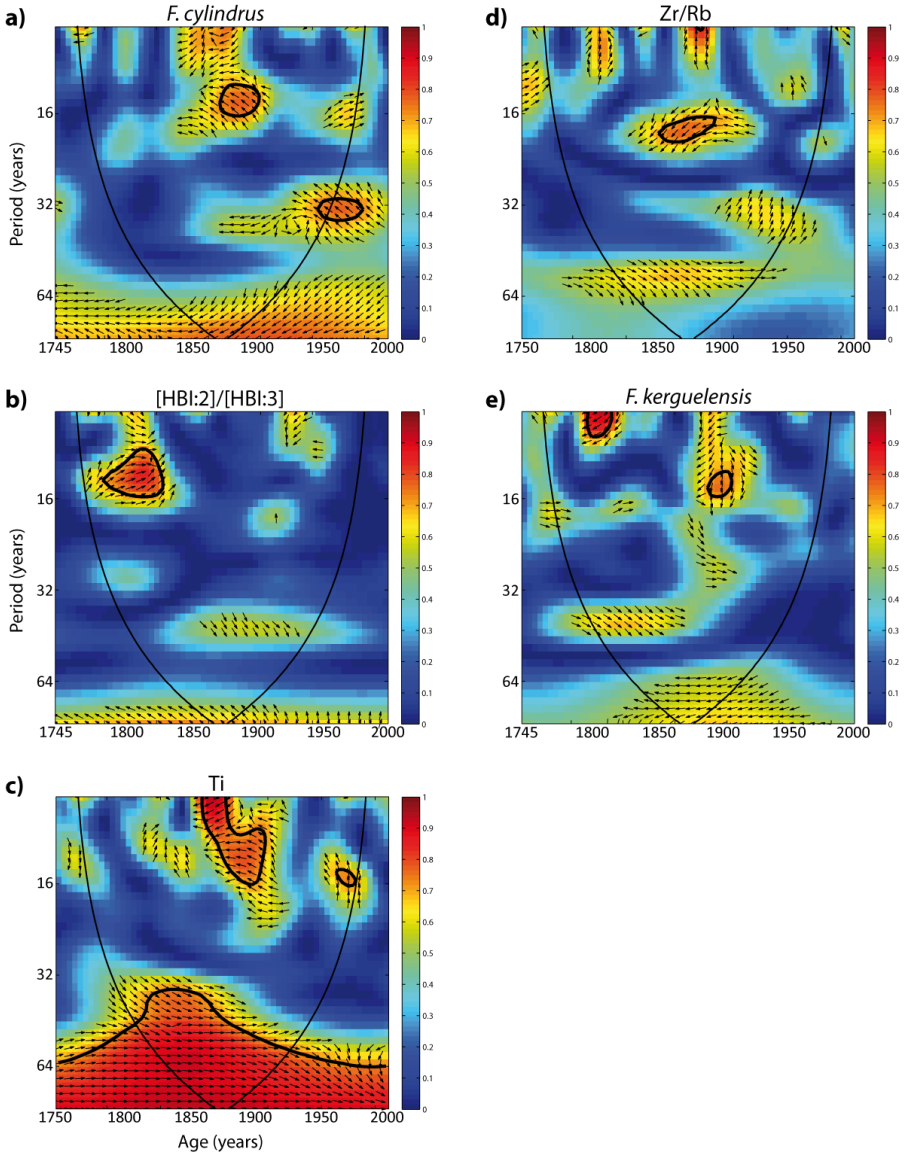

Figure 56. Cross wavelet correlation (XWT) between sedimentary signals from the core DTGC2011 and CB2010 over the last 250 years. a) XWT of *Fragilariopsis cylindrus*; b) XWT of [HBI:2]/[HBI:3]; c) XWT of Titanium; d) XWT of Zr/Rb; e) XWT of *F. kerguelensis*. Data has been resampled every 4 years. XWT analyses were done using Morlet wavelet and Monte Carlo methods according to Grinsted et al. (2004). Statistically significant periods are identified by the black circled red zones. Rightward pointed arrows indicate positively correlated signals while leftward pointed arrows indicate negatively correlated signals. Data has been resampled every 4 years.

5.2.3 Glacial dynamics in Adélie Land

Campagne et al. (2015) have recently discussed about the local influence of the Mertz Glacier (MG) dynamics off AGVL. Indeed, it has been suggested the MG generates well marked pluri decadal cycles (70-80 years) in sea surface and polynya conditions in the Adélie Trough over the last centuries. We have investigated the relationships between the Adélie Depression (more precisely Commonwealth Bay, CB, 200 km eastward of DDUT) and the DDUT sites over the last 250 years. Whereas heavier sea ice condition are recorded between 1760-1800 C.E., 1845-1880 C.E. and 1915-1960 C.E. immediately after each calving of the MG (Campagne et al., 2015; Fig 53 pink curves), the DDUT region was simultaneously characterized by open water conditions, notably with increasing *F. kerguelensis* during the 1765-1820 C.E., 1845-1895 C.E. and 1920-1955 C.E. periods (Fig. 53, blue curves). As such, the 1880-1920 C.E. and the 1950-1970 C.E. periods were characterized by increasing sea ice conditions (Fig. 53). These opposite trends are further supported by wavelet analyses between records from the two regions (Fig. 56), which highlight a strong and inverse relationships in the ~70-80 years band for *F. cylindrus*, [HBI:2]/[HBI:3] and *F. kerguelensis* over the last 250 years. Such repetitive and opposite behaviour between the two regions, distant from 200 km, exclude the implication of global climate forcing, but rather the influence of local processes. Additionally, recent observations show that the 2010 calving of the MG had profound impacts on the downstream area (Kusahara et al., 2011; Tamura et al., 2012; Lacarra et al., 2014), including CB and the DDUT. Indeed, the seaward extent of the MGT blocks pack ice and icebergs westward flow (Frezzotti et al., 1998), which are of particular importance for the build up of a fast ice buttress on the Adélie bank and, thence, on sea surface conditions over the DDUT (Chap III; Massom et al., 2001; Giles et al., 2008; Smith et al., 2011). Therefore, while the Adélie Depression region experiences open water conditions due to the presence of the MGP, the DDUT experiences heavy pack ice conditions because of the absence or reduction of fast ice and iceberg fields on the Adélie bank. In contrast, a reduced (or absent) MG tongue (MGT) allows the passage of pack ice reducing the MGP in the Adélie Depression region and icebergs which then ground onto the Adélie Bank and promote fast ice development which, in turn, promote the presence of open water conditions over the DDUT area. However, such pattern may be altered in time by the nature of the forcing themselves. Indeed, the MGT constitutes a relative continuous ice flow over decades while in the DDUT the fast ice buttress over the banks is related to both the MG dynamics along with strong interannual changes in atmospheric conditions (Chap III). More spatial and temporal analyses

of sea ice cover through the MODIS satellite imagery would help to assess the fast ice variability in the region and particularly over the DDUT. Concerning the polynya activity, the opposite pattern between both sites is a less obvious over the last 250 years. Our records indicate that at the sub decadal timescale the Zr/Rb records at CB and DDUT have been episodically and alternatively in phase **(**e.g. during 1800-1825 C.E., since 1960 C.E.) and out-of-phase (e.g. during 1845-1890 C.E. and1890-1950 C.E.) (Fig. 53). Wavelet analyses confirm such observations (Fig. 56). In phase relationship, as e.g. observed over the last decades, could suggest that polynya activity may have been driven by atmospheric forcing superimposed to local glacial dynamics, in agreement with previous findings (Chap III; Campagne et al., 2015).

6 Conclusion

Paleoclimate reconstructions from the DTGC2011 indicate that the DDUT region have experienced three distinct climate phases over the last 500 years. These changes in the mean climate state were linked to the synoptic scale reorganisations in the atmospheric and oceanic patterns. The 1540-1725 C.E. period, characterized by a delayed ice free season and low polynya activity, coincides with the beginning of the southward migration of the mid-latitude Westerly Winds conducting to more northerly to easterly winds in the AGVL region. The 1725-1890 C.E. interval was characterized by a progressive increase of the ice free season due to an early spring sea ice retreat and presence of a recurrent polynya over the 1725-1890 C.E. period. Our data however suggest that the polynya regime changed around 1850 C.E. from a coastal polynya to a seaward polynya. Such shift in sea ice and polynya dynamics might have been caused by changes in the wind pattern, from prevalent katabatic to dominant easterly winds. Finally, increasing sea ice seasonality since the late 19th century, characterized by icy spring and more open conditions in summer to autumn, was likely associated to the apparition of the persistent SAM+ pattern, promoting more frequent, weaker easterly winds and onshore wind circulation in our study area. Additionally, climate modes and solar activity may have continuously influenced sea surface conditions in the region at different timescales over the last centuries, but the mechanisms involved remain unclear. Additionally, out-of-phase records of sea ice and polynya activity between DDUT and CB, 200 km eastward, indicate that the MG dynamics played a major role on regional sea-surface conditions on top of global forcing. Studying impacts of the Dibble Glacier dynamics on sea surface conditions, notably

on fast ice coverage, would be required to complete the contribution of glacial forcing surrounding the DDUT. The polynya efficiency and terrigenous inputs may also be strongly impacted by intrusion and circulation of the warm CDW onto the shelf. Coupled atmospheric and oceanic variability, combined to the dynamics of the coupled MGP-MG system seem likely to drive inflow of CDW onto the Adélie shelf. Although very preliminary, oceanic exchanges between the Adélie Depression and the DDUT *via* the DDU bank have been recently observed (Houssais, M.N., personal communications), but their impacts on local oceanic surface conditions need to be identified. Analysis of additional sedimentary sections in or nearby the DDUT area would provide a better and finer spatial view of local processes that act in the region at interannual to decadal scale.

AUTHOR CONTRIBUTIONS

X. Crosta and G. Massé designed the study and P. Campagne carried it out. O. P. Campagne performed diatom analyses, biomarker analyses and PCA analyses; S. Schmidt performed ^{210}Pb analyses and helped to develop the age model of the core; P. Campagne prepared the manuscript with contributions from all co-authors.

ACKNOWLEDGMENTS

This research was funded by the ERC StG ICEPROXY project (203441), the ANR CLIMICE project and FP7 Past4Future project (243908). The French Polar Institute provided logistical support for sediment and data collection (IPEV projects 452 & 1010). This is ESF PolarClimate HOLOCLIP contribution n°24 and Past4Future contribution n°83.

SUPPLEMENTARY FIGURES are available in Annexe 2.

Chapitre V: Les derniers 2,000 ans en Antarctique de l'Est

La banquise antarctique exerce un rôle important sur les flux de chaleur et les échanges de gaz à l'interface océan-atmosphère, sur la circulation océanique globale, sur l'albédo de l'Hémisphère Sud et sur la productivité primaire de l'Océan Austral. Les reconstructions paléo-climatiques (PAGES 2k Network, 2013) couvrant l'Holocène tardif, ainsi que les récentes observations (Cavalieri et de Parkinson, 2008) en Antarctique montrent que les variations de températures et de couvert de banquise sont spatialement et temporellement hétérogènes, pour des raisons encore inconnues. L'étude à haute résolution des conditions passées du couvert de banquise en Antarctique au cours de l'Holocène est donc nécessaire afin de mieux évaluer ces changements, ainsi que les forçages naturels et les mécanismes impliqués.

Dans ce chapitre, notre objectif portait sur la reconstruction des conditions océanographiques et climatiques en Antarctique de l'Est au cours des deux derniers millénaires, là où d'autres enregistrements manquaient, étaient incomplets, où étaient d'assez faible résolution sur ces périodes. Dans ce chapitre final, grâce à la validation de nos outils (Chap III), ainsi qu'à l'étude fine des forçages climatiques au cours de derniers siècles (Chaps III & IV), nous avons pu distinguer quatre intervalles climatiques pluri centennales au cours de l'Holocène tardif. Les conditions moyennes de ces intervalles sont relativement opposées aux phases climatiques bien connues observées dans l'Hémisphère Nord. La mise en perspective de nos travaux à partir d'une carotte sédimentaire avec d'autres enregistrements glaciaires en Antarctique de l'Est, ainsi que l'analyse par ondelettes de nos données, révèlent des changements brusques des conditions de surface, de polynies et de saisonnalité de la banquise, en lien avec l'activité solaire à travers l'interaction couplée de la circulation atmosphérique et océanique de l'Hémisphère Sud. Les résultats présentés dans ce chapitre constituent également un article scientifique en préparation.

Article IV: High resolution reconstruction of climate and sea ice seasonality in Adélie Land, East Antarctica, over the Late Holocene

in preparation

Campagne, P.1,2,3, Etourneau, J.1, Massé, G.2,3, Crosta, X.1 and IODP Expedition 318 Scientists

1EPOC, UMR CNRS 5805, Université de Bordeaux, Allée Geoffroy St Hilaire, 33615 Pessac, France

2LOCEAN, UMR CNRS/UPCM/IRD/MNHN 7159, Université Pierre et Marie Curie, 4 Place Jussieu, 75252 Paris, France

3TAKUVIK, UMI 3376 UL/CNRS, Université Laval, G1V 0A6 Quebec (Quebec), Canada

Antarctic sea ice exerts a strong control on the ocean-atmosphere heat and gas fluxes, the Southern Hemisphere albedo, the global ocean circulation and the Southern Ocean primary productivity. From the Late Holocene onward, paleo reconstructions (PAGES 2K, 2013) along with recent observations (e.g. Cavalieri and Parkinson, 2008) indicate that temperatures and sea ice cover in Antarctica display spatial and temporal heterogeneous trends that are not fully understood. High resolution investigation of past Antarctic sea-ice conditions during the Holocene is thus required to better assess sea ice changes and the mechanisms involved under natural climate forcing. Here, new and well dated sediments from Integrated Ocean Discovery Program (IODP) Site U1357B, retrieved on the continental shelf off Adélie Land (East Antarctica), constitutes the first complete high-resolution marine-based paleoclimate records covering the last 2,000 years. A sequence of annual to near-annual laminated diatomaceous sediment enables reconstruction of past sea-ice conditions at an unprecedented interannual to decadal resolution over the Late Holocene. Diatom assemblages and diatom-specific lipid biomarkers (HBIs) allow to distinct four intervals over the last 2,000 years, which mean climate conditions were opposed to known climate phases observed in the Northern Hemisphere. Wavelet analyses of the datasets also reveal large abrupt changes in sea ice seasonality and polynya activity, which can be associated to solar activity forcing through the modification of the coupled SH atmospheric and oceanic circulation.

Key words: Late Holocene, Adélie Land, Sea ice, SAM, SOI, Westerlies, solar activity, diatoms, HBIs.

1 Introduction

While the Holocene has been traditionally considered as a relatively stable climatic period, significant changes have been reported on both regional and global scales. Notably, the late Holocene period is characterized by large and rapid changes in temperature. Although generally most pronounced in the Northern hemisphere (NH, e.g. Medieval Warm Period or Little Ice Age, see Mann et al., 2009; Crowley, 2000), such climatic phases may also be observed in marine records (e.g. Leventer et al., 1993; Leventer et al., 1996; Domack et al., 2001; Nielsen et al., 2004) and glacial records (e.g. Masson et al., 2000; Masson-Delmotte et al., 2004, Bertler et al., 2011; Orsi et al., 2012; PAGES 2k Network, 2013) from the Southern hemisphere (SH). However, SH paleoclimate reconstructions highlight the complex heterogeneous regional and temporal trends of the Late Holocene variability (Cook et al, 2000; Mann et al., 2008), particularly for the Antarctic region (Turner et al., 2005; Schneider et al., 2006; Steig et al., 2009; Goosse et al., 2012).

Although an extensive network of ice cores in Antarctica is revealing some of the nature of Late Holocene atmospheric variability, few marine records are available and, when available, these tend to be short and low resolution. In particular, in East Antarctica, the few high resolution records obtained from the marine environment lack the last millennium (JPC24, MD2603-2601; Crosta et al., 2007; Denis et al., 2010) and this period, which is essential for delineating climatic fluctuations induced by natural variability from those resulting from Anthropogenic activities, is studied using information only collected via ice core reconstructions. As such, very little is known on the interactions between the ocean, sea ice and atmosphere climatic sub-systems and their teleconnexions to low-latitude climate as the mechanism behind the regional climatic heterogeneity observed over the last millennium in Antarctica (Goosse et al., 2012). This is especially evident for sea ice dynamics, which ice-core records only cover the last 250 years (Curran et al., 2003).

Here we present the first high-resolution marine-based paleoclimate records from core IODP U1357 Hole B, retrieved on the continental shelf off Adélie Land and covering the last 2,000 years. Along the East Antarctic continental shelf zone, where high sedimentation rates have been previously reported (JPC24, MD2603-2601; Crosta et al., 2007; Denis et al., 2010), the Dumont d'Urville Trough (DDUT) site yields a ~180 meter long Holocene sediment archive and constitutes the most expanded Holocene sediment section yet discovered worldwide (Escutia et al., 2010). These exceptionally high sediment rates therefore allow for assessing

the evolution of sea ice cover and related surface ocean conditions in the area during the Late Holocene at a sub-decadal resolution. We use sea ice-related and open ocean-associated diatom assemblages, along with diatom specific biomarkers (HBIs) to reconstruct past sea ice variations in our study area. We further assess the amplitudes and frequencies of the forcing mechanisms involved in long- and short-term sea ice variability.

2 Material and Methods

2.1 General characteristic of the study area

Antarctic coastal and continental shelf zones (CCSZ) are some of the most ecologically productive regions of the Southern Ocean (Arrigo et al., 2008). Diatoms account for a large proportion of primary productivity in CCSZ and in Adélie Land, East Antarctica, they dominate (~80%) the phytoplanktonic assemblages, and occur mostly through intense spring blooms (Beans et al., 2008) influenced by changes in stratification and thus the stability of surface waters, that are, in turn, associated to oceanic dynamics and wind pattern variability (Leventer, 1992; Vaillancourt et al., 2003; Arrigo and van Dijken, 2003; Williams et al., 2008; Beans et al.,2008). Our study area, the Dumont d'Urville Trough (DDUT; Fig. 57), is punctuated by several glacial depressions, which act as natural sediment traps by focusing the local sedimentary material. The DDUT runs from the front of the Zélée and Astrolabe glaciers to the continental shelf break along a SE-NW orientation and is flanked by the Dumont d'Urville (DDU) Bank (Fig. 57), on its eastern side and the Dibble Bank on its western side.

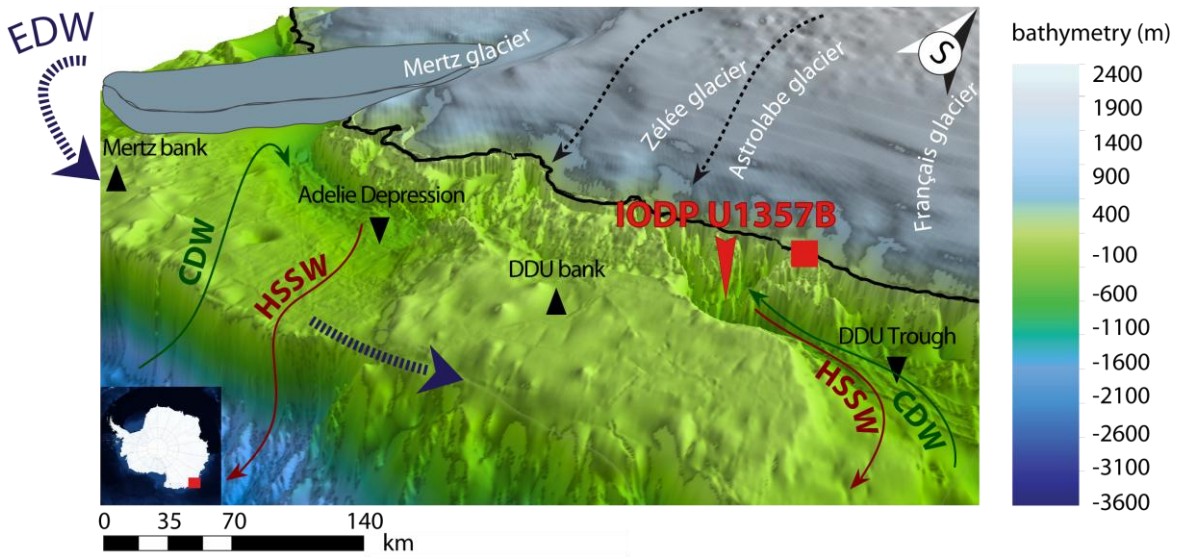

Figure 57. Study area. Map of the study area showing the location of sediment core IODP U1357 Hole B (downward red arrows) in the Dumont D'Urville Through (DDUT). Are also mentioned the Dumont D'Urville (DDU) french station (red square), the main glacial (in white) and topographic (upward black triangle for high relief and downward for troughs) features, the East Wind Drift (EWD; blue dashed arrow), the principal water masses as Circumpolar Deep Water (CDW; green arrow) and the High Salinity Shelf Water (HSSW; brown arrow) (Williams et al., 2008), and the katabatic winds (black dashed arrows; Massom et al., 1998). Bathymetry data were obtained from http://www.deepreef.org/publications/peer-review/82-gvdem.html.

The area is under the influence of several water masses and currents (Rintoul, 1998; Williams and Bindoff, 2003; Williams et al., 2008) with, at the surface, the wind-driven East Wind Drift, flowing westward. Close to the surface, the Antarctic Surface Water constitutes the summer sub-surface water mass. They are located on the continental shelf while the Circumpolar Deep Water (CDW) upwells near the Antarctic Divergence and can intrude onto the plateau during summer. At the bottom, the High Salinity Shelf Water, which is formed by brine rejection during winter sea ice formation and cooling of the CDW, flows northward (Fig. 57) as part of the dense shelf water that extrudes the plateau. This Adélie Land Bottom Water ultimately sources the Antarctic Bottom Water (Rintoul et al., 1998; Jacobs et al., 2004; Meredith et al., 2013).

The CCSZ of Adélie Land experiences the strongest katabatic winds ever observed (Périard and Pettré, 1993), due to the funnelling effect caused by presence of narrow glacial valleys close to the shoreline (Wendler et al., 1997). These winds blow from the south-east and support the occurrence of polynyas such as the DDU Polynya (DDUP; 66.11°S–139.31°E) in the region.

Sea ice covers ~80% of the area during winter and melt back to the coast in summer (Arrigo and van Dijken, 2003). Fast ice is also present during the winter months and extends to ~100 km offshore between the Dibble Tongue in the west and the Adélie Bank in the east (Massom et al., 2003; 2009; Smith et al., 2011; Wang et al., 2014). In summer, this fast ice buttress is characterized by a succession of several breakouts and re-freezes in the DDUT as a result of a lack of anchor points (Massom et al., 2009; Smith et al., 2011). In contrast, it remains more stable and persists later in the season over the banks where numerous icebergs act as grounding points. Recent studies suggest a strong inter-annual variability of sea ice cover in our study area, both in of term of extent and timing (formation and retreat), as sea ice conditions are closely linked to the fast-ice dynamics which are, in turn, largely related to synoptic scale wind (Adolph et al., 1995; Massom et al., 2003; 2009; Smith et al., 2011; see Chap III).

2.2 Core description

In February 2010, the Integrated Ocean Discovery Program (IODP) Expedition 318 (lead proponent: C. Escutia) recovered a ~180 meter long Holocene sediment archive in the DDUT. The Hole U1357B (66.4°S, 140.4°E; Fig. 57) has been drilled close to the DDU station in the most proximal depression of the DDUT at a depth of 1010 meters by an advanced piston coring (APC)/extended core barrel (XCB) drilling assembly. The loss of sediment due of gas evolution and section expansion was minimal throughout the core and the sequence recovered from Hole U1357B, composed of 19 sections, provides an intact Holocene sedimentary sequence (Escutia et al., 2010). The upper 170 m of the core consist of dark olive-brown to light greenish brown diatom ooze, and exhibits centimeter scale laminations defined by color changes between lighter greenish brown (spring season) and darker brown (summer season) intervals, as previously shown at the same site (Maddison et al., 2012). Laminations range from ~1 to ~4 cm of annual thickness, as a result of changing conditions between a high-productivity deposition during spring and a less organic-rich sedimentation during summer (e.g., Stickley et al., 2005; Maddison et al., 2006; Denis et al., 2006). The observation of hydrogen sulfide gas at very shallow depth (uppermost meter) in all holes and the presence of pervasive laminations throughout the sequence indicate anoxic conditions that prevented larger benthic organisms from disrupting the laminations. The diatom ooze is unusually pure and intervals with minor clay or fine silt grains only account for up to 10–20% of the smear

slide grains (Escutia et al., 2010). Radiolarians, sponge spicules, and silicoflagellates are also well preserved, further confirming the presence of preservation conditions highly suitable for paleoclimate reconstructions. In this study, we focus over the uppermost ~38 m of the archive that are corresponding to the last 2,000 years.

2.3 Core chronology

The chronological framework of the sediments was determined using radiometric techniques. Radiocarbon analyses were performed at the Center for Accelerator Mass Spectrometry from the Lawrence Livermore National Laboratory, Livermore, USA. Five carbonate shell dates and eighty AO dates (Suppl. Table 1) were obtained for Hole U1357B sediments. The dead carbon fraction (DCF) was determined by comparison of shells raw ^{14}C dates with raw ^{14}C dates derived from AO treated samples within Hole U1357B and nearby cores (Costa et al., 2007). A DCF correction of 425 years was subtracted from all AO raw ^{14}C dates prior to calibration. A reservoir age correction of 1200 +/- 100 years (with a Delta R of 800 years), as generally recommended for East Antarctic shelves (Ingólfsson et al., 1998), was assigned to all ^{14}C raw dates for calibration using CLAM software (Blaauw and Christen, 2011) which uses the marine13 calibration curve. Overall, Hole U1357B sediments cover the last 11,500 years in ~170 meters. For the interval of consideration here, the core covers the ~-129-1907 C.E. period (Fig. 58) in ~38 meters, with an average sedimentation rate of ~1,8 cm/yr.

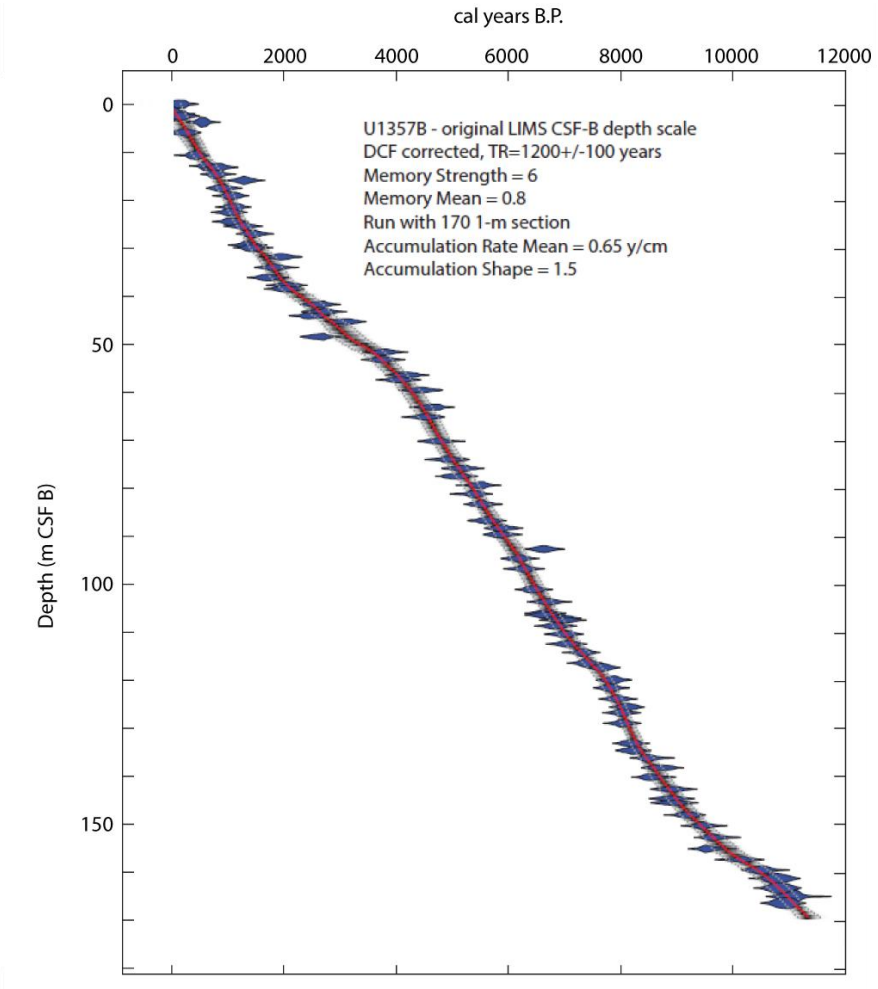

Figure 58. Chronology of the IODP U1357 based on AMS 14C dates. Ages were calibrated to calendar ages using BACON (Blaauw and Christen, 2011).

2.4 Diatoms analyses

Micropaleontological analyses were performed every 17-18 cm (~9.4 years resolution) according to the methodology described in Crosta and Koç (2007) in core U1357B. Diatom slides were prepared from ~0.5 g of dry sediment. After decarbonatation and oxidation of the organic matter, the residue was suspended in distilled water and settled onto a coverslip, dried and subsequently mounted on a glass slide with NOA61. Cell counts were done using an Olympus BH-2 at a magnification of x1000. For each sample, 300-350 diatom valves were counted and data are presented as species relative abundances. Diatom identification was performed to the species or species group level. More details about slide preparation and diatom identification are available in Crosta et al. (2004). Approximately 70 diatom species

were identified in down-core assemblages, from which less than a dozen species presented abundances higher than 2% of the total diatom population. Diatom species have been grouped according to their ecological preferences. Ecological interpretations were based on the modern data (chap III) as well as paleoclimate studies covering the Holocene.

2.5 Biomarker analyses

Few marine and freshwater diatoms belonging to *Haslea*, *Navicula*, *Pleurosigma* and *Rhizosolenia* genera were recently found to be synthesizing Highly Branched Isoprenoids (HBI) (Massé et al., 2011; Sinninghé et al., 2004). A di-unsaturated isomer [HBI:2] has been identified in Antarctic sea ice and isotopic analyses provide evidence for that this isomer is synthesized by sea ice dwelling diatoms, while a tri-unsaturated isomer [HBI:3] has been identified in water column phytoplankton (Massé et al., 2011). Biomarker analysis followed the technique described by Massé et al. (2011) and were performed every ~5-6 cm (~3 years resolution) along the upper ~38 meters of the core IODP U1357B. Briefly, an internal standard was added to the freeze-dried sediments, lipids were extracted using a Dichloromethane/Methanol mixture to yield a total organic extract (TOE), which was then purified using open column chromatography (silica). Hydrocarbons were analyzed using a Gas Chromatograph coupled to a Mass Spectrometry detector (GC-MS). More details about analyses are available in Massé et al. (2011).

2.6 Wavelet analyses

We used cross wavelet analysis and applied the Morlet wavelet as the mother function on our dataset, through the MATLAB package and the complete method written by Grinsted et al. (2004). This method provides a good balance between time and frequency localization, and we used Monte Carlo simulations to provide frequency-specific probability distribution (Global wavelet spectrum) that can be tested against wavelet coefficients. Statistical significance was estimated against a red noise model (Grinsted et al., 2004). In this study, to test the relevance of our proxies, their statistical relationships and to examine periodicities in a frequency domain, we compared the two time series by their continuous wavelet transform, which we hypothesized are linked in some way. The resulting Cross Wavelet Transform

exposed their common power and relative phase in time-frequency space of the two signals. Data were previously re-sampled at a 4 years constant step, close to the initial sampling step. Data were then standardised by subtracting to each values the mean of the dataset and then by dividing it with the standard deviation. Standardisation did not change the shape of the records but normalized the amplitude of the variations. Given the resolution of our analyses, cyclicities in the ~0-15 years band are not taken in consideration as they cannot be distinguished from those arising from the noise.

2.7 Sedimentary proxies

The FCC gp includes *Fragilariopsis curta* and *F. cylindrus*. Large abundances of both species were interpreted as an indication for the presence of a heavy sea ice cover in several paleoclimate studies, including those from our study area (Crosta et al., 2007; Denis et al., 2010). Recent studies have also proposed the use of [HBI:2] and [HBI:3] to reconstruct variations of Antarctic sea ice duration during the Holocene as complementary sea ice proxy to diatom counts (Denis et al., 2010; Collins et al., 2013). In the region, Campagne et al. (2015) have observe a good correlation between [HBI:2] and *F. cylindrus* in response to increasing sea ice conditions.

Chaetoceros Hyalochaete resting spores (CRS) in Holocene sediment from Adélie Land have been associated to an intermittent mixing of the stratified surface waters caused by intense katabatic winds during the ice free season (Maddison et al., 2006). Indeed, increasing abundances of CRS in surface sediment were coinciding with the dominances of strong southerly winds (Chap. III) that induced intense polynya activity along the DDU coast (Riaux-Gobin et al., 2013). Sedimentary distribution of CRS in the region has also been associated with high nutrient levels and the reduction of sea ice influence in spring (Leventer, 1991; Crosta et al., 1997; Denis et al., 2006).

Analysis of surface sediments (Chap. III) revealed that increasing abundances of large centric diatom (such as *Thalassiosira lentiginosa, T. oliverana, T. trifulta, T. gracilis, T. tumida, Actinocyclus actinochilus, Stellarima microtrias* and *Coscinodiscus* spp) indicate open water and relatively warm conditions during summer, and provides an indication of the length of the phytoplankton growing season.

Analysis of Holocene sediments indicate that *Thalassiosira antarctica* RS and the *Porosira* gp, composed of *P. glacialis* and *P. pseudodenticulata*, shares broadly similar sea surface temperature, sea surface salinity, sea ice proximity preferences as well as similar seasonal occurrences (Pike et al., 2009). In Holocene sediments, these species were used to infer late summer/autumn rapid deposition triggered by early sea ice return (Maddison et al., 2006; Denis et al., 2006). However, analysis of modern regional sediments indicate that *T. antarctica* prefers icier environments than the *Porosira* gp (Chap. III).

3 Results

Relative abundances of the FCC gp show a slightly increasing trend over the last 2,000 years, from which, large pluri decadal to centennial scale oscillations can be observed (Fig. 59). The FCC gp reaches a mean values of ~34% between ~-129-480 C.E., and decreases gradually to reach ~20% between ~480-850 C.E. (Fig. 59). Relative abundances of the FCC gp then increase rapidly toward a mean values of ~39% in the sediments deposited between ~850-1550 yrs C.E, and decreases gradually to ~30% between ~1550-1850 C.E. (Fig. 59). After 1850 C.E., the FCC gp relative abundance increase rapidly to reach a mean value of ~47% over the last decades (Fig. 59). At the pluri decadal scale, the FCC gp relative abundances display a strong variability throughout the entire record, with large amplitude shifts of up to 40%.

The [HBI:2]/[HBI:3] ratio record also exhibits a similar long-term trend with values increasing over the last 2,000 years (Fig. 59). The [HBI:2]/[HBI:3] ratio presents a mean value of ~0,032 between ~-129-480 C.E. and decreases to ~0,017 between ~480-850 C.E. (Fig. 59). The ratio increases toward its highest values between ~850-1550 C.E. with a mean value of ~0,043, and then decreases to ~0,03 between ~1550-1850 C.E (Fig. 59). After ~1850 C.E., the [HBI:2]/[HBI:3] ratio increases again toward a mean value of 0,04 although the last decades experienced a sharp decrease (Fig. 59). Greater variability of [HBI:2]/[HBI:3] ratio, traduced by large peak values up to 0,1, are discernible between 50-210 C.E. and between the 900-1900 C.E. intervals (Fig. 59), generally during periods of greater FCC gp relative abundances.

In contrast, relative abundances of the CRS exhibit an opposite long term trend, with a relatively slight decrease over the last 2,000 yrs. The record also displays large amplitude of pluri centennial scale oscillations (Fig. 59). The CRS abundances display a low mean values of ~21% between ~-129-480 C.E., and then increase toward their highest values between ~480-850 C.E., with a mean value of ~34% (Fig. 59). Then, the CRS cell abundance decreases to a mean value of ~19% between ~850-1550 C.E., and re-increases to 28% between ~1550-1850C.E. (Fig. 59). After 1850 C.E., CRS relative abundances drop to ~14% (Fig. 59). Beside these large periods, the CRS record further strongly varies and present large pluri-decadal shifts of 20-40% throughout the record (Fig. 59).

Relative abundances of the open water gp slightly decrease throughout the record (Fig. 59). The pluri centennial variability in relative abundances of the open water gp is less marked than for previous records, however a strong pluri decadal variability is evidenced throughout the whole core, characterized by large peak (values increasing up to 5-8 %) around ~-80 C.E., ~230 C.E., ~660 C.E., ~750-770 C.E., ~1010 C.E. and at 1330 C.E. (Fig. 59).

Relative abundances of *Thalassiosira antarctica* also display a long-term trend decrease with relatively high values at the beginning of the record (mean value of 7%) decreasing to low values at 450-900 C.E. (mean value of 2%) and increasing again during the most recent period (mean value of 9%). The pluri centennial variability is less marked than other spp. records but pluri decadal variability is high with large peak values of ~8-25% at ~-40 C.E., ~200 C.E., ~1150 C.E., ~1250 C.E., ~1680 C.E. and ~1790 C.E. (Fig. 59).

Relative abundances of the *Porosira* gp display some large pluri centennial scale oscillations over the last 2,000 years (Fig. 59), with mean values of 2.5% during the -129-480 C.E., 5% during the 480-850 C.E., 2% during the 850-1550 C.E. and 1% since 1550 C.E. (Fig. 59). The *Porosira* gp also exhibit large amplitude shifts from ~4,5 % to ~0,7% at ~150 C.E., from ~1 % to ~5,5 % around ~480 C.E. and from ~6 % to ~1,6 % at ~840 C.E., and further displays large peak values (up to 5 %) at ~570 C.E., ~680 C.E., ~730 C.E., ~780-800 C.E. and ~1320 C.E.

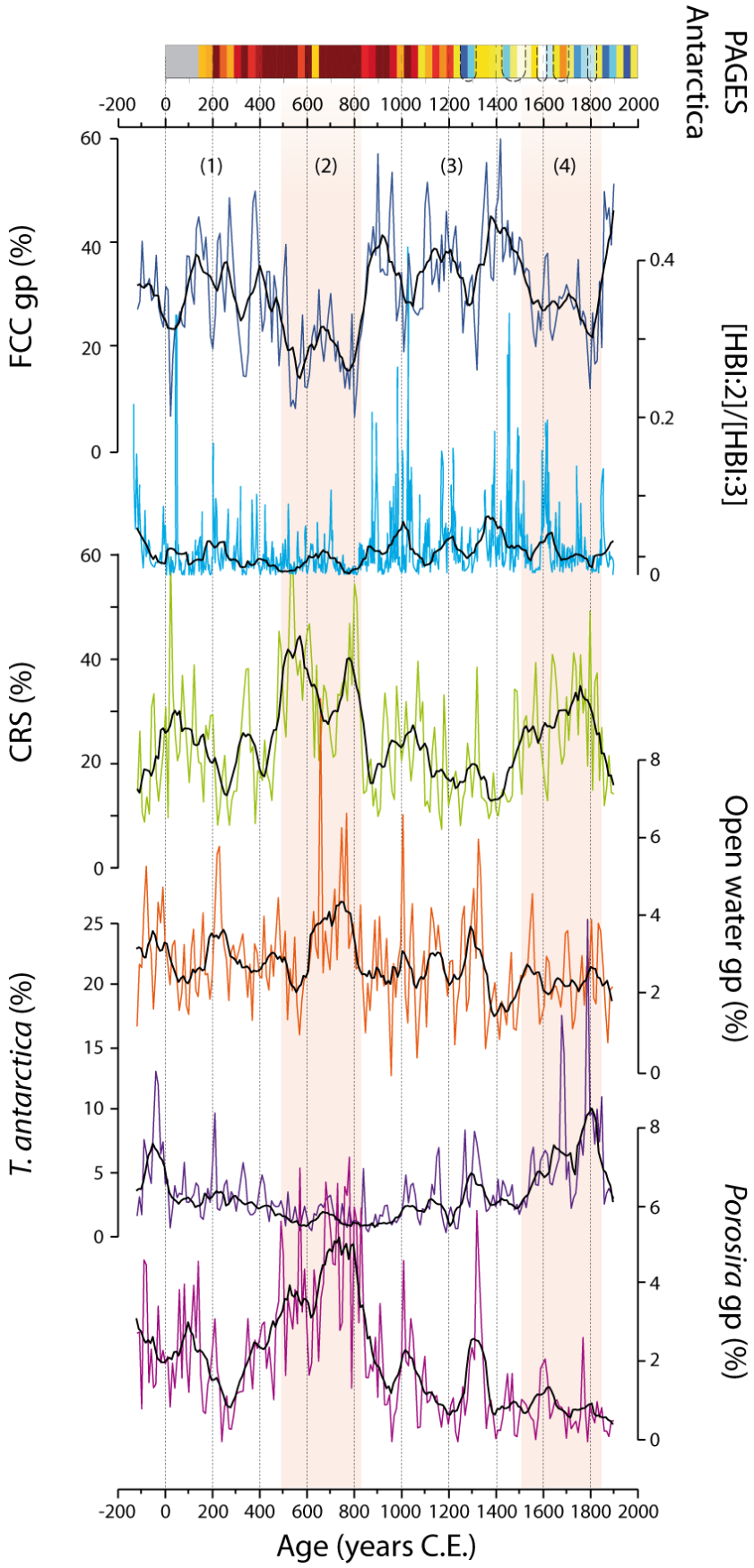
PAGES Antarctica
-200 0 200 400 600 800 1000 1200 1400 1600 1800 2000
(1)
(2)
(3)
(4)
FCC gp (%)
[HBI:2]/[HBI:3]
CRS (%)
Open water gp (%)
T. antarctica (%)
Porosira gp (%)
Age (years C.E.)

Figure 59. Variations of sea surface conditions through the sedimentary records from the IODP U1357B covering the last 2,000 years and continental scale temperature reconstructions from Antarctica. 30-year-mean standardized temperatures for the seven PAGES 2k Network regions, inferred from PAGES 2k consortium, 2013. Variations of the diatom assemblage relative abundances in IODP U1357 B covering the late Holocene, and sea ice related biomarkers: sea ice diatoms group (FCC; blue curve), [HBI:2]/[HBI:3] ratio (light blue curve), *Chaetoceros* resting spores group (CRS; green curve), open water group (red curve), *Thalassiosira antarctica* (violet curve), and *Porosira* group (pink curve). (1) to (4) indicate climate phases indentified, with red shading area indicating warmer periods. Black curves indicate the 90 years running mean.

4 Discussion

The late Holocene period is characterized by large and rapid changes in temperature that are spatially and temporarily heterogeneous in the SH. In Antarctica, the few marine-based paleorecords, which tend to be short and low resolution or incomplete, limit the understanding of the interactions between the ocean, sea ice and atmosphere climatic sub systems and the teleconnexion to low-latitude climate. Along the East Antarctic continental shelf zone, and particularly off Adélie Land, the high sedimentation rates allow for assessing the evolution of sea ice cover at a sub-decadal resolution over the Late Holocene. In section 4.1, we study the variability of sea surface conditions off Adélie Land over the last 2,000 years, in term of amplitudes and frequencies trough spectral analyses of our sedimentary signals. We also compare our data with regional temperature reconstructions based on ice cores in order to assess of the regional pattern of our results. Finally, in section 4.2 we discuss about the potential forcing mechanisms involved in long- and short-term sea surface variability.

4.1 2,000 years of climate evolution in East Antarctica

Our records from IODP U1357B display a long-term trend during the Late Holocene on which four contrasted climate phases lasting several hundred years are superimposed. Spectral analyses on the sedimentary signals also evidence pervasive pluri-decadal scale cyclicities over the last 2,000 years.

4.1.1 Long-term evolution

Most of our records indicate a long-term cooling trend over the Late Holocene period. Indeed, increasing relative abundances of FCC gp and of the [HBI:2]/[HBI:3] ratio over the last 2,000 years (Fig. 59) suggest enhanced concentration and duration of spring sea ice. Similarly, the slight decrease in relative abundances of both CRS and the Open Water gp (Fig. 59) indicate a reduction of DDU polynya and increasing sea ice concentrations (or less opened waters) during the summer season. These trends are even more evident if we focus on the last millennium with strong increase in FCC gp relative abundances and HBI content, along with strong decrease in CRS and Open Water gp relative abundances since 800 C.E. We congruently observe a steady increase in *T. antarctica* relative abundances along with a steady decrease in the *Porosira* gp relative abundances (Fig. 59) that reflect enhanced sea ice conditions in autumn. These results are in line with the global cooling trend observed over the last millennium with cold conditions between ~1000-1800 C.E. (Mann et al., 2009; Ljungqvist et al., 2010; Wanner et al., 2011) and, at the hemispheric scale, with the mean cooling trend recorded in Antarctica (Fig. 59; Orsi et al., 2012; PAGES 2k Network, 2013) despite the spatial heterogeneity in ice core temperature reconstructions over that period (Goosse et al., 2012).

4.1.2 Pluri-centennial variability

In addition to this long-term trend, our records further display strong short-scale variability over the Late Holocene. Indeed, wavelet analyses indicate that relative abundances of most diatoms (with the exception of *T. antarctica*) exhibit prominent periodicities (significant at the 95% confidence level) in the ~250 and the ~500 years bands over the last 2,000 years (Fig. 60). For *T. antarctica*, these frequencies are not significant and more diffuse during the first millennium, probably due to the low abundances of this species in the sediments at that time, but appear more distinctly during the second millennium when cells are more abundant. Unlike diatoms, wavelet spectrum of the [HBI:2]/[HBI:3] record shows significant power in the 80-200 years band over the last millennium and non-significant high power in the 300-400 years band throughout the last 2,000 years. Absence or unstructured periodicities in the [HBI:2]/[HBI:3] ratio signal during the first millennium is likely due to low ratio values at that time. As such, the sedimentary signals from core IODP U1357B exhibit four distinct

climatic periods, lasting several hundreds of years, each characterized by significant changes in seasonal sea ice dynamics.

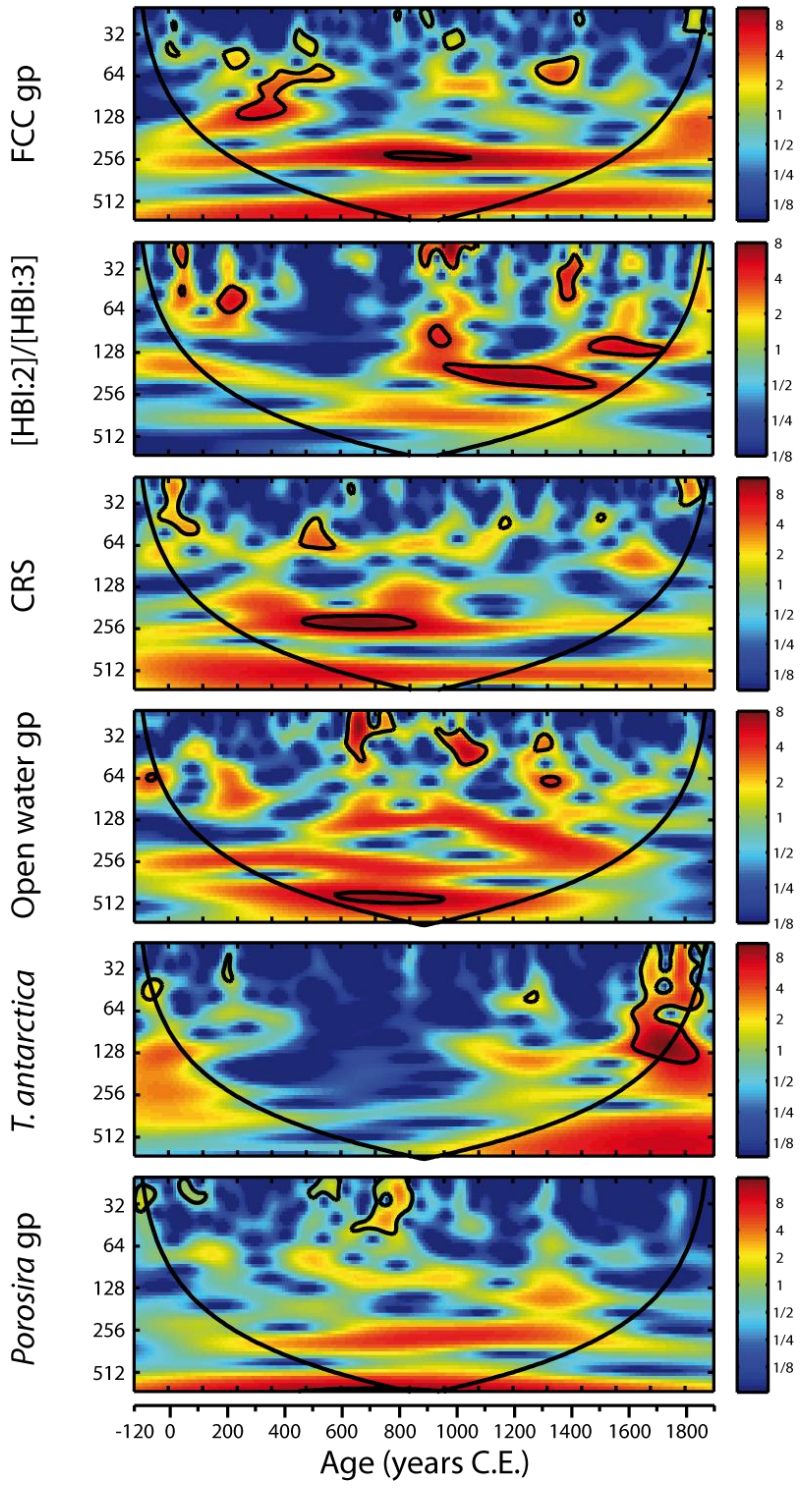

Figure 60. Cyclicities of sea surface conditions over the Late Holocene. Continuous wavelet transform applied on the FCC gp, the [HBI:2]/[HBI:3] ratio, the CRS assemblage, the Open Water gp, the *T.*

antarctica and the *Porosira* gp, using Morlet wavelet according to Grinsted et al. (2004). Data has been resampled every 10 years and standardized.

- *(1) The ~-129-480 C.E cold period*

This interval is marked by high FCC gp abundances and relatively high values of the [HBI:2]/[HBI:3] ratio (Fig. 59), suggesting icy conditions in spring resulting in cool, low salinity meltwaters injection upon sea ice waning. Highest abundances of *F. curta* and *F. cylindrus* are linked with locations that experience a sea ice cover duration of 9-11 month/yr and 8-9 month/yr respectively (Armand et al., 2005). Moderate relative abundances of CRS, centric diatoms (Open Water gp) and the *Porosira* gp suggest relatively cool summers and icy autumns, along with a moderate polynya extent or activity. This assemblage therefore indicates that surface oceanic conditions were characterized by a relatively late (although important) melting period in spring and a relatively early autumn waxing during this interval and, therefore, a reduced ice free season. The diatom assemblages in (1), when compared with surface sediment assemblages from the SH (Armand et al., 2005; Crosta et al., 2005), suggest an average sea ice duration of ~9-10 months/yr during this interval.

- *(2) The ~480-825 C.E warm/mild period*

This interval is characterized by the lowest relative abundances of the FCC gp and lowest [HBI:2]/[HBI:3] ratio values together with the highest CRS and open ocean diatom relative abundances throughout the entire record (Fig. 59). Relative abundances of the *Porosira* gp were maximum while those of *T. antarctica* were lowest. These data therefore indicate that (2) was characterized by an intense polynya activity and the most pronounced open water conditions of the last 2,000 years. Sea ice was probably melting early in spring but, most importantly, sea ice advance was also delayed in autumn, implying a short duration of the sea ice season. When compared with assemblages from surface sediment in the SH (Armand et al., 2005; Crosta et al., 2005), the species distribution in our sediments from that period suggests an approximately 8 months long sea ice season.

- *(3) The ~825-1550 C.E. cold period.*

In contrast to (2), this interval is characterized by maximum abundances of the FCC gp and high [HBI:2]/[HBI:3] ratio values along with low abundances of CRS, the Open Water gp and *T. antarctica* and *Porosira* gp (Fig. 59). This suggests the occurrence of very icy spring conditions and cool conditions during the summer/autumn season. Polynya extent and activity

may also have been strongly reduced at that time. Therefore, our records indicate that, as during (1), colder conditions rapidly took up at the end of (2) and prevailed between ~825-1550 C.E. Mean sea ice duration, based on comparison to modern assemblages (Armand et al., 2005; Crosta et al., 2005), can be estimated to a period lasting ~10-11 months/yr and was characterized by a late spring melting and early autumn waxing.

- *(4) The ~1550-1850 C.E. cold/mild period*

During interval (4), although the FCC gp and [HBI:2]/[HBI:3] ratio values decrease, they remained relatively elevated and coincided with increasing CRS abundances (Fig. 59). This suggests that enhanced polynya activity characterized the interval in contrast to (1) and (3). However, this time, the inverse relationship between sea ice and open water proxies characterizing previous intervals is less marked. This probably indicates the occurrence of still relatively cool summer conditions even if the spring conditions become progressively milder than during the previous interval. Interestingly, *T. antarctica* abundances increased during this interval while *Porosira* gp cells remained as low as during the previous interval suggesting that icier conditions during autumn progressively took place probably in line with cooler summers during this period. As such, between ~1550 and 1850 C.E., the sedimentary records suggest still some relatively cold conditions and enhanced coastal polynya activity, likely due to stronger and more persistent katabatic winds and, although the decrease in FCC gp abundances indicates an early spring melting, an early sea ice advance results in a short ice free season preventing the development of cells from the open water group. Comparison with modern diatom cell distributions in surface sediments (Armand et al., 2005; Crosta et al., 2005; Chap. III), would indicate a mean sea ice duration of ~9-10 months/yr during that interval. After 1850 C.E., relative abundances of the FCC gp increased again while relative abundances of CRS, open ocean and autumn diatoms markedly decreased. Although it is difficult to assess about the sea cover seasonality here given the short duration of the period, such sedimentary assemblage probably indicate icy spring conditions and reduced polynya activity.

Our records differ from global paleoclimate reconstructions covering the Late Holocene. Particularly over the last 1,000 years, the PAGES 2k network reconstructions based on ice core records suggest warmer conditions in Antarctica in the early part of the last millennium followed by colder conditions, at the opposite of our results (Fig. 59). The timing of alternating cold and warm phases in IODP U1357 B is relatively similar to the well-known

climatic phases described in the NH (e.g. Medieval Warm Period, Little Ice Age; Mann et al., 2008), but follows an opposite pattern as already observed (Tavernier et la., 2014; Neukom et al., 2014). This opposition could be linked to a delayed climatic response of the SH relative to the NH *via* oceanic and atmospheric connections (Goosse et al., 2004; 2012; PAGES 2k Network, 2013) but would imply a lag of several centuries that seems irrelevant.

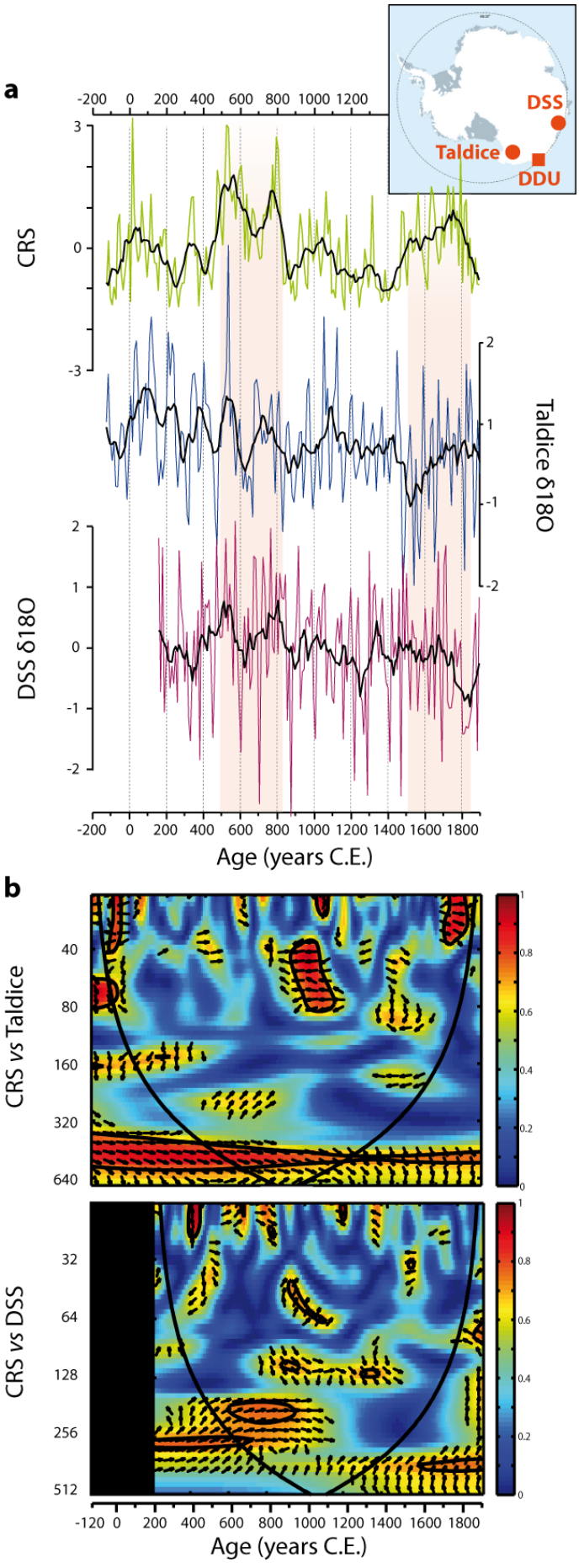
a
DSS
Taldice
DDU
CRS
Taldice δ18O
DSS δ18O
Age (years C.E.)
b
CRS vs Taldice
CRS vs DSS
Age (years C.E.)

Figure 61. Regional climate connexions between the Adélie Land area, the East Antarctic region and the Ross Sea regions. Map showing the location of the French station Dumont D'Urville (DDU; red square), the Talos Dome Ice Core site (Taldice; red spot) and the Law Dome Summit South site (DSS; red spot). a) Variations over the late Holocene period of standardized values of the CRS relative abundances (green), the δ18O (blue) records at Taldice (Stenni, unpublished data.) using timescale AICC2012, and the δ18O (violet) records at DSS (Moy et al., unpublished data, obtained from the National Climatic Data Center). Red shading area indicate warmer periods identified in IODP U1357B records. Black curves indicate the 90 years running mean. b) Wavelet cross correlation between the CRS relative abundances, the δ18O records at Taldice (upper panel) and δ18O records at DSS (lower panel), using Morlet wavelet according to Grinsted et al. (2004). Data has been sampled every 10 years.

Our records are, conversely, in much better agreement with East Antarctic climate as inferred from $\delta^{18}O$ records at Talos Dome Ice Core (Taldice; 159°04'21"E-72°47'14"S, 2318.5 m; Stenni, unpublished data) and at Law Dome Summit South (DSS; 112°50'5"E-66°43'47"S, 1368 m; Moy et al., unpublished data, NCDC) (Fig. 61a). Both ice core records show the long-term cooling observed in our diatom and biomarker records, and also contrasted climate phases at the pluri-centennial timescale. Taldice temperatures were amongst the highest (Fig. 61a) of the last 2,000 years during the (1) interval, while the DSS temperatures, although covering only half of the interval, seemed relatively low at that time similar to the cold conditions observed in our data. During the (2) interval, where we observe the warmest and less icy conditions of the last 2,000 years, DSS temperatures increased while Taldice temperatures stayed relatively elevated. Over the coldest and iciest period (3) of our data, both Taldice and DSS records are coherent with our results by exhibiting a pluri-centennial cooling. Finally, Taldice temperatures increased during the (4) period until 1850 C.E. (Fig. 61a), agreeing mostly with our sedimentary records. Conversely, DSS temperatures increased between 1300-1700 C.E. and decreased after 1700 C.E. (Fig. 61a), out-of-phase with our records. Interestingly, cross wavelet correlations between sedimentary signals from IODP U1357B and ice cores show higher correlation with CRS assemblages, with an in phase relationship in the 350-500 years band and in the 250-450 years band, for Taldice and DSS respectively (Fig. 61b). They also show non-stationary common cyclicities at the pluri-decadal timescale. These results ground truth the regional expression of our records and imply that East Antarctic coastal ocean and continental climate responded to similar forcing over the last 2,000 years.

4.1.3 Pluri-decadal variability

Wavelet analyses demonstrate that pervasive pluri-decadal variability in sea surface conditions off Adélie Land were present irrespective of the long-term cooling and mean environmental conditions recorded during the four climatic phases described above. The FCC gp displays significant power in 60-130 years band between 100-550 C.E. and 1300-1400 C.E. (Fig. 60). Similarly, CRS display non-significant high power in the ~130-150 years band between ~200-500 C.E. and ~700-950 C.E. (Fig. 60). *Thalassiosira antarctica* also shows significant high power in the ~20-150 years band during the ~1600-1850 C.E. interval, where large peaks are present, and *Porosira* gp shows a 30-40 years cycle during the period of its maximal abundance at 700-800 C.E. (Figs 59 & 60). The Open Water diatom gp shows significant periodicities of ~30-40 years and high power in the ~90-150 years band between ~500-1400 C.E (Fig. 60), successively coinciding with its maxima and minima abundances (Fig. 59). The [HBI:2]/[HBI:3] ratio signal shows two significant periodicities in the ~100-120 and ~120-150 years band during the 800-1800 C.E, and significant power in the ~30-70 years band, which coincide with two of its large peaks around ~200 C.E. and ~1400 C.E. (Figs 59 & 60).

Regarding the regional relationships at pluri decadal scale between our data and temperature reconstructions at Taldice and DSS, no stationary relationships are present over the last 2,000 years (Fig. 61b), which may imply that local forcing in Adélie Land may have dominated the pluri-decadal scale variability during the Late Holocene. However, non-stationary common cyclicities are present and, visually, we note that two maxima of temperatures around 550 C.E. and 750 C.E. at both Taldice and DSS coincide with minima of the FCC gp assemblages in our data, highlighting the potential contribution of global forcing at that time.

4.2 Potential forcing driving East Antarctic climate variability of the last 2,000 years

Sedimentary signals from IODP U1357B exhibit a large variability over the last two millennia characterized by persistent periodicities occurring at both low and high frequencies. We here aim to identify the potential forcing and mechanisms that acted at different timescales behind these cyclicities.

4.2.1 Long term forcing

The long cooling we observe in our data probably relies on external and natural climate forcing, that are changes in insolation and volcanic activity. Indeed, several studies have suggested that in Antarctica, declining temperatures and increasing sea ice cover over the Holocene are attributable to processional changes in local mean annual and spring insolation (Renssen et al., 2005; Shevenell et al., 2011; Etourneau et al., 2013). However, insolation changes associated to Milankovitch orbital evolution over the last 2,000 years are weak. Recent studies have also shown that repetitive volcanic eruptions may have further contributed to this general cooling by modulating these radiative forcing *via* injection into the stratosphere of large amounts of sulphur dioxide that converts to sulphate aerosol, thus increasing the Earth albedo and leading to short-term, global-scale cooling at the Earth surface (Robock et al., 2002). In particular during the last millennium, it has been suggested that volcanic activity have contributed to negative radiative forcing between 1400-1850 C.E. at global scale (Crowley et al., 2000; Cole Dai et al., 2000, McGregor et al., 2015; Sigl et al., 2015) and in the Southern Ocean to Antarctic region (Bertler et al., 2011; Orsi et al., 2012; Sigl et al., 2015).

4.2.2 Pluri centennial scale forcing

The pluri centennial scale variability exhibited by all sedimentary records and Taldice and DSS $d^{18}O$ records suggests that a common forcing played a major role over the Late Holocene. Robust long-term cyclicities at ~150-120 years, ~200-250 years and ~570 years have already been observed in Antarctic marine sediments and generally attributed to solar activity forcing (Domack et al., 2001; Leventer et al., 1996; Warner and Domack, 2002; Nielsen et al., 2004; Crosta et al., 2007). Indeed, latitudinal migration of the Southern Hemisphere Westerly Winds (SWW) and the circumpolar trough, that affected sea ice cover in Antarctica during the Holocene (Bentley et al., 2009; Denis et al., 2010; Etourneau et al., 2013. Kauffman et al., 2014), were associated to changes in solar activity (Mayewski et al.; 2004) with a 200 and a 400-500 years cycle over the Holocene (Lamy et al., 2001; Varma et al., 2011). More precisely, periods of higher (lower) solar activity were associated with mean southward (northward) shifts of the SWW, due to enhanced (weakened) meridional surface

temperature gradient (Varma et al., 2011). Strengthened and southward SWW increases zonal wind circulation (and so decreasing katabatic winds) off Adélie Land, in turn increasing sea ice presence and decreasing polynya activity in our study area (Chap III; Campagne et al., 2015). Our records suggest icier conditions off ALGV during the -129-480 C.E. and 825-1550 C.E. periods (intervals (1) and (3), respectively), in agreement with paleoclimate reconstructions suggesting poleward SWW during the ~0-450 C.E. and ~850–1400 C.E. periods (Lamy et al., 2001; Varma et al., 2011). Interestingly, the atmospheric configuration in (1) and (3) coincided with Southern Oscillation Index (SOI) negative phases (Fig. 62; Yan et al., 2011). Our data indicate less icy conditions, along with more intense polynya activity, during the 480-825 C.E. and 1550-1850 C.E. periods (intervals (2) and (4), respectively) in agreement with paleoclimate reconstructions indicating an equatorward position of the SWW during the ~450-850 C.E. and ~1400-1900 C.E. periods (Lamy et al., 2001; Varma et al., 2011). Such atmospheric configuration in (2) and (4) coincided with SOI+ phases (Fig. 62; Yan et al., 2011). However, differences in sea ice seasonality occur between the two warmer intervals of our records. Indeed, between ~1400-1900 C.E. several reconstructions (Fig. 62; Lamy et al., 2001; Varma et al., 2011) point a continuous poleward migration of the SWW (Mayewski et al., 2004; Bertler et al., 2011; Saunders et al., 2012), associated with the increasing SOI+/SAM+ (Southern Annular Mode) atmospheric pattern (Fig. 62; Villalba et al., 2012; Abram et al., 2014). Such atmospheric configuration may have progressively decreased katabatic winds and so, as we observe in our data, soften polynya conditions and increase the sea ice presence in the region over the (4) interval relative to (2). This scenario is supported by the concomitant large increase of diatom assemblages associated with icy conditions in autumn (*T. antarctica*) over the interval (4), whereas the (2) period experienced more open water related assemblages (*Porosira* gp) (Fig. 62). Finally, we suggest that increasing spring sea ice conditions and reduced polynya activity we observe since 1850 C.E. were likely due to continuous decreasing katabatic winds at that time, probably caused by persistent southward SWW and SAM+ trends (Fig. 62; Villalba et al., 2012; Abram et al., 2014).

It therefore appears that phasing between the influence of SOI and SAM at pluri centennial scale may strongly impact on Adélie Land sea ice dynamics and seasonality through modulation of the regional wind pattern, an hypothesis previously suggested over the instrumental period in the study area (Chap III; Campagne et al., 2015). Indeed, in our sedimentary data alternating spring assemblages (FCC gp *versus* CRS) follows well the SOI

pattern over the Late Holocene. At the opposite, autumnal assemblages in our records could be highly sensitive to the SAM pattern in addition to the SOI, suggesting the SAM have potential greater impacts on summer to autumnal conditions in our study area, in agreement with recent observations (Thompson and Solomon, 2002). However, longer SAM reconstructions recovering the (1) and (2) period in our records are required in order to verify these assumptions.

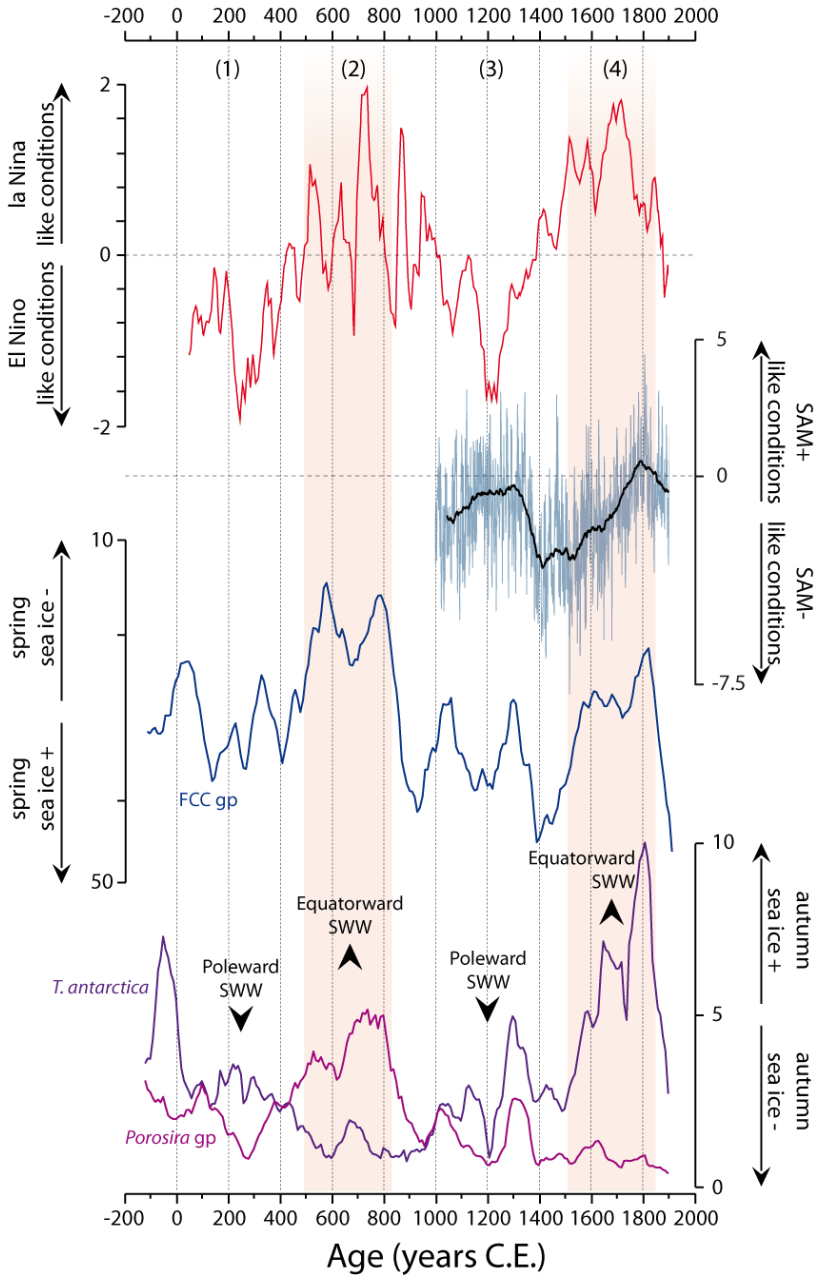

Figure 62. Relationships between sea surface conditions and polynya activity in Adélie Land and the synoptic scale SH atmospheric variability over the Late Holocene. Decadal Southern Oscillation Index

(SOI; red) precipitation-based reconstructions (Yan et al., 2011), negative (positive) values indicate more El Niño (la Nina) like conditions; Yearly Southern Annular Mode (SAM; blue) temperature-based reconstruction (Abram et al., 2014) and its 90 years running mean (black); 90 years running mean of the FCC gp relative abundances (blue); 90 years running mean of the *T. antarctica* relative abundances (violet); 90 years running mean of the *Porosira* gp relative abundances (pink); Southern Westerly Winds (SWW) long term changes (black arrows) inferred from Lamy et al. (2001) and Varma et al. (2011). (1) to (4) indicate the climatic phases inferred from the IODP U1357 B. Red shading area indicate warmer periods.

4.2.3 Pluri-decadal scale forcing

Cyclicities of 20-50 years appear in our sedimentary records but are strongly non stationary over the last 2,000 years (Fig. 60). We suggest that the observed non-stationary periods are partly due the mean climate state and resulting mean sedimentary content. Indeed, no significant pluri decadal cyclicity is present in sea ice proxies during the intervals 480-825 C.E. and 1550-1850 C.E., while no cyclicity is observed in open ocean proxies during the intervals -129-480 C.E. and 825-1550 C.E. Observations over the recent period in the SH (Enomoto et al., 1991; Zitto et al., 2015) and atmospheric circulation reconstructions in East Antarctica (Souney et al., 2002) attributed some pluri-decadal scale periodicities (20, 30, 40, 50 years) to the atmospheric teleconnexions between Southern high- and mid-latitudes, with possible links with the pluri-decadal expression of the SAM. As such, the presence of these non-stationary 20-50 years cyclicities in our records argument for similar atmospheric and oceanic teleconnexion between low latitudes and the AGVL at these timescales over the last 2,000 years. We note that minima of spring sea ice diatom assemblages in our data coincide well with maxima of SOI reconstructions over the last 2,000 years, while maxima of autumn sea ice diatom assemblages were concomitant with periods characterized by SAM+ pattern over the last 1,000 years (Fig. 62). However, wavelet analyses between the SAM reconstruction and sedimentary signals from IODP U1357B point a variant relationship (and are thus not presented here), with correlations which are sometimes in phase and sometimes reversed. Absence of clear trends could be possibly due to the smoothed impacts at pluri decadal scale of the climate modes over the last centuries, relative to longer timescale forcing mechanisms. In addition, the short decadal periodicities in our records might result from the expression of the interannual fluctuations of the AAO and El Nino indices (Stenseth et al., 2003; Jevrejeva et al., 2003), that can increase noise in the signal. Our results highlight the need for other regional long-term and high resolution paleoclimate reconstructions studies, in order to correctly assess climate modes impacts and processes involved at pluri decadal scale.

Additionally, local mechanisms may further trigger pluri-decadal scale variability in sea-surface conditions in the region. Previous results in core CB2010 from the Mertz Polynya in the region, demonstrated that the internal dynamics of the Mertz Glacier Tongue generated fluctuations in sea ice conditions and polynya activity with a ~70 years cyclicity (Campagne et al., 2015), which may imprint at the core site (Chapter IV). No constrain on the Mertz Glacier Tongue exist beyond the last 250 years and it appears tentative to extrapolate over the last 2,000 years when climate forcing may become as important as internal dynamics.

5 Conclusion

Analysis of the sedimentary archives retrieved in the DDUT in Adélie Land, allow for the reconstruction of sea ice cover and surface conditions at a decadal resolution. Our records are in agreement with other Antarctic reconstructions that indicate a long term cooling, and particularly in the East Antarctic region. Our reconstructions also suggest that the seasonal distribution of the sea ice cover, the length of the growing season and the polynya activity have changed at pluri centennial scale over the Late Holocene. As such, our reconstruction indicate four distinct climate intervals that show some similar evolutions with glacial records from the East Antarctica. These changes could be likely forced by solar activity modifying the SH synoptic scale atmospheric circulation pattern which is coupled to oceanic variability and changes of the regional wind pattern. Our results further suggest that, in our study area, sea ice seasonality and both spring and autumn assemblages might be sensitive to the phasing between SAM and SOI indices. Wavelet analyses also evidence periods of pluri decadal cyclicities in our record, potentially reflecting the relative contributions of atmospheric teleconnexions and local forcing (e.g. the Mertz Glacier calving cycle). Higher resolution marine records in the region would better assess the inter-annual to pluri-decadal scale forcing. Studies of the SH synoptic scale atmospheric variability and its impacts on sea surface conditions have been undertaken for the instrumental period but less is known about the longer timescale (e.g. Masson et al., 2000; Varma et al., 2011) especially with those focusing onto wind pattern variability in Antarctic coastal regions. Additionally, since observations of SH atmospheric circulation changes over the last decades might be biased due to the global warming effects and more regionally to the ozone hole depletion, those may not allow for assessing of the natural climate variability.

ACKNOWLEDGMENTS

We acknowledge Vincent Klein and Marie-Hélène Taphanel for technical assistance. We also thank the Intergrated Ocean Drilling Program (Expédition 318 et Ancillary Project 638) for providing samples. Funding for this research was provided by the ANR CLIMICE, the NERC-IODP-UK GRANT NE/G001294/1, the FP7 Past4Future 243908, the ESF PolarCLIMATE HOLOCLIP 625 and ERC ICEPROXY 203441.

SUPPLEMENTARY FIGURES are available in Annexe 3.

Conclusions générales et perspectives

Les assemblages de diatomées, ainsi que les éléments majeurs et mineurs mesurés par XRF core-scanner dans le sédiment, sont des outils communément utilisés pour reconstruire les variations paléo-environnementales dans l'Océan Austral. Plus récemment, l'utilisation de biomarqueurs spécifiques de diatomées (HBI) est venue compléter ce panel d'outils paléoclimatiques. Dans cette thèse, nous avons réalisé grâce à ces outils une étude à plusieurs échelles de temps des conditions paléoclimatiques en Terre Adélie-Georges V sur la période de l'Holocène tardif.

Un des buts de ce travail de thèse était, à partir d'une carotte d'interface, d'affiner la compréhension du système climat/océan/banquise actuel, grâce à l'étude très haute résolution de la réponse sédimentaire aux changements de conditions de surface sur la période instrumentale. L'étude de la période climatique actuelle a également porté sur la partie supérieure de deux carottes sédimentaires plus longues dans la région, ayant conservé leur interface, permettant ainsi de contraindre une certaine reproductibilité spatiale de nos résultats. Ces enregistrements sédimentaires ont de plus été confrontés, statistiquement quand cela était possible, à un éventail de données météorologiques sur les dernières décennies ainsi qu'à de la ré-analyses atmosphérique pour des échelles de temps un peu plus longues. La mise en perspective de nos signaux sédimentaires avec des données instrumentales saisonnières (direction et intensité du vent, température et concentration de glace) à l'échelle des sites d'études, a permis de valider les outils pour une utilisation ultérieure sur des échelles de temps plus longues, ce qui constituait l'objectif (1) de cette thèse. Le deuxième but (2) était d'identifier les forçages régionaux et/ou locaux ainsi que leurs mécanismes associés à diverses échelles temporelles de variabilité climatique (pluri centennale à décennale). Pour cela, des ondelettes ont été réalisées sur des enregistrements couvrant les derniers siècles, mais aussi sur une séquence sédimentaire recouvrant les derniers 2,000 ans, afin de documenter la variabilité des conditions de surface et de glace, et d'éventuels schémas répétitifs au cours de l'Holocène tardif. Enfin, la caractérisation des conditions océanographiques et climatiques en Antarctique de l’Est au cours des derniers siècles et millénaires, là où d'autres enregistrements manquaient, étaient incomplets sur ces périodes, où d'assez faible résolution, constituait l'objectif (3) de ce projet. De plus, la mise en perspective de nos travaux avec d'autres

enregistrements glaciaires en Antarctique de l'Est couvrant l'Holocène tardif est venue compléter les objectifs (2) et (3).

Principaux résultats

1. Validation de nos outils

L'étude des relations entre nos différents outils, combinée aux paramètres environnementaux à l'échelle annuelle et interannuelle atteste de la pertinence et de l'utilisation de nombreux indicateurs pour les études sédimentaires à plus long terme. Ainsi, les outils associés aux conditions libre de glace semblent répondre presque linéairement à l'allongement de la saison de croissance et à une faible concentration de glace, en accord avec les précédentes études régionales ou synoptiques. Cependant, nos résultats démontrent aussi que certains indicateurs environnementaux peuvent être caractéristiques de la zone d'étude, notamment dû à des conditions particulières (ex: la présence de polynie), ou encore que d'autres ne sont pas tout à fait en accord avec les interprétations auxquelles ils sont associés dans les précédentes études à longues échelles spatiales et/ou temporelles. En particulier, les indicateurs de conditions de banquise présentent une relation complexe avec les conditions environnementales, et apparaissent ainsi influencés par plusieurs facteurs tels que la concentration de banquise, la dynamique de fonte et/ou de reformation, la structure et la nature du couvert de glace, en lien étroit avec la circulation atmosphérique sur le plateau continental antarctique. A plus long terme, cette réponse multi-variée apparait cependant lissée en relation avec une expression moyennée des conditions environnementales dans les signaux sédimentaires ou encore l'action plus ou moins prépondérante de certains processus.

2. Identification des forçages et des mécanismes associés, Figure 63

Les enregistrements à l'échelle de l'Holocène tardif montrent que les changements d'état moyen à l'échelle interannuelle à décennale sont de plus faible amplitude que ceux à l'échelle centennale à millénaire, probablement parce que les variations d'énergie associées aux forçages à grandes échelles de temps sont plus grandes que celles associées aux forçages courtes échelles de temps. Ainsi, au cours des dernières décennies, dans un contexte de réchauffement climatique global et d'intensification du SAM, la direction du vent semble primordiale dans la modulation du cycle saisonnier du couvert de glace, premièrement

contrôlé par les changements saisonniers d'insolation et de température. A plus longue échelle temporelle cependant, les variations d'état moyen de l'insolation ainsi que les températures atmosphériques et océaniques semblent jouer un rôle plus important que la direction et l'intensité des vents sur les conditions de banquise dans la région.

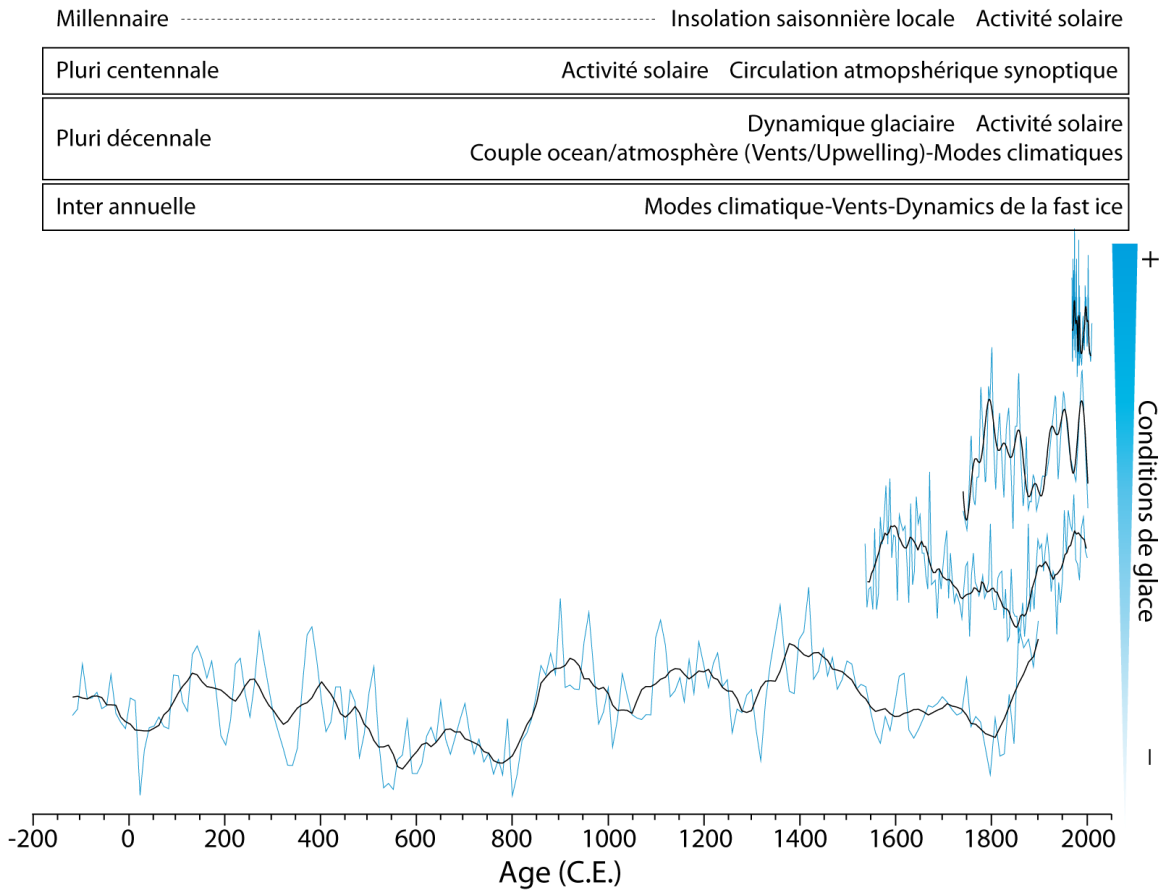

Figure 63. Schéma des forçages climatiques identifiés dans la thèse, ainsi que leurs échelles de temps d'action respectives au cours de l'Holocène tardif. Les courbes en bleu indiquent les enregistrements sédimentaires des diatomées de glace (*Fragilariopsis cylindrus* + *F. curta*) de toutes les carottes étudiées pendant la thèse; les courbes en noir représentent les moyennes lisées à 90 ans.

- Variabilité climatique interannuelle à décennale

Nos travaux réalisés sur les sédiments d'interface indiquent que la variabilité de la circulation atmosphérique sur le plateau continental de la Terre Adélie-Georges V constitue le forçage principal de la variabilité interannuelle des conditions de glace, notamment du point de vue de la présence du pack-ice et de la fast-ice et, ainsi, de la productivité siliceuse. Nos enregistrements tendent également à montrer que l'action couplée de l'atmosphère et de l'océan, à travers la variabilité des conditions d'upwellings et de circulation de masses d'eau au large du plateau, peut impacter saisonnièrement les conditions de surface au cours des

dernières décennies. Cependant, en raison du manque de données hydrologiques et océanographiques, qui nécessiterait un travail poussé en océanographie physique dans la région, à confronter notamment aux mesures météorologiques, ces hypothèses sont pour le moment invérifiables. Toutefois, en accords avec les d'études bibliographiques, nos observations tendent à indiquer que la variabilité atmosphérique interannuelle sur le plateau de la Terre Adélie-Georges V répond aux modes climatiques dominants de l'HS et, plus particulièrement à la tendance positive du SAM, très prononcée depuis les années 1950.

- Variabilité pluri décennale

Des variations décennales à pluri décennales relativement stationnaires ont également été mises en évidence dans nos divers enregistrements. Sur la base des observations de la période récente, nos résultats à plus longues échelles supportent le rôle important des relations modes climatiques-conditions de vent (synoptiques/régionales) sur la variabilité pluri décennale des conditions de surface dans notre zone d'étude. Nos résultats semblent également indiquer qu'à cette échelle les conditions d'upwelling et de circulation de masses d'eau sur le plateau jouent un rôle important sur les conditions de surface durant la saison de croissance du phytoplancton. Cette variabilité océanique semble associée à la dynamique atmosphérique, mais nos résultats tendent également à montrer un lien avec la dynamique glaciaire de la région. Ainsi, le cycle de vêlage du Glacier de Mertz apparaît comme l'un des forçages prépondérant des conditions de surface et de l'activité des polynies dans notre zone d'étude, avec une cyclicité de ~70 ans dans nos signaux sédimentaires. Des cyclicités pluri décennales proches de l'activité solaire n'apparaissent que partiellement dans nos données, ne permettant pas d'établir clairement un lien.

- Variabilité pluri centennale

A l'échelle pluri centennale, le changement d'état moyen des modes climatiques semble constituer le forçage prépondérant de la variabilité des conditions de surface au large du continent Antarctique *via* la réorganisation des télé-connexions moyennes-hautes latitudes et de la circulation atmosphérique synoptique résultante. Ainsi, nos résultats indiquent que la dynamique du couvert de glace *via* les changements de saisonnalité au printemps et à l'automne est sensible à l'expression des changements de phases des modes climatiques dominant de l'Hémisphère Sud. Sur la base d'études bibliographiques, nous avons émis l'hypothèse que ces changements d'état moyen des modes climatiques sont générés par la variabilité pluri centennale de l'activité solaire.

- Variabilité long-terme

Enfin, nos reconstructions à l'Holocène tardif attestent d'un refroidissement progressif au cours des derniers millénaires, probablement causé par la décroissance du rayonnement solaire dû à la précession (Steig et al., 2013) au long de l'Holocène, voir de la réponse de l'Antarctique et de l'Océan Austral au forçage volcanique (McGregor et al., 2015) comme observé pour l'Hémisphère Nord.

3. Caractérisation des conditions océanographiques et climatiques de l'Holocène tardif en Terre Adélie-Georges V

L'étude de nos archives sédimentaires longues a mis en évidence quatre intervalles climatiques successifs au cours des derniers 2,000 ans, caractérisés par des variations très prononcées de la saisonnalité du couvert de glace et des conditions régionales de polynie. Nos résultats sont relativement cohérents sur le long terme avec des enregistrements glaciaires en Antarctique de l'Est, indiquant un lien très prononcé avec les variations de températures dans cette région. Cependant, les phases climatiques enregistrées au large de la Terre Adélie semblent en opposition de phase par rapport à celles de l'HN. Par exemple, alors que la plupart des enregistrements marins et terrestres de l'HN témoignent d'un refroidissement entre le XIV-XIXe siècle, appelé Petit Age Glaciaire, nos enregistrements indiquent à l'inverse une tendance au réchauffement entre XVI-XIXe siècle, bien que cette période ne constitue pas l'intervalle le plus chaud (VI-IXe siècle) des derniers 2,000 ans dans nos enregistrements. Les raisons de cette opposition ou fort décalage pourraient résulter de la forte hétérogénéité spatiale du climat antarctique, comme enregistré dans les carottes de glace ou du temps nécessaire au transfert des anomalies climatiques de l'HN vers l'HS via l'atmosphère et l'océan (Goosse et al., 2004; 2012; PAGES 2k Network, 2013). D'autres études de carottes marines documentant le compartiment océanique à haute résolution temporelle et des études couplées données-modèles seront nécessaires pour mieux comprendre les mécanismes sous-jacents.

Limites et perspectives

(1): compréhension du système actuel

Cependant, le travail sur les sédiments de surface a été grandement limité par le manque de connaissance sur la compréhension du système actuel, quant à la formation des signaux sédimentaires dans la zone d'étude, leur transformation dans la colonne d'eau et leur enfouissement à l'échelle saisonnière. En effet, le modèle d'âge bien que contraint par un grand nombre de mesures du $^{210}Pb_{xs}$ et par leur reproductibilité, reste approximatif à l'échelle intra annuelle, et ne permet pas d'étudier la variabilité saisonnière des signaux sédimentaires, malgré la haute résolution de nos analyses. Deux lignes de pièges à sédiments ont été mouillées en janvier 2010 au large de Dumont D'Urville au droit de la carotte IODP U1357 et dans la Dépression Adélie, à proximité du Glacier de Mertz, et devaient fournir une vision des processus d'export et de sédimentation sur 4 ans. Cependant, en raison de contraintes technique fortes dû au milieu extrême, peu d'informations ont pu être extraites, et n'ont pas pu être reproduites spatialement à cause de la perte d'une partie du matériel. Sur le piège au large de DDU, le flux de masse a été caractérisé par un évènement unique de sédimentation massive (dont la valeur est proche des valeurs maximales observées dans diverses région antarctiques) restreint à deux semaines entre le 21 Janvier et le 6 Février (Closset, 2011), bien qu'il soit possible que le piège ait manqué le début de flux de masse. Sur le restant de l'année les flux ont été presque nuls, et ont ré-augmenté de nouveau lors de la récupération des pièges à sédiments en Janvier 2011 (Closset, 2011). Ces résultats vont à l'encontre des hypothèses basées sur les nombreuses études long terme portant sur la microstructure et la composition saisonnière des sédiments côtiers dans la région. En effet, Maddison et al. (2005), Denis et al. (2006) et Escutia et al. (2010) ont ainsi démontré que la sédimentation sur la marge du plateau résultait de la succession saisonnière de la production en surface entre le printemps et l'été austral, et ont également mis en évidence des couplets annuels de lamines d'épaisseur pluri-centimétrique dans la région et à notre site d'étude DDUT. Cependant, les nombreuses mesures d'activité du plomb radioactif ($^{210}Pb_{xs}$) réalisées au laboratoire EPOC ont montré des variations importantes du taux de sédimentation sur les périodes très récentes (Fig. 64; Schmidt et al., unpublished data). En effet, on note clairement l'apparition de plateaux, reproductibles sur plusieurs carottes, aux alentours des années 1983-1986 C.E. (Fig. 64), mais aussi des micro-lamines voir des hiatus potentiels de sédimentation sur certaines années, qui semblent correspondre à des variations de structures du sédiment, comme en témoignent les changements d'assemblages de diatomées et de la teneur en silice sur la carotte interface DTCI2010 (Fig. 64). Par ailleurs, les activités de $^{210}Pb_{xs}$ au top d'une carotte prélevée en Janvier 2011, montrent qu'approximativement 20 cm ont été déposés entre 2010-2011,

renforçant ainsi l'hypothèse d'un évènement de sédimentation massif au début de l'année 2010. L'étude des assemblages de diatomées et des concentrations de biomarqueurs sur cette section pourrait apporter des éléments de réponse quant à la composition/structure et l'origine de ces plateaux. Les raisons de la variabilité du taux de sédimentation n'ont pas encore été étudiées en détail mais notre étude portant sur les derniers 40 ans (Chapitre III) montre que ces années sont caractérisées par des conditions d'ouverture de banquise parmi les plus importantes des dernières décennies, ainsi que des températures élevées et des conditions peu venteuses. Ces conditions favoriseraient probablement une couche de surface relativement stable et chaude et diminueraient ainsi la productivité associée à la glace de mer. Pour expliquer la présence de plateaux, il a également été suggéré que cette sédimentation massive n'est pas originaire de la production primaire locale mais serait transportée depuis la région très productive du Mertz plus en aval, soit par le courant côtier en surface, soit par les courants de fond. Cette dernière hypothèse semble cependant peu probable en raison du Banc Adélie qui limite les échanges entre la Dépression Adélie et la région de DDUT. De plus, nos enregistrements sédimentaires au cours des derniers siècles indiquent des tendances opposées, notamment sur les courtes échelles de temps, entre nos signaux sédimentaires à CB et DDUT, réfutant une origine commune du sédiment aux deux sites.

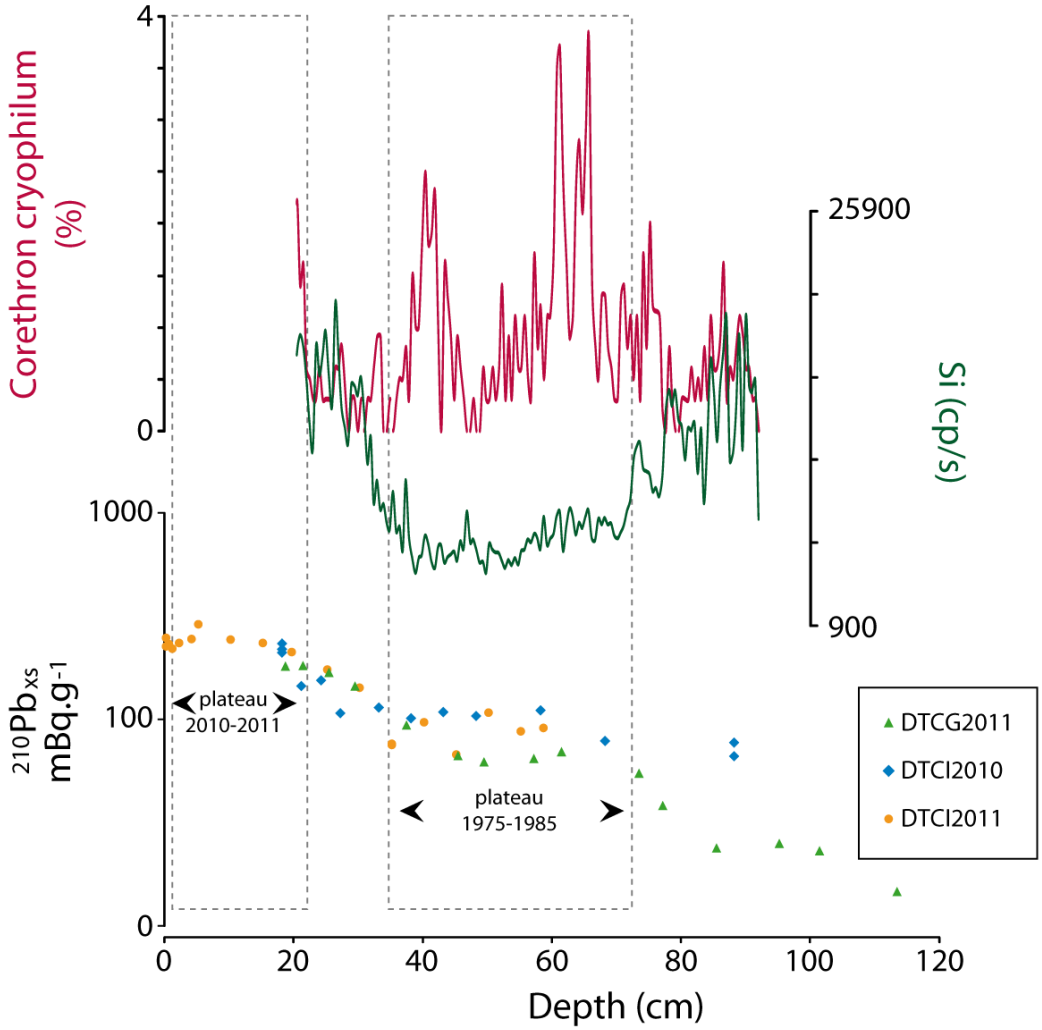

Figure 64. Variations interannuelles du taux de sédimentation en Terre Adélie. Activité du $^{210}Pb_{xs}$ dans trois enregistrements sédimentaires au site DDUT: DTCG2011 (triangle vert; *cf.* Chap IV); DTCI2010 (losange bleu; *cf.* Chap III) et DTCI2011 (cercle orange). Les âges des plateaux (rectangles en pointillés gris) sont préliminaires, et ont été estimés à partir de l'activité du ^{210}Pb (Schmidt et al., *unpublished data*). Variations de la structure sédimentaire au site DDUT basée sur l'analyse des assemblages de diatomées (rouge) et de la teneur XRF en silice (vert), réalisées sur la carotte DTCI2010.

Ainsi, le manque de connaissances quant aux variations spatio-temporelles de la productivité et notamment des blooms phytoplanctoniques en Terre Adélie-Georges V ne permet pas d'avoir une vision complète de la variabilité de la dynamique des polynie dans la région. Par exemple, un des points clés de nos reconstructions à court et long termes est les relations des assemblages de CRS aux conditions de polynie, associées aux vents catabatiques d'après les observations dans la région (Riaux Gobin et al., 2013). Il serait ici nécessaire de reconstruire plus finement les variations spatiales du couvert de glace ou de la productivité en surface afin de mieux contraindre la dynamique de la polynie au site DDUT. L'utilisation de données satellite de chlorophylle *a* en surface permettrait de mieux appréhender cette variabilité, mais

offre cependant une vision incomplète de la répartition spatiale du bloom en ne tenant pas compte de la productivité dans les cracks et les leads de la banquise. L'utilisation d'images MODIS, bien que disponible sur les dix dernières années, permettrait en revanche d'observer grâce à un maillage plus fin la variabilité du couvert de glace ainsi que de discriminer les conditions de fast ice de celle du pack ice, ayant un impact important sur les assemblages de diatomées et les HBIS. Une telle étude permettrait ainsi de contraindre la production *in situ* de celle exportée, et d'affiner ainsi la calibration et la validation de nos outils. Couplé à l'étude de sédiment de surface, cette technique permettrait d'infirmer ou de confirmer les relations démontrées dans le Chapitre III de certaines espèces de diatomées et également des HBIs avec les variations des conditions atmosphériques et de surface.

(2) et (3): connaissance de la variabilité climatique aux échelles pluri décennale à pluri centennale

La comparaison de simulations climatiques avec nos données pourrait nous aider à la compréhension des mécanismes responsables de la variabilité des conditions de surface dans notre zone d'étude au cours de l'Holocène et notamment sur le dernier millénaire. En collaboration avec le Pr. Hugues Goosse, Louvain la Neuve, nous avons pu travailler avec des données issues du modèle LOVECLIM, auxquelles nous avons confronter nos données sédimentaires. LOVECLIM est un modèle 3D de complexité intermédiaire développé à l'Université de Louvain (Belgique). Ce modèle est composé principalement de trois modèles simplifiés : le modèle atmosphérique quasi-géostrophique ECBilt, le modèle de circulation générale de l'océan et de la glace de mer (CLIO) et le modèle de la biosphère continentale (VECODE). A l'inverse des GCMs, LOVECLIM est caractérisé par une dynamique simple et une résolution horizontale et verticale plus grossière, ce qui permet une plus grande rapidité de calcul et rend possible l'assimilation de données (Goosse et al., 2010). Cette méthode relève d'un processus mathématique par lequel l'évolution d'un modèle numérique est contrainte à rester proche d'une réalité partiellement observée, en combinant les observations et les résultats des modèles afin d'obtenir une reconstruction optimale de l'état du système climatique dans le respect de la physique du modèle.

Nous utilisons ici deux simulations annuelles de concentration de glace de mer du modèle LOVECLIM, une sans assimilation de données, LOVECLIM_Last2k (LL), couvrant la

période 0-2,000 C.E., et une simulation avec assimilation de données, LOVECLIM_PR (LR), couvrant la période 851-2,000 C.E. (Fig. 65). LOVECLIM inclue les forçages climatiques naturels (activité solaire et volcanique, paramètres astronomiques) et anthropiques (GESs, aérosols, couverture terrestre). Une description des caractéristiques du modèle sans assimilation de donnée est disponible dans PAGES 2k Network (2013). L'assimilation de données dans LOVECLIM est contrainte par des reconstructions de température estivales et hivernales aux moyennes latitudes (ex: cernes d'arbres et sédiments lacustres) ainsi que par des enregistrements glaciaires aux hautes latitudes, de façon à intégrer les télé-connexions inter-latitudinales (Goosse et al., 2012). Une description des caractéristiques du modèle avec assimilation de donnée est disponible dans Goosse et al. (2012).

Sur le long terme, LL et LR indiquent une légère augmentation des concentrations de banquise au site de la carotte IODP U1357B au cours des derniers 2,000 ans et 1,000 ans, respectivement (Fig. 65), en accord avec nos reconstructions. LL montre une variabilité pluri centennale moins prononcée par rapport à nos données et à la simulation LR dont l'amplitude des changements est plus en accord avec nos données (Fig. 65). LL montre une diminution des SIC entre 0-150 C.E. et 400-800 C.E. traduisant une tendance au réchauffement sur ces périodes, entrecoupée d'une augmentation des SIC témoignant d'un refroidissement entre 150-400 C.E. et entre 800-1300 C.E. (Fig. 65), plus ou moins en accord avec ce que l'on observe dans nos données. Cependant, LL indique un réchauffement autour de 1350 C.E. suivit d'un refroidissement sur les derniers siècles à l'inverse de nos données (Fig. 65). LR montre un réchauffement entre 1100-1300 C.E., 1450-1650 C.E.et un refroidissement entre 900-1050 C.E. ainsi qu'entre 1300-1450 C.E. et 1650-1800 C.E., en désaccord avec nos données (Fig. 65). La variabilité pluri décennale dans LL et LR est bien représentée (Fig. 65). Toutefois, aucune relation claire ne semble apparaitre au cours des derniers 2,000 ans entre nos données et les deux sorties du modèle (Fig. 65). On note en cependant que les plus hautes valeurs de SIC dans LR coïncident avec le maximum d'abondances relatives de diatomées de glace (FCC gp) autour de 1350-1450 C.E., une période identifiée comme un épisode de froid extrême de l'HS (Neukom et al., 2014).

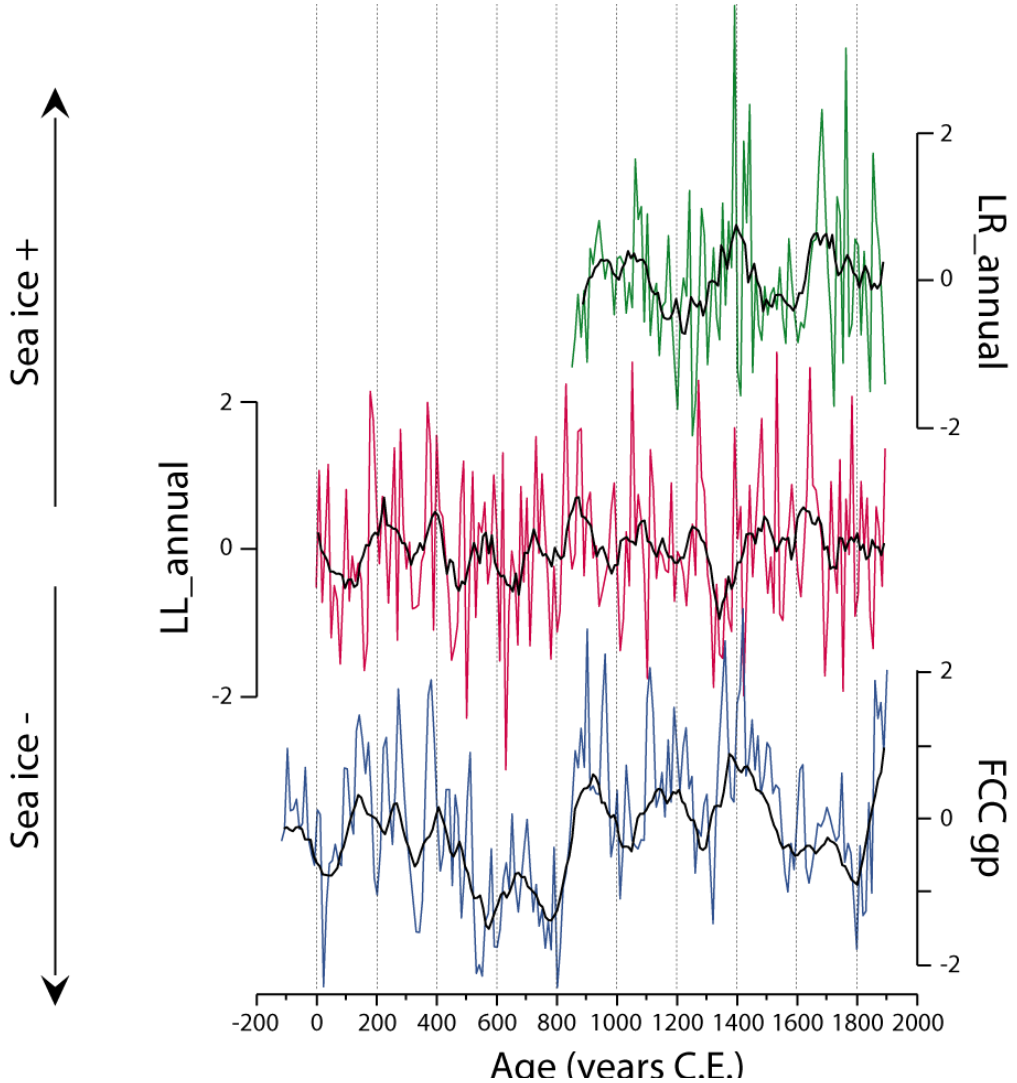

Figure 65. Comparaison entre les données sédimentaires de la IODP U1357B et la concentration de glace de mer annuelle (SIC), estimée grâce au modèle LOVECLIM. Les assemblages du groupe de diatomées de glace (FCC gp; bleu) ont été mis en perspective des résultats d'une simulation de SIC avec assimilation de données (LR; vert), et d'une simulation sans assimilation de données (LL; red). Les données sédimentaires et du modèle ont été standardisées.

Ainsi, la simulation LR reproduit les mêmes ordres de variabilité qu'observés dans nos signaux sédimentaires, mais avec des tendances globalement en désaccord avec nos données. Dans LL, la simulation sous-estime légèrement la variabilité pluri centennale, mais les tendances à cette échelle sont relativement en accord avec nos reconstructions jusqu'en 1300 C.E., puis sont inversées au cours des derniers siècles. LOVECLIM suggère que les paramètres astronomiques, l'activité solaire, l'activité volcanique ainsi que la couverture des sols constituent les forçages dominants responsables du refroidissement observé au cours du dernier millénaire (PAGES 2k Network, 2013). Ainsi, la comparaison modèle/données sédimentaires tend à indiquer que nos enregistrements témoignent de l'expression de la

variabilité climatique globale sur le long terme. En revanche, aux échelles pluri centennale à décennale il semble que les forçages climatiques majeurs inclus dans les simulations LOVECLIM ne suffisent pas à expliquer nos données. Dans la simulation avec assimilation de données, les différences observées indiquent que même en incluant des reconstructions paléoclimatiques, une part de la variabilité climatique est propre à notre zone d'étude. Cependant, les différences modèle/données sédimentaires pourraient aussi être dues au fait que les reconstructions à partir d'enregistrements marins ne sont pas incluses dans le modèle (Goosse et al., 2012), en raison d'une trop basse résolution. De ce fait, il n'existe pas d'assimilation de données pour le couvert de banquise dans LOVECLIM. De plus, la représentation de la variabilité des conditions de vent sur le plateau et notamment l'intensité des catabatiques, un des principaux forçages mais très localisé dans notre zone d'étude, peut être mal paramétrée dans le modèle. Les études tendent de plus en plus à démontrer que les modèles surestiment les forçages externes par rapport à la dynamique interne du climat (Goosse et al., 2012; Neukom et al., 2014), qui pourrait ici expliquer les tendances de nos enregistrements. La multiplication d'enregistrements sédimentaires marins complets, haute résolution, et leur intégration dans le modèle LOVECLIM pourraient offrir une vision plus complète du système climatique, en incluant par exemple les relations océan/banquise/vent, notamment à l'échelle locale.

Notre étude s'inscrit parmi les nombreuses évidences (Tavernier et la., 2014; Neukom et al., 2014) qui tendent à démontrer que le climat entre les deux hémisphères au cours des derniers 2,000 ans n'a finalement été en phase que sur quelques périodes de temps, correspondant à des extrêmes climatiques. Il se pourrait alors que la prépondérance de la recherche sur le climat dans l'HN, poussant à la recherche systématique de l'expression de phases climatiques type MWP ou LIA dans les enregistrements de l'HS, tende à biaiser la compréhension de la variabilité climatique au cours de l'Holocène. Il apparait que pour étudier la variabilité du climat et réduire les incertitudes notamment quant à la part de variabilité climatique naturelle et anthropique, les tendances de l'HN ainsi que l'HS doivent être prises en compte.

Références

A

Abram N.J., Mulvaney R.,Vimeux F., Phipps S.J.,Turner J., England M.H. Evolution of the Southern Annular Mode during the past millennium. *Nat. Clim. Change*, **4**, 564–569 (2014).

Adolphs, U. and Wendler, G. A pilot study on the interactions between katabatic winds and polynyas at the Adelie Coast, eastern Antarctica. *Ant. Sci. ,* **7**(3), 307- 314 (1995).

Allen, C.S., Oakes-Fretwell, L., Anderson, J.B. and Hodgson, D.A. A record of Holocene glacial and oceanographic variability in Neny Fjord, Antarctic Peninsula. *Holocene*, **20**(4): 551-564 (2010).

Annett, A. L., Carson, D. S., Crosta, X., Clarke, A., and Ganeshram, R. S. Seasonal progression of diatom assemblages in surface waters of Ryder Bay, Antarctica. *Pol. bio.*, **33**(1), 13-29 (2010).

Aoki, S., Rintoul, S., Ushio, S. and Watanabe, S. Freshening of the Adélie Land Bottom Water near 140°E. *Geophys. Res. Lett*. **32,** L23601 (2005).

Aoki, S., Sasai, Y., Sasaki, H., Mitsudera, H. and Williams, G. D. The cyclonic circulation in the Australian Antarctic basin simulated by an eddy resolving general circulation model. *Ocean Dyn.* **60**(3), 743-757 (2010).

Appleby, P.G. and Oldfield, F. Applications of 210Pb to sedimentation studies. *Uranium-series Disequilibrium: Applications to Earth, Marine and Environmental Sciences Claredon Press, Oxford*, 731-778 pp (1992).

Arblaster, J. M. and Meehl, G. A. Contributions of External Forcings to Southern Annular Mode Trends. *J. Clim.***19**, 2896–2905 (2006).

Armand, L. K., Crosta, X., Romero, O. and Pichon, J.-J. The biogeography of major diatom taxa in Southern Ocean sediments: 1. Sea ice related species. *Palaeogeog., Palaeoclim., Palaeoecol*. **223**, 93-126 (2005).

Armand, L. The use of diatom transfer functions in estimating sea-surface temperature and sea-ice in cores from the southeast Indian Ocean. PhD Thesis, Australian National University, Canberra, Australia; p. 932, pl. 17 (1997).

Arrigo, K. R., G. L. van Dijken, and S. Bushinsky. Primary production in the Southern Ocean, 1997–2006, *J. Geophys. Res*., **113**, C08004, (2008).

Arrigo, K. R. and van Dijken, G. L. Phytoplankton dynamics within 37 Antarctic coastal polynya systems. *J. Geophys. Res*. **108**(C8), 3271 (2003).

Arrigo, K. R., D. Worthen, A. Schnell, M. P. Lizotte, Primary production in Southern Ocean Waters, *J. Geophys. Res*., **103**, 15587–15600 (1998).

B

Ballarotta, M., Falahat, S., Brodeau, L., and Döös, K. On the glacial and interglacial thermohaline circulation and the associated transports of heat and freshwater. *Ocean Sci.*, **10**(6), 907-921 (2014).

Barbara, L., Crosta, X., Schmidt, S., Massé, G. Diatoms and biomarkers evidence for major changes in sea ice conditions prior the instrumental period in Antarctic Peninsula. *Quat. Sci. Rev.* **79**, 99e110 (2013).

Barbara, L., Crosta, X., Massé, G. and Ther, O. Deglacial environments in eastern Prydz Bay, East Antarctica. *Quat. Sci. Rev.*, **29**(19-20): 2731-2740 (2010).

Barber, D.G. and Massom, R.A. The role of sea ice in Arctic and Antarctic polynyas. In *Polynyas: windows to the world*, Smith Jr., W.O. *et al.* (Ed.), Elsevier Oceanography Series, **74**, 1-54 (2007).

Bárcena, M. Á., Isla, E., Plaza, A., Flores, J. A., Sierro, F. J., Masqué, P. et al. Bioaccumulation record and paleoclimatic significance in the Western Bransfield Strait. The last 2000 years. *Deep Sea Res. Part II: Topical Studies in Oceanography*, **49**(4), 935-950 (2002).

Bárcena, M., Gersonde, R., Ledesma, S., Fabrés, J., Calafat, A. M., Canals, M., et al. Flores, J. A. Record of Holocene glacial oscillations in Bransfield Basin as revealed by siliceous microfossil assemblages. *Ant. Sci*., **10**(03), 269-285 (1998).

Beaman, R.J., O'Brien, P.E., Post, A.L., and De Santis, L. A new high-resolution bathymetry model for the Terre Adélie and George V continental margin, East Antarctica. *Ant. Sci.* **23**(1), 95-103 (2011).

Beans, C., Hecq, J.H., Koubbi, P., Vallet, C., Wright, S. and Goffart, A. A study of the diatom-dominated microplankton summer assemblages in coastal waters from Terre Adélie to the Mertz Glacier, East Antarctica (139°E-145°E). *Pol. Bio.*, **31**(9): 1101-1117 (2008).

Beer, J., Mende, W., and Stellmacher, R. 'The role of Sun in climate forcing', *Quat. Sci. Rev.* **19**, 403–415 (2000).

Belt, S.T., Masse, G., Rowland, S.J., Poulin, M., Michel, C. and LeBlanc, B. A novel chemical fossil of palaeo sea ice: IP25. *Org. Geochem.*, **38**(1): 16-27 (2007).

Bentley, M.J., Hodgson, D.A., Smith, J.A., Cofaigh, C.Ã., Domack, E.W., Larter, R.D., Roberts, S.J., Brachfeld, S., Leventer, A., Hjort, C., Hillenbrand, C.D. and Evans, J. Mechanisms of Holocene palaeoenvironmental change in the Antarctic Peninsula region. *Holocene*, **19**(1): 51-69 (2009).

Bertler, N.A.N., Mayewski, P.A. and Carter, L. Cold conditions in Antarctica during the Little Ice Age - Implications for abrupt climate change mechanisms. *Earth Planet. Sci. Lett.*, **308**(1-2): 41-51 (2011).

Bindoff, N. L., Rosenberg, M. A. and Warner, M. J. On the circulation and water masses over the Antarctic continental slope and rise between 80 and 150°E. *Deep-Sea Res II* **47**, 2299-2326 (2000).

Blaauw, M., Christen, J.A. Flexible paleoclimate age-depth models using an autoregressive gamma process. *Bayesian Anal.***6**, 457-474 (2011).

Broecker, W.S. Paleoclimate - Was the medieval warm period global? *Science*, **291**, 1497-1499 (2001).

C

Campagne, P., Crosta, X., Houssais, M.N., Swingedouw, D., Schmidt, S., Martin, A., Devred, E., Capo, S., Marieu, V., Closset, I., Masse, G. Relative role of glacial ice and atmospheric forcing on the Mertz Glacier Polynya over the past 250 years, *Nat. Commun.*, **6**, 6642 (2015).

Cavalieri, D. J., and Parkinson, C. L. "Antarctic sea ice variability and trends, 1979–2006. *J. Geophys. Res.*, **113**.C7 (2008).

Cavalieri, D. J., St. Germain, K. and Swift, C. T. Reduction of weather effects in the calculation of sea ice concentration with the DMSP SSM/I. *J. Glaciol*. **41**, 455-464 (1995).

Chapman, W.L. and J.E. Walsh. A Synthesis of Antarctic Temperatures. *J. Clim.*, **20**, 4096-4117 (2007).

Closset, I. Le dernier millénaire en Antarctique de l'Est. UPMC, FRANCE (2011).

Cole-Dai, J., Moseley-Thompson, E., Wight, S. P., and Thompson, L. G.: A 4100-year record of explosive volcanism from an East Antarctica ice core, *J. Geophys. Res*., **105**, 24431–24441 (2000).

Collins, L. G., Allen, C. S., Pike, J., Hodgson, D. A., Weckström, K., and Massé, G. Evaluating highly branched isoprenoid (HBI) biomarkers as a novel Antarctic sea-ice proxy in deep ocean glacial age sediments. *Quat. Sci. Rev.*, **79**, 87-98 (2013).

Comiso, J. C. Variability and trends in Antarctic surface temperatures from in situ and satellite infrared measurements, *J. Clim*., **13**, 1674 – 1696 (2000).

Comiso, J.C., McClain, C.R., Sullivan, C.W., Ryan, J.P. and Leonard, C.L. Coastal Zone Color Scanner pigment concentrations in the Southern Ocean and relationships to geophysical surface features. *J. Geophys. Res.*, **98**(C2): 2419-2451 (1993).

Compo, G. P. *et al*. The Twentieth Century reanalysis Project. *Q.J.R. Meteor. Soc.* **137,** 1–28 (2011).

Cook, E. R., B. M. Buckley, R. D. D'Arrigo, and M. J. Peterson, Warmseason temperatures since 1600 B.C. reconstructed from Tasmanian tree rings and their relationship to large-scale sea surface temperature anomalies, *Clim. Dyn*., **16**, 79 – 91 (2000).

Cremer, H., Heiri, O., Wagner, B. and Wagner-Cremer, F. Abrupt climate warming in East Antarctica during the early Holocene, *Quat. Sci. Rev.*, **26**, 2012-2018 (2007).

Cremer, H., Roberts, D., McMinn, A., Gore, D. and Melles, M. The Holocene diatom flora of marine bays in the Windmill Islands, East Antarctica. *Bot. Mar.*, **46**: 82-106 (2003).

Crosta X. Marine diatoms in polar and sub-polar environments and their application to Late Pleistocene paleoclimate reconstruction, IOP Conference Series: Earth and Environmental *Science*, **14** (2011).

Crosta, X., Denis, D. and Ther, O. Sea ice seasonality during the Holocene, Adelie Land, East Antarctica. *Mar. Micropal.*, **66:** 222-232 (2008).

Crosta, X., Debret, M., Denis, D., Courty, M.A. and Ther, O. Holocene long- and short-term climate changes off Adelie Land, East Antarctica. *Geochem. Geophys.*, **8**: doi:10.1029/2007GC001718, 1-15 (2007).

Crosta, X. and Koc, N. Diatoms: From micropaleontology to isotope geochemistry. In Methods in Late Cenozoic Paleoceanography, Hilaire-Marcel, C. and de Vernal, A. (Ed.), *Elsevier*, Amsterdam, The Netherlands, 327-369 (2007).

Crosta, X., Crespin, J., Billy, I. and Ther, O. Major factors controlling Holocene d13Corg changes in a seasonal sea-ice environment, Adelie Land, East Antarctica. *Global Biogeochem. Cy.*, **19**: GB4029, (2005).

Crosta, X., Romero, O., Armand, L. K. and Pichon, J.-J. The biogeography of major diatom taxa in Southern Ocean sediments: 2. Open ocean related species. *Palaeogeog., Palaeoclim., Palaeoecol.* **223,** 66-92 (2005).

Crosta, X., Pichon, J.J. and Labracherie, M. Distribution of Chaetoceros resting spores in modern peri-Antarctic sediments. *Mar. Micropal.*, **29**: 238-299 (1997).

Crosta, X., Sturm, A., Armand, L. and Pichon, J.J. Late Quaternary sea ice history in the Indian sector of the Southern Ocean as recorded by diatom assemblages. *Mar. Micropal.*, **50**: 209-223 (2004).

Crowley, T.J. Causes of climate change over the past 1000 years. *Science* **289**, 270–277 (2000).

Cunningham, W.L., Leventer, A., Andrews, J.T., Jennings, A.E., Licht, K.J. Late Pleistocene-Holocene marine conditions in the Ross Sea, Antarctica: evidence from the diatom record. *Holocene* **9** (2), 129-139 (1999).

Cunningham, W. L. and Leventer, A. Diatom assemblages in surface sediments of the Ross Sea: Relationship to present oceanographic conditions. *Ant. Sci*. **10**(2), 134-146 (1998).

Curran, M. A., van Ommen, T. D., Morgan, V. I., Phillips, K. L., and Palmer, A. S. Ice core evidence for Antarctic sea ice decline since the 1950s. *Science*, **302**(5648), 1203-1206 (2003).

D

Debret, M., Chapron, E., Desmet, M., Rolland-Revel, M., Magand, O., Trentesaux, A., Bout-Roumazeille, V., Nomade, J. and Arnaud, F. North western Alps Holocene paleohydrology recorded by flooding activity in Lake Le Bourget, France. *Quat. Sci. Rev.*, **29**(17-18): 2185-2200 (2010).

Defelice, D.R., and S.W. Wise, Surface lithofacies, biofaces, and diatom diversity patterns as models for delineation of climatic change in the southeast Atlantic Ocean, *Mar. Micropal.*, **6**, 29-70 (1981).

Delmotte, M., Masson, V., Jouzel, J. A seasonal deuterium excess signal at Law Dome, coastal Antarctica: a southern ocean signature. *J. Geophys. Res*. **105**, 7187–7197 (2000).

Denis, D., Crosta, X., Barbara, L., Massé, G., Renssen, H., Ther, O. and Giraudeau, J. Sea ice and wind variability during the Holocene in East Antarctica: Insight on middle-high latitude coupling. *Quat. Sci. Rev.*, **29**(27-28): 3709-3719 (2010).

Denis, D. Variabilité climatique Holocène dans la zone marginale des glaces en Antarctique de l'Est, Université de Bordeaux 1 (2008).

Denis D. *et al*. Seasonal and sub-seasonal climate changes recorded in laminated diatom ooze sediments, Adélie Land, East Antarctica. *Holocene* **16,** 1137-1147 (2006).

Dinniman, M. S., Klinck, J. M. and Hofmann, E. E. Sensitivity of Circumpolar Deep Water Transport and Ice Shelf Basal Melt along the West Antarctic Peninsula to changes in the winds. *Amer. Meteor. Soc.* **25**(14), (2012).

Domack, E., Leventer, A., Burnett, A., Bindschadler, R., Convey, P. and Kirby, M. Antarctic Peninsula Climate Variability: Historical and Paleoenvironmental Perspectives. *Antarct. Res. Ser.* AGU, Washington, DC, 260 pp (2003).

Domack, E., Leventer, A., Dunbar, R., Taylor, F., Brachfeld, S. and Sjunneskog, C. Chronology of the Palmer Deep site, Antarctic Peninsula: A Holocene palaeoenvironmental reference for the circum-Antarctic. *Holocene*, **11**(1): 1-9 (2001).

Dypvik, H. and Harris, N. B. Geochemical facies analysis of fine-grained siliciclastics using Th/U, Zr/Rb and (Zr+Rb)/Sr ratios. *Chem. Geol.* **181**(1-4), 131-146 (2001).

E

Egger, J. Slope winds and the axisymmetric circulation over Antarctica. *J. atmos. sci.* **42**, 1859-1867 (1985).

Enomoto, H. Fluctuations of snow accumulation in the Antarctic and sea level pressure in the Southern Hemisphere in the last 100 years. *Climatic change*, **18**, no 1, p. 67-87 (1991).

Escutia, C., Party, S.S. Integrated Ocean drilling Program Expedition 318 Preliminary Report. Integrated Ocean drilling Program Management International, Inc., pp. 101 (2010).

Escutia, C., Warnke, D., Acton, G. D., Barcena, A., Burckle, L., Canals, M., and Frazee, C. S. Sediment distribution and sedimentary processes across the Antarctic Wilkes Land margin during the Quaternary. *Deep Sea Res. Part II:* Topical Studies in Oceanography, **50**(8), 1481-1508 (2003).

Etourneau, J., Collins, L. G., Willmott, V., Kim, J. H., Barbara, L., Leventer, A., et al. Massé, G. Holocene climate variations in the western Antarctic Peninsula: evidence for sea ice extent predominantly controlled by changes in insolation and ENSO variability. *Clim. Past*, **9**(4), 1431-1446 (2013).

F

Ferrari, R., Jansen, M. F., Adkins, J. F., Burke, A., Stewart, A. L., and Thompson, A. F. Antarctic sea ice control on ocean circulation in present and glacial climates. *Proceedings of the National Academy of Sciences*, **111**(24), 8753-8758 (2014).

Finocchiaro, F., Langone, L., Colizza, E., Fontolan, G., Giglio, F., et al. Record of the early Holocene warming in a laminated sediment core from Cape Hallett Bay (Northern Victoria Land, Antarctica). *Global Planet. Change*, **45**(1), 193-206 (2005).

Fogt, R. L., Bromwich, D. H., and Hines, K. M. Understanding the SAM influence on the South Pacific ENSO teleconnection. *Clim. Dyn.*, **36**(7-8), 1555-1576 (2011).

Fogt, R. L., Perlwitz, J., Monaghan, A. J., Bromwich, D. H., Jones, J. M. and Marshall, G. J. Historical SAM Variability. Part II: Twentieth-Century Variability and Trends from Reconstructions, Observations, and the IPCC AR4 Models. *J. Clim.*, **22**, 5346–5365 (2009).

Fogt, R.L. and Bromwich, D.H. Decadal Variability of the ENSO Teleconnection to the High-Latitude South Pacific Governed by Coupling with the Southern Annular Mode*. *J. Clim.*, **19**(6): 979-997 (2006).

Frezzotti, M., Cimbelli, A. and Ferrigno, J. G. Ice-front change and iceberg behavior along Oates and George V coasts, Antarctica, 1912–96. *Ann. Glaciol*. **27,** 643–650 (1998).

Froneman, J. W., McQuaid, G. D. and Perissinotto, R. Biogeographic structure of the microphytoplankton assemblages of the south Atlantic and Southern Ocean during austral summer. *J. Plankton Res.* **17**, 1791-1802 (1995).

G

Gersonde, R., Crosta, X., Abelmann, A. and Armand, L.K. Sea surface temperature and sea ice distribution of the Southern Ocean at the EPILOG Last Glacial Maximum - A circum-Antarctic view based on siliceous microfossil records. *Quat. Sci. Rev.*, **24**: 869-896 (2005).

Gersonde, R., and Zielinski, U. The reconstruction of late Quaternary Antarctic sea-ice distribution—the use of diatoms as a proxy for sea-ice.*Palaeogeog., Palaeoclim., Palaeoecol.*, **162**(3), 263-286 (2000).

Garrison, D. L. Antarctic sea ice biota. *American Zoologist*, **31**(1), 17-34 (1991).

Garrison, D. L., and Buck, K. R. The biota of Antarctic pack ice in the Weddell Sea and Antarctic Peninsula regions. *Pol. bio.*, **10**(3), 211-219 (1989).

Gersonde, R. and Wefer, G. Sedimentation of biogenic siliceous particles in Antarctic waters from the Atlantic sector. *Mar. Micropal.*, **11**: 311-322 (1987).

Giles, A. B., Massom, R. A., and Lytle, V. I. Fast-ice distribution in East Antarctica during 1997 and 1999 determined using RADARSAT data. *J. Geophys. Res.: Oceans* (1978–2012), **113**(C2) (2008).

Gleitz, M., Bartsch, A., Dieckmann, G.S. and Eicken, H. Composition and succession of sea ice diatom assemblages in the eastern and southern Weddell Sea, Antarctica. In: M.P. Lizotte and K.R. Arrigo (Editors), Antarctic sea ice biological processes, interactions, and variability. *Ant. Res. Ser*. American Geophysical Union, Washington, D.C., pp. 107-120 (1998).

Gleitz, M., Grossmann, S., Scharek, R. and Smetacek, V. Ecology of diatom and bacterial assemblages in water associated with melting summer sea ice in the Weddell Sea, *Antarctica. Ant. Sci.*, **8**: 135-146 (1996).

Gomez, B., Carter, L., Orpin, A.R., Cobb, K.M., Page, M.J., Trustrum, N.A. and Palmer, A.S. ENSO/SAM interactions during the middle and late Holocene. *Holocene*, **22**(1): 23-30 (2011).

Gong, D. and Wang, S. Definition of Antarctic Oscillation Index, *Geophys. Res. Lett*. **26,** 459-462 (1999).

Goodwin, I. D., Browning, S. A., and Anderson, A. *J. Clim.*windows for Polynesian voyaging to New Zealand and Easter Island. *Proceedings of the National Academy of Sciences*, **111**(41), 14716-14721 (2014).

Goosse, Hugues, and Violette Zunz. "Decadal trends in the Antarctic sea ice extent ultimately controlled by ice–ocean feedback." *The Cryosphere* 8.**2**: 453-470 (2014).

Goosse, H., Braida, M., Crosta, X., Mairesse, A., Masson-Delmotte, V., Mathiot, P., et al. Verleyen, E. Antarctic temperature changes during the last millennium: evaluation of simulations and reconstructions. *Quat. Sci. Rev.*, **55**, 75-90 (2012).

Goosse, H., Brovkin, V., Fichefet, T., Haarsma, R., Huybrechts, P., Jongma, J., et al. Weber, S. L. Description of the Earth system model of intermediate complexity LOVECLIM version 1.2. *Geoscientific Model Development*, **3**, 603-633 (2010).

Goosse, H., Masson-Delmotte, V., Renssen, H., Delmotte, M., Fichefet, T., Morgan, V., et al. Stenni, B. A late medieval warm period in the Southern Ocean as a delayed response to external forcing? *Geophys. Res. Lett. ,* **31**(6) (2004).

Gordon, A.L., Visbeck, M. and Huber, B. Export of Weddell Sea Deep and Bottom Water. *J. Geophys. Res.* C: Oceans, **106**(C5): 9005-9017 (2001).

Gregory, T. Holocene sea ice-ocean-climate variability from Adélie Land, East Antarctica. Ph.D. thesis, Cardiff University, UK., pp. 237 (2012).

Grinsted, A., Moore, J.C. and Jevrejeva, S. Application of the cross wavelet transform and wavelet coherence to geophysical time series. *Nonlin. Process. Geophys.* **11,** 561-566 (2004).

H

Hall, A. and Visbeck, M. Synchronous variability in the Southern Hemisphere atmosphere, sea ice, and ocean resulting from the Annular Mode. *J. Clim.* **15,** 3043-3057 (2002).

Hargraves, P.E. and French, F.W. Observations on the survival of diatom resting spores. *Beih. Nova Hedwigia,* **53,** 229-238 (1975).

Hargraves, P. E. Studies on marine plankton diatoms. I. Chaetoceros diadema (Ehr.) Gran: life cycle, structural morphology, and regional distribution. *Phycologia*, **11**(3), 247-257 (1972).

Hasle, G. R., Sims, P. A., and Syvertsen, E. E. Two recent Stellarima species: S. microtrias and S. stellaris (Bacillariophyceae). *Bot. Mar.*, **31**(3), 195-206 (1988).

Hasle, G. R. An analysis of the phytoplankton of the Pacific Southern Ocean: abundance, composition, and distribution during the Brategg Expedition, 1947-1948 (Vol. 52). Univ.-Forl (1969).

Haug, G. H., Hughen, K. A., Sigman, D. M., Peterson, L. C., and Röhl, U. Southward migration of the intertropical convergence zone through the Holocene. *Science*, **293**(5533), 1304-1308 (2001).

Heil, P. Atmospheric conditions and fast ice at Davis, East Antarctica: A case study. *J. Geophys. Res.: Oceans* (1978–2012) **111**.C5 (2006).

Hodgson, D. A., Verleyen, E., Sabbe, K., Squier, A. H., Keely, B. J., Leng, M. J., et al. Vyverman, W. Late Quaternary climate-driven environmental change in the Larsemann Hills, East Antarctica, multi-proxy evidence from a lake sediment core. *Quaternary Res.*, **64**(1), 83-99 (2005).

Holland, P. R., and Kwok, R. Wind-driven trends in Antarctic sea-ice drift. *Nat. Geosci.*, **5**(12), 872-875 (2012).

Hollibaugh, J. T., Seibert, D. L. R., and Thomas, W. H. Observations on the survival and germination of resting spores of three Chaetoceros (Bacillariophyceae) species 1, 2. *J. Phycol.*, **17**(1), 1-9 (1981).

J

Jacobs, S. Observations of changes in the Southern Ocean. *Phil. Trans. R. Soc. A.* **364,** 1657-1681 (2006).

Jacobs, S. Bottom water production and its links with the thermohaline circulation. *Ant. Sci.* **16**(4), 427-437 (2004).

Jansen, J. H. F., Van der Gaast, S. J., Koster, B. and Vaars, A. J. CORTEX, a shipboard XRF-scanner for element analyses in split sediment cores. *Mar. Geol.* **151,** 143-53 (1998).

Jenouvrier, S., Weimerskirch, H., Barbraud, C., Park, Y. H., and Cazelles, B. Evidence of a shift in the cyclicity of Antarctic seabird dynamics linked to climate. Proceedings of the Royal Society of London B: *Biological Sciences*, **272**(1566), 887-895 (2005).

Jevrejeva, S., Moore, J. C., and Grinsted, A. Influence of the Arctic Oscillation and El Niño-Southern Oscillation (ENSO) on ice conditions in the Baltic Sea: The wavelet approach. *J. Geophys. Res.*: *Atmospheres* (1984–2012), **108**(D21) (2003).

Johansen, J.R. and Fryxell, G.A. The genus Thalassiosira (Bacillariophyceae): Studies on species occurring south of the Antarctic Convergence Zone. *Phycologia* **24**(2), 155-179 (1985).

Johnson, G. C. Quantifying Antarctic Bottom Water and North Atlantic Deep Water volumes. *J. Geophys. Res*. **113,** C05027 (2008).

Jones, P.D. and Mann, M.E. Climate over past millennia. *Rev. Geophys.*, **42**(2): RG2002 (2004).

K

Kang, S.-H. and Fryxell, G. A. Fragilariopsis cylindrus (Grunow) Krieger: The most abundant diatom in water column assemblages of Antarctic marginal ice edge zones. *Pol. Biol.* **12**, 609-627 (1992).

Klinck, J. M. and Dinniman, M. S. Exchange across the shelf break at high southern latitudes. *Ocean Sci*., **6**, 513-524 (2010).

Koffman, B. G., Kreutz, K. J., Breton, D. J., Kane, E. J., Winski, D. A., Birkel, S. D., et al. Handley, M. J. Centennial-scale variability of the Southern Hemisphere westerly wind belt in the eastern Pacific over the past two millennia. *Clim. Past*, **10**(3), 1125-1144 (2014).

König-Langlo, G., J.C. King and P. Pettré. Climatology of the three coastal Antarctic stations Dumont d'Urville, Neumayer, and Halley. *J. Geophys. Res.*, **103**(D9), 10 935-10 946 (1998).

Krebs, W.N., Lipps, J.H. and Burckle, L.H. Ice diatom floras, Arthur Harbor, Antarctica. *Pol. bio.*, **7**: 163-171 (1987).

Kusahara, K., Hasumi, H. and Williams, G. Impact of Mertz Glacier Tongue calving on dense shelf water. *Nat. Commun.* **2,** 159 (2011).

Kwok, R. and Comiso, J.C. Southern Ocean climate and sea ice anomalies associated with the Southern Oscillation. *J. Clim.*, **15**(5): 487-501 (2002).

L

Lacarra, M., Houssais, M. N., Herbaut, C., Sultan, E. and Beauverger, M. Dense shelf water production in the Adélie Depression 2004-2012: Impact of the Mertz glacier calving. *J. Geoph. Res.* **119**(8), 5203-5220 (2014).

Lamy, F., Hebbeln, D., Röhl, U. and Wefer, G. Holocene rainfall variability in Southern Chile: A marine record of latitudinal shifts of the Southern Westerlies. *Earth Planet. Sci. Lett.*, **185**(3-4): 369-382 (2001).

Lefebvre, W., Goosse, H., Timmermann, R. and Fichefet, T. Influence of the Southern Annular Mode on the sea iceand#8211;ocean system. *J. Geophys. Res*., **109**(C9): C09005 (2004).

Legresy B., Wendt A., Tabacco I., Remy F. and Dietrich R. Influence of tides and tidal current on Mertz Glacier, Antarctica. *J. Glaciol.* **50**(170), 427-435 (2004).

Lescarmontier, L. *et al*. Vibration of the Mertz Glacier ice tongue, East Antarctica. *J. Glaciol.* **58**(210), 665-676 (2012).

Leventer, A., Domack, E., Dunbar, R., Pike, J., Stickley, C., Maddison, E. et al. Marine sediment record from the East Antarctic margin reveals dynamics of ice sheet recession. *GSA TODAY*, **16**(12), 4 (2006).

Leventer, A., Domack, E. W., Ishman, S. E., Brachfeld, S., McClennen, C. E., and Manley, P. Productivity cycles of 200–300 years in the Antarctic Peninsula region: understanding linkages among the sun, atmosphere, oceans, sea ice, and biota. *Geol. Soc. Am. Bull.*, **108**(12), 1626-1644 (1996).

Leventer, A., Dunbar, R. B., and DeMaster, D. J. Diatom evidence for late Holocene climatic events in Granite Harbor, Antarctica. *Paleoceanography*, **8**(3), 373-386 (1993).

Leventer, A. Modern distribution of diatoms in sediments from the Georges V coast, Antarctica. *Mar. Micropal.*, **19**: 315-332 (1992).

Leventer, A. Sediment trap diatom assemblages from the northern Antarctic Peninsula region. *Deep-Sea Res.*, **38**: 1127-1143 (1991).

Leventer, A. and Dunbar, R.B. Recent Diatom Record of McMurdo Sound, Antarctica: Implications for History of Sea Ice Extent. *Paleoceanography*, **3**(3): 259- 274 (1988).

Ljungqvist, F. C., Krusic, P. J., Brattström, G., and Sundqvist, H. S. Northern Hemisphere temperature patterns in the last 12 centuries. *Clim. Past*, **8**(1), 227-249 (2012).

Lumpkin, R. and Speer, K. Global ocean meridional overturning. *J. Phys. Oceanogr.*, **37**(10): 2550-2562 (2007).

Lund, D. C., Lynch-Stieglitz, J., and Curry, W. B. Gulf Stream density structure and transport during the past millennium. *Nature*, **444**(7119), 601-604 (2006).

M

Maddison, E. J., Pike, J. and Dunbar, R. Seasonally laminated diatom-rich sediments from Dumont d'Urville Trough, East Antarctic Margin: Late-Holocene Neoglacial sea-ice conditions. *Holocene* **22**(8), 857-875 (2012).

Maddison, E. J., Pike, J., Leventer, A., Dunbar, R., Brachfeld, S., Domack, E. W., et al. McClennen, C. Post-glacial seasonal diatom record of the Mertz Glacier Polynya, East Antarctica. *Mar. Micropal.*, **60**(1), 66-88 (2006).

Maddison, E.J. Seasonally Laminated Late Quaternary Antarctic Sediments. Cardiff University, unpublished PhD thesis (2006).

Maddison, E.J., Pike, J., Leventer, A. and Domack, E.W. Deglacial seasonal and subseasonal diatom record from Palmer Deep, Antarctica. *J. Quat. Sci.*, **20**: 435-446 (2005).

Mann, M. E., Zhang, Z., Rutherford, S., Bradley, R. S., Hughes, M. K., Shindell, D., et al. Ni, F. Global signatures and dynamical origins of the Little Ice Age and Medieval Climate Anomaly. *Science*, **326**(5957), 1256-1260 (2009).

Mann, M. E., Zhang, Z., Hughes, M. K., Bradley, R. S., Miller, S. K., Rutherford, S., and Ni, F. Proxy-based reconstructions of hemispheric and global surface temperature variations over the past two millennia. *Proceedings of the National Academy of Sciences*, **105**(36), 13252-13257 (2008).

Maqueda, M., Willmott, A. J., and Biggs, N. R. T. Polynya dynamics: a review of observations and modeling. *Rev. Geophys.*, **42**(1) (2004).

Marini, C., Frankignoul, C. and Mignot, J. Links between the Southern Annular Mode and the Atlantic Meridional Overturning Circulation in a Climate Model. *J. Clim.*, **24,** 624–640 (2011).

Marshall, G. J. Trends in the Southern Annular Mode from observations and reanalyzes. *J. Clim.* **16**, 4134-4143 (2003).

Martinson, D. G., Stammerjohn, S. E., Iannuzzi, R. A., Smith, R. C. and Vernet, M. Western Antarctic Peninsula physical oceanography and spatio-temporal variability. *Deep-Sea Res. Part II* **55,** 1964–1987 (2008).

Massé, G., Belt, S. T., Crosta, X., Schmidt, S., Snape, I., Thomas, D. N., and Rowland, S. J. Highly branched isoprenoids as proxies for variable sea ice conditions in the Southern Ocean. *Ant. Sci.*, **23**(05), 487-498 (2011).

Massé, G., Belt, S., Rowland, S., Sicre, M.-A. and Crosta, X. Highly branched isoprenoid biomarkers as indicators of sea-ice diatoms: implications for historical sea- ice records and future predictions, General Assembly of the European Geosciences Union. 04001, Vienna, Austria (2007).

Massé, G., Belt, S.T., Allard, W.G., Lewis, C.A., Wakeham, S.G. and Rowland, S.J. Occurrence of novel monocyclic alkenes from diatoms in marine particulate matter and sediments. *Org. Geochem.*, **35**(7): 813-822 (2004).

Massom, R., Reid, P., Stammerjohn, S., Raymond, B., Fraser, A., and Ushio, S. Change and variability in East Antarctic sea ice seasonality, 1979/80–2009/10 (2013).

Massom, R. A., Hill, K., Barbraud, C., Adams, N., Ancel, A., Emmerson, L., and Pook, M. J. Fast ice distribution in Adélie Land, East Antarctica: interannual variability and implications for emperor penguins Aptenodytes forsteri. *Mar. Ecol. Prog. Ser.*, **374**(January), 243-257 (2009).

Massom, R. A., Jacka, K., Pook, M. J., Fowler, C., Adams, N., and Bindoff, N. An anomalous late-season change in the regional sea ice regime in the vicinity of the Mertz Glacier Polynya, East Antarctica. *J. Geophys. Res.*: Oceans (1978–2012), **108**(C7) (2003).

Massom, R. A., Eicken, H., Haas, C., Jeffries, M. O., Drinkwater, M. R., Sturm, M., et al. Snow on Antarctic sea ice. *Rev. Geophys.*, **39**(3), 413-445 (2001).

Massom, R. A., Harris, P. T., Michael, K. J. and Potter, M. J. The distribution of formative processes of latent heat polynyas in East Antarctica. *Ann. Glaciol.*, **27**, 420-426 (1998).

Masson-Delmotte, V., Stenni, B. and Jouzel, J. Common millenial-scale variability of Antarctic and Southern Ocean temperatures during the past 5000 years reconsructed from the EPICA Dome C ice core. *Holocene*, **14**(2): 145-151 (2004).

Masson-Delmotte, V., Delmotte, M., Morgan, V., Etheridge, D., Van Ommen, T., Tartarin, S., and Hoffmann, G. Recent southern Indian Ocean climate variability inferred from a Law Dome ice core: New insights for the interpretation of coastal Antarctic isotopic records. *Clim. Dyn.*, **21**(2), 153-166 (2003).

Masson, V., Vimeux, F., Jouzel, J., Morgan, V., Delmotte, M., Ciais, P., et al. Vaikmae, R. Holocene climate variability in Antarctica based on 11 ice-core isotopic records. *Quaternary Res.*, **54**(3), 348-358 (2000).

Mayewski, P. A., Maasch, K. A., White, J. W., Steig, E. J., Meyerson, E., Goodwin, I., et al. Kreutz, K. A 700 year record of Southern Hemisphere extratropical climate variability. *Ann. Glaciol.*, **39**(1), 127-132 (2004).

Maykut, G.A. Energy Exchange Over Young Sea Ice in the Central Arctic. *J. Geophys. Res*., **83**(C7): 3646-3658 (1978).

McMinn, A., Bleakley, N., Steinburner, K., Roberts, D., and Trenerry, L. Effect of permanent sea ice cover and different nutrient regimes on the phytoplankton succession of fjords of the Vestfold Hills Oasis, eastern Antarctica. *J. Plankton Res.*, **22**(2), 287-303 (2000).

Meredith, M. P. Oceanography: Replenishing the abyss. *Nat. Geosci.*, **6**(3), 166-167 (2013).

Meredith, M. P. and Hogg, A. M. Circumpolar response of Southern Ocean eddy activity to a change in the Southern Annular Mode. *Geophys. Res. Lett.*, **33**, L16608 (2006).

Migeon, S., Weber, O., Faugères, J.-C. and Saint-Paul, J. SCOPIX : a new X-ray imaging system for core analysis. *Geo-Mar. Lett.* **18**, 251-255 (1999).

Moisan, T. A., and Fryxell, G. A. The distribution of Antarctic diatoms in the Weddell Sea during austral winter. *Bot. Mar.*, **36**(6), 489-498 (1993).

Moore, J. K., and Abbott, M. R. Phytoplankton chlorophyll distributions and primary production in the Southern Ocean. *J. Geophys. Res.: Oceans (1978–2012)*, **105(**C12), 28709-28722 (2000).

Moy, C.M., Seltzer, G.O., Rodbell, D.T. and Anderson, D.M. Variability of El Nino/SOuthern Oscillation activity at millenial timescales during the Holocene epoch. *Nature*, **420**: 162-165 (2002).

N

Neukom, R., Gergis, J., Karoly, D. J., Wanner, H., Curran, M., Elbert, J., et al. Frank, D. Inter-hemispheric temperature variability over the past millennium. *Nat. Clim. Change*, **4**(5), 362-367 (2014).

Neukom, R., Luterbacher, J., Villalba, R., Küttel, M., Frank, D., Jones, P. D., et al. Von Gunten, L. Multiproxy summer and winter surface air temperature field reconstructions for southern South America covering the past centuries. *Clim. Dyn.*, **37**(1-2), 35-51 (2011).

Nielsen, S.H.H., Koç, N. and Crosta, X. Holocene climate in the Atlantic sector of the Southern Ocean: Controlled by insolation or oceanic circulation? *Geology*, **32**(4): 317- 320 (2004).

O

Orsi, A. J., Cornuelle, B. D., and Severinghaus, J. P. Little Ice Age cold interval in West Antarctica: evidence from borehole temperature at the West Antarctic ice sheet (WAIS) divide. *Geophys. Res. Lett.* , **39**(9) (2012).

Orsi, A. H., Whitworth III, T. and Nowlin, W. D. Jr. On the meridional extent and fronts of the Antarctic Circumpolar Current. *Deep-Sea Res. Part I* **42,** 641–673 (1995).

P

Parish, T. R., and Bromwich, D. H. Reexamination of the near-surface airflow over the Antarctic continent and implications on atmospheric circulations at high southern latitudes*. *Monthly Weather Rev.*, **135**(5), 1961-1973 (2007).

Parish, N. J. P. and Bromwich, D. H. Continental-scale simulation of the Antarctic katabatic wind regime. *J. Clim.*, **4,** 135–146 (1991).

Périard, C. and Pettré, P. Some aspects of the climatology of dumont D'Irville, adélie land, Antarctica. *Int. J. Climatol.*, **13**: 313–328 (1993).

Pichon, J.J., G. Bareille, M. Labracherie, L.D. Labeyrie, A. Baudrimont, and J.L. Turon, Quantification of the biogenic silica dissolution in the Southern Ocean sediments. *Quat. Res.*, 3Z 361-378 (1992).

Pike, J., Swann, G. E., Leng, M. J., and Snelling, A. M. Glacial discharge along the west Antarctic Peninsula during the Holocene. *Nat. Geosci.*, **6**(3), 199-202 (2013).

Pike, J., Crosta, X., Maddison, E. J., Stickley, C. E., Denis, D., Barbara, L., and Renssen, H. Observations on the relationship between the Antarctic coastal diatoms Thalassiosira antarctica Comber and Porosira glacialis (Grunow) Jørgensen and sea ice concentrations during the late Quaternary. *Mar. Micropal.*, **73**(1), 14-25 (2009).

Presti, M., De Santis, L., Busetti, M. and Harris, P.T. Late Pleistocene and Holocene sedimentation on the George V Continental Shelf, East Antarctica. *Deep-Sea Res. Part II* **50**, 1441-1461 (2003).

Previdi, M. and Polvani, L. M. Climate system response to stratospheric ozone depletion and recovery. *Q.J.R. Meteorol. Soc.* **140**, 2401–2419 (2014).

Prokoph, A. and El Bilali, H. Cross-Wavelet Analysis: a Tool for Detection of Relationships between Paleoclimate Proxy Records. *Math. Geosc.* **40**(5), 575-586 (2008).

R

Ragueneau, O., Tréguer, P., Leynaert, A., Anderson, R. F., Brzezinski, M. A., DeMaster, D. J., et al. Quéguiner, B. A review of the Si cycle in the modern ocean: recent progress and missing gaps in the application of biogenic opal as a paleoproductivity proxy. *Global Planet. Change*, **26**(4), 317-365 (2000).

Rathburn, A.E., Pichon, J.J., Ayress, M.A. and De Deckker, P. Microfossil and stable- isotope evidence for changes in Late Holocene palaeoproductivity and palaeoceanographic conditions in the Prydz Bay region of Antarctica. *Palaeogeog., Palaeoclim., Palaeoecol.*, **131**(3-4): 485-510 (1997).

Renssen, H., Goosse, H., Fichefet, T., Masson-Delmotte, V. and Koc, N. Holocene climate evolution in the high-latitude Southern Hemisphere simulated by a coupled atmosphere-sea ice-ocean-vegetation model. *Holocene*, **15**: 951-964 (2005).

Riaux-Gobin, C., Romero, O. E., Coste, M., and Galzin, R. A new Cocconeis (Bacillariophyceae) from Moorea Island, Society Archipelago, South Pacific Ocean with distinctive valvocopula morphology and linking system. *Bot. Mar.*, **56**(4), 339-356 (2013).

Riaux-Gobin, C., Poulin, M., Dieckmann, G., Labrune, C., and Vétion, G. Spring phytoplankton onset after the ice break-up and sea-ice signature (Adélie Land, East Antarctica). *Pol. Res.*, **30** (2011).

Riaux-Gobin, C., Poulin, M., Prodon, R., and Tréguer, P. Land-fast ice microalgal and phytoplanktonic communities (Adélie Land, Antarctica) in relation to environmental factors during ice break-up. *Ant. Sci.*, **15**(03), 353-364 (2003).

Rintoul, S. R. Rapid freshening of Antarctic Bottom Water formed in the Indian and Pacific oceans. *Geophys. Res. Lett.* **34**, L06606 (2007).

Rintoul, S. R., and Sokolov, S. Baroclinic transport variability of the Antarctic Circumpolar Current south of Australia (WOCE repeat section SR3). *J. Geophys. Res.*: Oceans (1978–2012), **106**(C2), 2815-2832 (2001).

Rintoul, S. R. On the Origin and Influence of Adélie Land Bottom Water. In Ocean, Ice, and Atmosphere: Interactions at the Antarctic Continental Margin, Jacobs, S. and Weiss, R. (Ed.), *Ant. Res. Ser.*, **75**, 151-171 (1998).

Roberts, D., van Ommen, T. D., McMinn, A., Morgan, V., and Roberts, J. L. Late-Holocene East Antarctic climate trends from ice-core and lake-sediment proxies. *Holocene*, **11**(1), 117-120 (2001).

Robock, A. Volcanic eruptions and climate. Climate Change: Natural forcing factors for climate change timescales 10-1 to 10-5 years, *Rev. Geophys.*, **38**, 305 (2002).

Rowland, S.J., Belt, S.T., Wraige, E.J., Masse, G., Roussakis, C. and Robert, J.M. Effects of temperature on polyunsaturation in cytostatic lipids of Haslea ostrearia. *Phytochem.*, **56**(6): 597-602 (2001).

S

Sambrotto, R. N., Matsuda, A., Vaillancourt, R., Brown, M., Langdon, C., Jacobs, S. S., and Measures, C. Summer plankton production and nutrient consumption patterns in the Mertz Glacier Region of East Antarctica. *Deep Sea Res. Part II: Topical Studies in Oceanography*, **50**(8), 1393-1414 (2003).

Saunders, K. M., Kamenik, C., Hodgson, D. A., Hunziker, S., Siffert, L., Fischer, D., et al. Grosjean, M. Late Holocene changes in precipitation in northwest Tasmania and their potential links to shifts in the Southern Hemisphere westerly winds. *Global Planet. Change*, **92**, 82-91 (2012).

Schmidt, S., and De Deckker, P. Present-day sedimentation rates on the southern and southeastern Australian continental margins. *Australian J. Earth Sci.*, **62**(2), 143-150 (2015).

Schmidtko, S., Heywood, K. J., Thompson, H. and Shigeru, A. Multidecadal warming of antarctic waters. *Science* **346**, 1227-1231 (2014).

Schneider, D. P., Steig, E. J., van Ommen, T. D., Dixon, D. A., Mayewski, P. A., Jones, J. M., and Bitz, C. M. Antarctic temperatures over the past two centuries from ice cores. *Geophys. Res. Lett.* , **33**(16) (2006).

Schrader, H.J. and Gersonde, R. Diatoms and Silicoflagellates. In: Z.e. al. (Editor), Micropaleontological Counting Methods and Techniques - An exercise on an Eight Meters Section of the Lower Pliocene of Capo Rossello. *Utrecht Micropal. Bull*., Silicy, pp. 129-176 (1978).

Shevenell, A.E., Ingalls, A.E., Domack, E.W. and Kelly, C. Holocene Southern Ocean surface temperature variability west of the Antarctic Peninsula. *Nature*, **470**(7333): 250-254 (2011).

Sigl, M., Winstrup, M., McConnell, J. R., Welten, K. C., Plunkett, G., Ludlow, F., et al. Timing and climate forcing of volcanic eruptions for the past 2,500 years. *Nature,* **523**(2015).

Sinclair, M. R., Renwick, J. A., and Kidson, J. W. Low-frequency variability of Southern Hemisphere sea level pressure and weather system activity. *Monthly Weather Rev.*, **125**(10), 2531-2543 (1997).

Sinninghé Damsté, J. S. et al. The rise of the Rhizosolenoid diatoms. *Science,* **304**(5670), 584-587 (2004).

Souney, J. M., Mayewski, P. A., Goodwin, I. D., Meeker, L. D., Morgan, V., Curran, M. A., et al. A 700-year record of atmospheric circulation developed from the Law Dome ice core, East Antarctica. *J. Geophys. Res.: Atmospheres* (1984–2012), **107**(D22), ACL-1 (2002).

Speer, K., Rintoul, S. R., and Sloyan, B. The diabatic Deacon Cell*.*J. Phys. Oceanogr.*, **30**(12), 3212-3222 (2000).

Sprenk, D., Weber, M. E., Kuhn, G., Wennrich, V., Hartmann, T., and Seelos, K. Seasonal changes in glacial polynya activity inferred from Weddell Sea varves. *Clim. Past*, **10**(3), 1239-1251 (2014).

Stammerjohn, S. E., Martinson, D. G., Smith, R. C., Yuan, X. and Rind, D. Trends in Antarctic annual sea ice retreat and advance and their relation to El Niño-Southern Oscillation and Southern Annular Mode variability. *J. Geophys. Res*. **113**, C03S90, (2008).

Steig, E.J., Schneider, D.P., Rutherford, S.D., Mann, M.E., Comiso, J.C. and Shindell, D.T. Warming of the Antarctic ice-sheet surface since the 1957 International Geophysical Year. *Nature*, **457**(7228): 459-462 (2009).

Steinhilber, F., Abreu, J. A., Beer, J., Brunner, I., Christl, M., Fischer, H., et al. Wilhelms, F. 9,400 years of cosmic radiation and solar activity from ice cores and tree rings. *Proceedings of the National Academy of Sciences*,**109**(16), 5967-5971 (2012).

Steinhilber, F., Beer, J. and Fröhlich, C. Total solar irradiance during the Holocene. *Geophys. Res. Lett*., **36**(19): L19704 (2009).

Stenni, B., Proposito, M., Gragnani, R., Flora, O., Jouzel, J., Falourd, S. and Frezzotti, M. Eight centuries of volcanic signal and climate change at Talos Dome (East Antarctica). *J. Geophys. Res*., **107**(D9): 4076 (2002).

Stenseth, N. C., Ottersen, G., Hurrell, J. W., Mysterud, A., Lima, M., Chan, K. S., et al. Ådlandsvik, B. Studying climate effects on ecology through the use of climate indices: the North Atlantic Oscillation, El Nino Southern Oscillation and beyond. *Proceedings of the Royal Society of London B: Biological Sciences*, **270**(1529), 2087-2096 (2003).

Stickley, C. E., Pike, J., Leventer, A., Dunbar, R., Domack, E. W., Brachfeld, S., et al. McClennan, C. Deglacial ocean and climate seasonality in laminated diatom sediments, Mac. Robertson Shelf, Antarctica. *Palaeogeog., Palaeoclim., Palaeoecol.*, **227**(4), 290-310 (2005).

St-Laurent, P., Klinck, J.M. and Dinniman, M.S. On the Role of Coastal Troughs in the Circulation of Warm Circumpolar Deep Water on Antarctic Shelves. *J. Phys. Ocean.* **43**(1), 51-64 (2013).

Swingedouw, D., Mignot, J., Labetoulle, S., Guilyardi, E., and Madec, G. Initialisation and predictability of the AMOC over the last 50 years in a climate model. *Clim. Dyn.*, **40**(9-10), 2381-2399 (2013).

T

Tamura, T., Williams, G. D., Fraser, A. D. and Ohshima, K. I. Potential regime shift in decreased sea ice production after the Mertz Glacier calving. *Nat. Commun.* **3,** 826 (2012).

Tamura, T., Ohshima, K. I. and Nihashi, S. Mapping of sea ice production for Antarctic coastal polynyas. *Geophys. Res. Lett.* **35,** L07606 (2008).

Tavernier, I., Verleyen, E., Hodgson, D. A., Heirman, K., Roberts, S. J., Imura, S., et al. Vyverman, W. Absence of a Medieval Climate Anomaly, Little Ice Age and twentieth century warming in Skarvsnes, Lützow Holm Bay, East Antarctica. *Ant. Sci.*, **26**(05), 585-598 (2014).

Taylor, F., and McMinn, A. Evidence from diatoms for Holocene climate fluctuation along the East Antarctic margin. *Holocene*, **11**(4), 455-466 (2001).

Taylor, F., Whitehead, J., and Domack, E. Holocene paleoclimate change in the Antarctic Peninsula: evidence from the diatom, sedimentary and geochemical record. *Mar. Micropal.*, **41**(1), 25-43 (2001).

Taylor, F. Sedimentary diatom assemblages of Prydz Bay and Mac.Robertson Shelf, East Antarctica, and their use as paleoecological indicators. PhD thesis, University of Tasmania, Hobart (1999).

Taylor, F., McMinn, A., Franklin, D. Distribution of diatoms in surface sediments of Prydz Bay, Antarctica. *Mar. Micropal.* **32** (3/4), 209-230 (1997).

Tchernia, P. Océan Austral, Océanographie Régionale, Description Physique des Océans et des Mers. Ecole Nationale Supérieure de Techniques Avancées, pp. 45-85 (1978).

Thomas, E. R., Marshall, G. J., and McConnell, J. R. A doubling in snow accumulation in the western Antarctic Peninsula since 1850. *Geophys. Res. Lett.* , **35**(1) (2008).

Thompson, D. W., Solomon, S., Kushner, P. J., England, M. H., Grise, K. M., and Karoly, D. J. Signatures of the Antarctic ozone hole in Southern Hemisphere surface climate change. *Nat. Geosci.*, **4**(11), 741-749 (2011).

Thompson, D. W. J. and Solomon, S. Interpretation of recent Southern Hemisphere climate change. *Science* **296**, 895-899 (2002).

Thompson, D. W. J. and Wallace, J. M. Annular Modes in the Extratropical Circulation. Part I: Month-to-Month Variability. *J. Clim.***13**, 1000-1016 (2000).

Treguer, P., Nelson, D.M., Bennekom, A.J.V., DeMaster, D.J., Leynaert, A. and Queguiner, B. The silica balance in the world ocean: A reestimate. *Science*, **268**: 375-379 (1995).

Turner, J., Colwell, S.R., Marshall, G.J., Lachlan-Cope, T.A., Carleton, A.M., Jones, P.D., Lagun, V., Reid, P.A. and Iagovkina, S., 2005. Antarctic climate change during the last 50 years. *Int. J. Climatol.*, **25**(3): 279-294 (2009).

Turner, J. The El Niño–Southern Oscillation and Antarctica. *Int. J. Climatol.*, **24**(1), 1-31 (2004).

V

Vaillancourt, R. D., Sambrotto, R. N., Green, S., and Matsuda, A. Phytoplankton biomass and photosynthetic competency in the summertime Mertz Glacier Region of East Antarctica. *Deep Sea Res. Part II: Topical Studies in Oceanography*, **50**(8), 1415-1440 (2003).

Van der Broeke, M. and van Lipzig, N. P. M. Changes in Antarctic temperature wind and precipitation in response to Antarctic Oscillation. *Ann. Glaciol.* **39**, 119-126 (2004).

Van der Broeke, M. R., van Lipzig, N. P. M. and van Meijgaard, E. Momentum Budget of the East Antarctic Atmospheric Boundary Layer: Results of a Regional Climate Model. *J. Atmos. Sci.* **59**, 3117–3129 (2002).

van Ommen, T. D., and Morgan, V. Snowfall increase in coastal East Antarctica linked with southwest Western Australian drought. *Nat. Geosci.*, **3**(4), 267-272 (2010).

Varma, V., Prange, M., Merkel, U., Kleinen, T., Lohmann, G., Pfeiffer, M., et al. Schulz, M. Holocene evolution of the Southern Hemisphere westerly winds in transient simulations with global climate models. *Clim. Past*, **8**, 391-402 (2012).

Varma, V., Prange, M., Lamy, F., Merkel, U., and Schulz, M. Solar-forced shifts of the Southern Hemisphere Westerlies during the Holocene. *Clim. Past*, **7**(2), 339-347 (2011).

Verleyen, E., Hodgson, D. A., Sabbe, K., Cremer, H., Emslie, S. D., Gibson, J., et al. Vyverman, W. Post-glacial regional climate variability along the East Antarctic coastal margin—Evidence from shallow marine and coastal terrestrial records. *Earth-Sci. Rev.*, **104**(4), 199-212 (2011).

Villalba, R., Lara, A., Masiokas, M. H., Urrutia, R., Luckman, B. H., Marshall, G. J., et al. LeQuesne, C. Unusual Southern Hemisphere tree growth patterns induced by changes in the Southern Annular Mode. *Nat. Geosci.*, **5**(11), 793-798 (2012).

Vonmoos, M., Beer, J., and Muscheler, R. Large variations in Holocene solar activity: Constraints from 10Be in the Greenland Ice Core Project ice core. *J. Geophys. Res.: Space Physics (1978–2012)*, **111**(A10) (2006).

W

Wagner, B., Cremer, H., Hultzsch, N., Gore, D. B., and Melles, M. Late Pleistocene and Holocene history of Lake Terrasovoje, Amery Oasis, East Antarctica, and its climatic and environmental implications. *J. Paleolimnol.*, **32**(4), 321-339 (2004).

Wang, Z., Turner, J., Sun, B., Li, B., and Liu, C. Cyclone-induced rapid creation of extreme Antarctic sea ice conditions. *Scientific reports*, **4** (2014).

Wanner, H., Solomina, O., Grosjean, M., Ritz, S. P., and Jetel, M. Structure and origin of Holocene cold events. *Quat. Sci. Rev.*, **30**(21), 3109-3123 (2011).

Warner, N. R., and Domack, E. W. Millennial-to decadal-scale paleoenvironmental change during the Holocene in the Palmer Deep, Antarctica, as recorded by particle size analysis. *Paleoceanography*, **17**(3), PAL-5 (2002).

Wendler, G., Stearns, C., Weidner, G., Dargaud, G., and Parish, T. On the extraordinary katabatic winds of Adélie Land. *J. Geophys. Res.: Atmospheres (1984–2012)*, **102**(D4), 4463-4474 (1997).

Whitworth, T. I. I. I. Two modes of bottom water in the Australian-Antarctic Basin. *Geophys. Res. Lett.* , **29**(5), 17-1 (2002).

Williams, G. D., Aoki, S., Jacobs, S. S., Rintoul, S. R., Tamura, T., and Bindoff, N. L. Antarctic bottom water from the Adélie and George V Land coast, East Antarctica (140–149 E). *J. Geophys. Res.*: Oceans (1978–2012), **115**(C4) (2010).

Williams, G. D., Bindoff, N. L., Marsland, S. J. and Rintoul, S. R. Formation and export of dense shelf water from the Adélie Depression, East Antarctica. *J. Geophys. Res*. **113**, C04039 (2008).

Williams, G.D. and Bindoff, N.L. Wintertime oceanography of the Adélie depression. *Deep-Sea Res. Part II*, **50**, 1373-1392 (2003).

Wirth, S. B., Glur, L., Gilli, A., and Anselmetti, F. S. Holocene flood frequency across the Central Alps–solar forcing and evidence for variations in North Atlantic atmospheric circulation. *Quat. Sci. Rev.*, **80**, 112-128 (2013).

Wright, S. W., and van den Enden, R. L. Phytoplankton community structure and stocks in the East Antarctic marginal ice zone (BROKE survey, January–March 1996) determined by CHEMTAX analysis of HPLC pigment signatures. *Deep Sea Res. Part II: Topical Studies in Oceanography*, **47**(12), 2363-2400 (2000).

Wuite, J. Spatial and Temporal Dynamics of Three East Antarctic Outlet Glaciers and Their Floating Ice Tongues. Ph.D. thesis, Ohio State Univ., Columbus, pp. 190 (2006).

Y

Yan, H., Sun, L., Wang, Y., Huang, W., Qiu, S., and Yang, C. A record of the Southern Oscillation Index for the past 2,000 years from precipitation proxies. *Nat. Geosci.*, **4**(9), 611-614 (2011).

Yan, Y., Mayewski, P.A., Kang, S. and Meyerson, E. An ice-core proxy for Antarctic circumpolar zonal wind intensity. *Ann. Glaciol.*, **41**: 121-130 (2005).

Yasunari, T. and Kodama, S. Intraseasonal variability of katabatic wind over east Antarctica and planetary flow regime in the southern hemisphere. *J. Geophys. Res.* **98**(D7), 13063–13070 (1993).

Yuan, X. ENSO-related impacts on Antarctic sea ice: A synthesis of phenomenom and mechanisms. *Ant. Sci.*, **16**(4): 415-425 (2004).

Z

Zhai, M., Li, X., Hui, F., Cheng, X., Heil, P., Zhao, T. and Liu, J. Sea-ice conditions in the Adélie Depression, Antarctica, during besetment of the icebreaker RV Xuelong. *Ann. Glaciol.*, **56**(69), 160 (2015).

Zielinski, U. and Gersonde, R. Diatom distribution in Southern Ocean surface sediments (Atlantic sector): Implications for paleoenvironmental reconstructions. *Palaeogeog., Palaeoclim., Palaeoecol.*, **129**: 213-250 (1997).

Zitto, M. E., Barrucand, M. G., Piotrkowski, R., and Canziani, P. O. 110 years of temperature observations at Orcadas Antarctic Station: multidecadal variability. *Int. J. Climatol.* (2015).

Annexes

Annexe 1 - Informations, figures et tables supplémentaires relatives à l'article I

Supplement Note 1

We have focused on the relationships and response of sea surface conditions, through satellite data, to atmospheric forcings inferred from automatic weather forecast measurements in the region of Dumont D'Urville (Supplementary Fig. 1). The four seasons (DJF, MAM, JJA and SON) are considered independently. We decided to not take in consideration the seasonal lagged response that may exist between atmospheric forcings and sea ice conditions as this is beyond the scope of this study. Only significant correlation are shown, but high level non significant relationship (>± 0,200) between parameters are also discussed here.

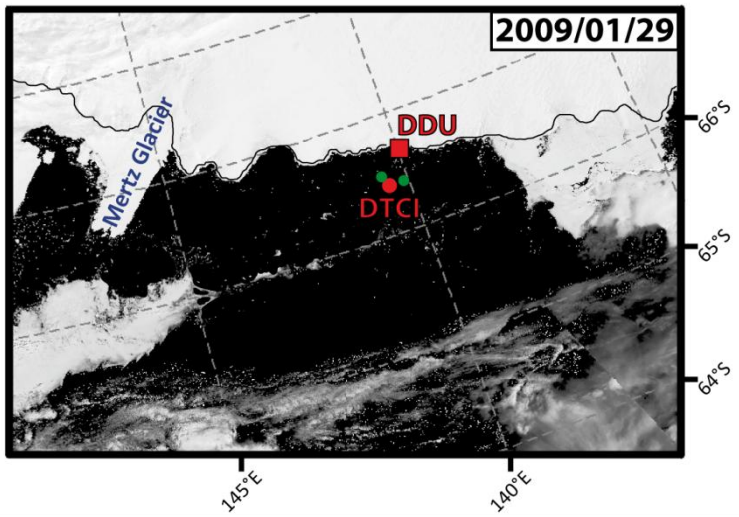

Supplement Figure 1: Location of satellite data pixels. MODIS satellite image (2009/01/29) of the Georges V Land indicating the grid points (green spots; -66,5481; 140,5149 and -66,4065; 140,0883) used for the extraction of the daily sea ice concentration values. The red spot indicates the DTCI core location, and the red square marks the Dumont D'Urville french station.

In spring (September to November, SON), wind direction displays positive relationship with the sea ice retreat date (Suppl. Table 1), indicating that more easterly (westerly) winds tend to promote early (late) sea ice melting, as observed for the summer period (see below). Spring SIC are positively linked with the sea ice retreat date and negatively related to the ice free season (Suppl. Table 1). Finally, wind speed is positively associated with spring temperatures (Suppl. Table 1), indicating that weak winds are cooler than strong ones for the season.

In summer (December to February, DJF), wind speed is significantly negatively correlated to wind direction (-0,601;Suppl. Table 1) indicating that more easterly winds are stronger than south to westerly ones in the area. Katabatic winds extend only to a limited distance over the open ocean during the summer season, due to less gravitational flow, whereas in winter with the sea ice cover, katabatic winds are not constrained and extend offshore (Pettré and Parish, 1993). Therefore, the opposite relationship we observed between wind speed and direction might reflect the increasing contribution of the more along shore wind pattern through the East Wind Drift, due to soften (meridional) katabatic winds in summer (Wendler et al., 1997). Additionally, a strong relationship exists between the summer wind direction and the sea ice retreat date while the wind speed displays an opposite relationship with the timing of sea ice retreat. The wind direction in summer is further negatively linked to temperatures and the length of the ice free season, suggesting that more easterly (westerly) winds would tend to be associated with higher (lower) temperatures and longer (shorter) ice free season. Additionally, wind speed displays opposite relationships with timing of sea ice advance, which in turn appears positively linked to summer temperature. These results suggest that a stronger easterly (weaker westerly) winds in spring-summer promote earlier (later) sea ice retreat in our study area. Results regarding the sea ice advance date and atmospheric parameters appear contradictory (see above), but looking at their relationships is question able as sea ice waxing conditions are attributable to the autumn and not summer period (see below). Unsurprisingly, summer SIC is significantly negatively correlated to the length of the ice free season (-0,868) and significantly positively correlated to the sea ice retreat date (0,930).

For the autumn period, wind speed is positively linked to wind direction, and displays a significant negative correlation with SIC (-0,472;Suppl. Table 1) and a significant positive correlation with the closing date (0,360). These results would suggest that easterly (westerly) winds are weaker (stronger) over the March to May period. In autumn, the katabatic phase becomes stronger due to the strengthening of the surface inversion, which results in a more downslope (increasing) wind direction (Wendler et al., 1997), likely explaining the opposite relationship between wind direction and speed we found in summer (see above). Additionally, our results show that years characterized by weaker easterly (stronger south to westerly) winds in autumn would be associated by increasing (decreasing) sea ice conditions and subsequently advanced (delayed) sea ice closing. Such sea ice conditions are further associated to low (high) temperatures in our study area, as this latter exerts negative relationship with SIC and positive link with the wind speed along with the closing time period. However, satellite data of SIC does not allow to discriminate if increasing SIC in autumn is due to increasing sea ice presence or sea ice formation in the area, whose characteristics may have large impacts on water column stratification through the dense water formation process. Unsurprisingly, for the autumn period SIC are significantly negatively correlated with the sea ice advance date (-0,917) and the length of the ice free season (-0,425).

During the winter season, the wind speed displays a positive correlation with the temperature (0.542;Suppl. Table 1), indicating that strong (weak) winds are associated to warmer (cooler) temperature. Interestingly, although the winter wind direction is not significantly correlated to winter wind speed and temperature, it displays high positive relationship with both, implying

that easterly winds are weaker and cooler in winter than westerly winds in the region. This might reflects the contribution of storms crossing the Adélie Land coastal area and bringing moist warmer air under a more westerly regime (Wang et al., 2014). SIC during winter are negatively linked with wind speed and temperature (Suppl. Table 1), suggesting that weak cold winds would promote increase of SIC.

Seasonal responses of sea ice conditions to atmospheric forcings highlight that summer and autumn display the highest correlations/relationships with weather forecast/satellite data, likely because both seasons at high latitude experience much of the environmental variability through the sea ice melting and regrowth. Opposite response of sea surface conditions further occurs between summer and autumn in our PCA, as stronger easterly (weak westerly) winds would reduce (increase) sea ice conditions in summer at the core site but increase (reduce) sea ice conditions during autumn. Relationship between wind conditions (notably wind direction) and temperature varies seasonally in our data, but it seems that for any season wind speed is negatively linked to temperature.

Supplement Note 2

Sea ice proxies

The *Banquisia* gp is composed by sea ice dwelling diatoms such as *Navicula directa*, *N. glaciei*, *Synedra* spp and *Ephemera* spp (Annett et al., 2010;Torstensson et al., 2012). These species are all localized in the F2- area (Fig. 38). *Navicula directa* is positively correlated to *Ephemera* spp (0,181;Suppl. Table 2), and *N. glaciei* is positively correlated to *Synedra recta* (0,265). Only *Entomoneis* spp and *Synedra fragilis*, known to be sea ice related, are located at the opposite in the F2+ axis and are not correlated to other species. We nonetheless chose to include them in the *Banquisia* gp as their low abundances may bias the PCA results. Combined relative abundances of the species included in the *Banquisia* gp are less than 2% of the total diatom assemblages (species noted in grey in Fig. 38), they were not compared with meteorological parameters.

Fragilariopsis obliquecostata has been associated with surface melt pools and with the water column under sea ice (Garrison, 1991; Armand et al., 2005; Gersonde et al., 2000). *Fragilariopsis obliquecostata* is often associated to other cold water *Fragilariopsis* species such as *F. ritscheri* and *F. sublinearis* in the literature, and they were found to present similar Holocene recordsas *F. curta*in the region (Crosta et al., 2008). On the PCA, *F. obliquecostata* is localized in the F1+/F2- quarter (Fig. 38) and displays its highest significant correlation with *F. rhombica* (0.454;Suppl. Table 2) and *Eucampia antarctica* (0.378) for example. *Fragilariopsis obliquecostata* is however not significatively related to *F. ritscheri* and *F. sublinearis* in our study area, conversely to what is presented in the literature.

The *Fragilariopsis* summer group combines *F. ritscheri* and *F. sublinearis*. Highest abundance of *F. ritscheri* is observed with SST ranging 0-3°C and can support a wide range

of an annual sea ice duration from 2 to 10.5 months, with a peak around 9 month/yr (Armand et al., 2005). Although *F. ritscheri* has been observed in surface melt pools, land-fast and pack-ice samples (Tanimura et al., 1990), it has been found in higher abundances in the adjacent water column than in sea ice samples (Gersonde, 1984), suggesting that this species potentially prefers melt water conditions (Armand et al., 2005). From its surface sediment occurrence, *F. sublinearis* have been related close to and at, the summer sea-ice edge, in areas characterized by year-round sea ice influence and summer surface water temperatures <−1°C (Zielinski and Gersonde, 1997; Gersonde et al., 2000). Both species have found to co-occur with other *Fragilariopsis* spp in the sea ice assemblage in Antarctic Peninsula (Crosta et al., 2008).*Fragilariopsis ritschieri* and *F. sublinearis* are both significantly located in the F1+/F2+ and in the F1+/F2- axes respectively (Fig. 38). Pearson correlation coefficient reveals that both species are highly positively correlated (0,501;Suppl. Table 2) in agreement with previous studies. *Fragilariopsissublinearis*is significantly correlated to*F. curta* (0.234), along with summer and autumn associated species (e.g. *T. antarctica*: 0.234; *E. antarctica*: 0.223). However, unlike in paleoclimate studies (Crosta et al., 2008), *F. sublinearis* and *F. ritschieri* display negative and significant correlation with *F. cylindrus* (-0.359 and 0.346, respectively) and show no relationship with *F. obliquecostata*.

Distribution pattern of *Eucampia antarctica* in surface sediments, along with Holocene sediment, indicates that the species is ubiquist and that its spatial distribution shows no clear relationship with the distribution of sea ice (Crosta et al., 1998; Zielinski and Gersonde, 1997; Crosta et al., 2008)probably because previous studies lumped together the two varieties *E. antarctica* var *antarctica* (“warm” variety) and *E. antarctica* var *recta* (“cold” variety). In core DTCI2010, only specimens of *E. antarctica* var *recta* were encountered. *Eucampia antarctica* is located on the F1+/F2- (Fig. 38), and presents significant positive correlation with several large centric diatoms (e.g. *Porosira glacialis*: 0.234; *Thalassiosira lentiginosa*: 0.260; Suppl. Table 2) and with *F. rhombica* (0.373). These results agree with the literature as the seasonal progression of diatom assemblages in surface waters over the Antarctic Peninsula suggests a concomitant occurrence of *E. antarctica* and large centrics diatoms (e.g. genera *Porosira*, *Stellarima* and *Thalassiosira*), which increases through the ice free season (Annett et al., 2010).

Open ocean proxies

The *Rhizosolenia* gp is composed of *Rhizolenia* spp and *Proboscia* spp (Fig. 38). Both genera belong to the same family (*Rhizosoleniaceae*). *Rhizosolenia* spp and *Proboscia* spp are generally associated to late summer season production, long diatom productivity season, linked with open ocean conditions (Armand et al. 2005; Crosta et al. 2005; Maddison et al. 2006; Willmott et al., 2010). Undetermined *Rhizosolenia* spp were observed around the Astrolabe Glacier, closely linked to mixed waters with higher surface densities and nutrient levels (Beans et al., 2008).*Rhizosolenia* spp thrive better in mixed waters than the smaller pennate diatoms due to drag-inducing adaptations that reduce their sinking rate compared to needle-like morphology. They can also regulate buoyancy to move between shallow high light

and deeper high nutrient areas of the water column (Kemp et al., 2000; Annett et al., 2010). Stickley *et al*. (2005) connected the occurrence of *Proboscia* spp in Iceberg Alley, East Antarctica, with an open ocean provenance and, thus, an increasing influence of offshore waters in this area. Similarly, Maddison et al. (2006) suggested that the presence of *P. inermis* in sediments in our study area constitutes a signal for warmer oligotrophic waters onto the shelf. As such, it is possible that the *Rhizosolenia* gp can survive in stable, nutrient poor surface waters associated to a strong seasonal thermocline and nutricline. The mass sinking of those diatoms (the ‘‘fall dump’’), is triggered by the breakdown of the water column stratification, therefore implying that *Rhizosolenia* gp may also indicates rapid deposition (Kemp *et al*. 2000; Taylor et al., 2002). *Proboscia inermis* and *Rhizosolenia* spp (here strongly dominated by *R. antennata* var *semispina*) are significantly located on the F1-/F2- area, while *P. truncata* is situated in the F1+/F2- area (Fig. 38). Pearson coefficient correlation confirms their positive relationship by indicating significant positive correlation between *P. truncata* and *P. inermis* (0,250; Suppl. Table 2) and between *Rhizosolenia* spp and *P. inermis* (0,639). Although *P. alata* is in the F1+/F2- axes (Fig. 38), Pearson coefficient correlation points a significant positive correlation between *P. truncata* and *P. alata* (0,261). From this and from the known similar ecologial preferences (see above), we decide to include all these species in the *Rhizosolenia* gp.

The *Thalassiothrix* gp is composed by *T. antarctica* and *Trichotoxon reinboldii.* Both species are found in low abundance in Holocene Antarctic shelf sediments (Crosta et al., 2008). Similarly to the *Rhizosolenia* gp, species from the *Thalassiothrix* gp are likely linked to a long diatom productivity season, and are an indicator for rapid deposition and good preservation in sediment, as its needle-like frustules generally do not preserve well (Leventer et al., 1996). However, due to their ubiquitous distributions in sediment, these species are not considered as good environmental indicators (Zielinski et al., 1997). *Thalassiothrix antarctica* and *T. reinboldii* are respectively located in the F1+/F2- and in the F1+/F2+ axes (Fig. 38). The Pearson correlation between both species indicates significant positive value (0,303), arguing for their combination, as suggested in the litterature.

In surface sediment samples, highest abundances were of *F. rhombica* are related to ice free conditions in February and generally highly consolidated sea ice conditions in September (between 65 and 90% concentration), in regions where sea ice cover persisted for 7-9 month/yr (Armand et al., 2005). In Holocene sediment, Denis et al. (2006) suggests that *F. rhombica* replaced the *F. curta* during the warmer mid-Holocene relative to the colder Late Holocene, and many chains of *F. rhombica* were found *in situ* in the spring laminae during the Hypsithermal against few single cells during the Neoglacial. It is therefore believed that *F. rhombica* would replace *F. cylindrus* and *F. curta* in the spring assemblage when sea ice is less present during the spring/summer season (Armand et al., 2005). On the PCA, *F. rhombica* is situated in F1+/F2- (Fig. 38). PCA indicate *F. rhombica* does not displays any relationship with *F. curta,* but the species is significantly and negatively correlated with *F. cylindrus* (-0,239; Suppl. Table 2).

Wind and stratification conditions related proxies

The *Chaetoceros* subgenus *Phaeoceros* is common in open water environment (Kang and Fryxell, 1993). *Chaetoceros dichaeta and C.cryophilum* were found in water samples to be the most abundant species of the *C. Phaeoceros* genus in the study area (Beans et al., 2008). In Holocene sediment in Antarctic Peninsula, presence of *Phaeoceros* vegetative cells suggests an oceanic influence (Maddison et al., 2005) and,inthe region, *Phaeoceros* spp with *F. rhombica* and CRS in light laminae (Denis et al., 2006) possibly indicate a late spring bloom when sea ice retreated. Wherever possible, *Chaetoceros* cells were counted at the species level. Indetermined species of *Phaeoceros* (referred as *Phaeoceros* spp) along with *C. atlantica* and *C. dichaeta* are positioned in the F1-/F2+ axes while *C. cryophilum* is situated at the opposite in the F1+/F2- area and *C. bulbosum* is located on the F1-/F2- area (Fig. 38). Pearson coefficient correlations indicate that *C. atlantica* and *C.dichaeta* are significatively linked (0,424;Suppl. Table 2) as well as *Phaeoceros* spp and *C.dichaeta* (0,336). However no clear relationship occurs for *C. cryophilum* and *C. bulbosum*. Based on PCA and Pearson analyses, *Phaeoceros* gp in our study is composed by *C. Phaeoceros* spp*, C. atlantica* and *C. dichaeta. Phaeoceros* species are generally considered having similar ecological preferences and are grouped all together (Denis et al., 2006) or are not identified at the species levelin moststudies (Riaux-Gobin et al., 2013). However, our observations highlight that differences exist between species in term of seasonal to interannual behaviour, which should be investigated in more details in future studies. *Chaetoceros atlantica* and *C. dichaeta* present high significant correlations with *T. Antarctica* and some large centric diatoms, while *C. cryophilus* displays significant correlation with the *Thalassiothrix* gp and *F. kerguelensis* suggesting a summer production and/or open ocean origin.

Benthic diatoms were extremely rare in our samples. *Cocconeis* spp, *Grammatophora* spp, *Trachyneis* spp, *Licmophora* spp, *Melosira sol*, *M. adelia*, *Achnantes brevipes*, *Amphora* spp, *Diploneis* spp, *Pseudogomphonema* spp and *O. weissflogii* are epiphitic species (Al-Handaland Wulff, 2008). The benthic taxa is not commonly used use for paleoenvironmental interpretation as it constitutes the less well-documented taxa (Taylor et al., 2000). However, *Cocconeis* spp occur in water depths >10 m (Whitehead and McMinn, 1997) and form spring/summer blooms and diatom mats in the coastal subtidal zone (Krebs, 1983). The mats disintegrate by late spring as wind strength increases and sea ice breaks up (Krebs, 1983). In sediment traps from the northern Antarctic Peninsula, Leventer et al. (1991) recorded an autumn diatom assemblage with increasing benthic and ice-related species as being the coastal flora resuspended by autumn storms (Leventer, 1991). Therefore the benthic group may be taken as an indicator for storm frequency and intensity and/or wave action implying strong turbulences in the water column (Barbara et al., 2013), during the ice free season (Heil et al., 2006). *Achnantes* spp is positively correlated to *Cocconeis fasciolata* (0,233;Suppl. Table 2) and to *Diploneis* spp (0,289), *Amphora* spp and *Odontella weissflogii* are also positively correlated (0,281), same for *Melosira adelia* and *Pseudogomphonema* spp (0,171). All these species are located in the F1+ (Fig. 38). Although not been significantly correlated to the species cited above, *Grammatophora* spp, *Trachyneis* spp, *Cocconeis costata*, *Licmophora* spp and *Melosira sol* are also present in the F1+ area and were thus added into

the Benthic gp along with the other species mentioned . *Cocconeis fasciolata* is one of the most abundant species of this group despite relative abundances less than 1% of the total diatom assemblage. *Cocconeis fasciolata* presents significant positive correlation with several open water related taxa (e.g. *F. kerguelensis, T. antarctica* and *T. lentiginosa*) supporting a summer deposition of this group as suggested in the literature.

Corethron spp is typically associated with open ocean conditions (Armand et al. 2005; Crosta et al. 2005). As such, *C. criophilum* occurs in open water with little sea ice (Fryxell and Hasle, 1971). Beans et al. (2008) also observed that *C. pennatum* in the region showed a positive relationship with surface mixed waters as it would thrive better in this environment than the smaller pennate diatoms due to drag-inducing adaptations that reduce their sinking rate. This species is part of the shade flora (Kemp et al., 2000). In Holocene sediment, *Corethron* spp has been used to indicate disruption of the pycnocline associated to return of atmospheric perturbations during summer/autumn (Denis et al., 2006). Given the difficulties to identify them properly (low preservation of long appendices), we have grouped both species during the counting process. On the PCA, *Corethron* spp is positioned in the F1+/F2- quarter (Fig. 38). *Corethron* spp displays significant positive correlation with *F. rhombica and* the *Thalassiothrix* gp along with some species of the open water gp, and negative significant correlation with e.g. CRS and [HBI: 2] supporting a summer production as suggested in the literature.

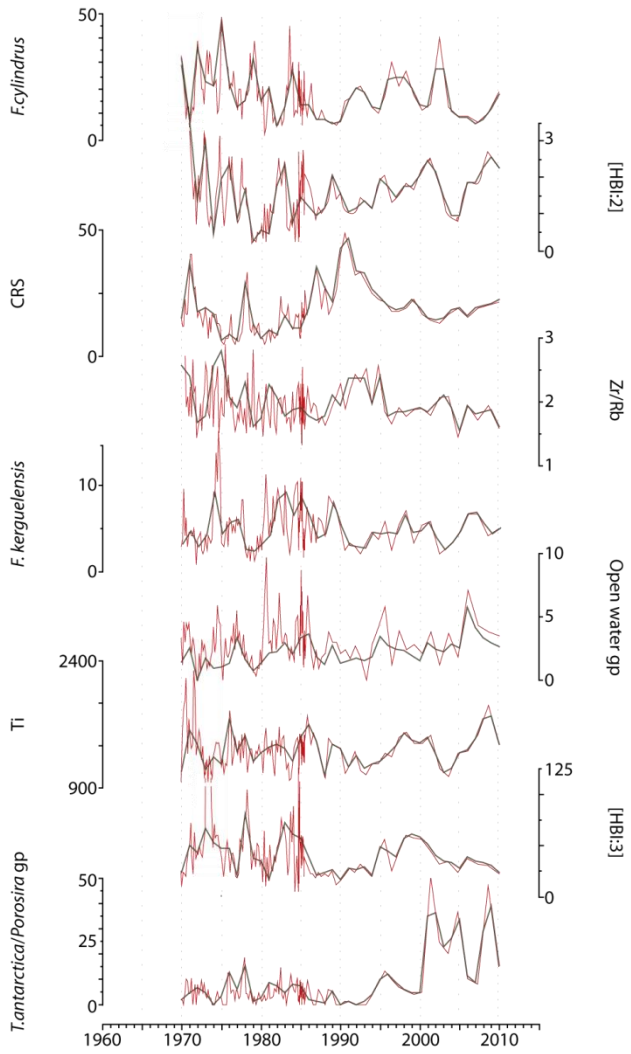

Supplement Figure 2: Raw versus standardised data. Raw data (red) and standardised data (grey) from the sediment core DTCI2010. Diatom relative abundances are expressed in (%), Titanium levels in (cps) and HBIs concentrations are expressed in ($\mu g.g^{-1}$).

Variables	Opening	Closing	MAM_sic	JJA_sic	SON_sic	DJF_sic	MAM_dir	JJA_dir	SON_dir	DJF_dir
Opening	1	0,051	0,060	-0,036	0,306	0,930	0,155	0,261	0,229	0,299
Closing	0,051	1	-0,917	-0,251	-0,121	0,009	0,202	-0,012	0,135	0,126
MAM_sic	0,060	-0,917	1	0,398	0,107	0,093	-0,307	0,023	-0,091	-0,074
JJA_sic	-0,036	-0,251	0,398	1	0,246	-0,045	-0,049	-0,020	-0,018	0,223
SON_sic	0,306	-0,121	0,107	0,246	1	0,278	0,329	0,184	0,158	0,374
DJF_sic	0,930	0,009	0,093	-0,045	0,278	1	0,019	0,192	0,182	0,140
MAM_dir	0,155	0,202	-0,307	-0,049	0,329	0,019	1	0,583	0,398	0,568
JJA_dir	0,261	-0,012	0,023	-0,020	0,184	0,192	0,583	1	0,679	0,728
SON_dir	0,229	0,135	-0,091	-0,018	0,158	0,182	0,398	0,679	1	0,586
DJF_dir	0,299	0,126	-0,074	0,223	0,374	0,140	0,568	0,728	0,586	1
MAM_speed	-0,068	0,360	-0,472	-0,263	-0,101	0,009	0,250	0,268	0,113	0,136
JJA_speed	0,196	0,154	-0,105	-0,295	0,254	0,211	0,172	0,304	0,314	0,157
SON_speed	0,072	0,219	-0,207	-0,121	-0,131	0,003	0,046	0,162	0,023	0,091
DJF_speed	-0,208	-0,236	0,189	-0,100	-0,086	-0,086	-0,299	-0,304	-0,230	-0,601
MAM_temp	0,369	0,419	-0,453	-0,218	0,025	0,344	0,154	0,075	0,226	0,049
JJA_temp	0,340	0,283	-0,244	-0,271	0,274	0,246	0,319	0,220	0,350	0,356
SON_temp	0,101	0,292	-0,247	-0,154	-0,094	0,060	0,073	-0,187	-0,195	0,038
DJF_temp	-0,022	0,216	-0,296	-0,250	-0,057	-0,088	0,103	-0,078	0,125	-0,254

Variables	MAM_speed	JJA_speed	SON_speed	DJF_speed	MAM_temp	JJA_temp	SON_temp	DJF_temp
Opening	-0,068	0,196	0,072	-0,208	0,369	0,340	0,101	-0,022
Closing	0,360	0,154	0,219	-0,236	0,419	0,283	0,292	0,216
MAM_sic	-0,472	-0,105	-0,207	0,189	-0,453	-0,244	-0,247	-0,296
JJA_sic	-0,263	-0,295	-0,121	-0,100	-0,218	-0,271	-0,154	-0,250
SON_sic	-0,101	0,254	-0,131	-0,086	0,025	0,274	-0,094	-0,057
DJF_sic	0,009	0,211	0,003	-0,086	0,344	0,246	0,060	-0,088
MAM_dir	0,250	0,172	0,046	-0,299	0,154	0,319	0,073	0,103
JJA_dir	0,268	0,304	0,162	-0,304	0,075	0,220	-0,187	-0,078
SON_dir	0,113	0,314	0,023	-0,230	0,226	0,350	-0,195	0,125
DJF_dir	0,136	0,157	0,091	-0,601	0,049	0,356	0,038	-0,254
MAM_speed	1	0,118	0,315	0,116	0,294	-0,024	0,346	-0,106
JJA_speed	0,118	1	0,107	0,070	-0,018	0,542	-0,187	0,168
SON_speed	0,315	0,107	1	0,092	0,258	0,166	0,263	0,004
DJF_speed	0,116	0,070	0,092	1	-0,243	-0,397	-0,037	0,044
MAM_temp	0,294	-0,018	0,258	-0,243	1	0,389	0,030	0,423
JJA_temp	-0,024	0,542	0,166	-0,397	0,389	1	0,049	0,336
SON_temp	0,346	-0,187	0,263	-0,037	0,030	0,049	1	-0,159
DJF_temp	-0,106	0,168	0,004	0,044	0,423	0,336	-0,159	1

Supplement Table 1:Pearson matrix of coefficient correlation, from the PCA between seasonal (3 months) averaged meteorological parameters.

Variables	[HBI:2]	HBI:2]/[HBI:3	[HBI:3]	. actinochylus	A. Curvatulus	A. hookerii	A. hyalinus	Acnanthes spp	Amphora spp
[HBI:2]	1	0,797	-0,043	0,170	0,142	-0,145	0,047	0,037	-0,011
[HBI:2]/[HBI:3]	0,797	1	-0,336	0,146	0,190	-0,188	-0,021	-0,054	-0,042
[HBI:3]	-0,043	-0,336	1	-0,003	-0,056	0,192	0,005	0,064	-0,006
A. actinochylus	0,170	0,146	-0,003	1	0,024	0,083	-0,033	0,095	-0,076
A. Curvatulus	0,142	0,190	-0,056	0,024	1	-0,060	-0,030	-0,091	-0,002
A. hookerii	-0,145	-0,188	0,192	0,083	-0,060	1	0,072	0,119	-0,060
A. hyalinus	0,047	-0,021	0,005	-0,033	-0,030	0,072	1	0,091	-0,069
Acnanthes spp	0,037	-0,054	0,064	0,095	-0,091	0,119	0,091	1	-0,036
Amphora spp	-0,011	-0,042	-0,006	-0,076	-0,002	-0,060	-0,069	-0,036	1
C. atlantica	-0,040	0,016	-0,109	-0,078	-0,082	0,028	0,113	0,075	-0,045
C. bulbosum	0,013	-0,016	0,096	-0,014	0,015	0,232	0,190	0,212	0,098
C. costata	0,124	0,078	0,086	0,226	0,034	-0,078	-0,104	-0,129	-0,074
C. cryophilum	-0,190	-0,169	-0,118	0,144	0,128	-0,018	-0,045	0,074	-0,022
C. dichaeta	0,080	0,085	-0,140	-0,068	-0,033	-0,190	0,002	0,033	-0,039
C. fasciolata	0,161	0,068	-0,032	0,122	-0,027	0,084	0,059	0,233	-0,067
C. hyalochaete RS	0,104	0,123	-0,167	-0,144	-0,119	-0,201	-0,146	-0,012	-0,088
C. Phaeoceros gp	0,122	0,110	-0,073	-0,044	0,013	-0,017	-0,035	-0,049	-0,071
Ch. cryophilus	0,149	0,213	-0,105	0,039	0,041	0,062	0,021	-0,071	-0,015
Cocconeis spp	0,022	-0,042	0,047	0,151	0,065	-0,057	0,063	-0,074	0,248
Coscinodiscus spp	0,084	0,021	0,020	0,244	0,013	-0,046	-0,009	0,035	0,103
Diploneis spp	-0,035	0,042	-0,101	0,034	-0,067	-0,006	0,040	0,289	-0,027
E. antarctica	0,057	0,022	-0,155	0,156	-0,007	-0,031	-0,016	0,032	0,010
Entomoneis spp	0,004	-0,041	0,014	-0,167	0,194	-0,045	-0,090	-0,048	-0,027
Ephemera spp	0,096	0,021	0,044	-0,119	0,095	0,066	0,183	0,008	-0,066
F. curta	0,018	-0,021	0,131	0,122	0,033	0,158	-0,017	0,038	-0,101
F. cylindrus	-0,124	-0,062	0,189	-0,233	0,007	-0,082	-0,015	-0,146	0,123
F. kerguelensis	0,128	0,046	-0,042	0,164	-0,031	0,264	0,255	0,243	-0,029
F. obliquecostata	-0,116	-0,090	-0,137	0,077	0,216	-0,113	-0,072	-0,099	0,152
F. peragalli	0,051	-0,021	0,056	-0,074	-0,030	-0,077	0,083	-0,021	-0,012
F. pseudonana	-0,043	-0,073	0,256	-0,121	0,027	0,151	0,166	-0,043	0,070
F. rhombica	-0,245	-0,169	-0,118	0,102	0,060	-0,013	-0,071	-0,013	-0,030
F. ritscherii	-0,148	-0,177	-0,071	0,029	-0,099	-0,046	-0,049	0,334	0,102
F. separanda	-0,054	-0,117	0,110	-0,081	-0,052	0,386	0,281	0,072	-0,063
F. sublinearis	-0,063	-0,123	-0,037	0,153	0,014	-0,033	-0,089	0,056	-0,002
F. vanheurckii	-0,005	0,090	-0,144	0,013	-0,070	0,071	-0,081	0,081	0,027
Gramatophora spp	-0,009	-0,031	-0,014	0,006	0,204	-0,058	-0,057	-0,030	-0,017
Licmophora spp	-0,053	0,022	-0,070	-0,037	-0,069	-0,109	0,133	-0,048	-0,027
M. adelia	0,451	0,366	-0,033	0,045	0,091	-0,137	-0,032	-0,038	-0,086
M. sol	0,199	0,181	-0,059	0,195	-0,021	0,093	0,073	0,064	-0,059
N. directa	0,056	0,124	-0,024	0,001	0,082	0,001	-0,001	-0,010	0,008
N. glaciei	0,108	0,121	-0,068	-0,139	0,055	-0,184	0,129	-0,075	0,064
Nitzschia spp	-0,029	-0,044	0,030	0,110	-0,086	0,194	-0,077	-0,082	-0,007
O. weissflogii	0,036	-0,040	0,107	-0,012	0,193	-0,051	0,011	0,104	0,281
P. alata	0,206	0,154	0,001	0,060	-0,042	0,089	0,139	0,109	0,012
P. glacialis	0,146	0,095	-0,097	0,225	0,026	0,004	0,149	0,007	0,121
P. inermis	-0,209	-0,244	0,635	-0,032	-0,077	0,241	0,076	-0,074	0,054
P. pseudodenticulata	-0,076	-0,144	0,104	-0,008	0,074	-0,026	-0,003	-0,032	-0,029
P. tronca	0,010	0,124	0,103	0,092	0,137	0,142	0,046	-0,124	0,097
Pseudogomphonema spp	0,266	0,262	-0,009	0,132	0,105	-0,090	-0,001	-0,020	-0,054
Pseudo-nitschia spp	-0,010	0,087	-0,042	-0,295	0,097	0,128	0,016	-0,124	-0,052
Rhizosolenia spp	-0,117	-0,177	0,491	0,097	-0,068	0,081	-0,031	-0,018	0,077
S. fragilis	0,198	0,152	-0,089	0,162	-0,135	0,027	0,104	-0,026	-0,054
S. microtrias	0,003	-0,020	-0,104	0,027	0,031	-0,082	-0,026	0,008	0,095
S. recta	-0,092	-0,076	-0,050	-0,084	0,144	0,007	0,005	-0,087	0,164
T. antarctica	0,218	0,087	-0,101	0,224	0,058	-0,080	0,237	0,133	0,053
T. frenguelli	-0,128	-0,082	0,091	0,075	-0,061	-0,047	0,168	-0,043	-0,024
T. gracilis	0,163	0,101	0,026	0,218	-0,064	0,297	0,096	0,116	-0,038
T. gravida	-0,138	-0,102	0,127	-0,018	-0,223	0,300	0,040	0,170	-0,098
T. lentiginosa	0,110	0,042	-0,195	0,330	-0,140	0,173	0,087	0,149	0,060
T. oliverana	-0,037	0,002	-0,157	0,166	-0,168	-0,006	-0,092	-0,069	-0,067
T. ritscheri	0,028	-0,009	0,123	0,142	0,033	0,100	-0,004	-0,018	-0,013
T. toxon	0,178	0,079	-0,053	-0,026	-0,139	0,033	0,051	0,077	-0,067
T. trifulta	0,002	-0,012	-0,070	0,152	0,039	-0,077	0,106	0,197	0,191
T. tumida	0,147	0,044	-0,049	0,125	0,033	0,072	0,052	-0,135	0,004
Ti	0,372	0,394	-0,218	0,150	0,063	-0,130	0,044	0,071	-0,033
Trachyneis spp	0,080	0,056	-0,040	0,044	0,001	-0,078	0,219	-0,038	-0,022
Tx. antarctica	0,000	-0,040	-0,162	0,283	-0,034	0,009	0,036	0,183	-0,012
Zr/Rb	0,060	0,063	0,081	0,023	0,024	-0,077	-0,226	-0,068	0,009

Variables	C. atlantica	C. bulbosum	C. costata	C. cryophilum	C. dichaeta	C. fasciolata	hyalochaete	Phaeoceros g	Ch. cryophilus
[HBI:2]	-0,040	0,013	0,124	-0,190	0,080	0,161	0,104	0,122	0,149
[HBI:2]/[HBI:3]	0,016	-0,016	0,078	-0,169	0,085	0,068	0,123	0,110	0,213
[HBI:3]	-0,109	0,096	0,086	-0,118	-0,140	-0,032	-0,167	-0,073	-0,105
A. actinochylus	-0,078	-0,014	0,226	0,144	-0,068	0,122	-0,144	-0,044	0,039
A. Curvatulus	-0,082	0,015	0,034	0,128	-0,033	-0,027	-0,119	0,013	0,041
A. hookerii	0,028	0,232	-0,078	-0,018	-0,190	0,084	-0,201	-0,017	0,062
A. hyalinus	0,113	0,190	-0,104	-0,045	0,002	0,059	-0,146	-0,035	0,021
Acnanthes spp	0,075	0,212	-0,129	0,074	0,033	0,233	-0,012	-0,049	-0,071
Amphora spp	-0,045	0,098	-0,074	-0,022	-0,039	-0,067	-0,088	-0,071	-0,015
C. atlantica	1	0,145	0,110	-0,118	0,424	0,082	0,082	0,032	0,061
C. bulbosum	0,145	1	0,021	-0,028	-0,113	0,075	-0,235	-0,077	0,094
C. costata	0,110	0,021	1	-0,019	-0,100	-0,053	0,007	-0,107	-0,093
C. cryophilum	-0,118	-0,028	-0,019	1	-0,061	-0,172	-0,277	-0,124	0,094
C. dichaeta	0,424	-0,113	-0,100	-0,061	1	0,179	0,156	0,336	0,112
C. fasciolata	0,082	0,075	-0,053	-0,172	0,179	1	0,026	0,016	0,004
C. hyalochaete RS	0,082	-0,235	0,007	-0,277	0,156	0,026	1	0,108	-0,333
C. Phaeoceros gp	0,032	-0,077	-0,107	-0,124	0,336	0,016	0,108	1	0,124
Ch. cryophilus	0,061	0,094	-0,093	0,094	0,112	0,004	-0,333	0,124	1
Cocconeis spp	-0,009	-0,083	0,047	0,085	-0,154	-0,004	-0,160	-0,080	-0,009
Coscinodiscus spp	-0,103	0,030	0,129	0,228	-0,160	-0,019	-0,065	-0,180	0,007
Diploneis spp	-0,038	0,083	-0,095	0,016	0,011	0,020	0,080	-0,055	-0,036
E. antarctica	0,037	0,094	0,166	0,363	-0,054	0,003	-0,206	-0,040	0,228
Entomoneis spp	-0,062	-0,050	-0,007	-0,005	0,088	0,060	0,165	0,325	-0,087
Ephemera spp	-0,048	0,155	-0,106	-0,090	-0,023	0,005	-0,118	0,075	0,050
F. curta	0,020	0,041	0,066	-0,140	-0,089	-0,073	-0,340	-0,138	-0,011
F. cylindrus	-0,061	0,155	-0,097	-0,051	-0,004	-0,165	-0,271	-0,087	0,026
F. kerguelensis	-0,049	0,171	-0,014	-0,094	-0,227	0,261	-0,248	-0,033	0,214
F. obliquecostata	-0,084	0,066	0,076	0,377	-0,077	-0,097	-0,384	-0,157	0,186
F. peragalli	-0,048	-0,049	-0,043	0,029	-0,070	-0,039	-0,010	-0,050	-0,002
F. pseudonana	-0,062	0,168	-0,131	-0,039	-0,109	-0,088	-0,278	-0,135	0,117
F. rhombica	-0,216	-0,037	0,089	0,442	-0,256	-0,080	-0,351	-0,146	0,026
F. ritscherii	-0,113	-0,045	0,017	0,181	-0,193	0,105	0,036	-0,212	-0,194
F. separanda	0,067	0,136	-0,093	-0,123	-0,054	0,000	-0,173	-0,067	0,065
F. sublinearis	0,042	-0,102	0,026	0,168	-0,096	0,250	-0,148	-0,207	-0,045
F. vanheurckii	-0,063	-0,148	-0,038	-0,027	-0,084	0,025	0,176	0,095	0,012
Gramatophora spp	-0,068	-0,070	-0,061	0,041	-0,014	-0,055	-0,101	0,015	0,067
Licmophora spp	0,041	-0,050	0,084	-0,046	0,014	0,109	0,079	-0,036	0,098
M. adelia	0,027	0,039	0,090	-0,033	-0,036	0,097	-0,078	0,128	0,235
M. sol	-0,083	-0,029	-0,014	0,007	-0,035	0,028	0,020	-0,039	-0,034
N. directa	0,007	-0,089	0,019	-0,099	0,004	-0,084	0,033	0,053	0,016
N. glaciei	-0,023	-0,045	0,031	-0,098	0,085	-0,064	-0,027	0,036	0,081
Nitzschia spp	0,089	0,009	0,011	0,086	-0,098	-0,074	-0,039	-0,062	0,032
O. weissflogii	0,035	-0,117	-0,102	0,112	-0,021	-0,015	-0,061	-0,044	-0,104
P. alata	-0,072	0,052	0,087	-0,003	-0,066	0,039	-0,073	-0,061	-0,019
P. glacialis	0,050	0,043	0,105	0,076	-0,068	0,085	-0,051	-0,092	0,001
P. inermis	-0,163	0,079	-0,014	-0,025	-0,174	-0,163	-0,261	-0,010	-0,078
P. pseudodenticulata	0,081	0,056	0,129	0,018	-0,078	0,054	-0,142	-0,167	-0,031
P. tronca	-0,077	-0,044	-0,072	-0,070	-0,061	-0,081	-0,311	0,054	-0,014
Pseudogomphonema spp	0,046	-0,048	0,085	-0,113	0,028	0,009	0,073	0,074	-0,064
Pseudo-nitschia spp	0,028	0,102	-0,190	-0,104	-0,042	-0,209	-0,151	0,065	0,195
Rhizosolenia spp	-0,112	0,031	-0,044	-0,022	-0,063	0,075	-0,180	0,104	0,086
S. fragilis	-0,012	-0,134	0,101	-0,039	-0,077	-0,002	0,054	0,052	0,170
S. microtrias	0,214	-0,074	0,041	0,094	0,014	0,002	-0,032	0,026	0,012
S. recta	-0,060	-0,106	-0,130	0,191	-0,042	-0,122	-0,132	-0,127	0,042
T. antarctica	0,299	-0,061	0,098	0,001	0,303	0,381	0,083	0,066	-0,010
T. frenguelli	0,026	0,036	-0,087	-0,088	0,023	0,004	-0,100	-0,121	0,005
T. gracilis	-0,080	0,047	0,008	-0,180	-0,143	0,063	-0,140	-0,046	0,069
T. gravida	-0,054	0,227	-0,052	-0,148	-0,167	0,031	0,029	-0,162	-0,123
T. lentiginosa	-0,100	-0,039	-0,002	0,187	-0,088	0,234	-0,072	-0,153	0,163
T. oliverana	0,071	-0,101	0,095	0,067	0,164	0,184	0,052	-0,007	0,089
T. ritscheri	0,165	-0,119	0,055	-0,014	0,230	0,049	0,052	0,050	0,051
T. toxon	-0,072	-0,050	-0,148	0,130	-0,028	0,100	-0,062	0,025	0,139
T. trifulta	0,076	0,067	-0,103	0,074	0,078	-0,043	-0,210	-0,072	0,042
T. tumida	0,017	-0,063	-0,015	0,139	0,043	0,095	-0,158	0,007	0,144
Ti	0,096	-0,013	0,176	0,027	0,125	0,086	0,087	0,147	0,167
Trachyneis spp	0,015	-0,003	-0,077	0,110	0,226	-0,018	0,077	0,021	-0,058
Tx. antarctica	-0,115	-0,043	-0,099	0,298	-0,083	0,112	-0,131	-0,040	0,186
Zr/Rb	-0,096	0,003	0,112	-0,067	0,022	-0,218	0,059	0,012	-0,060

Variables	Cocconeis spp	scinodiscus s	Diploneis spp	E. antarctica	ntomoneis sp	Ephemera spp	F. curta	F. cylindrus	F. kerguelensis
[HBI:2]	0,022	0,084	-0,035	0,057	0,004	0,096	0,018	-0,124	0,128
[HBI:2]/[HBI:3]	-0,042	0,021	0,042	0,022	-0,041	0,021	-0,021	-0,062	0,046
[HBI:3]	0,047	0,020	-0,101	-0,155	0,014	0,044	0,131	0,189	-0,042
A. actinochylus	0,151	0,244	0,034	0,156	-0,167	-0,119	0,122	-0,233	0,164
A. Curvatulus	0,065	0,013	-0,067	-0,007	0,194	0,095	0,033	0,007	-0,031
A. hookerii	-0,057	-0,046	-0,006	-0,031	-0,045	0,066	0,158	-0,082	0,264
A. hyalinus	0,063	-0,009	0,040	-0,016	-0,090	0,183	-0,017	-0,015	0,255
Acnanthes spp	-0,074	0,035	0,289	0,032	-0,048	0,008	0,038	-0,146	0,243
Amphora spp	0,248	0,103	-0,027	0,010	-0,027	-0,066	-0,101	0,123	-0,029
C. atlantica	-0,009	-0,103	-0,038	0,037	-0,062	-0,048	0,020	-0,061	-0,049
C. bulbosum	-0,083	0,030	0,083	0,094	-0,050	0,155	0,041	0,155	0,171
C. costata	0,047	0,129	-0,095	0,166	-0,007	-0,106	0,066	-0,097	-0,014
C. cryophilum	0,085	0,228	0,016	0,363	-0,005	-0,090	-0,140	-0,051	-0,094
C. dichaeta	-0,154	-0,160	0,011	-0,054	0,088	-0,023	-0,089	-0,004	-0,227
C. fasciolata	-0,004	-0,019	0,020	0,003	0,060	0,005	-0,073	-0,165	0,261
C. hyalochaete RS	-0,160	-0,065	0,080	-0,206	0,165	-0,118	-0,340	-0,271	-0,248
C. Phaeoceros gp	-0,080	-0,180	-0,055	-0,040	0,325	0,075	-0,138	-0,087	-0,033
Ch. cryophilus	-0,009	0,007	-0,036	0,228	-0,087	0,050	-0,011	0,026	0,214
Cocconeis spp	1	0,236	-0,054	0,129	-0,056	0,125	-0,045	-0,005	0,038
Coscinodiscus spp	0,236	1	0,037	0,305	-0,089	-0,052	-0,008	-0,203	0,026
Diploneis spp	-0,054	0,037	1	0,022	-0,035	0,056	-0,045	-0,094	0,026
E. antarctica	0,129	0,305	0,022	1	-0,004	-0,034	-0,054	-0,252	0,146
Entomoneis spp	-0,056	-0,089	-0,035	-0,004	1	-0,077	-0,147	0,022	-0,133
Ephemera spp	0,125	-0,052	0,056	-0,034	-0,077	1	-0,075	0,171	0,075
F. curta	-0,045	-0,008	-0,045	-0,054	-0,147	-0,075	1	-0,306	0,136
F. cylindrus	-0,005	-0,203	-0,094	-0,252	0,022	0,171	-0,306	1	-0,432
F. kerguelensis	0,038	0,026	0,026	0,146	-0,133	0,075	0,136	-0,432	1
F. obliquecostata	0,154	0,186	-0,031	0,378	-0,083	-0,085	0,040	-0,143	0,077
F. peragalli	-0,025	-0,039	-0,016	0,029	-0,016	0,072	-0,048	-0,038	0,150
F. pseudonana	-0,016	-0,193	-0,137	-0,180	-0,069	0,221	-0,183	0,535	0,063
F. rhombica	0,119	0,259	0,013	0,373	-0,088	-0,082	-0,051	-0,239	0,027
F. ritscherii	-0,044	0,215	0,278	0,083	-0,026	-0,219	0,114	-0,346	0,090
F. separanda	0,069	-0,131	0,019	-0,110	-0,110	0,102	0,225	-0,068	0,356
F. sublinearis	0,073	0,188	0,054	0,223	-0,012	-0,165	0,234	-0,349	0,138
F. vanheurckii	-0,128	-0,033	0,199	-0,116	-0,012	-0,141	0,037	-0,200	0,057
Gramatophora spp	-0,035	-0,056	-0,022	0,042	-0,023	0,102	0,063	-0,093	0,004
Licmophora spp	-0,056	-0,017	0,143	-0,004	-0,036	0,043	-0,016	-0,085	-0,016
M. adelia	-0,010	0,054	-0,067	0,264	-0,029	0,167	-0,016	-0,003	0,083
M. sol	-0,120	-0,075	0,020	0,063	-0,078	0,090	-0,099	-0,020	0,133
N. directa	0,178	-0,158	-0,049	-0,082	-0,081	0,181	0,050	0,083	-0,033
N. glaciei	0,028	-0,155	0,016	0,097	-0,029	0,135	-0,037	0,162	-0,117
Nitzschia spp	-0,022	0,002	-0,081	0,151	0,006	-0,016	0,055	-0,097	0,098
O. weissflogii	0,311	0,159	0,075	0,002	-0,038	-0,082	0,073	-0,162	0,088
P. alata	0,080	-0,007	0,021	0,065	-0,077	0,069	0,045	-0,063	0,293
P. glacialis	0,049	0,210	-0,059	0,234	0,062	-0,040	0,013	-0,303	0,235
P. inermis	0,041	-0,139	-0,078	-0,237	-0,074	0,128	0,010	0,353	-0,049
P. pseudodenticulata	0,051	0,004	0,081	0,046	0,263	-0,136	0,100	-0,040	0,074
P. tronca	0,259	-0,011	-0,091	-0,012	-0,093	0,155	0,130	-0,035	0,153
Pseudogomphonema spp	-0,067	0,019	-0,070	-0,045	-0,072	-0,150	0,144	-0,178	0,007
Pseudo-nitschia spp	-0,032	-0,247	-0,007	-0,208	-0,103	0,257	-0,038	0,337	-0,145
Rhizosolenia spp	0,136	0,029	-0,066	0,058	-0,040	-0,011	-0,143	0,093	0,097
S. fragilis	-0,053	-0,075	-0,069	0,004	-0,071	-0,011	0,048	-0,196	0,121
S. microtrias	0,107	0,211	0,024	0,155	-0,015	-0,138	0,120	-0,246	0,156
S. recta	0,289	-0,028	0,036	0,147	-0,066	0,027	-0,045	-0,058	-0,023
T. antarctica	0,081	0,100	-0,009	0,063	0,092	-0,118	-0,040	-0,363	0,184
T. frenguelli	-0,050	-0,079	-0,031	0,036	-0,032	0,079	0,099	0,049	-0,007
T. gracilis	-0,036	-0,080	-0,042	-0,038	-0,071	0,121	0,249	-0,216	0,485
T. gravida	0,000	0,040	0,157	-0,137	-0,129	0,061	0,092	0,036	0,001
T. lentiginosa	0,100	0,190	0,141	0,260	-0,137	0,068	-0,022	-0,378	0,507
T. oliverana	-0,136	0,032	0,074	0,234	0,046	-0,101	-0,143	-0,143	0,053
T. ritscheri	0,053	-0,055	-0,093	0,079	0,055	-0,109	0,088	-0,111	-0,011
T. toxon	-0,147	0,100	0,040	0,160	-0,086	0,082	0,092	-0,219	0,213
T. trifulta	0,032	0,174	0,106	0,130	0,015	-0,020	0,183	-0,200	0,136
T. tumida	0,076	0,105	-0,128	0,245	-0,031	0,041	0,137	-0,150	0,051
Ti	-0,033	-0,038	0,046	0,175	0,006	-0,019	-0,051	-0,283	0,248
Trachyneis spp	-0,044	0,114	-0,028	-0,092	-0,029	-0,025	0,033	-0,091	-0,035
Tx. antarctica	0,101	0,313	0,207	0,291	-0,162	-0,001	-0,008	-0,388	0,334
Zr/Rb	-0,150	-0,025	0,024	-0,034	0,125	0,097	0,011	0,151	-0,176

Variables	obliquecostat	F. peragalli	F. pseudonana	F. rhombica	F. ritscherii	F. separanda	F. sublinearis	F. vanheurckii	amatophora s
[HBI:2]	-0,116	0,051	-0,043	-0,245	-0,148	-0,054	-0,063	-0,005	-0,009
[HBI:2]/[HBI:3]	-0,090	-0,021	-0,073	-0,169	-0,177	-0,117	-0,123	0,090	-0,031
[HBI:3]	-0,137	0,056	0,256	-0,118	-0,071	0,110	-0,037	-0,144	-0,014
A. actinochylus	0,077	-0,074	-0,121	0,102	0,029	-0,081	0,153	0,013	0,006
A. Curvatulus	0,216	-0,030	0,027	0,060	-0,099	-0,052	0,014	-0,070	0,204
A. hookerii	-0,113	-0,077	0,151	-0,013	-0,046	0,386	-0,033	0,071	-0,058
A. hyalinus	-0,072	0,083	0,166	-0,071	-0,049	0,281	-0,089	-0,081	-0,057
Acnanthes spp	-0,099	-0,021	-0,043	-0,013	0,334	0,072	0,056	0,081	-0,030
Amphora spp	0,152	-0,012	0,070	-0,030	0,102	-0,063	-0,002	0,027	-0,017
C. atlantica	-0,084	-0,048	-0,062	-0,216	-0,113	0,067	0,042	-0,063	-0,068
C. bulbosum	0,066	-0,049	0,168	-0,037	-0,045	0,136	-0,102	-0,148	-0,070
C. costata	0,076	-0,043	-0,131	0,089	0,017	-0,093	0,026	-0,038	-0,061
C. cryophilum	0,377	0,029	-0,039	0,442	0,181	-0,123	0,168	-0,027	0,041
C. dichaeta	-0,077	-0,070	-0,109	-0,256	-0,193	-0,054	-0,096	-0,084	-0,014
C. fasciolata	-0,097	-0,039	-0,088	-0,080	0,105	0,000	0,250	0,025	-0,055
C. hyalochaete RS	-0,384	-0,010	-0,278	-0,351	0,036	-0,173	-0,148	0,176	-0,101
C. Phaeoceros gp	-0,157	-0,050	-0,135	-0,146	-0,212	-0,067	-0,207	0,095	0,015
Ch. cryophilus	0,186	-0,002	0,117	0,026	-0,194	0,065	-0,045	0,012	0,067
Cocconeis spp	0,154	-0,025	-0,016	0,119	-0,044	0,069	0,073	-0,128	-0,035
Coscinodiscus spp	0,186	-0,039	-0,193	0,259	0,215	-0,131	0,188	-0,033	-0,056
Diploneis spp	-0,031	-0,016	-0,137	0,013	0,278	0,019	0,054	0,199	-0,022
E. antarctica	0,378	0,029	-0,180	0,373	0,083	-0,110	0,223	-0,116	0,042
Entomoneis spp	-0,083	-0,016	-0,069	-0,088	-0,026	-0,110	-0,012	-0,012	-0,023
Ephemera spp	-0,085	0,072	0,221	-0,082	-0,219	0,102	-0,165	-0,141	0,102
F. curta	0,040	-0,048	-0,183	-0,051	0,114	0,225	0,234	0,037	0,063
F. cylindrus	-0,143	-0,038	0,535	-0,239	-0,346	-0,068	-0,349	-0,200	-0,093
F. kerguelensis	0,077	0,150	0,063	0,027	0,090	0,356	0,138	0,057	0,004
F. obliquecostata	1	-0,028	-0,132	0,454	0,117	-0,111	0,155	-0,189	0,160
F. peragalli	-0,028	1	-0,023	0,005	0,074	0,090	0,080	-0,056	-0,010
F. pseudonana	-0,132	-0,023	1	-0,156	-0,332	0,093	-0,319	-0,130	0,042
F. rhombica	0,454	0,005	-0,156	1	0,248	-0,123	0,196	-0,058	0,168
F. ritscherii	0,117	0,074	-0,332	0,248	1	-0,112	0,501	0,299	0,009
F. separanda	-0,111	0,090	0,093	-0,123	-0,112	1	-0,038	-0,179	-0,020
F. sublinearis	0,155	0,080	-0,319	0,196	0,501	-0,038	1	0,178	0,138
F. vanheurckii	-0,189	-0,056	-0,130	-0,058	0,299	-0,179	0,178	1	0,056
Gramatophora spp	0,160	-0,010	0,042	0,168	0,009	-0,020	0,138	0,056	1
Licmophora spp	-0,036	-0,016	-0,028	0,106	0,027	-0,047	0,007	0,104	-0,023
M. adelia	0,083	-0,050	0,033	-0,052	-0,145	-0,068	-0,021	-0,077	0,089
M. sol	-0,022	-0,035	0,125	-0,048	-0,087	0,032	-0,053	-0,023	-0,049
N. directa	-0,126	-0,077	0,139	-0,189	-0,200	0,035	-0,126	0,046	-0,036
N. glaciei	0,114	-0,039	0,032	-0,101	-0,208	-0,047	-0,121	-0,115	-0,055
Nitzschia spp	-0,001	-0,037	0,063	-0,040	0,048	0,066	0,073	-0,031	-0,052
O. weissflogii	0,141	-0,017	-0,096	0,041	0,136	-0,063	0,104	-0,012	-0,024
P. alata	-0,070	-0,034	0,142	-0,072	-0,137	0,304	0,028	-0,067	-0,048
P. glacialis	0,141	0,143	-0,160	0,051	0,129	-0,034	0,255	0,004	0,081
P. inermis	-0,097	-0,022	0,412	-0,090	-0,224	0,080	-0,203	-0,051	0,032
P. pseudodenticulata	0,115	0,055	-0,147	0,101	0,063	0,038	0,208	-0,202	-0,004
P. tronca	0,124	-0,041	0,173	0,155	-0,112	0,169	0,021	-0,141	0,197
Pseudogomphonema spp	-0,018	-0,032	-0,129	-0,009	0,107	-0,036	0,122	-0,086	-0,045
Pseudo-nitschia spp	-0,093	-0,110	0,198	-0,007	-0,230	0,071	-0,331	-0,030	-0,048
Rhizosolenia spp	0,053	0,005	0,146	-0,026	-0,150	-0,042	0,046	-0,038	0,038
S. fragilis	-0,060	-0,031	-0,005	-0,040	0,029	-0,037	0,011	0,122	-0,044
S. microtrias	0,100	0,010	-0,194	-0,008	0,065	-0,021	0,132	-0,007	-0,029
S. recta	0,258	0,431	0,035	0,222	0,006	-0,008	0,165	-0,073	0,122
T. antarctica	0,029	0,115	-0,271	-0,212	0,054	0,032	0,234	0,057	0,032
T. frenguelli	0,013	-0,014	0,033	0,039	-0,110	-0,063	0,052	-0,065	-0,020
T. gracilis	-0,206	-0,010	0,134	-0,068	-0,049	0,269	-0,013	0,012	-0,099
T. gravida	-0,084	-0,057	-0,069	-0,035	0,037	0,164	-0,163	-0,048	-0,081
T. lentiginosa	0,056	0,073	-0,157	0,079	0,155	0,035	0,092	0,101	-0,103
T. oliverana	0,087	-0,039	-0,189	0,028	0,029	-0,136	0,191	-0,075	-0,055
T. ritscheri	-0,019	0,031	-0,020	-0,140	-0,091	0,171	0,039	-0,066	-0,029
T. toxon	0,055	0,152	-0,106	-0,019	0,121	-0,017	0,149	0,051	0,095
T. trifulta	0,178	-0,048	-0,177	0,201	0,205	-0,104	0,270	0,007	0,125
T. tumida	0,248	0,165	-0,159	-0,016	-0,031	-0,061	0,249	0,004	-0,004
Ti	-0,001	-0,017	-0,104	-0,047	-0,058	0,166	0,107	0,061	0,029
Trachyneis spp	-0,099	-0,013	-0,086	-0,108	-0,059	0,172	0,105	-0,101	-0,018
Tx. antarctica	0,289	0,070	-0,244	0,238	0,253	-0,083	0,209	0,139	0,148
Zr/Rb	-0,076	-0,055	0,236	-0,042	-0,132	-0,173	-0,226	-0,018	0,000

Variables	icmophora sp	M. adelia	M. sol	N. directa	N. glaciei	Nitzschia spp	O. weissflogii	P. alata	P. glacialis
[HBI:2]	-0,053	0,451	0,199	0,056	0,108	-0,029	0,036	0,206	0,146
[HBI:2]/[HBI:3]	0,022	0,366	0,181	0,124	0,121	-0,044	-0,040	0,154	0,095
[HBI:3]	-0,070	-0,033	-0,059	-0,024	-0,068	0,030	0,107	0,001	-0,097
A. actinochylus	-0,037	0,045	0,195	0,001	-0,139	0,110	-0,012	0,060	0,225
A. Curvatulus	-0,069	0,091	-0,021	0,082	0,055	-0,086	0,193	-0,042	0,026
A. hookerii	-0,109	-0,137	0,093	0,001	-0,184	0,194	-0,051	0,089	0,004
A. hyalinus	0,133	-0,032	0,073	-0,001	0,129	-0,077	0,011	0,139	0,149
Acnanthes spp	-0,048	-0,038	0,064	-0,010	-0,075	-0,082	0,104	0,109	0,007
Amphora spp	-0,027	-0,086	-0,059	0,008	0,064	-0,007	0,281	0,012	0,121
C. atlantica	0,041	0,027	-0,083	0,007	-0,023	0,089	0,035	-0,072	0,050
C. bulbosum	-0,050	0,039	-0,029	-0,089	-0,045	0,009	-0,117	0,052	0,043
C. costata	0,084	0,090	-0,014	0,019	0,031	0,011	-0,102	0,087	0,105
C. cryophilum	-0,046	-0,033	0,007	-0,099	-0,098	0,086	0,112	-0,003	0,076
C. dichaeta	0,014	-0,036	-0,035	0,004	0,085	-0,098	-0,021	-0,066	-0,068
C. fasciolata	0,109	0,097	0,028	-0,084	-0,064	-0,074	-0,015	0,039	0,085
C. hyalochaete RS	0,079	-0,078	0,020	0,033	-0,027	-0,039	-0,061	-0,073	-0,051
C. Phaeoceros gp	-0,036	0,128	-0,039	0,053	0,036	-0,062	-0,044	-0,061	-0,092
Ch. cryophilus	0,098	0,235	-0,034	0,016	0,081	0,032	-0,104	-0,019	0,001
Cocconeis spp	-0,056	-0,010	-0,120	0,178	0,028	-0,022	0,311	0,080	0,049
Coscinodiscus spp	-0,017	0,054	-0,075	-0,158	-0,155	0,002	0,159	-0,007	0,210
Diploneis spp	0,143	-0,067	0,020	-0,049	0,016	-0,081	0,075	0,021	-0,059
E. antarctica	-0,004	0,264	0,063	-0,082	0,097	0,151	0,002	0,065	0,234
Entomoneis spp	-0,036	-0,029	-0,078	-0,081	-0,029	0,006	-0,038	-0,077	0,062
Ephemera spp	0,043	0,167	0,090	0,181	0,135	-0,016	-0,082	0,069	-0,040
F. curta	-0,016	-0,016	-0,099	0,050	-0,037	0,055	0,073	0,045	0,013
F. cylindrus	-0,085	-0,003	-0,020	0,083	0,162	-0,097	-0,162	-0,063	-0,303
F. kerguelensis	-0,016	0,083	0,133	-0,033	-0,117	0,098	0,088	0,293	0,235
F. obliquecostata	-0,036	0,083	-0,022	-0,126	0,114	-0,001	0,141	-0,070	0,141
F. peragalli	-0,016	-0,050	-0,035	-0,077	-0,039	-0,037	-0,017	-0,034	0,143
F. pseudonana	-0,028	0,033	0,125	0,139	0,032	0,063	-0,096	0,142	-0,160
F. rhombica	0,106	-0,052	-0,048	-0,189	-0,101	-0,040	0,041	-0,072	0,051
F. ritscherii	0,027	-0,145	-0,087	-0,200	-0,208	0,048	0,136	-0,137	0,129
F. separanda	-0,047	-0,068	0,032	0,035	-0,047	0,066	-0,063	0,304	-0,034
F. sublinearis	0,007	-0,021	-0,053	-0,126	-0,121	0,073	0,104	0,028	0,255
F. vanheurckii	0,104	-0,077	-0,023	0,046	-0,115	-0,031	-0,012	-0,067	0,004
Gramatophora spp	-0,023	0,089	-0,049	-0,036	-0,055	-0,052	-0,024	-0,048	0,081
Licmophora spp	1	-0,063	0,034	0,044	-0,029	-0,083	-0,038	-0,077	-0,083
M. adelia	-0,063	1	0,073	0,007	0,037	0,027	-0,088	0,117	-0,134
M. sol	0,034	0,073	1	-0,046	-0,059	0,088	-0,012	0,075	0,072
N. directa	0,044	0,007	-0,046	1	0,150	-0,040	0,043	0,062	-0,041
N. glaciei	-0,029	0,037	-0,059	0,150	1	-0,036	-0,056	0,202	-0,004
Nitzschia spp	-0,083	0,027	0,088	-0,040	-0,036	1	0,063	0,165	0,159
O. weissflogii	-0,038	-0,088	-0,012	0,043	-0,056	0,063	1	0,107	0,129
P. alata	-0,077	0,117	0,075	0,062	0,202	0,165	0,107	1	-0,018
P. glacialis	-0,083	-0,134	0,072	-0,041	-0,004	0,159	0,129	-0,018	1
P. inermis	-0,049	-0,068	-0,020	0,118	0,001	-0,073	-0,044	0,060	-0,154
P. pseudodenticulata	0,020	-0,126	-0,097	-0,197	-0,052	0,128	0,010	-0,035	0,252
P. tronca	-0,093	0,090	0,063	0,193	0,011	0,106	0,091	0,261	0,047
Pseudogomphonema spp	-0,072	0,171	0,127	-0,070	-0,035	-0,024	0,017	-0,034	0,089
Pseudo-nitschia spp	-0,046	-0,007	-0,089	0,119	0,169	-0,067	-0,005	-0,074	-0,234
Rhizosolenia spp	-0,020	0,037	0,022	0,059	0,021	-0,027	0,050	0,086	0,053
S. fragilis	0,024	0,074	0,177	0,069	0,026	0,250	-0,075	0,054	0,190
S. microtrias	-0,015	0,001	-0,098	-0,060	-0,068	0,025	0,113	-0,107	0,157
S. recta	-0,066	-0,155	-0,117	-0,005	0,263	0,024	0,173	-0,002	0,130
T. antarctica	-0,028	-0,023	0,023	-0,083	-0,040	0,059	0,162	0,023	0,356
T. frenguelli	0,199	0,012	0,055	0,175	0,031	-0,074	-0,034	-0,068	-0,068
T. gracilis	-0,044	0,131	0,055	0,022	-0,112	0,102	-0,019	0,145	0,042
T. gravida	0,023	-0,186	-0,018	-0,013	-0,108	-0,040	-0,004	-0,038	-0,023
T. lentiginosa	-0,005	0,035	0,172	-0,041	-0,111	0,177	0,097	0,105	0,304
T. oliverana	-0,021	-0,035	0,135	-0,167	-0,100	0,095	-0,022	-0,114	0,262
T. ritscheri	0,008	-0,076	0,080	0,143	0,056	-0,052	0,035	0,049	-0,056
T. toxon	0,021	0,243	0,104	-0,140	0,076	-0,033	0,139	0,091	0,066
T. trifulta	-0,047	0,107	-0,064	0,070	0,023	0,022	0,307	0,017	0,090
T. tumida	-0,048	0,198	0,079	-0,083	0,200	0,004	0,095	-0,004	0,215
Ti	0,077	0,155	0,112	0,076	0,025	0,033	0,007	0,200	0,228
Trachyneis spp	-0,029	-0,054	0,016	-0,040	0,082	-0,066	-0,030	0,017	0,004
Tx. antarctica	0,086	0,014	0,099	-0,068	-0,152	-0,009	0,187	-0,009	0,264
Zr/Rb	0,060	-0,041	0,019	-0,073	0,025	-0,087	-0,031	-0,043	-0,193

Variables	P. inermis	seudodenticu	P. tronca	ogomphonem	udo-nitschia	hizosolenia sp	S. fragilis	S. microtrias	S. recta
[HBI:2]	-0,209	-0,076	0,010	0,266	-0,010	-0,117	0,198	0,003	-0,092
[HBI:2]/[HBI:3]	-0,244	-0,144	0,124	0,262	0,087	-0,177	0,152	-0,020	-0,076
[HBI:3]	0,635	0,104	0,103	-0,009	-0,042	0,491	-0,089	-0,104	-0,050
A. actinochylus	-0,032	-0,008	0,092	0,132	-0,295	0,097	0,162	0,027	-0,084
A. Curvatulus	-0,077	0,074	0,137	0,105	0,097	-0,068	-0,135	0,031	0,144
A. hookerii	0,241	-0,026	0,142	-0,090	0,128	0,081	0,027	-0,082	0,007
A. hyalinus	0,076	-0,003	0,046	-0,001	0,016	-0,031	0,104	-0,026	0,005
Acnanthes spp	-0,074	-0,032	-0,124	-0,020	-0,124	-0,018	-0,026	0,008	-0,087
Amphora spp	0,054	-0,029	0,097	-0,054	-0,052	0,077	-0,054	0,095	0,164
C. atlantica	-0,163	0,081	-0,077	0,046	0,028	-0,112	-0,012	0,214	-0,060
C. bulbosum	0,079	0,056	-0,044	-0,048	0,102	0,031	-0,134	-0,074	-0,106
C. costata	-0,014	0,129	-0,072	0,085	-0,190	-0,044	0,101	0,041	-0,130
C. cryophilum	-0,025	0,018	-0,070	-0,113	-0,104	-0,022	-0,039	0,094	0,191
C. dichaeta	-0,174	-0,078	-0,061	0,028	-0,042	-0,063	-0,077	0,014	-0,042
C. fasciolata	-0,163	0,054	-0,081	0,009	-0,209	0,075	-0,002	0,002	-0,122
C. hyalochaete RS	-0,261	-0,142	-0,311	0,073	-0,151	-0,180	0,054	-0,032	-0,132
C. Phaeoceros gp	-0,010	-0,167	0,054	0,074	0,065	0,104	0,052	0,026	-0,127
Ch. cryophilus	-0,078	-0,031	-0,014	-0,064	0,195	0,086	0,170	0,012	0,042
Cocconeis spp	0,041	0,051	0,259	-0,067	-0,032	0,136	-0,053	0,107	0,289
Coscinodiscus spp	-0,139	0,004	-0,011	0,019	-0,247	0,029	-0,075	0,211	-0,028
Diploneis spp	-0,078	0,081	-0,091	-0,070	-0,007	-0,066	-0,069	0,024	0,036
E. antarctica	-0,237	0,046	-0,012	-0,045	-0,208	0,058	0,004	0,155	0,147
Entomoneis spp	-0,074	0,263	-0,093	-0,072	-0,103	-0,040	-0,071	-0,015	-0,066
Ephemera spp	0,128	-0,136	0,155	-0,150	0,257	-0,011	-0,011	-0,138	0,027
F. curta	0,010	0,100	0,130	0,144	-0,038	-0,143	0,048	0,120	-0,045
F. cylindrus	0,353	-0,040	-0,035	-0,178	0,337	0,093	-0,196	-0,246	-0,058
F. kerguelensis	-0,049	0,074	0,153	0,007	-0,145	0,097	0,121	0,156	-0,023
F. obliquecostata	-0,097	0,115	0,124	-0,018	-0,093	0,053	-0,060	0,100	0,258
F. peragalli	-0,022	0,055	-0,041	-0,032	-0,110	0,005	-0,031	0,010	0,431
F. pseudonana	0,412	-0,147	0,173	-0,129	0,198	0,146	-0,005	-0,194	0,035
F. rhombica	-0,090	0,101	0,155	-0,009	-0,007	-0,026	-0,040	-0,008	0,222
F. ritscherii	-0,224	0,063	-0,112	0,107	-0,230	-0,150	0,029	0,065	0,006
F. separanda	0,080	0,038	0,169	-0,036	0,071	-0,042	-0,037	-0,021	-0,008
F. sublinearis	-0,203	0,208	0,021	0,122	-0,331	0,046	0,011	0,132	0,165
F. vanheurckii	-0,051	-0,202	-0,141	-0,086	-0,030	-0,038	0,122	-0,007	-0,073
Gramatophora spp	0,032	-0,004	0,197	-0,045	-0,048	0,038	-0,044	-0,029	0,122
Licmophora spp	-0,049	0,020	-0,093	-0,072	-0,046	-0,020	0,024	-0,015	-0,066
M. adelia	-0,068	-0,126	0,090	0,171	-0,007	0,037	0,074	0,001	-0,155
M. sol	-0,020	-0,097	0,063	0,127	-0,089	0,022	0,177	-0,098	-0,117
N. directa	0,118	-0,197	0,193	-0,070	0,119	0,059	0,069	-0,060	-0,005
N. glaciei	0,001	-0,052	0,011	-0,035	0,169	0,021	0,026	-0,068	0,263
Nitzschia spp	-0,073	0,128	0,106	-0,024	-0,067	-0,027	0,250	0,025	0,024
O. weissflogii	-0,044	0,010	0,091	0,017	-0,005	0,050	-0,075	0,113	0,173
P. alata	0,060	-0,035	0,261	-0,034	-0,074	0,086	0,054	-0,107	-0,002
P. glacialis	-0,154	0,252	0,047	0,089	-0,234	0,053	0,190	0,157	0,130
P. inermis	1	-0,037	0,250	-0,094	0,096	0,639	-0,076	-0,118	0,014
P. pseudodenticulata	-0,037	1	-0,028	0,093	-0,073	0,045	0,013	0,152	0,019
P. tronca	0,250	-0,028	1	0,162	0,068	0,119	0,005	-0,114	0,137
Pseudogomphonema spp	-0,094	0,093	0,162	1	-0,022	-0,028	-0,040	-0,010	-0,093
Pseudo-nitschia spp	0,096	-0,073	0,068	-0,022	1	-0,126	-0,040	-0,147	0,030
Rhizosolenia spp	0,639	0,045	0,119	-0,028	-0,126	1	-0,054	-0,048	0,039
S. fragilis	-0,076	0,013	0,005	-0,040	-0,040	-0,054	1	-0,044	-0,107
S. microtrias	-0,118	0,152	-0,114	-0,010	-0,147	-0,048	-0,044	1	0,107
S. recta	0,014	0,019	0,137	-0,093	0,030	0,039	-0,107	0,107	1
T. antarctica	-0,308	0,093	-0,068	-0,007	-0,391	0,027	0,090	0,132	0,010
T. frenguelli	0,140	-0,005	0,008	0,018	0,058	0,090	0,043	-0,073	-0,058
T. gracilis	0,016	-0,099	0,208	0,033	-0,004	-0,093	0,114	-0,011	-0,081
T. gravida	0,114	0,008	0,035	-0,105	0,002	-0,052	-0,078	0,084	-0,087
T. lentiginosa	-0,197	0,038	-0,056	-0,028	-0,288	0,003	0,233	0,186	0,024
T. oliverana	-0,174	0,035	-0,095	-0,033	-0,159	0,003	0,001	-0,002	0,012
T. ritscheri	0,060	0,071	0,065	0,057	-0,105	0,108	-0,017	0,082	0,012
T. toxon	-0,128	-0,052	-0,096	-0,011	-0,050	-0,025	0,177	0,129	0,095
T. trifulta	-0,139	0,080	0,170	0,006	-0,035	-0,017	-0,099	0,026	-0,007
T. tumida	-0,045	-0,020	0,068	0,009	-0,054	0,020	0,048	0,059	0,210
Ti	-0,265	0,049	-0,026	0,066	-0,085	-0,091	0,155	0,087	-0,009
Trachyneis spp	-0,101	-0,071	-0,074	-0,006	-0,090	-0,076	0,010	0,084	0,021
Tx. antarctica	-0,118	-0,016	-0,040	-0,079	-0,260	0,117	0,073	0,217	0,065
Zr/Rb	0,099	-0,004	0,092	-0,031	-0,020	-0,090	-0,072	-0,097	-0,061

Variables	T. antarctica	T. frenguelli	T. gracilis	T. gravida	T. lentiginosa	T. oliverana	T. ritscheri	T. toxon	T. trifulta
[HBI:2]	0,218	-0,128	0,163	-0,138	0,110	-0,037	0,028	0,178	0,002
[HBI:2]/[HBI:3]	0,087	-0,082	0,101	-0,102	0,042	0,002	-0,009	0,079	-0,012
[HBI:3]	-0,101	0,091	0,026	0,127	-0,195	-0,157	0,123	-0,053	-0,070
A. actinochylus	0,224	0,075	0,218	-0,018	0,330	0,166	0,142	-0,026	0,152
A. Curvatulus	0,058	-0,061	-0,064	-0,223	-0,140	-0,168	0,033	-0,139	0,039
A. hookerii	-0,080	-0,047	0,297	0,300	0,173	-0,006	0,100	0,033	-0,077
A. hyalinus	0,237	0,168	0,096	0,040	0,087	-0,092	-0,004	0,051	0,106
Acnanthes spp	0,133	-0,043	0,116	0,170	0,149	-0,069	-0,018	0,077	0,197
Amphora spp	0,053	-0,024	-0,038	-0,098	0,060	-0,067	-0,013	-0,067	0,191
C. atlantica	0,299	0,026	-0,080	-0,054	-0,100	0,071	0,165	-0,072	0,076
C. bulbosum	-0,061	0,036	0,047	0,227	-0,039	-0,101	-0,119	-0,050	0,067
C. costata	0,098	-0,087	0,008	-0,052	-0,002	0,095	0,055	-0,148	-0,103
C. cryophilum	0,001	-0,088	-0,180	-0,148	0,187	0,067	-0,014	0,130	0,074
C. dichaeta	0,303	0,023	-0,143	-0,167	-0,088	0,164	0,230	-0,028	0,078
C. fasciolata	0,381	0,004	0,063	0,031	0,234	0,184	0,049	0,100	-0,043
C. hyalochaete RS	0,083	-0,100	-0,140	0,029	-0,072	0,052	0,052	-0,062	-0,210
C. Phaeoceros gp	0,066	-0,121	-0,046	-0,162	-0,153	-0,007	0,050	0,025	-0,072
Ch. cryophilus	-0,010	0,005	0,069	-0,123	0,163	0,089	0,051	0,139	0,042
Cocconeis spp	0,081	-0,050	-0,036	0,000	0,100	-0,136	0,053	-0,147	0,032
Coscinodiscus spp	0,100	-0,079	-0,080	0,040	0,190	0,032	-0,055	0,100	0,174
Diploneis spp	-0,009	-0,031	-0,042	0,157	0,141	0,074	-0,093	0,040	0,106
E. antarctica	0,063	0,036	-0,038	-0,137	0,260	0,234	0,079	0,160	0,130
Entomoneis spp	0,092	-0,032	-0,071	-0,129	-0,137	0,046	0,055	-0,086	0,015
Ephemera spp	-0,118	0,079	0,121	0,061	0,068	-0,101	-0,109	0,082	-0,020
F. curta	-0,040	0,099	0,249	0,092	-0,022	-0,143	0,088	0,092	0,183
F. cylindrus	-0,363	0,049	-0,216	0,036	-0,378	-0,143	-0,111	-0,219	-0,200
F. kerguelensis	0,184	-0,007	0,485	0,001	0,507	0,053	-0,011	0,213	0,136
F. obliquecostata	0,029	0,013	-0,206	-0,084	0,056	0,087	-0,019	0,055	0,178
F. peragalli	0,115	-0,014	-0,010	-0,057	0,073	-0,039	0,031	0,152	-0,048
F. pseudonana	-0,271	0,033	0,134	-0,069	-0,157	-0,189	-0,020	-0,106	-0,177
F. rhombica	-0,212	0,039	-0,068	-0,035	0,079	0,028	-0,140	-0,019	0,201
F. ritscherii	0,054	-0,110	-0,049	0,037	0,155	0,029	-0,091	0,121	0,205
F. separanda	0,032	-0,063	0,269	0,164	0,035	-0,136	0,171	-0,017	-0,104
F. sublinearis	0,234	0,052	-0,013	-0,163	0,092	0,191	0,039	0,149	0,270
F. vanheurckii	0,057	-0,065	0,012	-0,048	0,101	-0,075	-0,066	0,051	0,007
Gramatophora spp	0,032	-0,020	-0,099	-0,081	-0,103	-0,055	-0,029	0,095	0,125
Licmophora spp	-0,028	0,199	-0,044	0,023	-0,005	-0,021	0,008	0,021	-0,047
M. adelia	-0,023	0,012	0,131	-0,186	0,035	-0,035	-0,076	0,243	0,107
M. sol	0,023	0,055	0,055	-0,018	0,172	0,135	0,080	0,104	-0,064
N. directa	-0,083	0,175	0,022	-0,013	-0,041	-0,167	0,143	-0,140	0,070
N. glaciei	-0,040	0,031	-0,112	-0,108	-0,111	-0,100	0,056	0,076	0,023
Nitzschia spp	0,059	-0,074	0,102	-0,040	0,177	0,095	-0,052	-0,033	0,022
O. weissflogii	0,162	-0,034	-0,019	-0,004	0,097	-0,022	0,035	0,139	0,307
P. alata	0,023	-0,068	0,145	-0,038	0,105	-0,114	0,049	0,091	0,017
P. glacialis	0,356	-0,068	0,042	-0,023	0,304	0,262	-0,056	0,066	0,090
P. inermis	-0,308	0,140	0,016	0,114	-0,197	-0,174	0,060	-0,128	-0,139
P. pseudodenticulata	0,093	-0,005	-0,099	0,008	0,038	0,035	0,071	-0,052	0,080
P. tronca	-0,068	0,008	0,208	0,035	-0,056	-0,095	0,065	-0,096	0,170
Pseudogomphonema spp	-0,007	0,018	0,033	-0,105	-0,028	-0,033	0,057	-0,011	0,006
Pseudo-nitschia spp	-0,391	0,058	-0,004	0,002	-0,288	-0,159	-0,105	-0,050	-0,035
Rhizosolenia spp	0,027	0,090	-0,093	-0,052	0,003	0,003	0,108	-0,025	-0,017
S. fragilis	0,090	0,043	0,114	-0,078	0,233	0,001	-0,017	0,177	-0,099
S. microtrias	0,132	-0,073	-0,011	0,084	0,186	-0,002	0,082	0,129	0,026
S. recta	0,010	-0,058	-0,081	-0,087	0,024	0,012	0,012	0,095	-0,007
T. antarctica	1	-0,116	-0,050	-0,131	0,266	0,280	0,129	0,097	0,102
T. frenguelli	-0,116	1	0,191	0,076	0,024	-0,079	-0,042	0,015	0,225
T. gracilis	-0,050	0,191	1	0,141	0,266	0,064	-0,105	0,076	0,047
T. gravida	-0,131	0,076	0,141	1	0,051	-0,097	-0,113	-0,057	-0,034
T. lentiginosa	0,266	0,024	0,266	0,051	1	0,251	-0,006	0,233	0,131
T. oliverana	0,280	-0,079	0,064	-0,097	0,251	1	0,036	0,011	-0,083
T. ritscheri	0,129	-0,042	-0,105	-0,113	-0,006	0,036	1	-0,075	-0,017
T. toxon	0,097	0,015	0,076	-0,057	0,233	0,011	-0,075	1	0,062
T. trifulta	0,102	0,225	0,047	-0,034	0,131	-0,083	-0,017	0,062	1
T. tumida	0,130	-0,024	-0,027	-0,134	0,097	0,045	0,053	0,306	0,153
Ti	0,238	0,016	0,148	-0,164	0,119	0,089	0,052	0,075	0,015
Trachyneis spp	0,294	-0,026	-0,033	-0,062	-0,018	0,055	0,170	0,090	-0,043
Tx. antarctica	0,161	0,072	0,159	0,081	0,528	0,054	-0,050	0,303	0,151
Zr/Rb	-0,188	-0,158	0,119	-0,027	-0,133	0,106	0,097	-0,158	-0,112

Supplement Table 2:Pearson matrix of coefficient correlation, from the PCA between sedimentary raw data/proxies from the DTCI 2010.

Variables	EAST	SOUTH	WEST	NORTH	Temperature	Wind direction	Wind speed	SIC	Opening	Closing	Ice free season	Open water gp	Benthic gp	Banquisia gp	Thalassiothrix gp	C.phaeoceros gp	CRS
EAST	1	-0,949	-0,451	-0,248	0,063	-0,848	0,220	-0,035	-0,221	-0,385	0,048	0,209	-0,051	-0,190	0,239	0,308	-0,251
SOUTH	-0,949	1	0,207	0,039	0,026	0,771	-0,052	0,081	0,223	0,281	-0,093	-0,193	-0,012	0,188	-0,157	-0,386	0,289
WEST	-0,451	0,207	1	0,143	-0,470	0,666	-0,456	-0,130	0,062	0,366	0,093	-0,004	0,192	-0,065	-0,352	0,371	0,090
NORTH	-0,248	0,039	0,143	1	0,151	-0,004	-0,355	-0,038	0,039	0,259	0,070	-0,201	0,088	0,213	-0,078	-0,298	-0,163
Temperature	0,063	0,026	-0,470	0,151	1	-0,222	0,085	0,040	0,104	0,272	0,014	-0,062	-0,362	0,338	0,140	-0,441	0,004
Wind direction	-0,848	0,771	0,666	-0,004	-0,222	1	-0,302	0,054	0,233	0,207	-0,130	-0,096	-0,025	-0,011	-0,456	0,021	0,396
Wind speed	0,220	-0,052	-0,456	-0,355	0,085	-0,302	1	0,045	-0,060	-0,030	0,039	-0,283	-0,069	0,131	0,191	-0,175	0,364
SIC	-0,035	0,081	-0,130	-0,038	0,040	0,054	0,045	1	0,916	-0,259	-0,962	-0,077	-0,341	-0,178	-0,220	-0,158	0,091
Opening	-0,221	0,223	0,062	0,039	0,104	0,233	-0,060	0,916	1	0,051	-0,915	-0,122	-0,288	-0,053	-0,220	-0,211	0,044
Closing	-0,385	0,281	0,366	0,259	0,272	0,207	-0,030	-0,259	0,051	1	0,355	-0,139	0,146	0,259	0,243	-0,114	-0,066
Ice free season	0,048	-0,093	0,093	0,070	0,014	-0,130	0,039	-0,962	-0,915	0,355	1	0,061	0,328	0,160	0,303	0,156	-0,070
Open water gp	0,209	-0,193	-0,004	-0,201	-0,062	-0,096	-0,283	-0,077	-0,122	-0,139	0,061	1	0,367	-0,172	0,145	0,183	-0,237
Benthic gp	-0,051	-0,012	0,192	0,088	-0,362	-0,025	-0,069	-0,341	-0,288	0,146	0,328	0,367	1	-0,144	0,016	0,123	-0,224
Banquisia gp	-0,190	0,188	-0,065	0,213	0,338	-0,011	0,131	-0,178	-0,053	0,259	0,160	-0,172	-0,144	1	0,154	-0,254	-0,252
Thalassiothrix gp	0,239	-0,157	-0,352	-0,078	0,140	-0,456	0,191	-0,220	-0,220	0,243	0,303	0,145	0,016	0,154	1	-0,086	-0,383
C.phaeoceros	0,308	-0,386	0,371	-0,298	-0,441	0,021	-0,175	-0,158	-0,211	-0,114	0,156	0,183	0,123	-0,254	-0,086	1	-0,061
CRS	-0,251	0,289	0,090	-0,163	0,004	0,396	0,364	0,091	0,044	-0,066	-0,070	-0,237	-0,224	-0,252	-0,383	-0,061	1
Fragilariopsis summer gp	0,187	-0,155	-0,233	0,041	-0,271	-0,377	0,229	0,057	-0,040	-0,097	-0,005	0,193	0,517	-0,017	0,350	-0,209	-0,277
F.obliquecostata	-0,139	0,184	-0,053	-0,073	-0,089	-0,058	0,060	-0,092	0,005	0,145	0,056	0,155	0,340	0,345	0,338	-0,129	-0,539
F.kerguelensis	0,028	-0,017	-0,066	0,017	-0,121	-0,120	-0,073	-0,354	-0,360	-0,058	0,316	0,560	0,594	0,205	0,283	-0,108	-0,341
F.cylindrus	0,089	-0,143	-0,135	0,399	0,266	-0,240	-0,172	0,171	0,162	0,016	-0,148	-0,418	-0,324	0,152	-0,014	-0,318	-0,226
C. cryophilum	-0,001	0,059	-0,043	-0,231	-0,085	0,052	-0,236	0,116	0,111	-0,264	-0,211	0,178	-0,220	-0,091	0,192	-0,132	-0,432
T. antarctica	0,535	-0,624	0,154	-0,086	-0,262	-0,211	-0,236	-0,223	-0,288	-0,272	0,162	0,467	0,083	-0,288	-0,036	0,567	-0,306
E. Antarctica	0,129	-0,195	-0,003	0,255	0,017	-0,247	-0,072	0,194	0,222	0,008	-0,202	0,161	0,291	0,303	0,103	-0,095	-0,526
P.glacialis	0,453	-0,472	-0,110	-0,031	-0,228	-0,435	0,081	-0,340	-0,431	-0,217	0,312	0,299	0,232	-0,003	0,234	-0,017	-0,342
Rhizosolenia gp	-0,112	0,065	-0,078	0,411	0,102	-0,159	-0,296	-0,038	-0,020	0,064	0,042	-0,226	0,231	0,308	0,060	-0,265	-0,520
F. rhombica	-0,208	0,288	-0,221	0,026	0,215	-0,100	0,073	0,170	0,318	0,334	-0,163	-0,214	0,092	0,278	0,285	-0,445	-0,476
Ti	0,011	-0,105	0,162	0,244	-0,045	0,068	-0,175	-0,227	-0,121	0,056	0,141	0,351	0,273	-0,077	0,191	-0,045	-0,178
Zr/Rb	-0,338	0,330	0,091	0,121	0,146	0,344	0,095	0,269	0,306	0,100	-0,243	0,062	-0,016	0,219	-0,484	-0,105	0,345
[HBI:3]	0,361	-0,412	-0,199	0,303	-0,039	-0,482	-0,206	-0,097	-0,206	-0,140	0,132	0,235	0,334	-0,008	0,250	-0,173	-0,467
[HBI:2]	0,158	-0,260	0,218	0,119	-0,305	0,025	-0,085	-0,180	-0,178	-0,011	0,163	0,463	0,329	-0,126	0,046	0,173	-0,027
[HBI:2]/[HBI:3]	-0,283	0,220	0,398	-0,052	-0,270	0,520	0,022	-0,127	-0,026	0,082	0,061	0,155	0,064	-0,073	-0,221	0,220	0,459

Variables	ariopsis summ	obliquecostat	F.kerguelensis	F.cylindrus	C. cryophilum	T. antarctica	E. Antarctica	P.glacialis	hizosolenia g	F. rhombica	Ti	Zr/Rb	[HBI:3]	[HBI:2]	[HBI:2]/[HBI:3
EAST	0,187	-0,139	0,028	0,089	-0,001	0,535	0,129	0,453	-0,112	-0,208	0,011	-0,338	0,361	0,158	-0,283
SOUTH	-0,155	0,184	-0,017	-0,143	0,059	-0,624	-0,195	-0,472	0,065	0,288	-0,105	0,330	-0,412	-0,260	0,220
WEST	-0,233	-0,053	-0,066	-0,135	-0,043	0,154	-0,003	-0,110	-0,078	-0,221	0,162	0,091	-0,199	0,218	0,398
NORTH	0,041	-0,073	0,017	0,399	-0,231	-0,086	0,255	-0,031	0,411	0,026	0,244	0,121	0,303	0,119	-0,052
Temperature	-0,271	-0,089	-0,121	0,266	-0,085	-0,262	0,017	-0,228	0,102	0,215	-0,045	0,146	-0,039	-0,305	-0,270
Wind direction	-0,377	-0,058	-0,120	-0,240	0,052	-0,211	-0,247	-0,435	-0,159	-0,100	0,068	0,344	-0,482	0,025	0,520
Wind speed	0,229	0,060	-0,073	-0,172	-0,236	-0,236	-0,072	0,081	-0,296	0,073	-0,175	0,095	-0,206	-0,085	0,022
SIC	0,057	-0,092	-0,354	0,171	0,116	-0,223	0,194	-0,340	-0,038	0,170	-0,227	0,269	-0,097	-0,180	-0,127
Opening	-0,040	0,005	-0,360	0,162	0,111	-0,288	0,222	-0,431	-0,020	0,318	-0,121	0,306	-0,206	-0,178	-0,026
Closing	-0,097	0,145	-0,058	0,016	-0,264	-0,272	0,008	-0,217	0,064	0,334	0,056	0,100	-0,140	-0,011	0,082
Ice free season	-0,005	0,056	0,316	-0,148	-0,211	0,162	-0,202	0,312	0,042	-0,163	0,141	-0,243	0,132	0,163	0,061
Open water gp	0,193	0,155	0,560	-0,418	0,178	0,467	0,161	0,299	-0,226	-0,214	0,351	0,062	0,235	0,463	0,155
Benthic gp	0,517	0,340	0,594	-0,324	-0,220	0,083	0,291	0,232	0,231	0,092	0,273	-0,016	0,334	0,329	0,064
Banquisia gp	-0,017	0,345	0,205	0,152	-0,091	-0,288	0,303	-0,003	0,308	0,278	-0,077	0,219	-0,008	-0,126	-0,073
Thalassiothrix gp	0,350	0,338	0,283	-0,014	0,192	-0,036	0,103	0,234	0,060	0,285	0,191	-0,484	0,250	0,046	-0,221
C.phaeoceros	-0,209	-0,129	-0,108	-0,318	-0,132	0,567	-0,095	-0,017	-0,265	-0,445	-0,045	-0,105	-0,173	0,173	0,220
CRS	-0,277	-0,539	-0,341	-0,226	-0,432	-0,306	-0,526	-0,342	-0,520	-0,476	-0,178	0,345	-0,467	-0,027	0,459
Fragilariopsis summer gp	1	0,192	0,621	-0,233	-0,010	0,011	0,404	0,480	0,347	0,324	0,294	-0,284	0,594	0,373	-0,100
F.obliquecostata	0,192	1	0,331	-0,146	0,297	-0,063	0,286	0,235	0,245	0,503	0,005	-0,023	-0,001	-0,129	-0,217
F.kerguelensis	0,621	0,331	1	-0,441	0,067	0,192	0,295	0,407	0,230	0,111	0,421	-0,181	0,474	0,449	0,096
F.cylindrus	-0,233	-0,146	-0,441	1	-0,028	-0,273	0,171	-0,208	0,376	0,001	-0,258	0,038	0,256	-0,288	-0,476
C. cryophilum	-0,010	0,297	0,067	-0,028	1	0,222	0,019	0,265	0,041	0,387	0,218	-0,359	-0,027	-0,100	-0,129
T. antarctica	0,011	-0,063	0,192	-0,273	0,222	1	0,005	0,506	-0,233	-0,391	0,442	-0,284	0,164	0,586	0,262
E. Antarctica	0,404	0,286	0,295	0,171	0,019	0,005	1	0,198	0,403	0,285	0,181	0,044	0,322	-0,006	-0,296
P.glacialis	0,480	0,235	0,407	-0,208	0,265	0,506	0,198	1	0,061	0,008	0,344	-0,269	0,530	0,436	-0,120
Rhizosolenia gp	0,347	0,245	0,230	0,376	0,041	-0,233	0,403	0,061	1	0,395	-0,117	-0,170	0,547	-0,247	-0,551
F. rhombica	0,324	0,503	0,111	0,001	0,387	-0,391	0,285	0,008	0,395	1	-0,008	-0,194	0,026	-0,357	-0,375
Ti	0,294	0,005	0,421	-0,258	0,218	0,442	0,181	0,344	-0,117	-0,008	1	-0,273	0,185	0,561	0,363
Zr/Rb	-0,284	-0,023	-0,181	0,038	-0,359	-0,284	0,044	-0,269	-0,170	-0,194	-0,273	1	-0,193	0,024	0,141
[HBI:3]	0,594	-0,001	0,474	0,256	-0,027	0,164	0,322	0,530	0,547	0,026	0,185	-0,193	1	0,364	-0,474
[HBI:2]	0,373	-0,129	0,449	-0,288	-0,100	0,586	-0,006	0,436	-0,247	-0,357	0,561	0,024	0,364	1	0,582
[HBI:2]/[HBI:3]	-0,100	-0,217	0,096	-0,476	-0,129	0,262	-0,296	-0,120	-0,551	-0,375	0,363	0,141	-0,474	0,582	1

Supplement Table 3:Pearson matrix of coefficient correlation, from the PCA between significant sedimentary data and meteorological parameters, averaged over the November to March period.

Annexe 2 - Figures supplémentaires relatives à l'article III

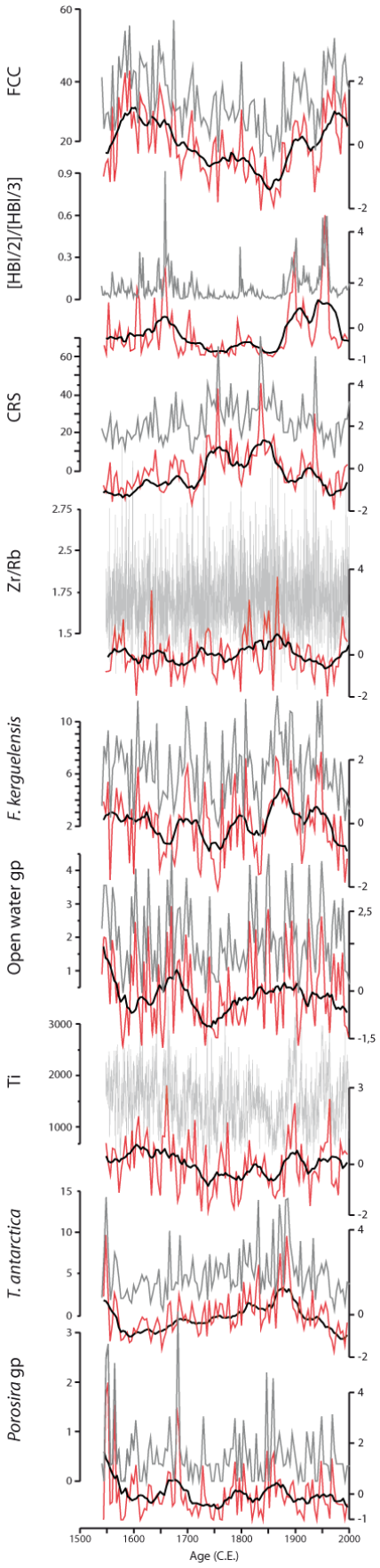

Suppl. Figure 1

Raw versus standardised data. Raw data (grey) and standardised data (orange) from the sediment core DTGC2011.

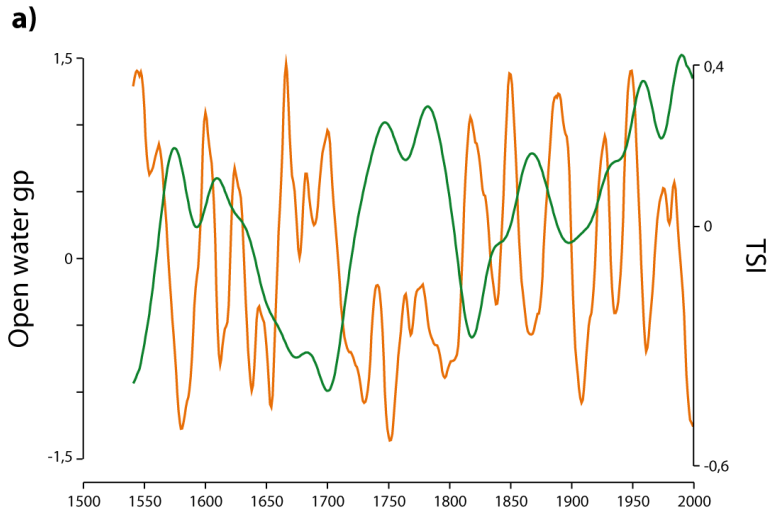

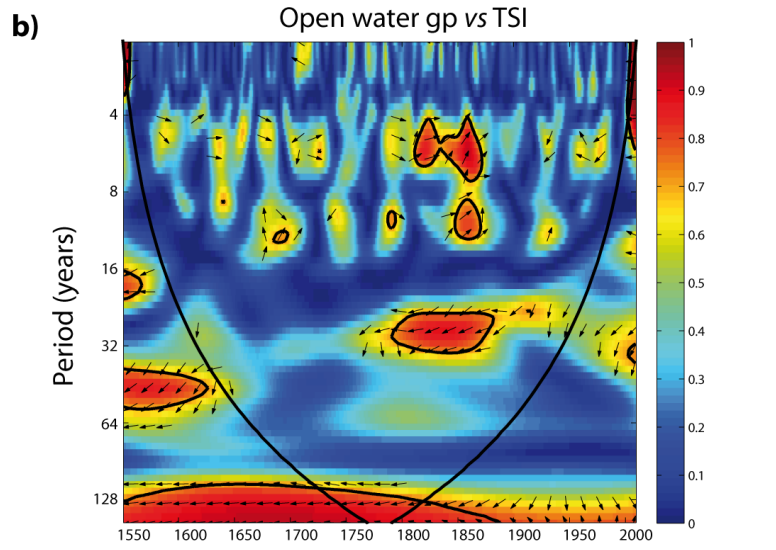

Suppl. Figure 2

Solar forcing over the last centuries on sea surface conditions in Adélie Land. **a)** Open Water gp composed of large centric diatoms (orange) from the DTCG 2011, and total solar irradiance (TSI, green) based on variability of cosmogenic ^{10}Be (Steinhilber et al., 2009); **b)** Cross wavelet correlation between the Open Water gp and ΔTSI, using Morlet wavelet and Monte Carlo methods according to Grinsted et al. (2004). Statistically significant periods are identified by the black circled red zones. Rightward pointed arrows indicate positively correlated signals while leftward pointed arrows indicate negatively correlated signals. Data has been resampled every 4 years.

Annexe 3 - Tables supplémentaires relatives à l'article IV

Core & section	cm bsf	Median CSFB (m)	Material	D 14C	±	Reported 14C age	DCF corrected
1HCCW	17-18	2,48	AO bulk	-197,4	3,3	1765	1340
2H1W	129-130	3,76	AO bulk	-237,0	2,9	2170	1745
2H3W	52-53	5,92	AO bulk	-203,6	2,8	1830	1405
2H6W	90-91	10,66	AO bulk	-222,5	2,3	2020	1595
3H1W	96-97	12,90	shell	-205,6	3,1	1850	1850
3H1W	126-127	13,17	AO bulk	-269,5	2,6	2520	2095
3H2W	130-131	14,60	AO bulk	-264,1	2,2	2465	2040
3H3A	122-123	15,91	shell	-271,1	3,1	2540	2540
3H4W	146-147	17,52	AO bulk	-274,8	2,7	2580	2155
3H6W	17-18	19,10	AO bulk	-289,5	2,1	2745	2320
3HCCW	51-52	21,44	AO bulk	-293,5	2,5	2790	2365
4H1W	111-112	22,54	AO bulk	-286,9	2,5	2715	2290
4H3W	19-20	24,48	AO bulk	-288,4	2,0	2735	2310
4H3W	123-124	25,44	shell	-269,9	3,1	2525	2525
4H4W	144-145	27,04	AO bulk	-321,8	2,4	3120	2695
4H6W	93-94	29,37	AO bulk	-313,2	2,1	3020	2595
4H7W	5-6	29,94	shell	-282,7	3,1	2670	2670
5H1W	89-90	31,83	AO bulk	-357,6	2,5	3555	3130
5H3W	28-29	34,03	AO bulk	-349,6	2,6	3455	3030
5H4W	105-106	36,13	AO bulk	-340,8	2,0	3350	2925
5H5W	133-134	37,76	AO bulk	-363,8	2,7	3635	3210
5H6W	63-64	38,50	AO bulk	-362,5	2,7	3615	3190
6H1W	130-131	41,75	AO bulk	-401,1	1,8	4120	3695
6H2W	136-137	43,25	AO bulk	-405,2	2,6	4175	3750
6H3W	76-77	44,11	AO bulk	-389,9	2,4	3970	3545
6H4W	54-55	45,34	AO bulk	-429,0	2,3	4500	4075
6H6W	95-96	48,47	AO bulk	-401,1	2,0	4120	3695
7H2W	27-28	51,66	AO bulk	-467,0	1,9	5055	4630
7H3W	67-68	53,26	AO bulk	-465,8	1,7	5035	4610
7H5W	42.5-143.	56,45	AO bulk	-486,4	2,1	5355	4930
7H6W	91-92	57,44	AO bulk	-480,1	2,3	5255	4830
8H1W	7-8	59,58	AO bulk	-498,6	1,7	5545	5120
8H3W	65-66	63,16	AO bulk	-508,5	2,2	5705	5280
8H4W	118-119	65,19	AO bulk	-502,0	1,8	5600	5175
9H1W	122-123	70,23	AO bulk	-513,4	1,5	5785	5360
9H4W	73-74	74,03	AO bulk	-520,4	1,8	5905	5480
9H5W	08.5-109.	75,88	AO bulk	-532,3	2,2	6105	5680
9H7W	46-47	77,54	AO bulk	-527,3	1,7	6020	5595
10H1W	90-91	79,41	AO bulk	-547,3	1,4	6365	5940
10H2W	121-122	81,22	AO bulk	-541,9	1,7	6270	5845
10H4W	42-43	83,36	AO bulk	-549,2	1,9	6400	5975
10H6W	83-84	86,77	AO bulk	-553,3	2,0	6475	6050
11H1W	32-33	88,33	AO bulk	-567,2	1,6	6730	6305
11H2W	104-105	89,68	AO bulk	-566,1	1,6	6705	6280
11H4W	128-129	92,71	AO bulk	-602,8	1,5	7415	6990

Core & section	cm bsf	Median CSFB (m)	Material	D 14C	±	Reported 14C age	DCF corrected
11H6W	25-26	94,68	AO bulk	-582,5	2,0	7015	6590
11H 7W	89-90	96,82	AO bulk	-586,6	1,5	7095	6670
12H4W	25-26	101,13	AO bulk	-594,0	1,4	7240	6815
12H5W	131-132	103,69	AO bulk	-605,9	1,8	7480	7055
12H7W	68-69	106,06	AO bulk	-603,8	1,5	7435	7010
12H7W	106-107	106,44	AO bulk	-603,5	1,2	7430	7005
13H1W	13-14	107,13	AO bulk	-615,8	1,6	7685	7260
13H1A	52-53	107,50	shell	-596,5	3,5	7290	7290
13H2W	56-57	108,73	AO bulk	-611,3	1,4	7590	7165
13H3W	87.5-88.5	110,43	AO bulk	-617,9	1,3	7730	7305
13H5W	6.5-7.5	112,47	AO bulk	-620,0	1,2	7775	7350
13H6W	63.5-64.5	114,25	AO bulk	-632,7	1,9	8045	7620
13HCCW	27.5-28.5	116,45	AO bulk	-635,4	1,4	8105	7680
14H2W	26-27	117,38	AO bulk	-650,2	1,7	8435	8010
14H3W	135-136	119,95	AO bulk	-659,0	1,2	8640	8215
14H5W	3-4	121,62	AO bulk	-656,5	1,3	8585	8160
14H6W	86-87	123,92	AO bulk	-661,7	1,3	8705	8280
14H7W	107-108	125,61	AO bulk	-669,2	1,3	8885	8460
15H1W	78-79	126,79	AO bulk	-664,9	1,3	8785	8360
15H3W	27-28	129,00	AO bulk	-665,6	1,1	8800	8375
15H5W	146-147	133,18	AO bulk	-671,9	1,6	8950	8525
15H6W	143-144	134,66	AO bulk	-673,1	1,3	8980	8555
16H1W	71-72	136,21	AO bulk	-683,9	1,0	9250	8825
16H3W	13-14	138,26	AO bulk	-690,8	1,2	9430	9005
16H4W	77-78	140,23	AO bulk	-685,4	1,2	9290	8865
16H6W	31-32	142,72	AO bulk	-696,9	0,9	9590	9165
16H7W	81-82	144,68	AO bulk	-696,2	1,3	9570	9145
17H1W	60-61	145,57	AO bulk	-697,4	1,2	9605	9180
17H3W	30-31	148,09	AO bulk	-704,2	1,0	9785	9360
17H4W	122-123	150,35	AO bulk	-713,3	1,2	10035	9610
17H6W	82-83	152,76	AO bulk	-718,6	1,1	10185	9760
18H1W	68-69	155,14	AO bulk	-715,8	0,9	10105	9680
18H3W	13-14	157,41	AO bulk	-731,6	1,1	10565	10140
18H4W	97-98	159,57	AO bulk	-741,3	1,0	10860	10435
18H5W	137-138	161,33	AO bulk	-747,7	1,0	11065	10640
18H7W	52-53	163,32	AO bulk	-748,9	1,0	11100	10675
19H1W	108-109	165,08	AO bulk	-755,7	1,5	11320	10895
19H2W	97-98	166,44	AO bulk	-751,7	1,0	11190	10765
19H3W	64-65	167,60	AO bulk	-760,3	0,9	11475	11050
19H4W	66-67	169,10	AO bulk	-788,8	1,5	12490	12065
19H4W	102-103	169,46	AO bulk	-771,6	1,4	11860	11435
19H5W	61-62	170,53	AO bulk	-989,4	1,4	36560	36135

Suppl. Table 1

IODP U1357B ^{14}C dates. Carbonate shell dates and acid only dates from IODP U1357B.

Annexe 4 - Article complémentaire

Crespin, J., Yam, R., Crosta, X., Massé, G., Schmidt, S., Campagne, P., & Shemesh, A. Holocene glacial discharge fluctuations and recent instability in East Antarctica. *Earth and Planetary Science Letters*, **394**, 38-47 (2014).

Earth and Planetary Science Letters 394 (2014) 38–47

Contents lists available at ScienceDirect

Earth and Planetary Science Letters

www.elsevier.com/locate/epsl

Holocene glacial discharge fluctuations and recent instability in East Antarctica

Julien Crespin [a,*], Ruth Yam [a], Xavier Crosta [b], Guillaume Massé [c,d], Sabine Schmidt [b], Philippine Campagne [b], Aldo Shemesh [a]

[a] Weizmann Institute of Science, Rehovot, 76100 Israel
[b] EPOC, UMR CNRS 5805, Université Bordeaux I, 33405 Talence, France
[c] LOCEAN, UMR 7159, Université Pierre et Marie Curie, 4 Place Jussieu, 75252 Paris Cedex 05, France
[d] TAKUVIK, UMI 3367, Université Laval, G1V0A6 Québec, Canada

ARTICLE INFO

Article history:
Received 12 June 2013
Received in revised form 17 February 2014
Accepted 7 March 2014
Available online xxxx
Editor: J. Lynch-Stieglitz

Keywords:
East Antarctica
Holocene
glaciers
diatoms
oxygen isotopes
ENSO

ABSTRACT

Antarctica holds the largest ice sheet in the world, the East Antarctic Ice Sheet (EAIS), and plays a significant role in both local and global climate through the interactions between ice sheets, ocean, sea ice, and atmosphere. Our understanding of East Antarctica Holocene climate variability relies mainly on ice cores that however do not document glacial discharge history. Here, we present the first high resolution $\delta^{18}O_{diatom}$ record derived from two marine sediment cores retrieved on the East Antarctic continental shelf to reconstruct glacial discharge off Adélie Land and George V Land (AL–GVL) over the last 11,000 years from decadal to centennial resolution. Our results suggest multi-centennial glacier advances and retreats until 2000 cal yr BP, followed by a period of relative instability marked by two major glacial retreats centered at ~1700 cal yr BP and ~1980 CE. We suggest that the multi-centennial oscillations during the Early/Mid-Holocene reflect glacier fluctuations in response to long-term local seasonal insolation and short-term solar variability. We also propose that $\delta^{18}O_{diatom}$ variability over the last 2000 years was the result of a recent change in the AL–GVL region to increasing atmospheric influence, linked to ENSO intensification and teleconnections strengthening between low and high latitudes.

1. Introduction

Antarctica and its ice sheets have played, and continue to play, a major role in the global ocean–atmosphere system. The East Antarctic Ice Sheet (EAIS), the largest in the world, stores 79% of Antarctica ice and influences directly both Antarctic and global climate through interactions with the ocean, the sea ice, and the atmosphere of the Southern Hemisphere. Ice sheet morphology (e.g. through the presence of glacier ice tongues) has an important impact on sea ice cycle and thus on bottom ocean circulation and primary productivity. As such, a better understanding of the impact of glacier systems and the associated climate feedbacks of the east Antarctic region is important for future climate predictions (Denis et al., 2009a).

Scarce environmental reconstructions based on ice cores, marine sediments, lake sediments, and terrestrial records revealed that Antarctic climate shows three contrasted intervals during the Holocene (Mayewski et al., 2009): a Deglacial period (also termed the Early Holocene Climate Optimum), a Mid-Holocene warm period or Hypsithermal, and a Late Holocene period or Neoglacial cooling (Hodgson et al., 2009a; Denis et al., 2009a; Verleyen et al., 2011), followed by the recent climate warming.

The climatic periods are not always synchronous in the different regions of Antarctica due to the spatial heterogeneity in the intensities of the forcing mechanisms. As a result, the Antarctic climate system is regionally partitioned with heterogeneous surface air temperature trends and ice-sheet/glacier fluctuations on millennial to decadal timescales (Masson et al., 2000; Denis et al., 2009a; Hall, 2009; Mayewski et al., 2009; Verleyen et al., 2011). This partitioning was also monitored over the last 50 years whereby East Antarctica (EA) and Antarctic Peninsula (AP) surface air temperature increased by ~1 °C and ~3 °C, respectively (Turner et al., 2005a). However, even if EA currently appears less sensitive to recent global warming, numerical models predict that warming, and therefore melting of the EAIS, will greatly increase in the next decades, which will drastically impact ocean circulation (Summerhayes et al., 2009). Over the last few decades, the most profound changes in the ice-sheets result from glacier dynamics at ocean margins (Pritchard et al., 2009). Moreover, it has been

* Corresponding author.
E-mail address: julien.crespin@weizmann.ac.il (J. Crespin).

http://dx.doi.org/10.1016/j.epsl.2014.03.009
0012-821X/

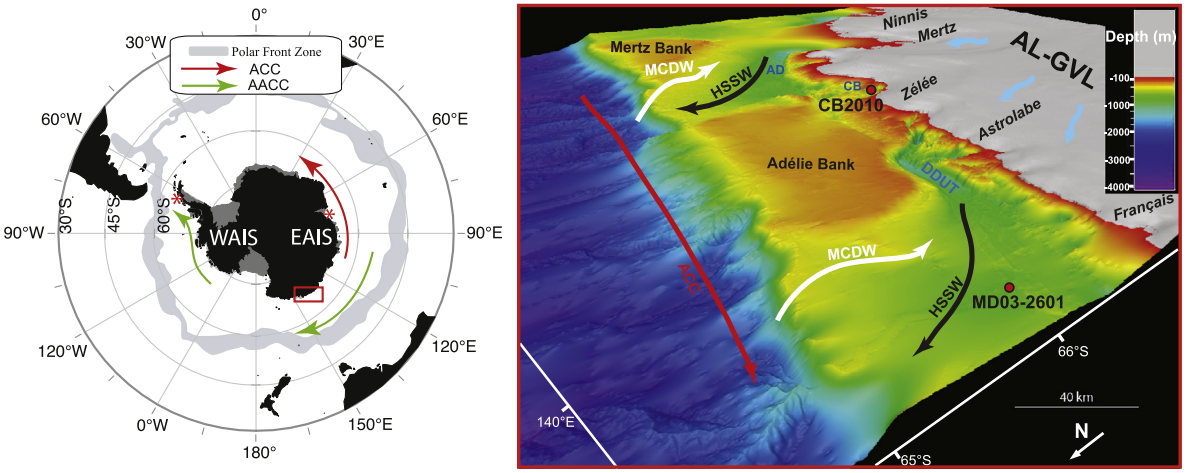

Fig. 1. Study area (modified from Beaman et al., 2011): location of cores MD03-2601 and CB2010 (red dots) and coastal cores from Berg et al. (2010) and Pike et al. (2013) (red asterisks), glaciers (in italic), katabatic winds (light blue arrows), and details of oceanographic currents and different water masses in the region. HSSW: High Salinity Shelf Water; MCDW: Modified Circumpolar Deep Water; ACC: Antarctic Coastal Current; AACC: Antarctic Circumpolar Current. Features include the Adélie Land–George V Land (AL–GVL), the Adélie Depression (AD), Commonwealth Bay (CB), Dumont d'Urville Trough (DDUT). (For interpretation of the references to color in this figure legend, the reader is referred to the web version of this article.)

evidenced that large parts of the EAIS margin are more vulnerable to external forcing than previously recognized (Miles et al., 2013). Hence, it is important to reconstruct the glacial discharge history (iceberg and brash-ice discharge together with basal melting of floating glaciers/ice shelves) to the coastal waters off EA in order to further improve numerical predictions.

We present the first high-resolution diatom oxygen isotope ($\delta^{18}O_{diatom}$) records obtained from two marine sediment cores collected on the Adélie Land–George V Land (AL–GVL) continental shelf (EA). The down core $\delta^{18}O_{diatom}$ records enable to reconstruct the glacial discharge history of AL–GVL at decadal to centennial resolution to better understand the relationship between East Antarctic climate variability and local glacier fluctuations. This could provide potential insights on the sensitivity of the EAIS to future climatic changes.

2. Material and methods

Two marine sediment cores (piston core MD03-2601: 66°03.07′S, 138°33.43′E; 746 m water depth; interface core CB2010: 66°54.33′S; 142°26.20′E; 780 m water depth; Fig. 1) were analyzed to investigate changes in glacial discharge during the Holocene on the AL–GVL in the Indian sector of the Southern Ocean. These high accumulation sites from the coastal continental shelf zones are located below one of the most productive ecological provinces in the Southern Ocean (Arrigo et al., 2008). Several glaciers, releasing freshwater to the surface water of the marine environment, dissect the coastal area off AL–GVL region. The Zélée, Astrolabe, and Français glaciers predominantly affect the MD03-2601 site off AL, whereas the CB2010 site off GVL is influenced by both the Mertz and Ninnis glaciers (Fig. 1). The two cores are located ~200 km apart and are separated by the Adélie Bank. Piston core MD03-2601 is composed of a 4000-cm-long sequence of laminated diatom ooze, while interface core CB2010 is composed of a 30-cm-long of massive diatom ooze.

2.1. Chronology

The age model used for piston core MD03-2601 is based on seven Accelerator Mass Spectrometry ^{14}C dates of the humic fraction of bulk organic matter calibrated to calendar ages using CALIB 5.0 and a reservoir age of 1300 years (see Denis et al., 2009a for further details on the age model). Core MD03-2601 spans the period between 11,000 and 1000 calendar years BP (cal yr BP).

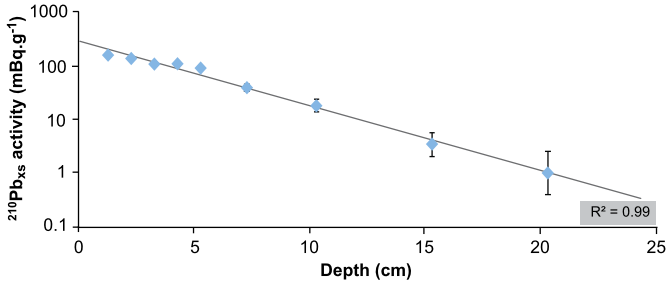

Fig. 2. Down core profile of $^{210}Pb_{xs}$ activity (blue diamonds). Error bars correspond to 1SD. (For interpretation of the references to color in this figure legend, the reader is referred to the web version of this article.)

The age model of interface core CB2010 (Fig. 2) was developed from the excess ^{210}Pb activity ($^{210}Pb_{xs}$), which yields a mean sedimentation rate of 0.11 cm yr^{-1} and taking into account that the interface of the core is contemporaneous to the retrieval date as shown by the presence of an oxydated fluffly layer. $^{210}Pb_{xs}$ profile was determined as the difference of the total (^{210}Pb) and supported (^{226}Ra) activities in sediment, measured by low-background high-efficiency gamma spectrometry (Schmidt et al., in press). Individual sample ages were calculated by fitting a smooth curve to the chronological data. Core CB2010 spans the past 250 years.

2.2. Diatom extraction and analysis

Cores MD03-2601 and CB2010 were sampled every 32 cm and 1 cm leading to a sampling resolution of ~80–100 years and ~10 years, respectively. Diatoms were separated from the sediment and purified using a combination of previously published cleaning techniques adapted for our Antarctic marine samples (Juillet-Leclerc, 1986; Morley et al., 2004; Shemesh et al., 1995; Swann and Leng, 2009). Sediment samples were pretreated with 30% H_2O_2 for 4 h at 60 °C and 10% HCl for 2 h at room temperature, followed by sonication for a few seconds. Samples were then sieved and the 10–32 μm size fraction was retained for density separation by sodium polytungstate (SPT) (specific gravities from 2.1 to 2.25 g/ml) to separate diatoms from detrital minerals. Following oxidation of the labile organic matter coating the diatom valves by using a 1:1 mixture of HNO_3 (65%)/$HClO_4$ (70%) at 60 °C for 1 h, samples were centrifuged 8 times with deionized water and dried at 60 °C. All samples were subjected to light

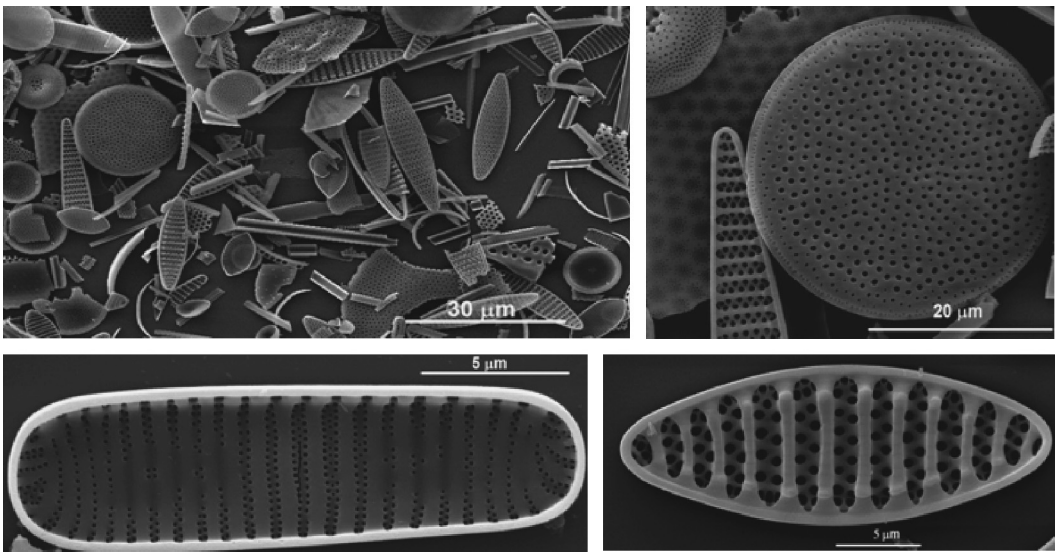

Fig. 3. Scanning electron microscope (SEM) images of clean diatom material analyzed for oxygen isotopes from MD03-2601 core showing the excellent preservation of the diatoms, the complete removal of adhering clays and the absence of any significant contamination.

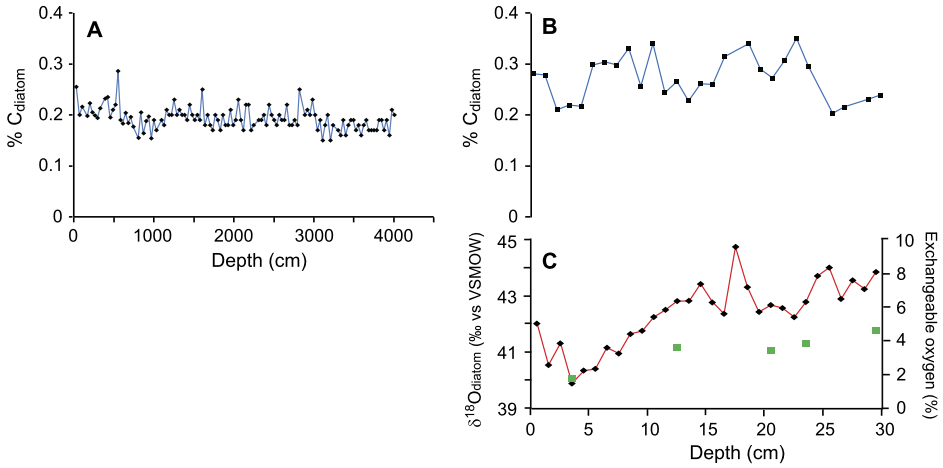

Fig. 4. % of organic carbon in core MD03-2601(A) and in core CB2010 (B). Panel C shows the $\delta^{18}O_{diatom}$ record (red curve; black diamonds representing the $\delta^{18}O_{diatom}$ measurements) and the percentage of exchangeable oxygen (green squares) from core CB2010. (For interpretation of the references to color in this figure legend, the reader is referred to the web version of this article.)

microscopy inspection in order to evaluate their purity prior to isotope analysis. Several samples, along the two cores, were subjected to SEM inspection in order to evaluate a possible dissolution effect and to ensure the purity of the samples (Fig. 3). The percentage of carbon content (%C), ranging from 0.15% to 0.35%, indicates that these procedures efficiently removed extraneous organic matter (Crosta et al., 2002; Jacot Des Combes et al., 2008; Hurrell et al., 2011) (Fig. 4).

Samples were then subjected to controlled isotopic exchange followed by high-temperature re-crystallization (to minimize the isotope effect associated with opal-bound water) with two water samples having different isotopic compositions ($\delta^{18}O_{w1} = +34.6‰$ and $\delta^{18}O_{w2} = -10.7‰$ vs. VSMOW). This allows the determination of the amount of exchangeable oxygen in the samples and to correct the measured isotopic composition of the stable fraction. $\delta^{18}O_{diatom}$ measurements were performed on 124 samples from MD03-2601 and on 30 samples from CB2010, using an Infra Red (IR) laser extraction technique. A Merchanteck 25W CO_2 IR laser, combined with BrF_5 reagent, was used to extract molecular O_2 from 200 µg of purified diatom. Following extraction and purification, O_2 was analyzed using a Thermo Finnigan Delta Plus XL isotope-ratio mass spectrometer. Absolute calibration was achieved by using NBS 28 and the PS diatom standard (Chapligin et al., 2011). The $\delta^{18}O_{diatom}$ values are expressed relative to VSMOW and showed a mean standard deviation of $\pm 0.36‰$ (1σ). The %C of the intrinsic organic matter encased within the cleaned diatom opal was measured on 145 samples from both the MD03-2601 and CB2010 cores using a Carlo Erba EA1110 elemental analyzer in line with a Finnigan MAT 252 stable isotope ratio mass spectrometer. We point out that the isotope measurements were made on the 10–32 µm size fraction and that the species counts were carried out on the bulk assemblage. However, the cleaning procedure showed that most of the diatoms from cores MD03-2601 and CB2010 are within the 10–32 µm size fraction, with very few diatoms in the size fractions of <10 µm and >32 µm.

3. Results

$\delta^{18}O_{diatom}$ values obtained from MD03-2601 and CB2010 cores vary between 39.9‰ and 45.0‰ (Fig. 5A). MD03-2601 $\delta^{18}O_{diatom}$ record does not show any trend throughout the Holocene as the 0.4‰ decrease between 11,000 cal yr BP and 2000 cal yr BP is within 1 standard deviation of the measure. MD03-2601 $\delta^{18}O_{diatom}$ record presents absolute variations up to 1.5‰ until 2000 cal yr BP. Major low events are found at ~10,500 cal yr BP,

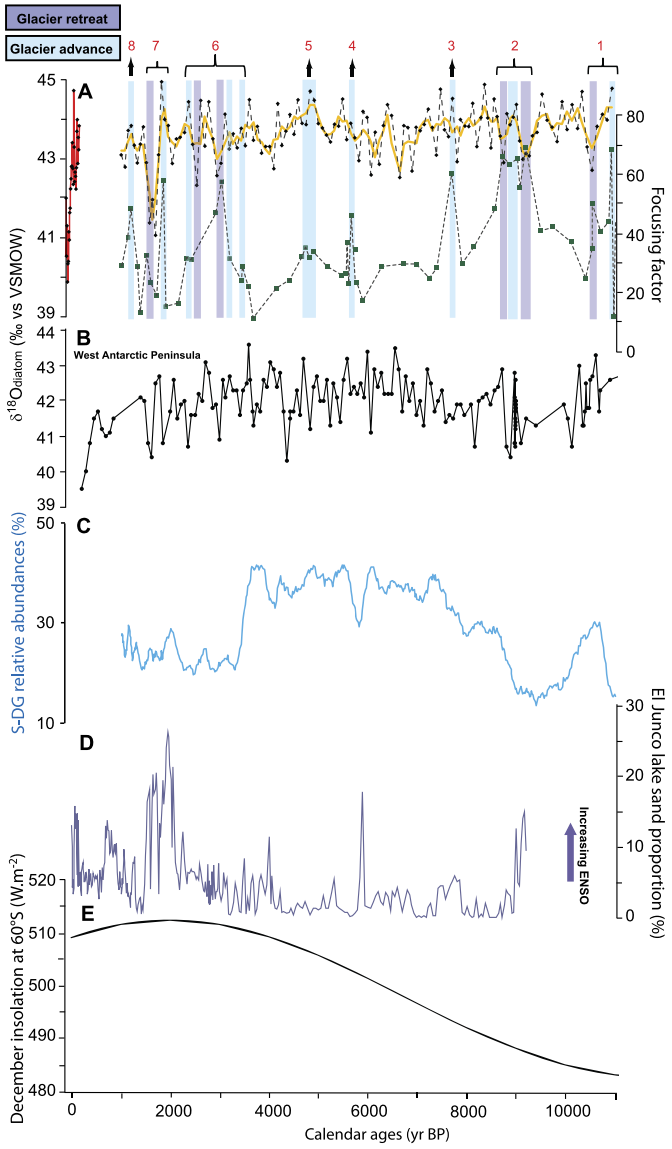

Fig. 5. (A) Composite $\delta^{18}O_{diatom}$ record from the AL–GVL (this study) (CB2010 in red and MD03-2601 3-points running mean in orange) with measured values (black diamonds) and focusing factor (ψ) record (Denis et al., 2009a) with measured values (dark green squares); Numbers in red refers to the focusing events mentioned in the text. Glacier advances and retreats are based on the $\delta^{18}O_{diatom}$ record; (B) $\delta^{18}O_{diatom}$ record (in black) with measured values (black dots) from the West Antarctic Peninsula (ODP site 1098A; Pike et al., 2013); (C) relative abundances of the summer diatom group (S-DG) (in light blue; 10-points running mean) as defined by Denis et al. (2009b); (D) percentage of sand (in purple) from El Junco Crater Lake, Galápagos (Conroy et al., 2008); (E) Summer (December) insolation at 60°S (Berger and Loutre, 1991). (For interpretation of the references to color in this figure legend, the reader is referred to the web version of this article.)

~9200 cal yr BP, ~6700–5800 cal yr BP, ~3000 cal yr BP and ~2500 cal yr BP. However, the most prominent low is found after 2000 cal yr BP when a 3.9‰ drop, with values as low as 40.9‰, is recorded at ~1700 cal yr BP.

CB2010 record expands the MD03-2601 record to the present, and allows generating a quasi-continuous record due to the good agreement between the top and the bottom values of two independent parameters from the two cores: percentage of carbon and $\delta^{18}O_{diatom}$ values (Figs. 4 and 5, respectively). Core CB2010 presents values varying between 42‰ and 44.5‰ during the 1750–1850 CE when an abrupt drop occurred. Lowest $\delta^{18}O_{diatom}$ of the combined records, with values as low as 39.9‰, are then recorded at 1980 CE. $\delta^{18}O_{diatom}$ values subsequently recovered to reach back 42‰ at the core top.

4. Discussion

4.1. Controls on $\delta^{18}O_{diatom}$

To date, there have been no studies relating $\delta^{18}O_{diatom}$ to local processes along the AL–GVL coastal margin. However, it has been evidenced that $\delta^{18}O_{diatom}$ depends on both temperature and $\delta^{18}O$ of the sea surface water ($\delta^{18}O_{water}$) from which it was deposited (Juillet-Leclerc and Labeyrie, 1987; Shemesh et al., 1992; Swann and Leng, 2009 and references therein). Secondary processes, such as vital effect, dissolution, and silica maturation can also influence the $\delta^{18}O_{diatom}$ signal and are discussed below.

4.1.1. Species effect – dissolution

A species effect on marine $\delta^{18}O_{diatom}$ has been proposed based on the $\delta^{18}O_{diatom}$ offset recorded between two different diatom size fractions in Plio-Pleistocene and late Pleistocene samples from the north Pacific (Swann et al., 2007, 2008). Conversely, culture and sediment trap experiments along with other down-core studies indicated that species effects are either non-existent or within analytical error (Shemesh et al., 1995; Brandriss et al., 1998; Schmidt et al., 2001; Moschen et al., 2005; Schiff et al., 2009). In core MD03-2601, we observed insignificant correlations between relative abundances of the four main diatom species (*Chaetoceros Hyalochaete* spp. resting spores (CRS), *Fragilariopsis curta*, *Fragilariopsis kerguelensis* and *Thalassiosira antarctica*) and $\delta^{18}O_{diatom}$ values ($0.01 < R^2 < 0.04$), spanning different size fractions and shape, which strongly argue here against any potential species vital effect (Fig. 6).

Opal dissolution may lead to isotope fractionation, thus altering the original signal. Two studies showed minimal isotopic alteration in fresh diatoms under pH conditions of 7–8 (Schmidt et al., 2001; Moschen et al., 2006) and no isotope alteration in old diatom material under variable pH (Moschen et al., 2006). SEM scans show that MD03-2601 diatoms are well preserved and do not exhibit signs of dissolution or diagenesis (Fig. 3), as already pointed out by Crosta et al. (2007). Taking into account the fact that the pH of Southern Ocean water is ca. 8, we infer that $\delta^{18}O_{diatom}$ signature has not been significantly altered by dissolution.

4.1.2. Silica maturation

Biogenic silica maturation during sedimentation/early burial leads to ^{18}O enrichment in the sedimentary opal (Schmidt et al., 1997, 2001; Moschen et al., 2005, 2006; Dodd et al., 2012). However, the extent to which these changes may impart on palaeoenvironmental inferences from $\delta^{18}O_{diatom}$ remains unknown, especially in marine environments. In conjunction with other evidences, a number of studies have documented strong correlations between records of $\delta^{18}O_{diatom}$ and other $\delta^{18}O$-based proxy data that would not have been expected if silica maturation significantly altered the fossilized $\delta^{18}O_{diatom}$ record (Shemesh et al., 1992; Leng and Barker, 2006; Swann and Leng, 2009). We here observed a 2‰ decrease within the top four centimeters of core CB2010 $\delta^{18}O_{diatom}$ record, opposite to the expected effect of silica maturation. We also observed a down-core increase in the percentages of exchangeable oxygen (from the –Si–OH layer of the diatom frustule), from 1.8% to 4.6%, (Fig. 4C) where a decrease (a reduction of –Si–OH groups with depth) would have been expected from silica maturation (Schmidt et al., 2001; Moschen et al., 2006). Moreover, cores CB2010 and MD03-2601 bear a similar range of exchangeable oxygen ($2.97 \pm 1.28\%$, $n = 5$; $3.06 \pm 0.86\%$, $n = 13$; respectively), indicating similar amounts of –Si–OH groups on centennial to millennial timescales and sediment thickness of 30 cm to 4000 cm.

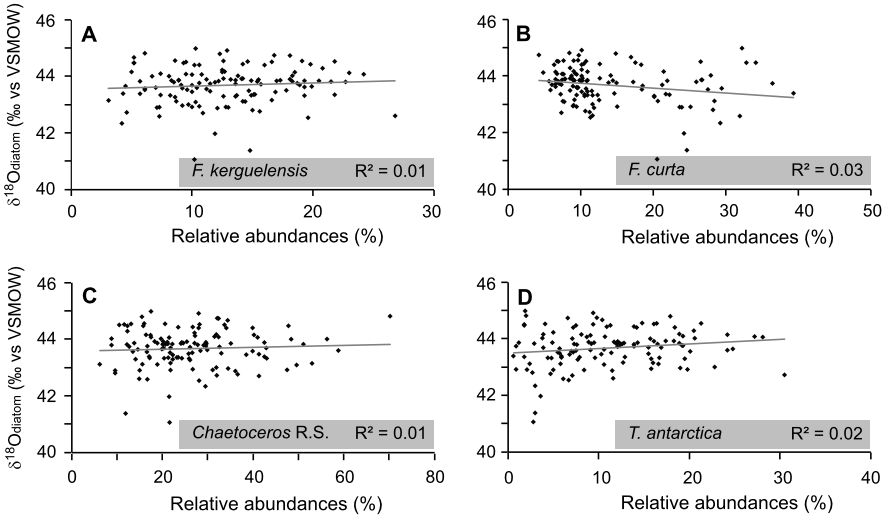

Fig. 6. $\delta^{18}O_{diatom}$ measurements vs. relative abundances of (A) *Fragilariopsis kerguelensis*, (B) *Fragilariopsis curta*, (C) *Chaetoceros Hyalochaete* spp. resting spores (CRS) and (D) *Thalassiosira antarctica*.

These observations argue against significant impact of silica maturation on our $\delta^{18}O_{diatom}$ records.

4.1.3. Influence of sea-surface temperature and water masses on $\delta^{18}O_{diatom}$

Previous temperature reconstructions, based on diatom census counts (summer diatom group – S-DG) in core MD03-2601, argue for warmer sea-surface waters and lesser sea ice cover between 8000 cal yr BP and 4000 cal yr BP, and colder sea-surface waters, and icier conditions from 4000 cal yr BP to 1000 cal yr BP (Denis et al., 2009b; Fig. 5C). Transient climate simulations of the last 9000 years, additionally show a cooling of the Southern Ocean south of 60°S since ~4000 cal yr BP (Renssen et al., 2005, 2012). However, the Mid-Holocene optimum and subsequent Neoglacial cooling periods, previously recorded both in AP (Taylor et al., 2001) and EA (Denis et al., 2009b, 2010), are not evidenced in the MD03-2601 $\delta^{18}O_{diatom}$ record. Moreover, subsurface ocean temperatures, derived from TEX^{L}_{86} measurements in the same core, do not indicate long-term variability until 2000 cal yr BP (Kim et al., 2012). Finally, if we use a diatom-temperature coefficient within the acknowledged −0.2‰/°C and −0.5‰/°C range (Brandriss et al., 1998; Crespin et al., 2010; Dodd and Sharp, 2010; Juillet-Leclerc and Labeyrie, 1987; Moschen et al., 2005; Shemesh et al., 1992), the $\delta^{18}O_{diatom}$ maximum amplitude of 3.9‰ recorded in core MD03-2601 will lead to an implausible temperature range of 7.8 °C to 19.5 °C. The temperature range derived from the TEX^{L}_{86} measurements is 4–5 °C for the Holocene (Kim et al., 2012), while diatom counts suggest a 1–2 °C drop between the Hypsithermal and the Neoglacial periods (Crosta et al., 2007). It is, therefore, very unlikely that $\delta^{18}O_{diatom}$ variations are controlled by temperature in agreement with a previous study for the west Antarctic Peninsula (WAP) (Pike et al., 2013).

Additionally, though no specific environmental study about the surface ocean water composition (water masses and sea-ice $\delta^{18}O$ contributions to the photic zone) along the AL–GVL area has been undertaken, available data for the area between 130°E–150°E and 60°S–68°S (569 values) indicate that most of $\delta^{18}O_{water}$ values for water depths between 0 m and 3500 m are between −0.2‰ and −0.3‰ with a maximum amplitude of 0.5‰ (Schmidt et al., 1999; http://data.giss.nasa.gov/o18data/). Hence, it is difficult to attribute the Holocene trend in $\delta^{18}O_{diatom}$ to drastic changes in the water masses occupying these sites, as no surface water masses present very different $\delta^{18}O_{water}$. Moreover, meteoric water derived from snow shows mean $\delta^{18}O$ values of ~−18‰ at Dumont d'Urville on the Adélie coast (Masson-Delmotte et al., 2008). Then, by assuming that meteoric water mean $\delta^{18}O$ values were comparable during the Holocene, a relatively small change in glacial discharge reaching the surface ocean was likely to have a strong impact on $\delta^{18}O_{water}$.

Thus, we argue that changes in $\delta^{18}O_{diatom}$ are governed by $\delta^{18}O_{water}$ which is, in turn, mainly regulated by glacial discharge via iceberg and brash ice discharge (Domack and Ishman, 1993; Domack et al., 1995) and/or frontal melting of glaciers (Pritchard et al., 2012) as already suggested by Pike et al. (2013) for the WAP. The $\delta^{18}O_{diatom}$ interpretation for the last 2000 years is consistent with the diatom assemblages showing icier sea-surface conditions (Denis et al., 2009b) probably because increased glacial ice discharge to the coastal ocean, further acting to cool surface waters.

Grounded icebergs, resulting from calving, might be the source of the isotopically depleted water rather than frontal melting of glaciers as calving of icebergs accounts for most of the mass loss from the Antarctic glaciers (Jacobs et al., 1992). Recently, for the Mertz and Ninnis glacier system, iceberg calving has been identified as the major contributor of the total mass loss compared to basal melting for the last thirty years (Rignot et al., 2013). Moreover, the George V coast is known to be an "iceberg trap" where large icebergs ground on Mertz Bank and Adélie Bank of the continental margin (Frezzotti et al., 1998b; Legrésy et al., 2004) where their long residence time is likely to have a significant impact on the ocean freshwater budget (Massom, 2003). Hence, a critical component recorded in the Holocene $\delta^{18}O_{diatom}$ record could be the production of icebergs from the surrounding glaciers, which might be indirectly related to the glacier fluctuations through climate forcing as suggested by Miles et al. (2013) for the current period.

4.2. AL–GVL glacial discharge history during the Holocene

4.2.1. Comparison with Southern Ocean $\delta^{18}O_{diatom}$ records

The range of $\delta^{18}O_{diatom}$ values obtained in MD03-2601 and CB2010 cores (39.9‰–45.0‰) is similar to the range measured by Pike et al. (2013) for the same period in Palmer Deep, WAP region (39.5‰–43.5‰) (Fig. 5B). These values are also consistent with $\delta^{18}O_{diatom}$ Holocene values published by Shemesh et al. (1995) and Hodell et al. (2001) for the Atlantic sector of the Southern Ocean. However, much lower values with significant scatter (34.0‰–41.0‰) were measured by Berg et al. (2010) in a Holocene core from Prydz Bay (EA). We note that the later core was retrieved

at much shallower depth and in an archipelago nearby the continent.

The high-resolution $\delta^{18}O_{diatom}$ record from the WAP (Pike et al., 2013) shows some similarities compared to the MD03-2601 $\delta^{18}O_{diatom}$ record during the last 5000 years (Fig. 5B). Both records show a decreasing trend since 5000 years with lowest $\delta^{18}O_{diatom}$ values during the last 2000 years. The records differ in the period between 10,000 cal yr BP and 5000 cal yr BP probably because of different climatic forcings in the WAP and EA during the early Holocene and different local responses due to very different oceanographic settings. The $\delta^{18}O_{diatom}$ record from the WAP shows important variations throughout the Holocene (~10,200 cal yr BP, ~8900 cal yr BP, ~4400 cal yr BP, and ~1700 cal yr BP) with events of ~150–200 yr duration presenting maximum amplitude of 2.4‰. During the Holocene, our composite $\delta^{18}O_{diatom}$ record shows less important variations, except during the last 2000 years with two major events of ~150 years duration presenting a $\delta^{18}O_{diatom}$ decrease of 3.9‰ (centered at ~1700 cal yr BP) and 4.9‰ (centered at ~1980 CE). As such, the youngest glacial discharge (iceberg and brash ice discharge and/or frontal melting of glaciers) recorded in core CB2010 (~1700 cal yr BP) appears unprecedented during the Holocene. We note that the upper part of the WAP $\delta^{18}O_{diatom}$ record shows a strong $\delta^{18}O_{diatom}$ decrease with very low Holocene values (39.5–40‰), similar to the event observed in core CB2010 (39.9–40.3‰), though leading it by a couple of hundred years.

The low resolution $\delta^{18}O_{diatom}$ from Prydz Bay (Berg et al., 2010) shows a different pattern with very low $\delta^{18}O_{diatom}$ values (<35‰, the lowest values of the three $\delta^{18}O_{diatom}$ records) during the early Holocene, interpreted by the authors as input of meltwater from melting of local ice sheets, with higher $\delta^{18}O_{diatom}$ values between 9000 cal yr BP and 6000 cal yr BP and lower values since 6000 cal yr BP. However, the very low resolution of this record (~10 measurements for the Holocene) does not allow a detailed comparison with our record.

4.2.2. AL–GVL glacial discharge history during the Early/Mid-Holocene

The glacier mass balance (the change in vertical thickness) is the direct signal of annual atmospheric conditions – with no delay – whereas the advance or retreat of glacier tongues (the change in horizontal length) is an indirect, delayed, and filtered signal of climatic change (Haeberli, 1995; Haeberli and Hoelzle, 1995; Haeberli, 1998; Oerlemans, 2001). At the low frequencies and long timescales (multidecadal to millennial) we are interested in, glaciers are in quasi-equilibrium with the climate forcing and the long-term trends observed in glacial discharge could not be random glacier dynamics.

At the Holocene timescale, no trend is observed in our $\delta^{18}O_{diatom}$ record and the main variability of this record is expressed in the low amplitude high frequency domain. Spectral analysis of the MD03-2601 $\delta^{18}O_{diatom}$ (11,000–2000 cal yr BP) was performed with RedFit 3.8 using 1000 Monte Carlo simulations, an oversampling factor of 4 for the Fourier transform, four segments with a 50% overlapping, and a Welch window-type. The program works directly from unevenly spaced data, avoiding the introduction of bias during interpolation. Two significant periods, at the 95% confidence level, were identified at ~220 years and ~440 years (see Supplementary material). The 220 years periodicity is very similar to the Suess period of solar activity (Turney et al., 2005); we suggest that the ~440 years periodicity is probably the resonance of the 220 years periodicity. This similarity may suggest, ultimately, a link between solar activity and the main parameter influencing $\delta^{18}O_{diatom}$, namely glacial discharge, probably through changes in atmospheric circulation, sea ice seasonality, and oceanic conditions modulating the energy balance at southern high latitude (Crosta et al., 2007).

The multi-centennial timescale variations observed in the down-core record of $\delta^{18}O_{diatom}$ allow us to refine previously published AL–GVL glacier fluctuations during the Holocene. Denis et al. (2009a) documented millennial AL–GVL glacier advances or retreats through a combination of diatom census counts (*Chaetoceros* resting spores, high stratification indicator, or *F. curta*, sea ice indicator) and focusing factor (ψ), the latter one been based on the ^{230}Th excess method and used as a qualitative proxy of changes in lateral sedimentary input to the core site (Denis et al., 2009a). Based on these proxies, the authors identified eight focusing events as glacial retreat or advance.

Event 1 (11,000–10,300 cal yr BP) and Event 2 (9400–8600 cal yr BP) during the deglaciation were suggested to represent glacial discharge. Event 3 (8100–7300 cal yr BP) during the cool reversal, Events 4 (6900–5600 cal yr BP) and 5 (5100–4800 cal yr BP) during the Hypsithermal, and Events 6 (3500-2200 cal yr BP), 7 (2000–1600 cal yr BP) and 8 (1300–1000 cal yr BP) were identified as glacial advances of different amplitudes. The focusing factor and diatom proxies are, however, ambiguous as both retreat and advance of glaciers bring particles to the core site and that glacial discharge via basal melting of ice shelf may also favor sea ice freezing (Bintanja et al., 2013) and, thereof, the production of *F. curta*.

Event 1 falls in line with high $\delta^{18}O_{diatom}$ values at ~10,900 cal yr BP and low $\delta^{18}O_{diatom}$ values at ~10,500 cal yr BP, indicating a two-phased event (Fig. 5A) with first a glacier advance followed by an important glacial discharge. Similarly, Event 2 might be understood as a three-phased event with an advance of the glacier system at ~9000 cal yr BP interrupting the general glacial discharge observed by Denis et al. (2009a). Event 3 occurred concomitantly to high $\delta^{18}O_{diatom}$ values and represents a glacial advance in phase with a large atmospheric negative anomaly in EA (Masson et al., 2000). Similarly, Event 4 and Event 5 are congruent with high $\delta^{18}O_{diatom}$ values and represent glacial advances as inferred by Denis et al. (2009a). The long-duration of event 6 might be separated in several phases of glaciers advance and retreat at the initiation of the Neoglacial (Fig. 5A). Event 7 might be separated in two phases with a glacial advance at 2000 cal yr BP and a glacial discharge at 1700 cal yr BP, while Event 8 is seemingly a glacial advance (Denis et al., 2009a).

We note that several low $\delta^{18}O_{diatom}$ values between 6000 cal yr BP and 7000 cal yr BP are not expressed in the focusing factor and may represent glacial retreats that did not result in sediment transport to the core site. These variations at the multi-centennial scale are not imprinted in the focusing factor, partly because of the low resolution of the later record and partly because the focusing factor is linked to bottom water transport while the $\delta^{18}O_{diatom}$ is a surface water signal. We also notice that glacial advances occurred during cool phases as recorded in East Antarctic ice cores while glacial discharges occurred 500–1000 years after the main Holocene warming events at 11,500 cal yr BP, 10,000 cal yr BP, 3800 cal yr BP and 1200 cal yr BP (Masson et al., 2000).

4.2.3. AL–GVL glacial discharge history during the last 2000 years

Due to the gap in time between the two cores, the last 2000 years hereafter refer to two periods: one between 2000 and 1000 cal yr BP and another one covering the last 250 years. These two periods are represented by the upper part of core MD03-2601 and by core CB2010, respectively (Fig. 5A) and characterized by higher amplitude variations of the isotopic signal culminating in two major events with much lower $\delta^{18}O_{diatom}$ values (39.9‰–41.1‰) (Fig. 5A). Higher climate variability in terms of amplitude and frequency has been evidenced both at global scale (Mayewski et al., 2004) and in Antarctica (Mayewski et al., 2009) since 2000 yr BP. In AL–GVL region, greater variability in subsurface temperature (Kim et al., 2012), atmospheric circulation, upwelling intensity, and sea-ice extent (Denis et al., 2010) were

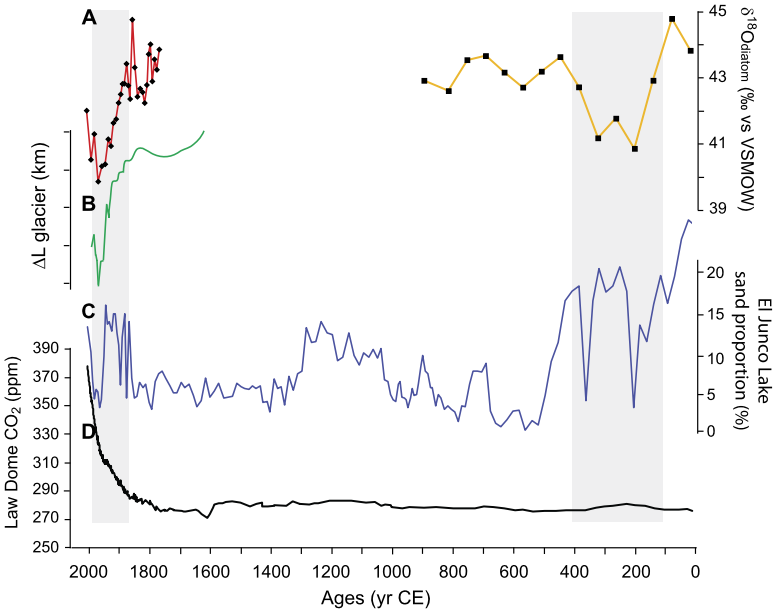

Fig. 7. (A) Composite $\delta^{18}O_{diatom}$ record from the AL–GVL (this study) (CB2010 in red and MD03-2601 in orange with measured values (black diamonds and black squares, respectively) for the last 2000 years; (B) Franz Joseph glacier length record (New Zealand's Southern Alps) in green (Leclercq and Oerlemans, 2012). (C) percentage of sand (in purple) from El Junco Crater Lake, Galápagos, for the last 2000 years (Conroy et al., 2008); (D) CO_2 concentration from Law Dome ice core (in black) for the past 2000 years (MacFarling Meure et al., 2006). (For interpretation of the references to color in this figure legend, the reader is referred to the web version of this article.)

observed during the late Holocene and was attributed to the impact of stronger and more frequent ENSO (Fig. 5). During the last 2000 years, the ENSO conditions at low-latitudes (Moy et al., 2002; Cane, 2005) were linked to orbitally induced changes in insolation seasonality: a maximum Holocene ENSO frequency since ~2200 cal yr BP (Conroy et al., 2008) (Fig. 5D) coupled with peak summer insolation at 60°S (Berger and Loutre, 1991) (Fig. 5E).

The two major events, centered at ~300 CE and ~1980 CE (Fig. 7A), are attributed to two important glacial discharges. The lowest $\delta^{18}O_{diatom}$ values recorded at 1870–2010 CE may result from the proximity of CB2010 to the Mertz–Ninnis glacier complex that could make its isotopic record more sensitive to glacial discharge than MD03-2601 record. Historical observations demonstrated different advance/retreat dynamics of the Mertz and Ninnis glaciers. While the Mertz ice tongue calved between 1912–1956 CE and subsequently grew until the last calving in February 2010, the Ninnis glacier calved in the early 1950s and in 1980–1982 CE (Wendler et al., 1996; Frezzotti et al., 1998b). Therefore, the amplitude and duration of the $\delta^{18}O_{diatom}$ low values event between 1870 CE and 2010 CE in core CB2010 could reflect the out-of-phase response of the two local glacial systems, probably initiated by a global forcing.

The two major events observed in our composite $\delta^{18}O_{diatom}$ record were congruent with high ENSO activity (Fig. 7C). The glacial discharge recorded in core MD03-2601 at ~300 CE is synchronous with a major glacial ice discharge observed in the WAP region, which was attributed to greater ENSO activity (Pike et al., 2013). However, in the AL–GVL region this event presents a higher magnitude ($\delta^{18}O_{diatom}$ decrease of 2.3‰ and 3.9‰ in ~150 years for the WAP and AL–GVL regions, respectively, Fig. 5). The event recorded in core CB2010, centered at ~1980 CE, presents an unprecedented $\delta^{18}O_{diatom}$ decrease of 4.9‰ in ~150 years. This event is congruent with a large reduction in length records of Cameron (Putnam et al., 2012) and Franz Joseph glaciers (Leclercq and Oerlemans, 2012) from New Zealand Southern Alps (Fig. 7B) and the exponential increase in atmospheric CO_2 concentrations recorded in Law Dome ice core (the most coastal ice core available for EA) (Fig. 7D). The similarities are especially striking when comparing the $\delta^{18}O_{diatom}$ record of CB2010 with the Franz Joseph glacier length record (Fig. 7A and B), one of the most responsive temperate maritime glaciers in New Zealand's Southern Alps (Leclercq and Oerlemans, 2012) and thus, highly sensitive to climatic changes. We also note that the increase towards higher $\delta^{18}O_{diatom}$ values in CB2010 after ~1980 CE is congruent with the increased mass balance of the Franz-Joseph glacier, which was coincident with a change in Interdecadal Pacific Oscillation and an associated increase in ENSO events (Chinn et al., 2005; Jones and Mann, 2004; Fitzharris et al., 2007). This further reinforces the idea of a possible coupling between New Zealand's cryosphere and southern high-latitude climate during the recent period.

Given the similarities between our record off EA with records from the WAP and New Zealand we infer that only large scale atmospheric processes such as ENSO can explain such a similarity between New Zealand and Antarctica, as already suggested above (Fig. 7C). The link among the behavior of the Southern Ocean, the southern atmospheric circulation, atmospheric CO_2, and New Zealand glaciers behavior was established for the last deglaciation (Kaplan et al., 2010). Moreover, atmospheric temperature, modulated by large scale changes in atmospheric circulation, has been evidenced as the dominant climate control on Southern Alps glaciers behavior for the modern period (Anderson and MacKintosh, 2006; Chinn et al., 2012; Clare et al., 2002; Hoelzle et al., 2007; Purdie et al., 2011), as well as for the late Holocene (Schaefer et al., 2009). Additionally, low to high-latitude teleconnections are today recognized in ENSO-sea ice (Stammerjohn et al., 2008) and in ENSO-glacial ice discharge relationships in the WAP region (Pike et al., 2013).

Synchronicity of the unprecedented $\delta^{18}O_{diatom}$ decrease at ~1980 CE with the CO_2 exponential increase suggests that atmospheric CO_2 could have intensified the decadal expression of the ENSO over the last decades (Fowler et al., 2012; Li et al., 2013), and may have amplified the last glacial discharge observed in core CB2010. We, however, acknowledge that higher resolution marine records of glacier activity spanning the instrumental period and the last millennia are pivotal to better document the interaction between climate and glacier fluctuations.

5. Conclusions

We showed that our $\delta^{18}O_{diatom}$ record off AL–GVL area generally does not bear the Holocene climatic features recorded in Antarctic marine and ice core records. Conversely, our $\delta^{18}O_{diatom}$ record does not present any trend until 2000 cal yr BP when two high amplitudes centennial-scale events occurred. We argue that $\delta^{18}O_{diatom}$ signal off AL–GVL area is controlled by glacial discharge forced by glacier fluctuations in response to long-term local seasonal insolation and short-term solar variability during the Early/Mid-Holocene. Our $\delta^{18}O_{diatom}$ record, thus suggests for the last 2000 years that two major periods (centered at ~1700 cal yr BP and ~1980 CE) of substantially increased iceberg and glacial discharge to the ocean occurred probably as a result of increasing atmospheric influence. We propose that the increased atmospheric forcing was linked with the intensification of centennial ENSO-like variability at low-latitudes, together with peak summer insolation at 60°S. The magnitude of the last major glacial discharge, as documented by our composite $\delta^{18}O_{diatom}$ record (Fig. 5A) and starting 100 years ago, is unprecedented for the last 11,000 years in the AL–GVL region and bears strong similarities to the Franz Josef Glacier length record in New Zealand, thus arguing for a large-scale connection southern mid- and high-latitude climate. It is also possible that the important increase in atmospheric CO_2 concentration during the past 200 years may have led to an amplification of the most recent glacial discharge during the past few decades. More $\delta^{18}O_{diatom}$ records along EA will potentially improve our knowledge of Antarctic ice sheet/glaciers system evolution and its consequences for global environmental changes.

Acknowledgements

Thanks to I. Brailovsky for the dedicated laboratory and office assistance. We are grateful to the anonymous reviewers for their highly constructive comments which greatly improved the paper. This research was partially supported by a Feinberg Graduate School post doctoral fellowship from the Weizmann Institute to J.C. Logistic support was obtained from the French IPEV and the international IMAGES program, ALBION and HOLOCLIP projects. The HOLOCLIP Project, a joint research project of ESF PolarCLIMATE programme, is funded by national contributions from Italy, France, Germany, Spain, Netherlands, Belgium, and the United Kingdom. This is a HOLOCLIP publication number 21.

Appendix A. Supplementary material

Supplementary material related to this article can be found online at http://dx.doi.org/10.1016/j.epsl.2014.03.009.

References

Anderson, B., MacKintosh, A., 2006. Temperature change as the major driver of late glacial and Holocene glacier fluctuations in New Zealand. Geology 34 (2), 121–124.

Arrigo, K.R., van Dijken, G.L., Bushinsky, S., 2008. Primary production in the Southern Ocean, 1997–2006. J. Geophys. Res. 113, C08004. http://dx.doi.org/10.1029/2007JC004551.

Beaman, R.J., O'Brien, P.E., Post, A.L., De Santis, L., 2011. A new high-resolution bathymetry model for the Terre Adélie and George V continental margin, East Antarctica. Antarct. Sci. 23 (1), 95–103.

Berg, S., Wagner, B., Cremer, H., Leng, M.J., Melles, M., 2010. Late Quaternary environmental and climate history of Rauer Group, East Antarctica. Palaeogeogr. Palaeoclimatol. Palaeoecol. 297, 201–213.

Berger, A., Loutre, M.F., 1991. Insolation values for the climate of the last 10 million years. Quat. Sci. Rev. 10 (4), 297–317. http://dx.doi.org/10.1016/0277-3791(91)90033-Q.

Bintanja, R., van Oldenborgh, G.J., Drijfhout, S.S., Wouters, B., Katsam, C.A., 2013. Important role for ocean warming and increased ice-shelf melt in Antarctic sea-ice expansion. Nat. Geosci. 6, 376–379. http://dx.doi.org/10.1038/ngeo1767.

Brandriss, M.E., O'Neil, J.R., Edlund, M.B., Stoermer, E.F., 1998. Oxygen isotope fractionation between diatomaceous silica and water. Geochim. Cosmochim. Acta 62, 1119–1125.

Cane, M.A., 2005. The evolution of El Niño, past and future. Earth Planet. Sci. Lett. 230, 227–240. http://dx.doi.org/10.1016/j.epsl.2004.12.003.

Chapligin, B., Leng, M.J., Webb, E., Alexandre, A., Dodd, J.P., Ijiri, A., Lücke, A., Shemesh, A., Abelmann, A., Herzschuh, U., Longstaffe, F.J., Meyer, H., Moschen, R., Okazaki, Y., Rees, N.H., Sharp, Z.D., Sloane, H.J., Sonzogni, C., Swann, G.E.A., Sylvestre, F., Tyler, J.J., Yam, R., 2011. Inter-laboratory comparison of oxygen isotope compositions from biogenic silica. Geochim. Cosmochim. Acta 75, 7242–7256.

Chinn, T.J., Winkler, S., Salinger, M.J., Haakensen, N., 2005. Recent glacier advances in Norway and New Zealand, a comparison of their glaciological and meteorological causes. Geogr. Ann. 87A (1), 141–157.

Chinn, T., Fitzharris, B.B., Willsman, A., Salinger, M.J., 2012. Annual ice volume changes 1976–2008 for the New-Zealand Southern Alps. Glob. Planet. Change 92–93, 105–118.

Clare, G.R., Fitzharris, B.B., Chinn, T.J., Salinger, M.J., 2002. Interannual variation in end of-summer-snowlines of the Southern Alps of New Zealand, in response to changes in Southern Hemisphere atmospheric circulation and sea surface temperature patterns. Int. J. Climatol. 22 (1), 121–128.

Conroy, J.L., Overpeck, J.T., Cole, J.E., Shanahan, T.M., Steinitz-Kannan, M., 2008. Holocene changes in eastern tropical Pacific climate inferred from a Galápagos lake sediment record. Quat. Sci. Rev. 27, 1166–1180.

Crespin, J., Sylvestre, S., Alexandre, A., Sonzogni, C., Paillès, C., Perga, M.E., 2010. Re-examination of temperature dependent relationship between $\delta^{18}O_{diatom}$ and $\delta^{18}O_{diatom}$ and implications for paleoclimate inferences. J. Paleolimnol. 44, 547–557.

Crosta, X., Shemesh, A., Salvignac, M.E., Gildor, H., Yam, R., 2002. Late Quaternary variations of elemental ratios (C/Si and N/Si) in diatom-bound organic matter from the Southern Ocean. Deep-Sea Res., Part 2, Top. Stud. Oceanogr. 49, 1939–1952.

Crosta, X., Debret, M., Courty, M.-A., Denis, D., Ther, O., 2007. Holocene long- and short-term climate changes off Adélie Land, East Antarctica. Geochem. Geophys. Geosyst. 8, Q11009. http://dx.doi.org/10.1029/12007GC001718.

Denis, D., Crosta, X., Schmidt, S., Carson, D., Ganeshram, R., Bout-Roumazeilles, V., Zaragosi, S., Martin, B., 2009a. Holocene glacier and deep water dynamics, Adélie Land, East Antarctica. Quat. Sci. Rev. 28 (13–14), 1291–1303.

Denis, D., Crosta, X., Schmidt, S., Carson, D., Ganeshram, R., Renssen, H., Crespin, J., Ther, O., Billy, I., 2009b. Holocene productivity changes off Adélie Land (East Antarctica). Paleoceanography 24, PA3207. http://dx.doi.org/10.1029/2008PA001689.

Denis, D., Crosta, X., Barbara, L., Massé, G., Renssen, H., Ther, O., Giraudeau, J., 2010. Sea ice and wind variability during the Holocene in East Antarctica: insight on middle–high latitude coupling. Quat. Sci. Rev. 29, 3709–3719.

Dodd, J.P., Sharp, Z.D., 2010. A laser fluorination method for oxygen isotope analysis of biogenis silica and new oxygen isotope calibration of modern diatoms in freshwater environments. Geochim. Cosmochim. Acta 74, 1381–1390.

Dodd, J.P., Sharp, Z.D., Fawcett, P.J., Brearley, A.J., McCubbin, F.M., 2012. Rapid post-mortem maturation of diatom silica oxygen isotope values. Geochem. Geophys. Geosyst. 13 (9), Q09014. http://dx.doi.org/10.1029/2011GC004019.

Domack, E.W., Ishman, S.E., 1993. Oceanographic and physiographic controls on modern sedimentation within Antarctic fjords. Geol. Soc. Am. Bull. 105, 1175–1189.

Domack, E.W., Ishman, S.E., Stein, A.B., McClennen, C.E., Jull, A.J.T., 1995. Late Holocene advance of the Müller Ice Shelf, Antarctic Peninsula: sedimentological, geochemical and paleontological evidence. Antarct. Sci. 7, 159–170.

Fitzharris, B.B., Clare, G.R., Renwick, J., 2007. Teleconnections between Andean and New-Zealand glaciers. Glob. Planet. Change 59, 159–174.

Fowler, A., Boswijk, G., Lorrey, A., Gergis, J., Pirie, M., McCloskey, S.P.J., Palmer, J.G., Wunder, J., 2012. Multi-centennial tree-ring record of ENSO-related activity in New Zealand. Nat. Clim. Change 2, 172–176. http://dx.doi.org/10.1038/NClimate1374.

Frezzotti, M., Cimbelli, A., Ferrigno, J., 1998b. Ice-front change and iceberg behavior along Oates and George V Coasts, Antarctica, 1912–96. Ann. Glaciol. 27, 643–650.

Haeberli, W., 1995. Glacier fluctuations and climate change detection. Geogr. Fis. Din. Quat. 18, 191–199.

Haeberli, W., 1998. Historical evolution and operational aspects of worldwide glacier monitoring. In: Haeberli, W., Hoelzle, M., Suter, S. (Eds.), Into the Second Century of World Glacier Monitoring: Prospects and Strategies. UNESCO, Paris.

Haeberli, W., Hoelzle, M., 1995. Application of inventory data for estimating characteristics of and regional climate-change effects on mountain glaciers: A pilot study with the European Alps. Ann. Glaciol. 21, 206–212.

Hall, B.L., 2009. Holocene glacial history of Antarctica and the Sub-Antarctic islands. Quat. Sci. Rev. 28, 2213–2230.

Hodell, D.A., Kanfoush, S.L., Shemesh, A., Crosta, X., Charles, C.D., Guilderson, T.P., 2001. Abrupt cooling of Antarctic surface waters and sea ice expansion in the South Atlantic sector of the Southern Ocean at 5000 cal yr BP. Quat. Res. 6, 191–198.

Hodgson, D.A., Abram, N., Anderson, J., Bargelloni, L., Barrett, P., Bentley, M.J., Bertler, N.A.N., Chown, S., Clarke, A., Convey, P., Crame, A., Crosta, X., Curran, M., di Prisco, G., Francis, J.E., Goodwin, I., Gutt, J., Massé, G., Masson-Delmotte, V., Mayewski, P.A., Mulvaney, R., Peck, L., Pörtner, H.-O., Röthlisberger, R., Stevens, M.I., Summerhayes, C.P., van Ommen, T., Verde, C., Verleyen, E., Vyverman, W., Wiencke, C., Zane, L., 2009a. Antarctic climate and environment history in the pre-instrumental period. In: Turner, J., Convey, P., Di Prisco, G., Mayewski, P.A., Hodgson, D.A., Fahrbach, E., Bindschadler, R., Gutt, J. (Eds.), Antarctic Climate Change and the Environment. Scientific Committee for Antarctic Research, Cambridge, pp. 115–182.

Hoelzle, M., Chinn, T., Stumm, D., Paul, F., Zemp, M., Haeberli, W., 2007. The application of glacier inventory data for estimating past climate change effects on mountain glaciers: A comparison between the European Alps and the Southern Alps of New Zealand. Glob. Planet. Change 56, 69–82.

Hurrell, E.R., Barker, P.A., Leng, M.J., Vane, C.H., Wynn, P., Kendrick, C.P., Verschuren, D., Street-Perrott, F.A., 2011. Developing a methodology for carbon isotope analysis for lacustrine diatoms. Rapid Commun. Mass Spectrom. 25, 1567–1574.

Jacobs, S.S., Helmer, H.H., Doake, C.S.M., Jenkins, A., Frolich, R.M., 1992. Melting of ice shelves and the mass balance of Antarctica. J. Glaciol. 38 (130), 375–387.

Jacot Des Combes, H., Esper, O., De La Rocha, C.L., Abelmann, A., Gersonde, R., Yam, R., Shemesh, A., 2008. Diatom δ^{13}C and δ^{15}N and C/N since the last galcial maximum in the Southern Ocean: potential impact of species composition. Paleoceanography 28, PA4209. http://dx.doi.org/10.1029/2008PA001589.

Jones, P.D., Mann, M.E., 2004. Climate over past millennia. Rev. Geophys. 42, RG2002. http://dx.doi.org/10.1025/2003RG000143.

Juillet-Leclerc, A., 1986. Cleaning process for diatomaceous samples. In: Ricard, M. (Ed.), Proceedings of the 8th International Diatom Symposium. Koeltz Scientific Books, Koenigstein, pp. 733–736.

Juillet-Leclerc, A., Labeyrie, L., 1987. Temperature dependence of the oxygen isotopic fractionation between diatom silica and water. Earth Planet. Sci. Lett. 84, 69–74.

Kaplan, M.R., Schaefer, J.M., Denton, G.H., Barrell, D.J.A., Chinn, J.H., Putman, A.E., Andersen, B.G., Finkel, R.C., Schwartz, R., Doughty, A.M., 2010. Glacier retreat in New Zealand during the Younger Dryas stadial. Nature 467, 194–197. http://dx.doi.org/10.1038/nature09313.

Kim, J.-H., Crosta, X., Willmott, W., Rensenn, H., Bonnin, J., Helmke, P., Schouten, S., Sinninghe Damsté, J.S., 2012. Holocene subsurface temperature variability in the eastern Antarctic continental margin. Geophys. Res. Lett. 39, L06705. http://dx.doi.org/10.1029/2012GL051157.

Leclercq, P.W., Oerlemans, J., 2012. Global and hemispheric temperature reconstruction from glacier length fluctuations. Clim. Dyn. 38, 1065–1079. http://dx.doi.org/10.1007/s00382-011-1145-7.

Legrésy, B., Wendt, A., Tabacco, I., Rémy, F., Dietrich, R., 2004. Influence of tides and tidal current on Mertz Glacier, Antarctica. J. Glaciol. 50 (170), 427–435.

Leng, M.J., Barker, P.A., 2006. A review of the oxygen isotope composition of lacustrine diatom silica for paleoclimate reconstruction. Earth-Sci. Rev. 75, 5–27.

Li, J., Xie, S.-P., Cook, E., Morales, M.S., Christie, D.A., Johnson, N.C., Chen, F., D'Arrigo, R., Fowler, A.M., Gou, X., Fang, K., 2013. El Nino modulations over the past seven centuries. Nat. Clim. Change 3, 822–826. http://dx.doi.org/10.1038/NCLIMATE1936.

MacFarling Meure, C., Etheridge, D., Trudinger, C., Steele, P., Langenfelds, R., van Ommen, T., Smith, A., Elkins, J., 2006. The Law Dome CO_2, CH_4 and N_2O ice core records extended to 2000 years BP. Geophys. Res. Lett. 33 (14), L14810. http://dx.doi.org/10.1029/2006GL026152.

Massom, R.A., 2003. Recent iceberg calving events in the Ninnis Glacier region, East Antarctica. Antarct. Sci. 15 (2), 303–313.

Masson, V., Vimeux, F., Jouzel, J., Morgan, V., Delmotte, M., Ciais, P., Hammer, C., Johnsen, S., Lipenkov, V.Y., Mosley-Thompson, E., Petit, J.R., Steig, E.J., Stievenard, M., Vaikmae, R., 2000. Holocene climate variability in Antarctica based on 11 icecore isotopic records. Quat. Res. 54, 348–358.

Masson-Delmotte, V., Hou, S., Ekaykin, A., Jouzel, J., Aristarain, A., Bernardo, R.T., Bromwich, D., Cattani, O., Delmotte, M., Falourd, S., Frezzotti, M., Gallée, H., Genoni, L., Isaksson, E., Landais, A., Helsen, M.M., Hoffmann, G., Lopez, J., Morgan, V., Motoyama, Noone D, H., Oerter, H., Petit, J.R., Royer, A., Uemura, R., Schmidt, G.A., Schlosser, E., Simoes, J.C., Steig, E.J., Stenni, B., Stievenard, M., Van Den Broeke, M.R., Van De Wal, R.S.W., Van De Berg, W.J., Vimeux, F., White, J.W.C., 2008. A review of Antarctic surface snow isotopic composition: observations, atmospheric circulation, and isotopic modeling. J. Climate 21, 3359–3387. http://dx.doi.org/10.1175/2007JCLI2139.1.

Mayewski, P.A., Rohling, E., Stager, C., Karlén, K., Maasch, K., Meeker, L.D., Meyerson, E., Gasse, F., van Kreveld, S., Holmgren, K., Lee-Thorp, J., Rosqvist, G., Rack, F., Staubwasser, M., Schneider, R., 2004. Holocene climate variability. Quat. Res. 62, 243–255.

Mayewski, P.A., Meredith, M.P., Summerhayes, C.P., Turner, J., Worby, A., Barrett, P.J., Casassa, G., Bertler, N.A.N., Bracegirdle, T., Garabato, A.C.N., Bromwich, D., Campbell, H., Hamilton, G.S., Lyons, W.B., Maasch, K.A., Aoki, S., Xiao, C., Van Ommen, T., 2009. State of the Antarctic and Southern Ocean climate system. Rev. Geophys. 47, 1–38.

Miles, B.W.J., Stokes, C.R., Vieli, A., Cox, N.J., 2013. Rapid, climate-driven changes in outlet glaciers on the Pacific coast of East Antarctica. Nature 500, 563–567. http://dx.doi.org/10.1038/nature12382.

Morley, D.W., Leng, M.J., Mackay, A.W., Sloane, H.J., Rioual, P., Battarbee, R.W., 2004. Cleaning of lake sediment samples for diatom oxygen isotope analysis. J. Paleolimnol. 31, 391–401.

Moschen, R., Lücke, A., Schleser, G., 2005. Sensitivity of biogenic silica oxygen isotopes to changes in surface water temperature and palaeoclimatology. Geophys. Res. Lett. 32, L07708. http://dx.doi.org/10.1029/2004GL022167.

Moschen, R., Lücke, A., Parplies, J., Radtke, U., Schleser, G.H., 2006. Transfer and early diagenesis of biogenic silica oxygen isotope signals during settling and sedimentation of diatoms in a temperate freshwater lake (Lake Holzmaar, Germany). Geochim. Cosmochim. Acta 70, 4367–4379.

Moy, C.M., Seltzer, G.O., Rodbell, D.T., Anderson, D.M., 2002. Variability of El Niño/Southern Oscillation activity at millennial timescales during the Holocene epoch. Nature 420, 162–165. http://dx.doi.org/10.1038/nature01194.

Oerlemans, J., 2001. Glaciers and Climate Change. A.A. Balkema Publishers, Lisse.

Pike, J., Swann, G.E.A., Leng, M.J., Snelling, A.M., 2013. Glacial discharge along the west Antarctic Peninsula during the Holocene. Nat. Geosci. 6, 199–202. http://dx.doi.org/10.1038/NGEO1703.

Pritchard, H.D., Arthern, R.J., Vaughan, D.G., Edwards, L.A., 2009. Extensive dynamic thinning on the margins of the Greenland and Antarctic ice sheets. Nature 461, 971–975. http://dx.doi.org/10.1038/nature08471.

Pritchard, H.D., Ligtenberg, S.R.M., Fricker, H.A., Vaughan, D.G., van den Broecke, A.R., Padman, L., 2012. Antarctic ice-sheet-loss driven by basal melting of ice shelves. Nature 484, 502–505.

Purdie, H., Mackintosh, A., Lawson, W., Anderson, B., Morgenstern, U., Chinn, T., Mayewksi, P., 2011. Interannual variability in net accumulation on Tasman Glacier and its relationship with climate. Glob. Planet. Change 77 (3–4), 142–152. http://dx.doi.org/10.1016/j.gloplacha.2011.04.004.

Putnam, A.E., Schaefer, J.M., Denton, G.H., Barrell, D.J.A., Finkel, R.C., Andersen, B.G., Schwartz, R., Chinn, T.J.H., Doughty, A.M., 2012. Regional climate control of glaciers in New Zealand and Europe during the pre-industrial Holocene. Nat. Geosci. 5, 627–630. http://dx.doi.org/10.1038/NGEO1548.

Renssen, H., Goose, H., Fichefet, T., Masson-Delmotte, V., Koç, N., 2005. Holocene climate evolution in the high-latitude Southern Hemisphere simulated by a coupled atmosphere–sea ice–ocean-vegetation model. Holocene 15 (7), 951–964.

Renssen, H., Seppä, H., Crosta, X., Goose, H., Roche, D.M., 2012. Global characterization of the Holocene Thermal Maximum. Quat. Sci. Rev. 48, 7–19.

Rignot, E., Jacobs, S., Mouginot, J., Scheuchl, P., 2013. Ice-shelf melting around Antarctica. Science 341, 266–270. http://dx.doi.org/10.1126/science.1235798.

Schaefer, J., Denton, G.H., Kaplan, M., Putman, A., Finkel, R.C., Barrell, D.J.A., Andersen, B.G., Schwartz, R., Mackintosh, A., Chinn, T., Schlüchter, C., 2009. High-frequency Holocene glacier fluctuations in New Zealand differ from the Northern signature. Science 324, 622–625.

Schiff, C., Kaufman, D.S., Wolfe, A.P., Dodd, J., Sharp, Z., 2009. Late Holocene storm-trajectory changes inferred from the oxygen isotope composition of lake diatoms, south Alaska. J. Paleolimnol. 41, 189–208. http://dx.doi.org/10.1007/s10933-008-9261-z.

Schmidt, G.A., Bigg, G.R., Rohling, E.J., 1999. Global seawater oxygen-18 database – v1.21. http://data.giss.nasa.gov/o18data/.

Schmidt, M., Botz, R., Stoffers, P., Anders, T., Bohrman, G., 1997. Oxygen isotopes in marine diatoms: A comparative study of analytical techniques and new results on the isotope composition of recent marine diatoms. Geochim. Cosmochim. Acta 61 (11), 2275–2280.

Schmidt, M., Botz, R., Rickert, D., Bohrman, G., Hall, S.R., Mann, S., 2001. Oxygen isotopes of marine diatoms and relations to opal-A maturation. Geochim. Cosmochim. Acta 65, 201–211.

Schmidt, S., Howa, H., Diallo, A., Martín, J., Cremer, M., Duros, P., Fontanier, Ch., Deflandre, B., Metzger, E., Mulder, Th., in press. Recent sediment transport and deposition in the Cap-Ferret Canyon, South–East margin of Bay of Biscay. Deep-Sea Res., Part 2, Top. Stud. Oceanogr. http://dx.doi.org/10.1016/j.dsr2.2013.06.004.

Shemesh, A., Charles, C.D., Fairbanks, R.G., 1992. Oxygen isotopes in biogenic silica: global changes in ocean temperature and isotopic composition. Science 256, 1434–1436.

Shemesh, A., Burckle, L.H., Hays, J.D., 1995. Late Pleistocene oxygen isotope records of biogenic silica from the Atlantic sector of the Southern Ocean. Paleoceanography 10, 179–196.

Stammerjohn, S.E., Martinson, D.G., Smith, R.C., Yuan, X., Rind, D., 2008. Trends in annual sea ice retreat and advance and their relation to El Niño–Southern Oscillation and Southern Annular Mode variability. J. Geophys. Res. 113, C03S90. http://dx.doi.org/10.1038/nature09751.

Summerhayes, C., Barnes, D., Bergstrom, D., Bindschadler, R., Bockheim, J., Bodeker, G., Bopp, L., Bracegirdle, T., Chown, S., Convey, P., di Prisco, G., Fahrbach, E., Forcada, J., Frenot, Y., Goose, H., Gutt, J., Hodgson, D., Huiskes, A., Jones, A., Leaper, R., Lefebvre, W., Lenton, A., Lynch, A., Metzl, N., Muray, A., O'Farrell, S., Peck, L., Pörtner, H., Roscoe, H., Smale, D., Smetacek, V., Turner, J., Vanreusel, A., Vaughan, D., Verde, C., Wang, Z., 2009. The Antarctic environment in the global system/the next 100 years. In: Turner, J., Convey, P., di Prisco, G., Mayewski, P.A., Hodgson, D.A., Fahrbach, E., Bindschadler, R., Gutt, J. (Eds.), Antarctic Climate Change and the Environment. Scientific Committee for Antarctic Research, Cambridge, pp. 299–387.

Swann, G.E.A., Leng, M.J., 2009. A review of diatom $\delta^{18}O$ in palaeoceanography. Quat. Sci. Rev. 28, 384–398.

Swann, G.E.A., Leng, M.J., Sloane, H., Maslin, M.A., Onodera, J., 2007. Diatom oxygen isotopes: Evidence of a species effect in the sediment record. Geochem. Geophys. Geosyst. 8 (6), Q06012. http://dx.doi.org/10.1029/2006GC001535.

Swann, G.E.A., Leng, M.J., Sloane, H.J., Maslin, M.A., 2008. Isotope offset in marine diatom $\delta^{18}O$ over the last 200 ka. J. Quat. Sci. 23 (4), 389–400. http://dx.doi.org/10.1002/jqs.1185.

Taylor, F., Whitehead, J., Domack, E., 2001. Holocene paleoclimate change in the Antarctic Peninsula: Evidence from the diatom, sedimentary and geochemical record. Marine Micropaleontology 41, 25–43. http://dx.doi.org/10.1016/S0377-8398(00)00049-9.

Turner, J., Colwell, S.R., Marshall, G.J., Lachlan-Cope, T.A., Carleton, A.M., Jones, P.D., Lagun, V., Reid, P.A., Iagovnika, S., 2005a. Antarctic climate change during the last 50 years. Int. J. Climatol. 25, 279–294.

Turney, C., Baillie, M., Clemens, S., Brown, D., Palmer, J., Pilcher, J., Reimer, P., Leuschner, H.H., 2005. Testing solar forcing of pervasive Holocene climate cycles. J. Quat. Sci. 20 (6), 511–518.

Verleyen, E., Hodgson, D.A., Sabbe, K., Cremer, H., Emslie, S., Gibson, J., Hall, B., Imura, S., Kudoh, S., Marshall, G.J., McMinn, A., Melles, M., Newman, L., Roberts, D., Singh, S.M., Sterken, M., Tavernier, I., Verkulich, S., Van de Vyver, E., Van Nieuwenhuyze, W., Wagner, B., Vyverman, W., 2011. Post-glacial regional climate variability along the East Antarctic coastal margin – Evidence from shallow marine and coastal terrestrial records. Earth-Sci. Rev. 104, 199–212.

Wendler, G., Ahlnas, K., Lingle, G.S., 1996. On the Mertz and Ninnis Glaciers, East Antarctica. J. Glaciol. 42 (142), 447–453.